Combined spectral and stimulated luminescence study of charge trapping and recombination processes in α-Al_2O_3:C

By: Angel Newton Nyirenda

Supervisor: Professor Makaiko Chithambo

Submitted to the Department of Physics and Electronics, Faculty of Science, Rhodes University, in fulfilment of the requirements of the degree of PhD (Science)

March 14, 2018

Abstract

The main objective of this project was to gain a deeper and better understanding of the luminescence processes in α-Al_2O_3:C, a highly-sensitive dosimetric material, using a combined spectral and stimulated luminescence study. The spectral studies concentrated on the emission spectra obtained using X-ray induced radioluminescence (XERL), thermoluminescence (XETL) and time-resolved X-ray excited optical luminescence (TR-XEOL) techniques. The stimulated luminescence studies were based on thermoluminescence (TL), optically stimulated luminescence (OSL) and phototransferred TL (PTTL) methods that were used in the study of the radiation-induced defects at high beta-doses and the deep traps, that is, traps with thermal depths beyond 500°C. The spectral and stimulated luminescence measurements were carried out using a high sensitivity luminescence spectrometer and a Risø TL/OSL Model DA-20 Reader, respectively. The XERL emission spectrum measured at room temperature shows seven gaussian peaks associated with F-centres (420 nm), F^+-centres (334 nm), F_2^{2+}-centres (559 nm), Stoke's vibronic band of Cr^{3+} (671 nm), Cr^{3+} R-line emission (694 nm), anti-Stokes vibronic band of Cr^{3+} (710 nm) and an unidentified emission band (260-300 nm) which we associate with hole recombinations at a luminescence centre. The 694-nm R-line emission from Cr^{3+} impurity ions is most likely due to recombination of holes at Cr^{2+} during stimulated luminescence and as a result of an intracentre excitation of Cr^{3+} in photoluminescence (PL) due to photon absorption. The Cr^{3+} emission decreases in intensity, whereas the intensity of F-centre emission band is almost constant with repeated XERL measurements. Depending on the amount of X-ray irradiation dose, both holes and/or electrons may take place in the emission processes of peaks I (30-80°C), II (90-250°C) and III (250-320°C) during a TL readout, albeit, electron recombination is dominant regardless of dose. At higher doses, the XETL emission spectra indicate that the dominant band associated

with TL peak III (250-320°C) in the material, shifts from F-centre to Cr^{3+}. Using the deep-traps OSL, it has been confirmed that the main TL trap is also the main OSL trap whereas the TL traps lying in the temperature range of 400-550°C constitute the secondary OSL traps. There is evidence of strong retrapping at the main trap during optical stimulation of charges from the secondary OSL traps and the deep traps and that the retrapping occurs via the delocalized bands. At high-irradiation beta-doses, aggregate defect centres which significantly alter the TL and OSL properties, are induced in the material. The induced aggregate centres get completely obliterated by heating a sample to 700°C. The radiation-induced defects cause the main TL peak to shift towards higher temperatures, increase its FWHM, reduce its maximum intensity and cause an underestimation of both the activation energy and order of kinetics of the peak. On the other hand, the OSL response of the material is enhanced following a high-irradiation dose. During sample storage in the dark at ambient temperature, charges do migrate from the deep traps (donors) to the main and intermediate traps (acceptors) and that the major donor traps during this charge transfer phenomenon lie between 500-600°C.

Acknowledgements

Most heartfelt thanks should go to my supervisor, Professor Makaiko Chithambo, who has mentored me since my MSc days. He extended to me the National Research Foundation PhD Bursary at a time I did not expect it. Prof. Chithambo has immeasurably sharpened both my research skills and writing skills through and through. I shall remain indebted to him for according me such rare opportunities in life.

Let me also thank the NRF and Rhodes University in a special way for funding our trip to the University of St Andrews in Scotland to carry out spectral studies. The journey was eye opening and the purpose of our visit, so rewarding. In the same vein, I would like to thank Dr. A.A. Finch of the University of St Andrews who provided us with technical and moral support during our stay in St Andrews.

It would be criminal not say thank you to my wife Louisa Gondwe-Nyirenda for her encouraging words during this treacherous journey. I dedicate this work to my two boys, Malumbo and Lumbani Nyirenda.

Contents

List of Figures

List of Tables

Chapter 1

Introduction

α-Al_2O_3:C has been a material of topical research interests since the early 1990's. Thermoluminescence detectors based on α-Al_2O_3:C (TLD-500K) were first developed and established at the Urals Polytechnic Institute (Ekaterinburg, Russia) in the form of a single crystal [1]. The TLD-500K showed high TL sensitivity to ionising radiation, simple TL glow curve, low background and dose threshold (0.1 μGy), low fading when stored in the dark, good reproducibility and re-usability with anneal, simple emission spectrum, wide dynamic range ($10^{-7} - 10$ Gy) of dose response and relatively low effective atomic number (10.2) [1]. Akselrod, et al [2] attributed the high-sensitivity of TLD-500K to the large concentration of trapping and luminescence centres. The material has since been widely adopted for environmental monitoring, personal, medical and retrospective dosimetry. The amount of research output yielded from studying the material is voluminous. However, some mechanisms of luminescence in the material remain unclear to date. Details of the defects responsible for charge trapping in the material are not fully known. Due to advancement of experimental techniques, more and more information on the trapping and recombination processes is being uncovered. The fact that more and more research output, based on the material, continues to be published yearly, is proof enough that α-Al_2O_3:C remains an unfinished product.

In our current work, we present a study of luminescence processes i.e. trapping, retrapping, radiative and non-radiative recombinations, in α-Al_2O_3:C using various spectral and stimulated luminescence techniques. The stimulated luminescence techniques were significantly used in the study of deep traps in the material. Spectra

techniques were emphasized in the study of the emission spectra i.e. recombination centres and the temperature-dependence of these emission spectra. In a detailed way, we also studied the effect of high-irradiation doses on thermoluminescence (TL) and optically stimulated luminescence (OSL) properties of the material.

In this chapter, we briefly introduce the content covered in each of the chapters in the thesis.

Chapter 2 deals with theoretical aspects of the luminescence phenomena. The different types of luminescence processes have been defined. The simple band model used to describe the stimulated luminescence phenomena i.e. TL and OSL, has been presented. The equations governing TL and OSL have been provided. Furthermore, we have accounted for the emission and absorption spectra i.e. luminescence spectroscopy, using the configurational coordinate model. The phenomenon of thermal quenching has also been explained using the configurational coordinate diagram.

In Chapter 3, details of the samples used in our study have been provided. The various pieces of instrumentation used during our investigations have also been thoroughly described in this chapter.

The results of the spectral studies have been presented in Chapter 4. Herein, we describe and explain the results based on the methods of X-ray induced radioluminescence (XERL), thermoluminescence (XETL) and time-resolved X-ray excited OSL (TR-XEOL). The temperature-dependence of the F-centre and chromium impurity ion, Cr^{3+}, has been discussed considerably. The radioluminescence spectra recorded while heating a sample at a controlled rate i.e XERL-TL spectra have been presented and compared against the conventional TL spectra. Efforts have also been made to understand the multi-component nature of the main TL peak in the material.

The study of the deep traps using the stimulated phenomena i.e. thermoluminescence (TL), optically stimulated luminescence (OSL) and phototransferred thermoluminescence (PTTL), has been covered at length in Chapter 5. A detailed analysis of the phenomenon of thermal assistance in the material has been provided. We have also put forward a reasonable debate concerning the deep hole traps in the material.

In Chapter 6, we discuss the effects of high-beta irradiation doses on the TL and OSL response of the material. These effects are discussed in terms of the aggregate F- and F^+-centres, introduced in the material by the high-irradation doses. The induced

aggregate centres are thermally unstable and produce high-temperature TL peaks.

Chapter 7 deals with charge migration from the deep traps (donors) to the main and intermediate traps (acceptors) during sample storage in the dark at ambient temperature. In this chapter, we also demonstrate that the major donor traps during this charge transfer phenomenon lie between 500-600°C.

In the final chapter, Chapter 8, we summarize the important results presented in Chapters 4, 5 and 6. We also point out potential areas of further research which we could not tackle because of equipment limitations and/or time factor.

Chapter 2

Theoretical aspects

Luminescence is a process in which a material emits non-thermal radiation due to absorption of ionising radiation i.e. ultraviolet light (UV), gamma rays, beta particles, etc. Upon absorbing ionising radiation, the electronic states of the absorbing material are raised to higher states i.e. metastable states. The relaxation of these excited states to ground state produces light termed as luminescence. For this to occur, the material must necessarily be an insulator or a wide-band gap semiconductor. The luminescence may either be spontaneous ($\sim 10^{-8}$ s) in which case it is called fluorescence or delayed ($\sim 10^{-3}$ s or longer) in which case it is called phosphorescence or stimulated luminescence. Radioluminescence (RL) is a form of spontaneous or prompt luminescence which occur simultaneously with sample irradiation. In radioluminescence, the characteristic exciting agents of a sample are nuclear particles i.e. gamma rays, X-rays, beta and alpha particles.

In this chapter, we provide a brief account of the theoretical underpinnings of stimulated luminescence and luminescence spectroscopy.

2.1 Stimulated luminescence phenomena

Solid state theory tells us that even the 'purest' crystalline solid contains defects. Crystal defects are simply disruptions to the periodicity of a crystalline solid. These defects may either be intrinsic i.e. introduced during crystal growth or extrinsic i.e. impurities. In whatever form, defects tend to alter the chemical, physical and electrical properties of the material. Defects introduce energy levels in the otherwise

forbidden band i.e. the energy gap between the bottom of the conduction band and top of the valence band. A valence band is a completely filled band, whereas a conduction band is a completely empty band at absolute zero. The energy levels introduced in the forbidden band act as traps and/or recombination centres for free charge carriers during irradiation. Whereas an electron is completely free in the conduction band, a hole is completely free in the valence band.

Let us consider a simple band model of a crystalline solid shown in Figure 2.1. It has to be stated at the outset that the band structure of real crystalline materials is too complex to be modeled by Figure 2.1. However, this simple model describes the luminescence processes in a simplified manner and can easily be extrapolated to more complex systems of real materials. The simple band model consists of a single trapping state (trap) and a single recombination centre (RC). The energy difference between the bottom of the conduction band and the trap level is called the trap or energy depth, E_t. When a material is exposed to ionising radiation i.e. excitation energy, ionization of atoms in the valence band occurs which generates free electron-hole pairs. The free electrons and holes may immediately recombine to produce fluorescence or radioluminescence. Alternatively, the free electrons may be captured by the trap and the free holes, by the recombination centre. If an external energy i.e. stimulation energy, with the right amount of energy is now added to the material, the trapped electron is released back into the conduction band from where it can either be recaptured by the trap i.e. retrapping, or transition to the recombination centre to unite with a hole with subsequent emission of a photon i.e. luminescence. Since an external stimulating agent is required to excite the trapped charges into the delocalised bands, this kind of luminescence is called stimulated luminescence. If the external stimulation energy is heat, it is called thermoluminescence. If instead, light is used as an external stimulating agent, the ensuing luminescence is called optically stimulated luminescence (OSL). In either case, the intensity of the luminescence is proportional to the number of trapped charges. Since the number of trapped charges is dependent upon the excitation energy i.e. the ionizing radiation, the luminescence intensity is therefore proportional to the amount of ionizing radiation absorbed by the sample. For this reason, a luminescent material can be used in radiation dosimetry applications.

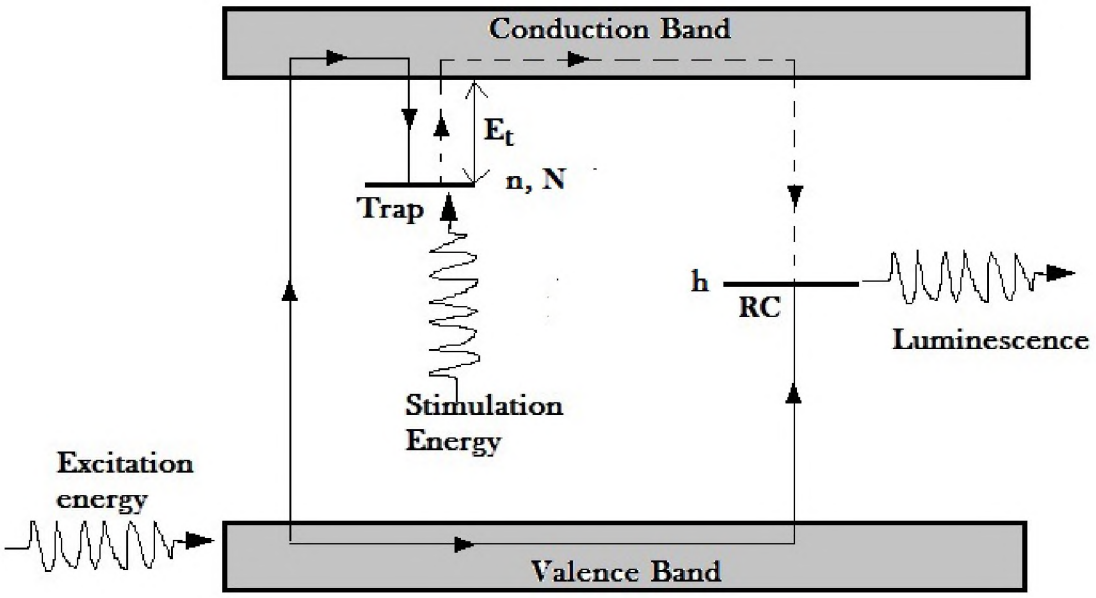

Figure 2.1: A simple band model for a luminescent material. RC represents recombination centre, E_t is the trap depth or the activation energy, n is the instantaneous number of trapped electrons, N is the concentration of electron traps and h is the instantaneous number of trapped holes. The solid arrows represent transitions of charges generated by the excitation energy, whereas the dotted arrows represent the transitions of a trapped electron during stimulation.

2.2 Thermoluminescence

As already pointed out in the previous section, thermoluminescence (TL) is a stimulated luminescence phenomenon in which heat is a stimulus. To yield thermoluminescence, a material (insulator or semiconductor) must first be exposed to ionizing radiation, then heated at a controlled rate to some maximum temperature. A plot of TL intensity against temperature produces a set of temperature-resolved peaks. Such a plot is called a TL glow-curve. Each peak in the TL glow-curve represents a species of traps with a unique trap depth. The peaks in a TL glow curve are analyzed in order to extract important parameters that can be used to describe TL processes in the material. Commonly extracted parameters include the trap depth, E, the attempt-to-escape frequency, s and the order of kinetics, b. The technique of thermoluminescence has proved worthy for the study of crystal defects which act as

trapping sites for electrons and holes, besides its application to radiation dosimetry and to dating techniques in archaeology and geology [3].

2.2.1 Models of thermoluminescence

We now present the equations governing thermoluminescence processes during thermal stimulation. We assume that the irradiation of the material has already taken place.

Let n (cm^{-3}) represent the instantaneous electron concentration in the traps of a particular species with an average trap depth, E (eV) and characteristic attempt-to-escape frequency, s (s^{-1}). The equations governing the thermoluminescence processes are as follows [4]:

$$I(t) = -\frac{dn}{dt} = sn \exp\left(-\frac{E}{kT}\right) \tag{2.1}$$

$$I(t) = -\frac{dn}{dt} = \frac{n^2}{N} s \exp\left(-\frac{E}{kT}\right) \tag{2.2}$$

$$I(t) = -\frac{dn}{dt} = s' n^b \exp\left(-\frac{E}{kT}\right) \tag{2.3}$$

where T is the absolute temperature (K) and k is the Boltzmann's constant (K/eV). Equation 2.1 is the Randall-Wilkins [4] equation which is based on the assumption of negligible retrapping during thermal stimulation i.e. **first order kinetics**. The solution of Equation 2.1 is:

$$I(T) = sn_0 \exp(-\frac{E}{kT}) \exp[-(s/\beta) \int_{T_0}^{T} \exp(-\frac{E}{kT'}) dT'] \tag{2.4}$$

where n_0 is the initial concentration of trapped electrons prior to heating, T_0 is the initial temperature, and T' is the dummy integration variable representing temperature.

Equation 2.2 is the Garlick-Gibson [4] equation which is based on the assumption of substantial retrapping during thermal stimulation i.e. **second order kinetics** and has the following solution:

$$I(T) = \frac{n_0 s'' \exp(-\frac{E}{kT})}{[1 + (s''/\beta) \int_{T_0}^{T} \exp(-\frac{E}{kT'} dT']^2} \tag{2.5}$$

where $s'' = s' n_0$, and other parameters as previously defined.

Equation 2.3 is the May-Partridge [4] equation which is based on the assumption of moderate/intermediate retrapping during thermal stimulation i.e. **general order kinetics** and whose solution is:

$$I(T) = s'' n_0 \exp(-\frac{E}{kT})[1 + (b-1)(s''/\beta) \int_{T_0}^{T} \exp(-\frac{E}{kT'})dT']^{-\frac{b}{b-1}} \tag{2.6}$$

where $s'' = s' n_0^{b-1}$ and other parameters as previously defined.

Using numerical approximation methods, Equations 2.4, 2.5 and 2.6 can be expressed in the form of Equations 2.7, 2.8 and 2.9, respectively, as follows [4]:

$$I(T) = I_M \exp[1 + \frac{E}{kT}\frac{T - T_M}{T_M} - \frac{T^2}{T_M^2}(1 - \frac{2kT_M}{E}\exp(\frac{E}{kT}\frac{T - T_M}{T_M}) - \frac{2kT_M}{E}] \tag{2.7}$$

$$I(T) = 4I_M \exp(\frac{E}{kT}\frac{T - T_M}{T_M})[\frac{T^2}{T_M^2}(1 - \frac{2kT}{E})\exp(\frac{E}{kT}\frac{T - T_M}{T_M}) + 1 + \frac{2kT_M}{E}]^{-2} \tag{2.8}$$

$$I(T) = I_M b^{\frac{b}{b-1}} \exp(\frac{E}{kT}\frac{T - T_M}{T_M})[1+(b-1)\frac{2kT_M}{E}+(b-1)(1-\frac{2kT}{E})(\frac{T^2}{T_M^2}\exp(\frac{E}{kT}\frac{T - T_M}{T_M}))]^{-\frac{b}{b-1}} \tag{2.9}$$

where I_M is the maximum intensity of the peak in arbitrary units, T_M is the absolute temperature of the maximum intensity, and the rest of the parameters as previously defined. Both I_M and T_M are obtained from experimental data. Equations 2.7, 2.8 and 2.9 become handy when curve fitting is chosen as a method of peak analysis.

2.2.2 Methods of kinetic analysis

This section provides an account of the techniques that are used in order to establish physical parameters of the traps. We will only concentrate on the methods that have been applied in later sections, namely, Chen's peak shape method and glow-curve computer deconvolution (GCCD). These two methods were preferred because of their appropriateness for our TL data analysis. However, we provide short descriptions of the other popular methods of kinetic analysis.

2.2.2.1 Glow-curve computer deconvolution

Glow-curve computer deconvolution (GCCD) also known as curve fitting is a computerized technique in which a function involving kinetic parameters is defined and

fitted to the experimental TL glow-curve. The curve fitting exercise starts by making intelligent guesses of the number of glow peaks in a given glow curve. The second step is to identify an appropriate mathematical function i.e. Equations 2.7, 2.8 and 2.9, for each of the peaks.

The objective of the curve fitting exercise is to find values of the parameters which give the optimal fit in terms of least-squares criterion [3]. The most common way of minimizing the difference between the experimental and predicted data (i.e. the residuals) is the Marquardt nonlinear least-squares fitting [5] in which a better fit yields high value of regression squared, R^2.

Alternatively, a goodness of fit and hence the reliability of the parameter values can be determined by using the figure of merit (FOM) which is calculated as follows:

$$FOM = \sum_i \frac{100|y_{experimental} - y_{fit}|}{\sum_i y_{fit}} \tag{2.10}$$

where $y_{experimental}$ is the experimental data and y_{fit} represents the values predicted by the fitting function. The smaller the value of FOM, the better the fit.

2.2.2.2 Chen's peak shape method

Chen's peak shape method uses geometrical parameters for the evaluation of the trap depth, E and order of kinetics, b of a TL glow peak. The peak points of interest used in this method include the position of the maximum intensity of the peak, T_M, the low temperature, T_1 and high temperature, T_2 at full width at half maximum (FWHM) of the peak.

Based on Figure 2.2: $\tau = T_M$-T_1, $\sigma = T_2$- T_M, and $\omega = T_2$- T_1.

The geometrical factor μ_g determines the symmetry of the peak and is calculated using the following equation:

$$\mu_g = \frac{\sigma}{\omega} \tag{2.11}$$

For first-order kinetics, $\mu_g \approx 0.42$, whereas for second-order kinetics, $\mu_g \approx 0.52$ [5]. Chen's equation is a general order equation for the calculation of the trap depth and is given by:

$$E_\alpha = c_\alpha(kT_M^2/\alpha) - b_\alpha(2kT_M) \tag{2.12}$$

where α may be σ, τ, or ω. The coefficients c_α are

$$c_\tau = 1.51 + 3(\mu_g - 0.42); \qquad b_\tau = 1.58 + 4.2(\mu_g - 0.42) \tag{2.13}$$

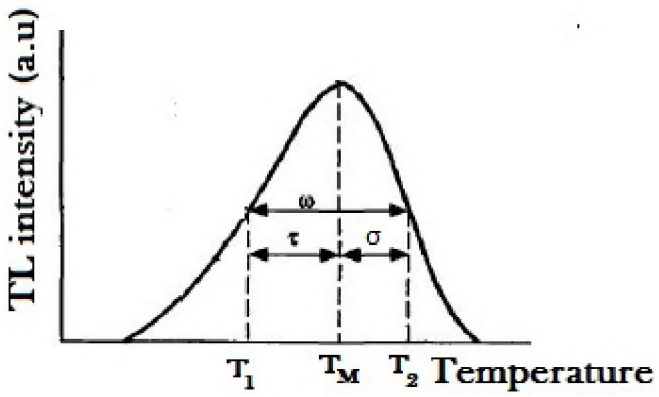

Figure 2.2: Chen's peak shape method: a single TL peak showing T_M, T_1, T_2 at FWHM and the geometrical parameters ω, τ, σ.

$$c_\sigma = 0.976 + 7.3(\mu_g - 0.42); \qquad b_\sigma = 0, \tag{2.14}$$

$$c_\omega = 2.52 + 10.2(\mu_g - 0.42); \qquad b_\omega = 1. \tag{2.15}$$

The expressions for first-order and second-order kinetics can be derived from Equations 2.13, 2.14 and 2.15 above by inserting μ_g=0.42 and μ_g=0.52, respectively.

2.2.3 Other methods of kinetic analysis

2.2.3.1 Initial rise method

Useful in the evaluation of the activation energy of a trap, the initial rise (IR) method applies to any order of kinetics and uses the assumption that the amount of trapped electrons in the low temperature region of the glow peak is approximately constant. Thus, in the low temperature region, the intensity, *I(T)* is proportional to Boltzmann factor i.e. $I(T) \propto \exp(-E/(kT))$. where E is the activation energy and other parameters as previously defined. A plot of $ln(I)$ against $1/kT$ is a straight that yields a slope equal to $-E$ As a rule of thumb, T must fall within 10-15% of maximum intensity, I_M [4].

2.2.3.2 Variable heating rate method

The variable heating rate method, abbreviated as VHR, is one of the methods of analysis based on the changes in position of the maximum intensity of a TL peak. It involves heating a sample at predefined heating rates, β. The values of T_M and I_M obtained at various values of β are thus used for the calculation of E, s and b.

2.2.3.3 Isothermal decay method

The isothermal decay method involves heating a sample to a specific temperature following irradiation and holding the sample at that temperature while recording the luminescence. The emitted light (also called phosphorescence decay), is measured as a function of time. This method makes it possible for evaluation of the decay rate of trapped electrons, E, s and b.

2.2.3.4 $T_m - T_{stop}$ method

The T_m-T_{stop} method, introduced by McKeever [4], involves heating an irradiated sample at a linear rate to a temperature T_{stop} corresponding to a point on the lower temperature interval of a glow peak. The sample is then cooled and TL taken to get all of the glow curve from which temperature of maximum TL intensity is noted [3]. This procedure is repeated at slightly higher values of T_{stop} each time incrementing by 2 to 5°C. A plot of T_m versus T_{stop} may show a stepwise curve with each flat region corresponding to a different activation energy, E [4]. The method allows for the estimation of the number and positions of individual peaks within a composite glow peak.

2.2.3.5 Whole glow peak method

The whole glow peak method also known as the area method is based on the calculation of the integral under a glow peak. The whole glow peak method is normally applied to a peak that is well isolated i.e. one that does not have subsidiary peaks on its rising and falling edges. This method helps in the evaluation of E, s and b.

2.2.3.6 The temperature-dependence of the area under an isothermal decay-curve

Proposed by Chithambo [6], the method is based on the temperature-dependence of the area under an isothermal decay-curve. It is best suited to the calculation of the activation energy of first-order kinetics, the order of kinetics and can be used to study thermal quenching [6].

2.3 Optically stimulated luminescence

Optically stimulated luminescence (OSL) is a stimulated luminescence phenomenon which uses light as a stimulation agent. When light of wavelength λ_{stim} is incident on a previously irradiated insulator or semiconductor material, charges localised in the traps may be released into the delocalized bands i.e. electrons into the conduction band and holes into the valence band. From the delocalised bands, these charges may either get recaptured by the traps i.e. retrapping, or may recombine with holes at recombination sites to produce photons of wavelength λ_{OSL} i.e. radiative recombination, or phonons i.e. non-radiative recombination. The wavelength of the emitted photon, λ_{OSL}, is usually greater than the stimulation wavelength, λ_{stim}. The aforementioned is the statement of Stoke's law and the mechanisms by which this occurs will be made clear in the section of luminescence spectroscopy.

The probability per unit time, p, of the photoionization of the traps and the subsequent release of the trapped charges into the delocalised bands is directly proportional to the stimulation light intensity and the photoionization cross-section. This probability is given by:

$$p = \sigma(\lambda)\phi \tag{2.16}$$

where ϕ (photons.m^{-2} s^{-1}) is the stimulation light intensity or the rate of photon flux and $\sigma(\lambda)$ (m^2) is the photoionization cross-section. $\sigma(\lambda)$ strongly depends on the wavelength of the stimulation light. Photoionization cross-section is an important parameter that governs trap ionization and determines the stability of a trap during optical stimulation [7]. For a given stimulation wavelength, λ_{stim}, a trap with a large photoionization cross-section is quickly emptied i.e. ionized.

The mathematical descriptions of the OSL processes during optical stimulation depend largely on whether the stimulation light intensity is constant, pulsed or ramped. The simple band model shown in Figure 2.1 has been used to describe the OSL processes.

2.3.1 Continuous-wave optically stimulated luminescence

Continuous-wave optically stimulated luminescence (CW-OSL) is a method of measuring OSL in which the intensity (as well as the wavelength of the stimulation light) is kept constant through out the stimulation period while continuously recording the OSL signal. This method makes use of a stimulation filter to separate between the stimulation and an emission signal. A detection filter is placed between the sample and the detector in order to block the scattered stimulation light from reaching the detector. The observed luminescence usually decays in time due to depletion of the trapped charges and their subsequent recombinations at luminescence centres.

Let n (cm^{-3}) be the instantaneous electron concentration in the traps of a particular species of concentration N (cm^{-3}) characterized by photoionization cross-section $\sigma(\lambda)$. In the analysis that follows, we assume that a sample was irradiated to ionizing radiation prior to optical stimulation. In the case of **first-order kinetics** of OSL i.e. negligible retrapping during optical stimulation, all the released electrons recombine with holes at the recombination centre. The intensity of resultant OSL is then given by:

$$I_{OSL}(t) = -\frac{dn}{dt} = np \tag{2.17}$$

whose solution is

$$I_{OSL}(t) = n_0 p \exp(-pt) = I_0 \exp(-\frac{t}{\tau}) \tag{2.18}$$

where $\tau = \mathrm{p}^{-1} = [\sigma(\lambda)\phi]^{-1}$ is the decay time constant in seconds, and $I_0 = n_0 p$ is the initial intensity at t =*0*. Note that an OSL signal is, in this case, a simple exponential decay (Equation 2.18).

For **second-order kinetics** i.e. strong charge retrapping during optical stimulation, the intensity of the OSL signal is given by:

$$I_{OSL}(t) = -\frac{dn}{dt} = \frac{n^2 p}{N} \tag{2.19}$$

whose solution is

$$I_{OSL}(t) = \frac{n_0^2 p}{[1 + \frac{n_0 pt}{N}]^{-2}} \tag{2.20}$$

Finally, in the intermediate retrapping case i.e. **general-order kinetics**, the OSL processes are proposed to be governed by the following equation [7]:

$$I_{OSL}(t) = -\frac{dn}{dt} = \frac{n^b p}{N^{b-1}} \tag{2.21}$$

where b is a dimensionless kinetic parameter representing the order of kinetics. The solution to Equation 2.21 which governs the OSL processes of general-order kinetics is:

$$I_{OSL} = \frac{n_0^b p}{N^{(b-1)}}[1 + (b-1)(\frac{n_0}{N})^{(b-1)} pt]^{-\frac{b}{b-1}} \tag{2.22}$$

It can be easily shown that Equation 2.22 reduces to first-order and second-order kinetics for *b=1* and *b=2* respectively.

2.3.2 Linear modulation optically stimulated luminescence

Proposed by Bulur [8], linear modulation optically stimulated luminescence (LM-OSL) involves linear ramping of the intensity of the constant-wavelength stimulating signal while the OSL is being recorded. The LM-OSL signal increases proportionally with the constant increase in the stimulation power until a maximum is achieved after which the signal decreases. When plotted against time, LM-OSL signal is seen as a series of peaks, with each peak corresponding to optical release of charge from different trap types [7]. Traps with a large photoionization cross-section empty quickly and show a peak at earlier times. Thus one can use the technique to separate overlapping OSL components which are assumed to originate from different traps.

The expressions for **first-order** and **general-order kinetics**, respectively, are:

$$I_{OSL}(t) = n_0 \sigma \gamma t \exp\left(-\frac{\sigma \gamma t^2}{2}\right) \tag{2.23}$$

and

$$I_{OSL}(t) = n_0 \sigma \gamma t \left[(b-1)\frac{\sigma \gamma t^2}{2} + 1\right]^{\frac{b}{1-b}} \tag{2.24}$$

where γ is the linear ramping rate of the stimulation light intensity, t is the recording time, $b > 1$ is a positive number and other parameters as previously defined.

Note that LM-OSL has simply being included here for the sake of completeness of OSL techniques and will not be discussed any further.

2.3.3 Time-resolved optically stimulated luminescence

Time-resolved optically stimulated luminescence (TR-OSL) also known as pulsed optical stimulation is a stimulation scheme that uses a short light pulse to stimulate luminescence. The stimulation source sends out pulses of light and the OSL signal is recorded during the pulse as well as after the pulse. A time-resolved OSL spectrum therefore consists of two parts: the luminescence signal during the pulse and the luminescence signal after the pulse [9]. Analysis of the TR-OSL signal provides information regarding the luminescence lifetimes and thus helps to improve our understanding of the dynamics that underlie the emission of the luminescence [10]. TR-OSL also allows for the study of recombination and/or relaxation pathways in the material, and therefore provides important information on the underlying luminescence mechanisms [11].

We now present the mathematical formulation of the kinetics of charges during TR-OSL based on the model proposed by Chithambo [12] for first-order kinetics. Let A be the initial electron concentration in a trap, s, the probability of stimulation per unit time and λ, the probability per unit time that a stimulated electron will produce luminescence. The time-rate of change of the number $N(t)$ of stimulated electrons during stimulation is given by

$$\frac{dN(t)}{dt} = sA - \lambda N(t) \tag{2.25}$$

whose solution is

$$N(t) = \frac{sA}{\lambda}\left[1 - \exp(-\lambda t)\right]. \tag{2.26}$$

If $L(t)$ is the production of luminescence, then

$$\frac{dL(t)}{dt} = \lambda N(t) \tag{2.27}$$

represents the rate of decay of stimulated electrons. Thus, the rate of luminescence emission during stimulation is

$$L_1(t) = I_{ON}(t) = sA\left[1 - \exp(-\lambda t)\right], \tag{2.28}$$

which is a saturating exponential.

The rate of luminescence emission after a stimulation pulse of width t_1 based on Equation 2.27 is therefore

$$L_2(t) = \lambda N(t_1) \exp\left[-\lambda(t - t_1)\right]. \tag{2.29}$$

Substituting for $N(t_1)$ into Equation 2.29 using Equation 2.26, one gets

$$L_2(t) = sA \exp(-\lambda t)\left[\exp(\lambda t_1) - 1\right] \tag{2.30}$$

Equation 2.30 is an exponential decay of luminescence after the end of the stimulation pulse.

In practice, the luminescence spectrum after the pulse can be fitted to an exponential of the form [12]:

$$I_{OFF}(t) = \Sigma_i A_i \exp(-\lambda_i t) + B \tag{2.31}$$

where λ_i is a decay constant for the ith component, A_i, the scaling parameter for the ith component and B is a constant that accounts for the background. The luminescence lifetime, $\tau = 1/\lambda$, represents the time duration between the eviction of a charge from a trap and the emission of luminescence.

The other notable model for TR-OSL is the model proposed by Yukihara and McKeever [9]. Yukihara and McKeever [9] derived the expressions for the OSL intensity when stimulation is on and off by writing the equations for the concentration of luminescence centres in excited state during stimulation. The time-resolved photoluminescence (TR-PL) model proposed by Pagonis [13], is another model that successfully accounts for time-resolved phenomena.

2.4 Phototransferred thermoluminescence

In conventional TL described earlier, a sample is initially irradiated using ionizing irradiation to fill the available traps. During heating at a controlled rate, the filled traps are emptied producing peaks in the recorded TL glow-curve. The smaller the energy depth of the trap being emptied, the lower the position in temperature of its corresponding peak i.e. the energy depth determines the temperature position of a

peak in the TL glow-curve. Traps with relatively lower energy depths are preferably called shallow traps whereas those with relatively higher energy depths ($> 500°C$), deep traps. There are also intermediate traps with moderate energy depths.

Let us consider a situation in which the shallow traps of a previously irradiated sample are emptied due to the heating to some preset temperature that clears the shallow traps but keeps the charge in the deep traps and/or intermediate traps intact. If the sample is now exposed to light of suitable wavelength at a temperature lower than the thermal depths of the shallow traps, OSL will be produced due to recombinations of the charges that get optically released from the deep and intermediate traps. When a TL is measured immediately following the light exposure to the same preset temperature used to clear the shallow traps, the resulting glow-curve may (or may not) reproduce the TL peaks associated with the shallow traps. In the event that the peak(s) associated with the shallow traps is (are) reproduced, we can conclude that during the optical stimulation, charges were transferred to the empty shallow traps from the occupied deep and intermediate traps. As a result, the recorded TL is called the phototransferred thermoluminescence (PTTL). In this case, the shallow traps behave like charge acceptors relative to the deep and intermediate traps i.e donor traps. A noteworthy fact is that any trap may be a donor or acceptor trap depending on whether it is accepting or donating charges. However, in PTTL, the term acceptor traps usually refer to the shallow and/or intermediate traps, whereas donor traps, to the deep traps.

PTTL is used for dose-reassessment in dosimetry and dating [14]. In using the PTTL technique, one avoids thermal quenching effects, interference by thermal radiation at high temperatures and non-radiation induced TL [15]. As Alexander and McKeever [16] put it, understanding the properties of PTTL lead to useful information regarding optical energies likely to be most efficient in transferring charge between centres and help to identify the mechanisms involved in OSL and TL processes. Bulur [17] describes PTTL as one of the sources of information in understanding the luminescence processes in the material of interest. Recently, Chithambo, et al [18] used the PTTL technique as a means to study mechanisms of luminescence in α-Al_2O_3:C.

2.5 Luminescence spectroscopy

Solé, et al [19] define spectroscopy as a branch of physics that deals with the study of the radiation absorbed, reflected, emitted, or scattered by a substance. When electromagnetic radiation interacts with matter, there is absorption, emission, reflection and scattering of radiation. By measuring the properties of these radiations, one can characterize the optical properties of the material under study. A spectrum (plural, spectra) is a plot of the radiation intensity as a function of wavelength (or energy). Therefore, luminescence spectroscopy refers to the analysis and interpretation of the spectra recorded during various luminescence processes. Thus, one talks about TL spectra, OSL spectra, RL spectra, etc. Furthermore, luminescence spectroscopy measures the energy levels of luminescence centres [20].

In luminescence spectroscopy, the focus is placed on the absorption/excitation and emission spectra of the material under study. The emission and excitation spectra refer to the spectral wavelength distribution of the emission and the excitation, respectively. In order to understand the underlying basic theory of luminescence spectroscopy, a configurational coordinate diagram shown in Figure 2.3 is used. All the necessary annotations in Figure 2.3 have been defined in the caption.

When light of suitable wavelength is incident on the luminescence centre, an electron in the ground state and vibrational level $n=0$ absorbs the excitation energy U_a, making a vertical transition A$\longrightarrow$B to a vibrational level $m=2$ in the excited state. Alternatively, a luminescence centre may be excited by capturing an electron that has been released from a trap during optical stimulation, a common process in OSL. The vertical transition is assumed on the basis of the Franck-Condon principle i.e. an approximation than an electronic transition occurs fast enough without changes in the positions of the relatively heavy nuclei of the centre and its environment. The probability of an excited electron to lose energy by generating lattice vibrations i.e. phonons, is $10^{12} - 10^{13}$/s, while the probability for light emission is at most 10^9/s [20]. Consequently, the centre in the excited state relaxes to a new equilibrium position Q_1 and vibrational level $m=0$, releasing phonons in the process. After some finite time, depending on the selection rules governing the electronic transition between the excited and ground states, an electron returns to the ground state via vibrational

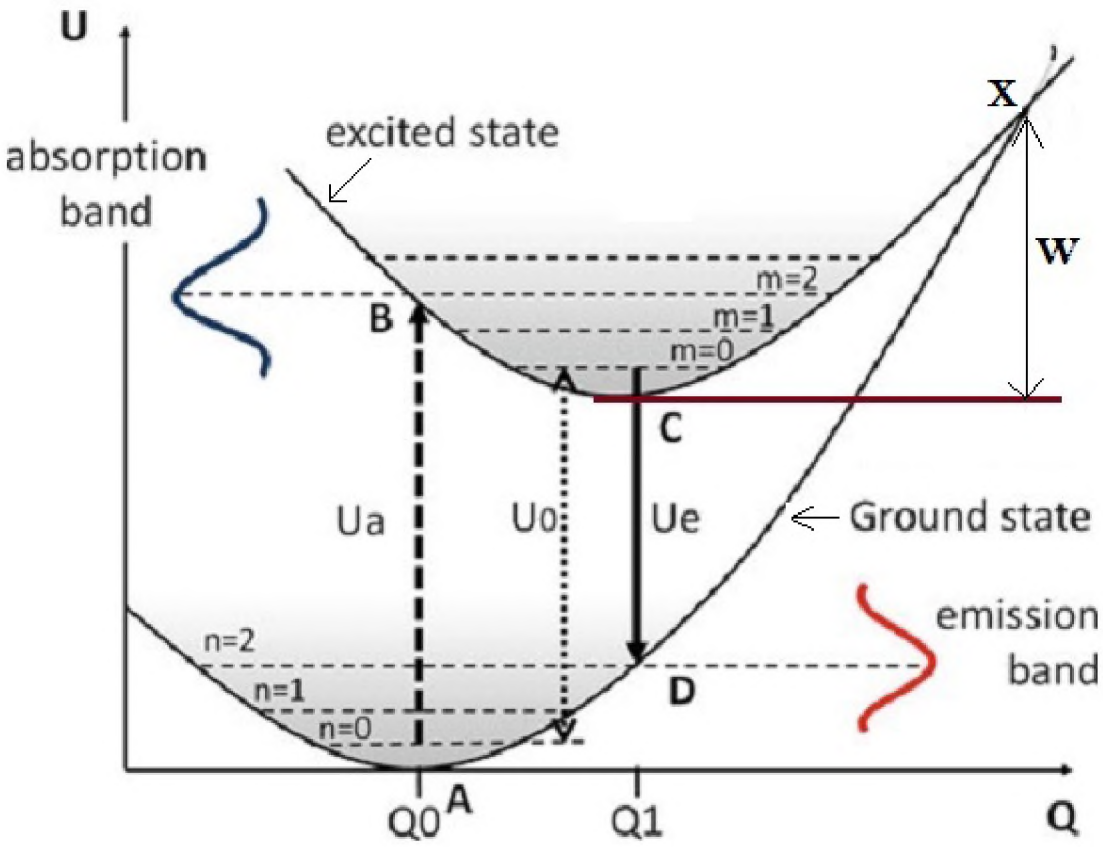

Figure 2.3: 1-D configurational coordinate diagram showing luminescence transitions according to the Franck-Condon principle during optical absorption where U represents the potential energy of the luminescence centre; Q, the configuration coordinate; n_i and m_i, *i=0, 1, 2, 3, ...* represent the vibrational levels in the ground and excited states respectively; Q_0 and Q_1 are the equilibrium positions for the ground and excited states respectively; U_a is the absorbed excitation energy and U_e is the emitted luminescence energy. The diagram has been reproduced (with slight modifications) from Gaft, et al [20].

level *n=2*, emitting luminescence i.e. photons of energy U_e. Finally, the centre relaxes back to the vibrational level *n=0* in the ground state, releasing more phonons in the process. It is obvious that the energy of absorption U_a is higher than that of emission U_e due to phonon-emitting relaxation processes in both the excited and ground states. This is called Stoke's law and the difference, U_a-U_e is the Stoke's shift.

Another important parameter in the optical absorption and emission processes is the Huang-Rhys factor, S which represents a number of emitted phonons accompa-

nying the optical transitions [20]. S is a measure of electron-phonon coupling in the lattice: $S < 1$ represents weak coupling, $1 < S < 5$ represents intermediate coupling and $S > 5$, is the strong coupling case [20].

As further explained by Gaft, et al [20], at a finite temperature, T, an electron state oscillates about the equilibrium position along the potential curve up to thermal energy, kT. It is the amplitude of these oscillations that results into the spectral width i.e. line broadening of the absorption transition.

To obtain an emission spectrum, the wavelength of the excitation wavelength is fixed and the luminescence intensity is monitored over a wide range of emission wavelengths. Similarly, to obtain an absorption/excitation spectrum, the luminescence intensity is monitored at a fixed emission wavelength while varying the excitation wavelengths. Experimentally, the emission and absorption intensities are recorded as a function of wavelength. However, in the configurational coordinate diagram shown in Figure 2.3, the absorption and emission intensities are functions of emission energy and not wavelength. Thus, there is need to convert the wavelength-resolved spectra to energy-resolved spectra for valid analyses of the spectra. The following equations make the conversions possible:

$$E = \frac{hc}{\lambda} \tag{2.32}$$

and

$$I(E)dE = I(\lambda)d\lambda \Longrightarrow I(E) = I(\lambda)|\frac{d\lambda}{dE}| = I(\lambda)\frac{\lambda^2}{hc} \tag{2.33}$$

where E represents the energy, λ, the wavelength, h, the Planck's constant and c, the speed of light in vacuum. Equation 2.32 converts the wavelength scale to energy scale, whereas Equation 2.33 converts the wavelength-resolved intensities to energy-resolved intensities. The modulus symbol in Equation 2.33 ensures that $I(E)$ is a positive quantity.

2.5.1 Thermal quenching

The explanations offered here are based on the configuration coordinate model shown in Figure 2.3. At low temperatures, an excited centre experiences small oscillations about its equilibrium position i.e. $Q_1 - Q_0$ is small. In this case, the excited state does not intersect with the ground state. At high temperatures on the other hand,

$Q_1 - Q_0$ is large and the centre experiences large-amplitude oscillations in the excited state. As a result, the equilibrium position is shifted further away from the ground state equilibrium position. This large shift causes the ground state and the excited to intersect at point X. An electron in an excited state executing oscillatory motion with energy $kT \geq W$ may return to the ground state non-radiatively accompanied by multi-phonon emission. This causes a reduction in the luminescence efficiency hence the luminescence yield of the material at higher temperatures, a phenomenon known as thermal quenching. The temperature dependence of the luminescence efficiency is given by the following relation:

$$\eta(T) = \frac{1}{1 + C \exp\left[-\frac{W}{kT}\right]} \tag{2.34}$$

where $\eta(T)$ is the temperature-dependent luminescence efficiency, W is the activation energy of thermal quenching, C is a constant related to the lattice vibration frequency and other parameters as previously defined. Equation 2.34 quantifies thermal quenching. The temperature T at which a material starts experiencing thermal quenching is called the onset temperature. It has been experimentally observed that the luminescence lifetimes and intensities of most luminescent materials show a similar temperature dependence to the luminescence efficiency.

Chapter 3

Equipment and sample details

This chapter gives a considerable account of the instrumentation and samples used during our investigations The pieces of apparatus used for the present work consisted of the high sensitivity luminescence spectrometer used in spectral studies of the material, a luminescence pulsing system for measuring TR-OSL and a Risø Reader for measuring both thermoluminescence (TL) and optically stimulated luminescence (OSL).

3.1 TR-OSL read-out system

The TR-OSL system used in our study is the LED based pulsing system designed and described by Chithambo and Galloway [21], and later on improved by Chithambo [22]. Figure 3.1 presents the schematic diagram of the pulsing system that was improved by Chithambo [22]. The components of this system are discussed below.

3.1.1 Stimulation unit

The stimulating unit consists of a set of 15 blue LEDs (Nichia NSPB-500) driven by pulses generated from a multivibrator using integrated circuit (IC) 2N74221 at some pulsewidth determined by the RC timing components connected externally to the IC. The Multichannel Scaler (EG and G ORTEC MCS-plus^{TM}) generates the trigger signal for the initiation of the stimulation process. It is also in the Multichannel Scaler (MCS) where the dynamic range and the number of sweeps are both set.

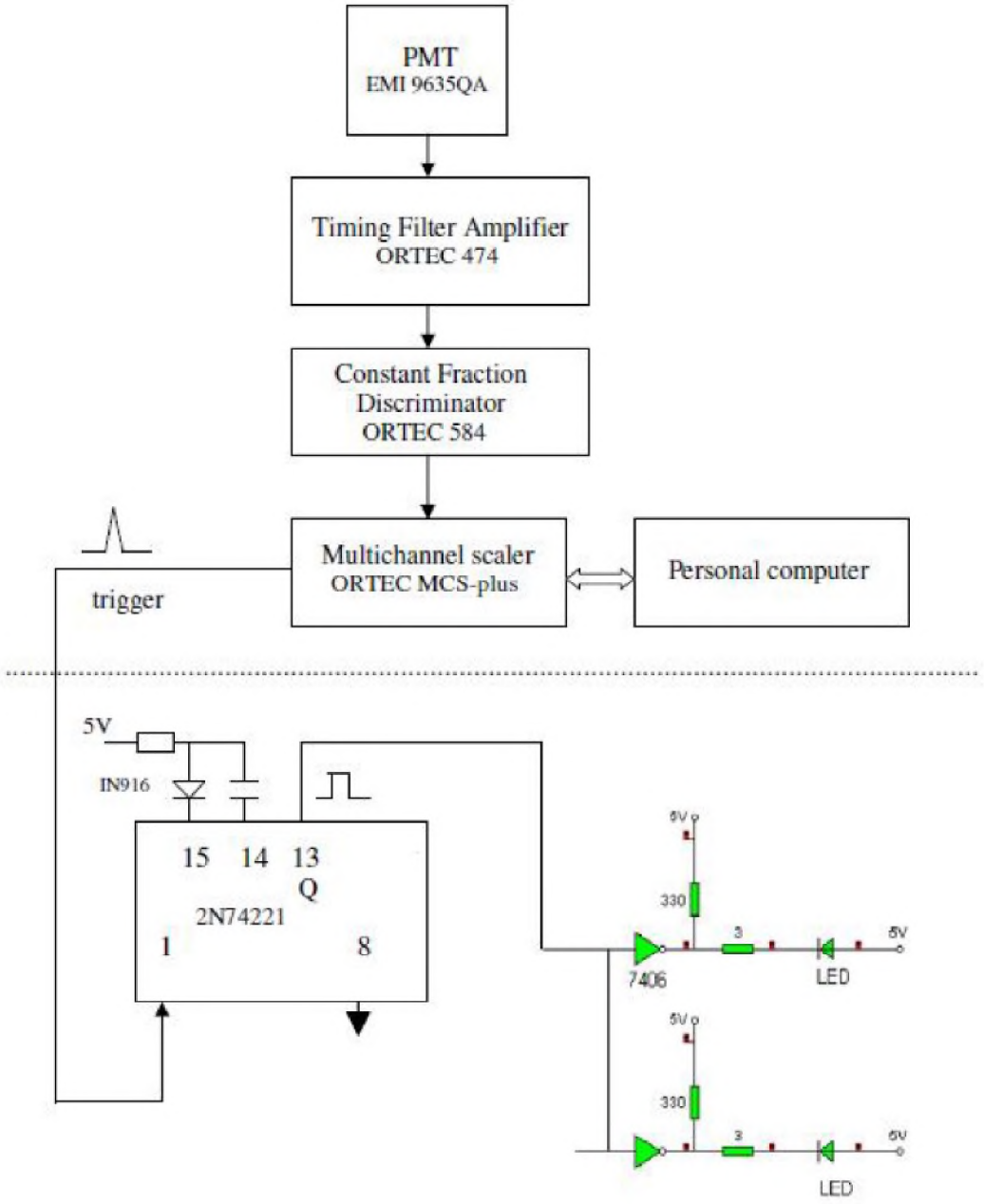

Figure 3.1: A schematic diagram of pulsing system for stimulation, detection and processing of a time-resolved luminescence spectrum. Drawing adapted from Chithambo [22].

3.1.2 Detection unit

The detection of luminescence is done by the photomultiplier tube (EMI 9635QA PMT). The detected luminescence signal is amplified by the timing filter amplifier (Ortec 474) and then counted by the constant fraction discriminator (Ortec 584)

[22]. A combination of Schott GB39 (transmission band 340-620 nm) and UG11 (transmission band 270-380 nm) was used as the detection filter.

3.1.3 Data acquisition and processing unit

The data recording process is initiated by the MCS. Once the scan is started, the MCS begins to acquire photon counts, sequentially recording data in its memory one channel after another, with no dead time between channels. The time-resolved luminescence spectrum is a plot of cumulative photon counts against time for dynamic range selected [22].

3.1.4 Sample stage and temperature control unit

The Annealing Oven Model AO500 (MBE-Komponenten), shown in Figure 3.2, provides both a sample stage, and a temperature control unit that controls sample heating. The oven provides heat treatment from 30°C up to 500°C. Optical access to the sample is provided by an opening on the top of the heater where LEDs are placed. At the centre of the oven (b), there is a dc driven ceramic thin film heater strip with adapted PT100 temperature sensor, an arrangement that ensures rapid heating up of the heater due to minimized thermal inertia, precise temperature control and provides a low thermal load to the sample.

3.2 The Risø TL/OSL-DA-20 Luminescence Reader

The Risø TL/OSL Luminescence Reader Model TL/OSL-DA-20 (Risø, DTU) is a luminescence system that measures both TL and OSL. Its primary components comprise the light detection unit, thermal stimulation unit, optical stimulation unit, and beta irradiation unit. The Reader is capable of holding up to 48 samples at once on its carousel. Samples can be heated for temperature ranges from room temperature up to a maximum of 700°C. Figure 3.3 shows a schematic diagram of the Risø Reader.

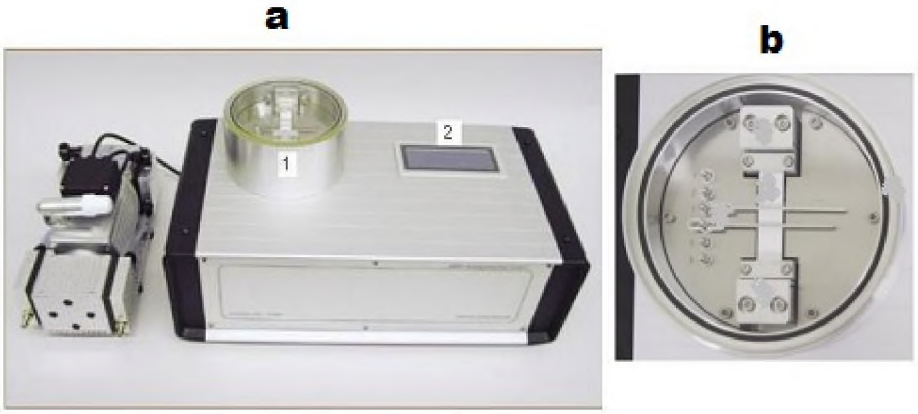

Figure 3.2: A diagram of the Annealing Oven Model AO500 (a) showing the recipient for the sample (1), and the user control panel (2). The top view of the sample stage (b) has been amplified for visual clarity. The diagram has been reproduced from the unpublished MSc thesis [23].

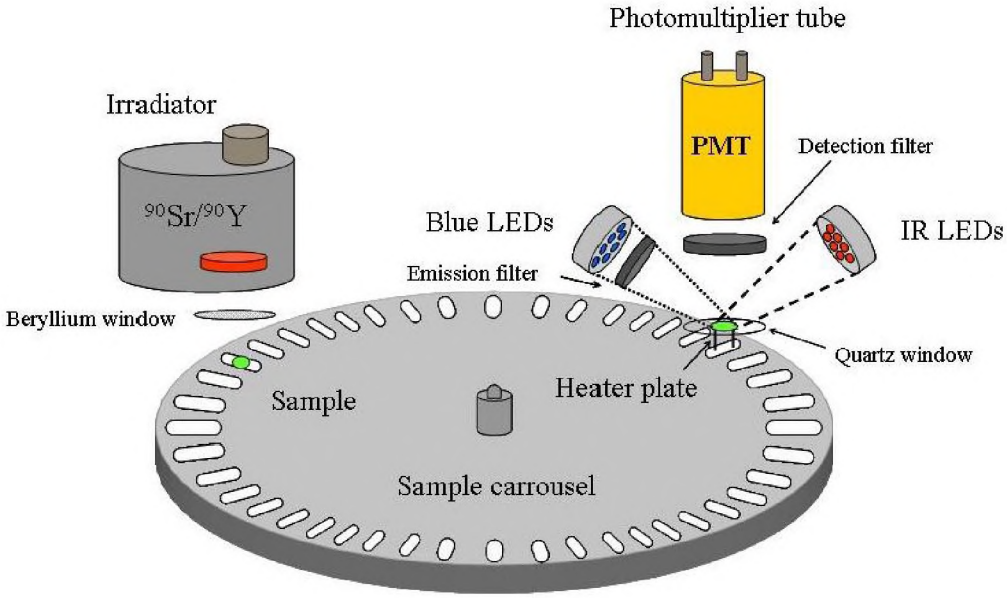

Figure 3.3: A schematic diagram of the TL/OSL Risø Reader showing the irradiation unit ($^{90}Sr/^{90}Y$), the sample carousel, the detection unit (PMT) and the stimulation units (blue LEDs for OSL, heater plate for TL, and IR LEDs for IRSL). Drawing taken from the Risø user manual.

3.2.1 Light detection unit

The light detection unit is comprised of the photomultiplier tube (EMI 9635 QA PMT) and the detection filters. Detection filters discriminate wanted signals against unwanted signals i.e. they prevent stimulation light that has scattered off the sample from reaching the PMT. They also define the spectral window and ensure that spectral stimulation is well separated from the detection window. The detection filter used in this project was a 7.5 mm thick Hoya U-340 (transmission band 250-390 nm).

3.2.2 Thermal Stimulation unit

The thermal stimulation unit is made up of the heating element and the lift mechanism that places the sample into the measurement position. Sample heating is achieved by feeding controlled direct current through the heating element. The heating system is able to heat samples at temperatures ranging from room temperature up to 700°C at various heating rates from 0.01°Cs^{-1} to 10 °Cs^{-1}. Nitrogen flow into the chamber allows for the cooling of the heating element in addition to protecting the heating system from oxidation at higher temperatures. The nitrogen atmosphere minimises the occurrence of spurious signals and ensures uniform heating of the samples.

3.2.3 Irradiation source

TL/OSL Reader uses a beta source for irradiation although alpha and X-irradiation sources are optional. A detachable beta irradiator is located above the sample carousel and accommodates a ^{90}Sr/^{90}Y beta source. Irradiation is software controlled allowing minimum single irradiation times of 1 s. The beta irradiation source used in the study was calibrated and the dose rate at sample position was found to be 0.1 Gy/s.

3.3 High sensitivity luminescence spectrometer

The high sensitivity luminescence spectrometer is a luminescence facility housed in the department of Geology and Environmental Sciences at the University of St Andrews in Scotland, UK. The system is capable of performing X-ray excited radioluminescence (XERL), optical luminescence (XEOL), cathodoluminescence (CL), thermolumines-

cence (TL), photoluminescence (PL) and time-resolved luminescence measurements. Time-resolved measurements can be made to provide estimates of lifetimes down to the μs range. The system described here is an improvement of the high sensitivity thermoluminescence spectrometer originally developed by Luff and Townsend [24].

Figure 3.4 shows the schematic diagram of the high sensitivity luminescence spectrometer [25]. The descriptions of the sytem provided herein have been adapted from the unpublished user manual of the system that was prepared by Dr A. Finch [26] of the department of Geology and Environmental Sciences at the University of St Andrews.

3.3.1 The sample chamber

The sample chamber has two sample stages, namely, the low-temperature or cyrogenic stage and the high-temperature stage. The cyrogenic stage enables measurements from -253°C to room temperature (25°C), whereas the high-temperature stage provides temperature control for measurements made from room temperature to 400°C. The cyrogenic stage is a Cyrophysics M22 Cyrostage, cooled by a CTI Cyrogenics 8200 water-cooled Helium compressor. Temperature is controlled by a Eurother 2404 controller connected to Au-Fe thermocouple and has a maximum rate of 0.1 °C/s. On the other hand, the high-temperature stage consists of a Nichrome strip and a chromel/alumel thermocouple controlled by Eurother 818 P controller and enables measurements up to a maximum heating rate of 3°C/s. Only the high temperature stage was used during our investigations.

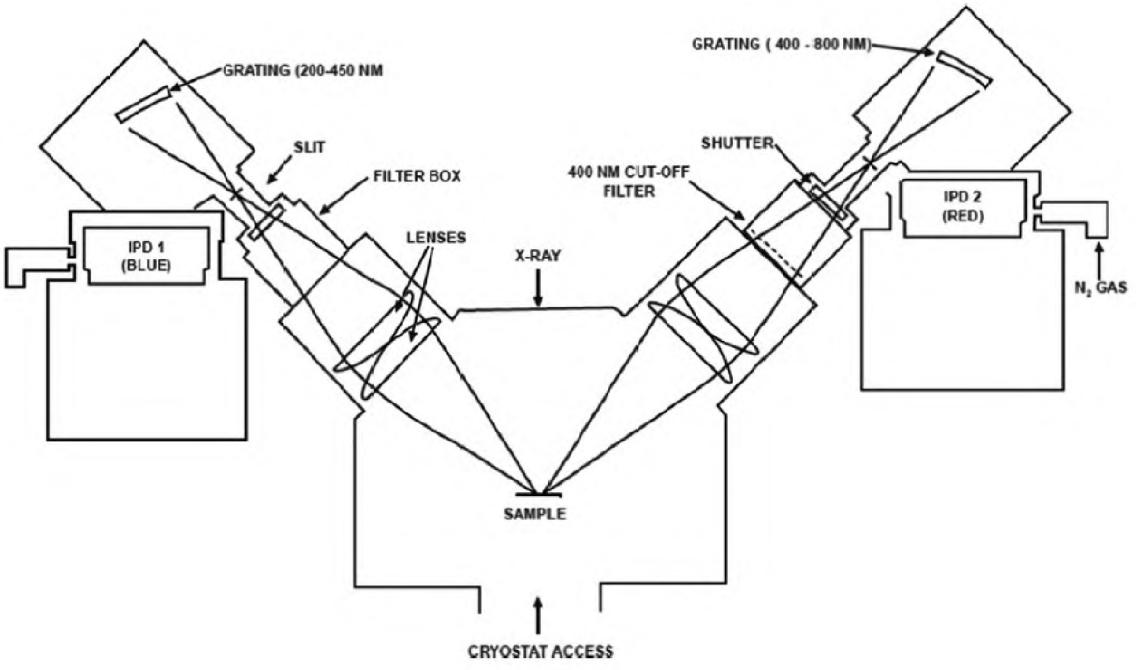

Figure 3.4: A schematic diagram of the high sensitivity luminescence spectrometer reproduced from Chithambo et al [25].

3.3.2 The irradiation unit

The irradiation unit is comprised of a Phillips MCN-101 X-ray tube operating at 20 kV/4 mA providing a nominal dose rate of 1.8 Gy/min and an electron gun operating between 10-25 kV and 200 nA of beam current providing an incident power density of approximately 1 kWm^{-2} at the sample position. X-ray irradiation takes place during radioluminescence measurements, whereas an electron gun is used for cathodoluminescence investigations.

3.3.3 The luminescence detection system

The luminescence detection system consists of a combination of two spectrometers which operate simultaneously. These two spectrometers, named as blue and red detectors, are capable of recording emissions over the wavelength range 230-800 nm i.e. from UV-NIR range. The blue detector covers the UV-Blue (230-530 nm) region, whereas the red detector covers the VIS-NIR (350-800 nm) region. The spectrometers use 0.5 mm entrance slits to provide a 0.5 nm resolution across the whole wavelength

range. Two sets of fused silica plano-convex lenses are used to focus the light from the sample onto the detectors. A Precision Optical Instruments GG400 400 nm longpass filter is permanently installed into the light path of the red detector to eliminate second-order scattering of longer wavelengths into the first-order spectrum. However, this cut-off filter is not opaque between 397-400 nm hence spectra of samples with high sensitivity are likely to show second-order response between 795-800 nm. This experimental artefact remains in processed spectra of samples that are strong in the UV-Blue. The two detectors provide two separate sets of spectral data with a substantial overlap.

Both the blue and red detectors are imaging plate detectors (IPDs). Imaging plate detectors (IPDs) use standard photomultiplier photocathode materials in which case electron multiplication is achieved by microchannel plates as opposed to dynodes. The IPDs were chosen to allow for high sensitivity and sub-μs switching of the power in the detector plate for time-resolved measurements.

The blue detector is a bialkali photocathode IPD whereas the red detector is an S25 based photocathode. Each detector type was chosen to maximise signal and minimise noise in the relevant spectral range. Blackbody radiation in the infrared is seen as a background in all runs using the high-temperature stage above 330°C and becomes progressively intense as temperature rises to the maximum i.e. 400°C.

Where necessary, the neutral density filters (10% transmission) were used in both detectors to attenuate excessive intensities from the samples. Spectral data were corrected for wavelength response of the system.

3.4 Sample details

All samples used in this particular project were Al_2O_3 disks measuring 5 mm in diameter and 1 mm thick, obtained from Rexon TLD Systems (Ohio, USA) characterized by narrow TL peaks. These samples are reportedly grown from a melt at $\sim$ 2050°C in the form of long, single crystal rods which are then cut to 5mm diameter and 1 mm thick single crystal disks [27]. The crystal growth is carried out in a highly reducing atmosphere in the presence of graphite which induces into the samples high concentration of oxygen vacancies i.e. F^+ and F-centres [27]. The end result contains

100-5000 parts per million (ppm) of carbon [27]. The high concentration of oxygen vacancies is responsible for the high sensitivity of the material to ionizing radiation. According to the recent study by Chithambo and Costin [28], the material also contains other impurities, namely, Si (1215), Fe (930), Cu (124), Ni (291), Ca (457), Mn (89), Zn (153), Mg (96) and Cr (452) where the values in the brackets represent impurity concentration in ppm.

Figure 3.5 shows a typical thermoluminescence (TL) glow curve plotted in semi-log scale and normal scale (inset) measured from α-Al_2O_3:C. The glow curve shown in Figure 3.5 was recorded at a heating rate of 1°C/s following beta irradiation to 5.0 Gy. In the normal scale, only the main peak (II) is clearly visible using the 5.0

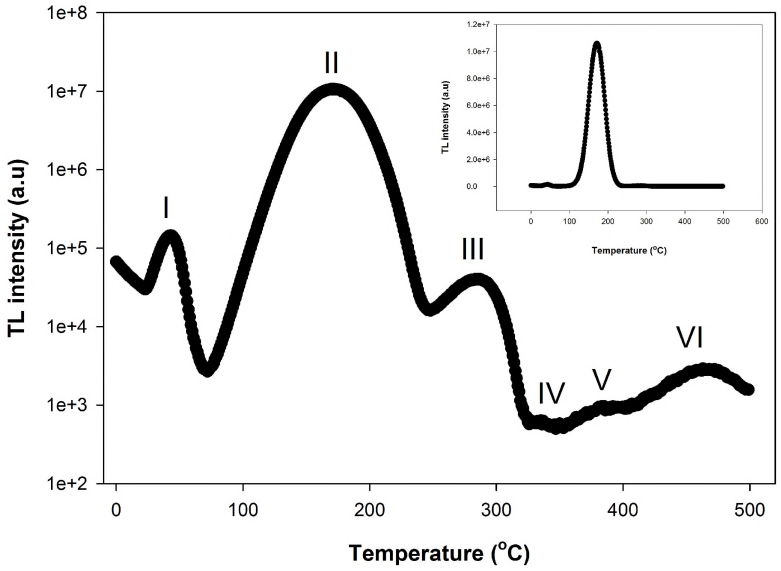

Figure 3.5: A TL glow curve plotted in semi-log scale measured from α-Al_2O_3:C at a heating rate of 1°C/s following beta irradiation to 5.0 Gy. The inset shows the same TL glow curve in normal scale. Peaks I, II, III, IV, V and VI are situated at $\sim$ 43°C, $\sim$ 171°C, $\sim$ 284°C, $\sim$ 335°C, $\sim$ 381°C and $\sim$ 463°, respectively.

Gy beta irradiation dose. The highly intense peak II obscures the presence of the weaker high-temperature peaks. The low temperature peak (I) is centered at $\sim$ 43°C (30-80°C) and has a full-width at half maximum (FWHM) of 19°C. The main peak (II) is situated at $\sim$ 171°C (90-250°C) and has a FWHM of 48°C. Peak III with a FWHM of 45°C is situated at $\sim$ 284°C (250-330°C). Peaks IV, V and VI have poorly

defined FWHM and are situated at $\sim 335°C$, $\sim 381°C$ and $\sim 463°C$ respectively. The traps associated with peak I shall be referred to as shallow traps; those associated with the main peak (II), the main traps and those associated with peaks III, IV, V, VI, the intermediate traps. In the subsequent chapters, we will refer to these TL peaks according to their labels in Figure 3.5.

Chapter 4

Spectral features of α-Al_2O_3:C

In this chapter, we report on the spectral emission features of α-Al_2O_3:C using three (3) different luminescence techniques, namely, X-ray excited radioluminescence (XERL), X-ray excited thermoluminescence (XETL) and time-resolved X-ray excited optical luminescence (TR-XEOL). All the measurements, whose results are presented in this chapter, were carried out using the High Sensitivity Luminescence Spectrometer. The spectral data were corrected for both system wavelength response and blackbody radiation at high temperatures.

The results and discussion on X-ray excited radioluminescence (XERL) are presented first. These will be followed by the results and discussion on X-ray excited time-resolved optical luminescence (TR-XEOL) then X-ray excited thermoluminescence (XETL). At the end of this chapter, a summary of results based on the spectral features of α-Al_2O_3:C is presented. Our analyses, results and discussions primarily focus on the spectral emission and the dependence of these emission features on temperature. Greater effort has been placed on the analysis of the temperature-dependence of the F-centre and Cr^{3+} emissions. Despite the fact these two defect centres i.e. F-centre and Cr^{3+} ions have been widely studied, some of their luminescence behaviour particularly in α-Al_2O_3:C, still remain unaccounted for. The results provided in this chapter provide further insight into the electron/hole recombination processes during different luminescence phenomena in α-Al_2O_3:C.

4.1 X-ray excited radioluminescence

X-ray excited radioluminescence (XERL) is the luminescence that is produced from a sample during X-ray irradiation. Unlike thermoluminescence (TL) or optically stimulated luminescence (OSL) where an external energy source is required to release trapped charges for recombination, radioluminescence involves spontaneous recombinations of holes and electrons at the luminescence centres. Radioluminescence is widely used for real-time optical fibre dosimetry during *in vivo* radiotherapy for which α-Al_2O_3:C is one of its associated dosimeters [29].

In this section, we report the spectral emission features of X-ray excited radioluminescence (XERL) of α-Al_2O_3:C. The temperature dependence of the XERL emission bands, with emphasis on F-centre and Cr^{3+} emission bands, is presented. The response of the F-centres and Cr^{3+} emission to repeated XERL measurements has also been covered. We have also presented the XERL spectra of α-Al_2O_3:C recorded while ramping the temperature of a sample at a constant rate.

4.1.1 Radioluminescence emission spectrum

Figure 4.1 presents an X-ray induced radioluminescence emission spectrum of α-Al_2O_3:C in wavelength scale (a) and energy scale (b). In the insets are corresponding semi-log plots to aid clarity. The XERL measurement was made on a sample that was exposed to X-ray dose at a rate of 1.8 Gy/min at room temperature. The spectrum was measured at an integration time of 30 s at room temperature. Note that the energy spectrum in Figure 4.1b was obtained using Equations 2.32 and 2.33.

The XERL spectra presented in Figures 4.1a and b show seven apparent emission peaks as clarified in the semi-log plots in the insets. Consequently, the XERL emission spectrum was deconvoluted into energy-resolved spectrum using a sum of seven gaussian functions. Table 4.1 lists the central emission energies of the gaussian-resolved peaks. The defect types associated with each emission as identified with reference to literature are included.

The emission bands of F, F^+ and F_2^{2+} are associated with the following recombination processes [30, 31]:

$F^+ + e^- \longrightarrow F^* \longrightarrow F +$ 420-nm luminescence

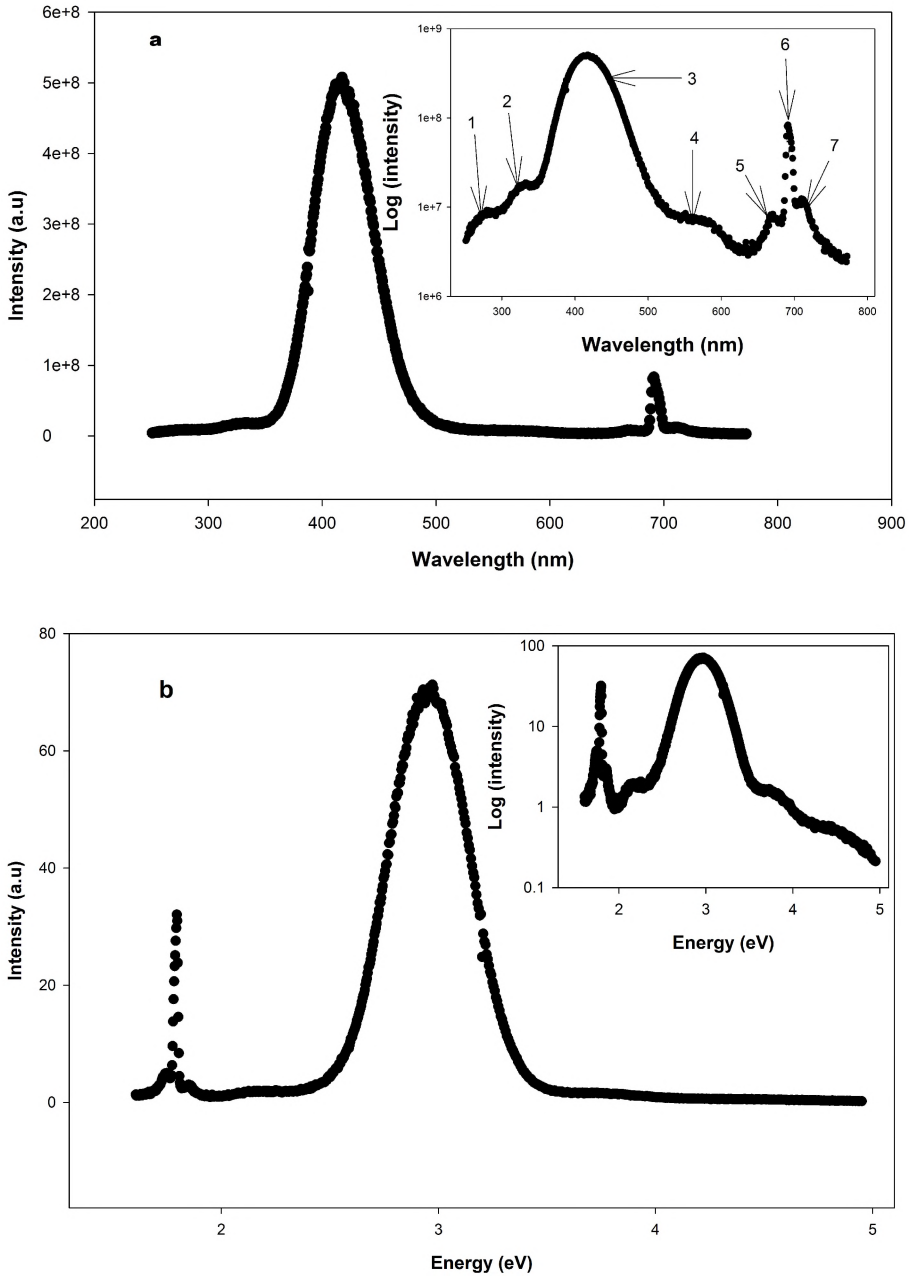

Figure 4.1: X-ray induced radioluminescence spectrum of α-Al_2O_3:C in wavelength scale (a) and energy scale (b) showing one dominant broad emission band peaking at 2.96 eV (420 nm) and a narrow emission band at 1.78 eV (694 nm). The insets are the corresponding semi-log plots showing seven apparent emission peaks centred at 1.75 eV (710 nm), 1.79 eV (694 nm), 1.85 eV (671 nm), 2.22 eV (559 nm), 2.96 eV (420 nm), 3.72 eV (334 nm) and 4.44 eV (280 nm).

Table 4.1: A summary of the apparent emission peaks in the X-ray induced radioluminescence spectrum measured at room temperature.

Peak number	λ_{max} (nm)	E_{max} (eV)	Defect type
1	280	4.44	unknown
2	334	3.72	F^+
3	420	2.96	F
4	559	2.22	F_2^{2+}
5	671	1.85	Cr^{3+}
6	694	1.79	Cr^{3+} (R-line)
7	710	1.75	Cr^{3+}

$F+h \longrightarrow F^{+*} \longrightarrow F^+ +$ 330-nm luminescence

$F_2+2h \longrightarrow F_2^{2+*} \longrightarrow F_2^{2+} +$ 550-nm luminescence

where e^- represents an electron, h, a hole and an asterisks (*) denotes an excited defect centre. The recombination processes associated with the Cr^{3+} emission will be dealt with in later sections.

Based on the existing literature, the Cr^{3+} impurity ion is associated with the R-line (694 nm), the Stoke's (710 nm) and anti-Stoke's (671 nm) vibronic sidebands superimposed on a broad emission band (660-750 nm). The R-line (694 nm) and the broad band (660-750 nm) are associated with the $^2E \longrightarrow {}^4A_2$ and $^4T_2 \longrightarrow {}^4A_2$ intracenter transitions, respectively [32]. Previous spectral studies of Cr^{3+} in different host lattices (e.g [20, 33, 34, 32]) have shown that the anti-stokes vibronic lines are not visible at cryostat temperatures and that at such low temperatures, the 694-nm emission band shows two R-lines that are 0.15 nm apart due to the splitting of the ^2E energy level in a strong crystal field. These R-lines can only be detected by a high-resolution spectrometer i.e. <0.15 nm resolving power. It is also worth pointing out that in the wavelength space, the Stoke's vibronic sideband is more intense than the anti-Stoke's one (see Figure 4.1). The emission band centred at 4.44 eV (280 nm) has not been reported previously and remains unidentified. In the next section we explore the responses of these emission bands when the XERL spectrum is measured at elevated temperatures.

4.2 Temperature dependence of some XERL emissions

In order to understand the behaviour of the XERL emissions at higher temperatures, the XERL spectrum was studied at various temperatures between 30 and 300°C. The integration time of the XERL spectrum at each temperature was 60 s. Gaussian deconvolution of the energy-resolved RL spectrum was carried out for each temperature to evaluate peak parameters pertaining to a specific emission. The peak parameters of interest were the central emission energy, the FWHM and the maximum intensity. The temperature-dependence was done specifically for F-centre (420 nm) and Cr^{3+} R-line (694 nm) emission.

4.2.1 Temperature dependence of Cr^{3+} R-line emission

The dependence of the Cr^{3+} R-line emission on temperature was analysed between 30-160°C. Beyond 160°C, the Cr^{3+} R-line emission is highly diminished hence not suitable for analysis. Figure 4.2 shows the plots of the temperature dependence of the central emission energy (a), the FWHM (b), the maximum intensity (c) and the bandshape (d) of the Cr^{3+} emission.

It can be seen from Figure 4.2a that the central emission energy is unaffected by the temperature at which XERL is measured, whereas the FWHM (Figure 4.2b) does not show any systematic dependence on measurement temperature. The central emission energy has a constant nominal value of 1.79 eV, whereas the FWHM has a mean value of 0.0449±0.0008 eV. The peak intensity of the Cr^{3+} emission (Figure 4.2c), on the other hand, generally decreases with increasing temperature. The decrease of luminescence intensity with temperature can be attributed to the effects of thermal quenching.

Thermal quenching of Cr^{3+} R-line emission has been previously reported for Al_2O_3:Cr^{3+} [34, 32], $Y_3Al_{5-x}Ga_xO_{12}$:Cr^{3+} [33] and numerous other host lattices in which Cr^{3+} produces luminescence when excited. These researchers attributed the observed luminescence quenching of the R-line emission to the depopulation of the ^2E excited state following thermal promotion of electrons from the ^2E state to an upper

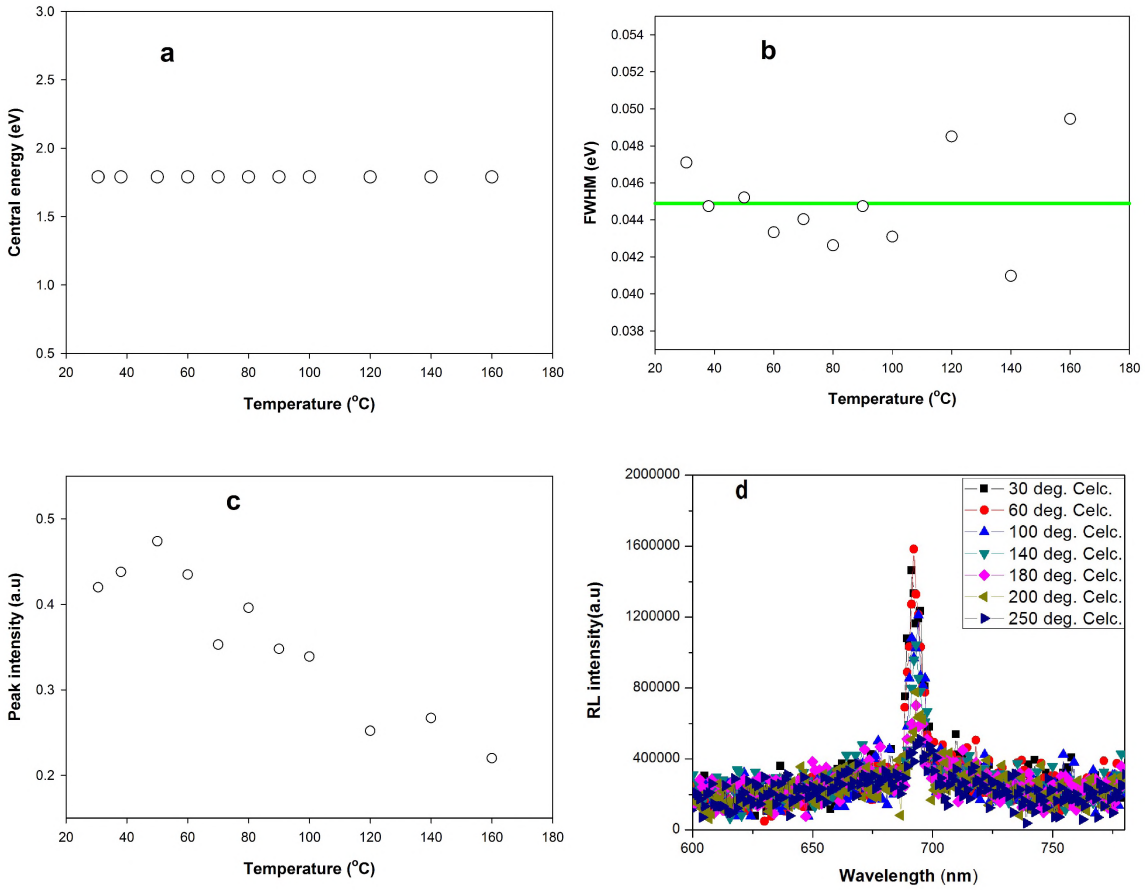

Figure 4.2: Plots of the temperature dependence of Cr^{3+} R-line emisssion: central emission energy vs. temperature (a); the FWHM vs. temperature (b), the peak intensity vs. temperature (c) and the bandshape vs. temperature (d).

excited state, namely, $^4T_2$. This reduces the $^2E \longrightarrow {}^4A_2$ transitions responsible for the R-line emission and at the same time increases the $^4T_2 \longrightarrow {}^4A_2$ transitions responsible for the 660-750 nm broad emission band. As a result, the R-line emission intensity is reduced and the broad emission band is enhanced. However, this seems not to be the case in α-Al_2O_3 host lattice. It is clear from Fig. 4.2d that the reduction in R-line emission is not accompanied by an enhanced broad emission band. This difference (particularly for the Al_2O_3 host lattice) may be attributed to the differences in lattice crystal fields most probably induced by the C-doping.

4.2.2 Temperature dependence of F-centre emission

The temperature dependence of the F-centre emission is presented in Figure 4.3. Figure 4.3a shows the emission energy against temperature; Figure 4.3b, the FWHM

against temperature and Figure 4.3c, the emission intensity against temperature. For purposes of comparison, Figure 4.3c presents plots of normalised intensities in both wavelength and energy spaces i.e. energy-resolved peak intensity (Peak intensity (E)), wavelength-resolved peak intensity (Peak intensity (λ)) and wavelength-resolved integrated intensity (Area (λ)).

Figure 4.3a shows that the central energy of the F-centre emission peak is independent of the temperatures used in this investigation. The solid line in Figure 4.3a represents the mean emission energy i.e. 2.964±0.0002 eV for the F-centre emission band. On the other hand, the FWHM of the F-centre emission peak increases with temperature (see Figure 4.3b).

As shown in Figure 4.3c, the energy-resolved intensity, wavelength-resolved intensity and wavelength-resolved integrated area, all yield similar curves against temperature. The intensity of F-centre emission seems fairly constant between 30-120°C, increases between 140-160°C, then decreases monotonically with temperature. This behaviour, except for the small peak in the curve, is typical of F-centre quenching. The plot of intensity vs. temperature in Figure 4.3c is comparable to the plot reported by Nikiforov et al[35] that shows the experimentally derived quenching curves of RL of F-centres for different temperatures and different states of deep traps. The plot of Nikiforov et al [35] has been reproduced in Figure 4.3d for comparison.

The FWHM data in Figure 4.3b were fitted with the following expression [32] in order to extract some electron-phonon coupling parameters:

$$\Gamma(T) = \sqrt{8 \ln 2}\, \hbar\omega \sqrt{S \coth\left[\frac{\hbar\omega}{2kT}\right]} \tag{4.1}$$

where $\Gamma(T)$ is the temperature-dependent FWHM; S, the Huang-Rhys factor; $\hbar$, the modified Planck's constant; ω, the angular frequency of phonons and other parameters as previously defined. The effective phonon energy, $E_p = \hbar\omega$ is responsible for electron-lattice coupling in the crystal. The result of this fit is shown in Figure 4.4 and yields $S = 5.0 \pm 0.9$ and $E_p = 0.079 \pm 0.008$ eV. Thus, the lattice vibrational frequency associated with the phonons is $(1.91 \pm 0.19) \times 10^{13}$ Hz. The obtained value of $S = 5.0 \pm 0.9$ suggests strong coupling between the F-centre and crystal lattice.

The intensity vs. temperature data in Figure 4.3c were analysed for thermal

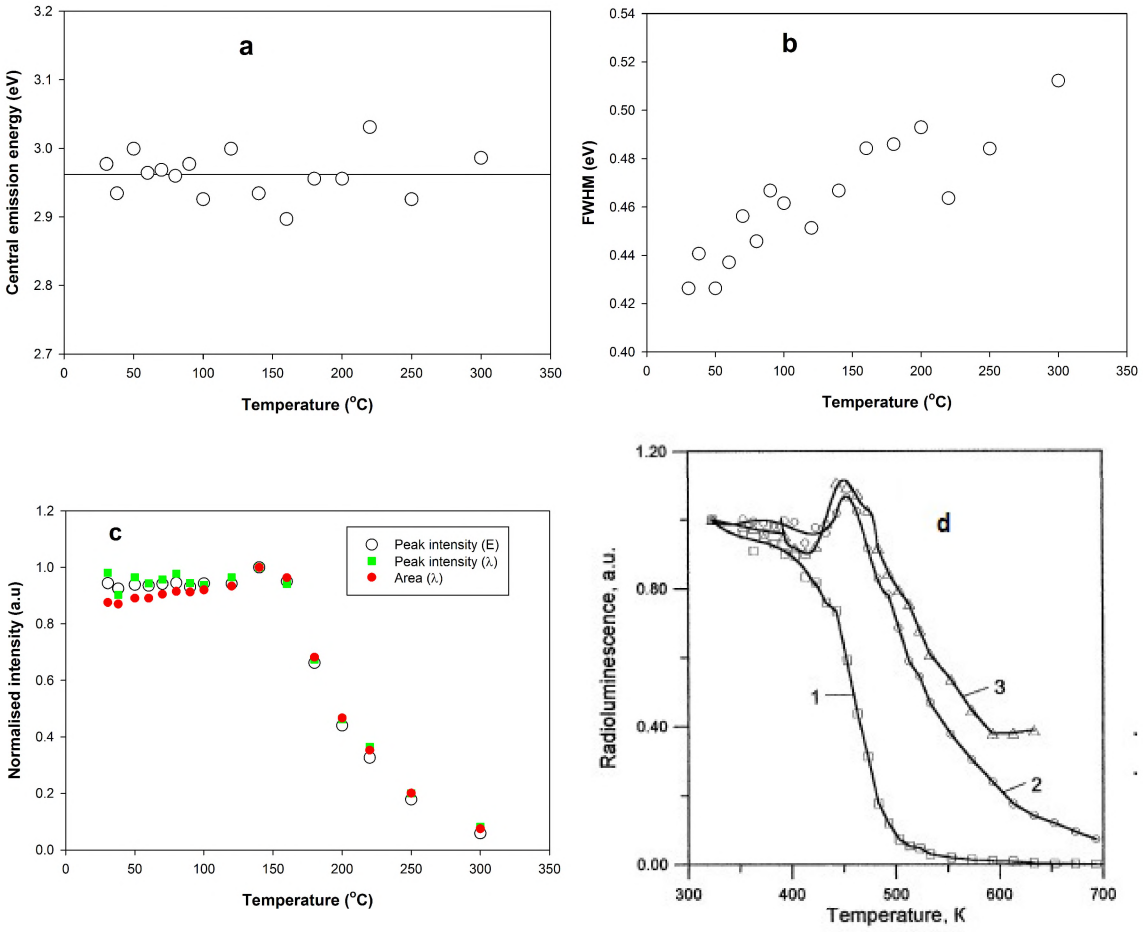

Figure 4.3: Plots of temperature dependence of the F-centre emission: central emission energy against temperature (a); FWHM against temperature (b),and light intensity against temperature (c). The plot of RL intensity vs. temperature (d) is adapted from Nikiforov et al [35] that shows the experimentally derived quenching curves of RL of F-centres for different temperatures and different states of deep traps. The solid line in (a) represents the mean energy value.

quenching parameters using the well-known thermal quenching equation [36] i.e.

$$I(T) = \frac{I_0}{1 + C\exp\left[-\frac{W}{kT}\right]} \tag{4.2}$$

where $I(T)$ is the temperature-dependent luminescence intensity; I_0, the luminescence intensity at absolute zero and other parameters as previously defined. The fit is shown in Figure 4.5 and yields $W = 1.07$ eV and $C = 2.1 \times 10^{11}$. Thus, the lattice vibrational frequency, $\nu = \tau_0 C = 6.0 \times 10^{12}$ Hz where $\tau_0 = 35$ ms is the mean radiative lifetime of F-centres at low temperatures in α-Al_2O_3:C. The calculated activation

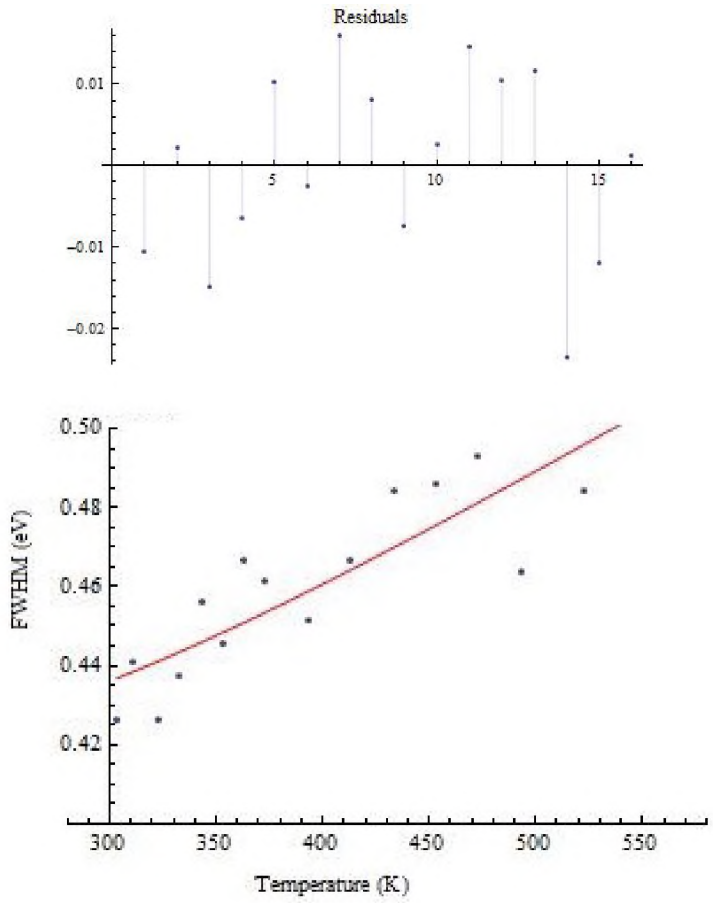

Figure 4.4: A fit of the FWHM vs. temperature data of the F-centre emission using Equation 4.1 and the concomitant residuals. The fit yields $S = 5.0 \pm 0.9$ and $E_p = \hbar\omega = 0.079 \pm 0.008$ eV for Huang-Rhys constant and phonon energy respectively. The associated lattice vibration frequency is 1.91×10^{13} Hz.

energy of thermal quenching is consistent with other published values i.e. 1.085 eV [36], 1.0 eV [13] and 1.045 eV [25]. It is also important to note that the lattice vibrational frequency i.e $\nu = 6.0 \times 10^{12}$ Hz, as calculated from the thermal quenching equation (Equation 4.2) is in close agreement with the lattive vibrational frequency of phonons i.e $\nu = 1.91 \times 10^{13}$ Hz, obtained by fitting the F-centre FWHM temperature-dependence data using Equation 4.1.

To quantify thermal assistance from the RL data, an Arrhenius plot of ln(Intensity) against 1/kT was drawn. The negative slope of a linear region of such plots yield a value that is numerically equal to the activation energy of thermal assistance, E_a. Figure 4.6 shows a plot of ln(Intensity) against 1/kT corresponding to the wavelength-resolved integrated area vs. temperature data of Figure 4.3c. Only the linear region

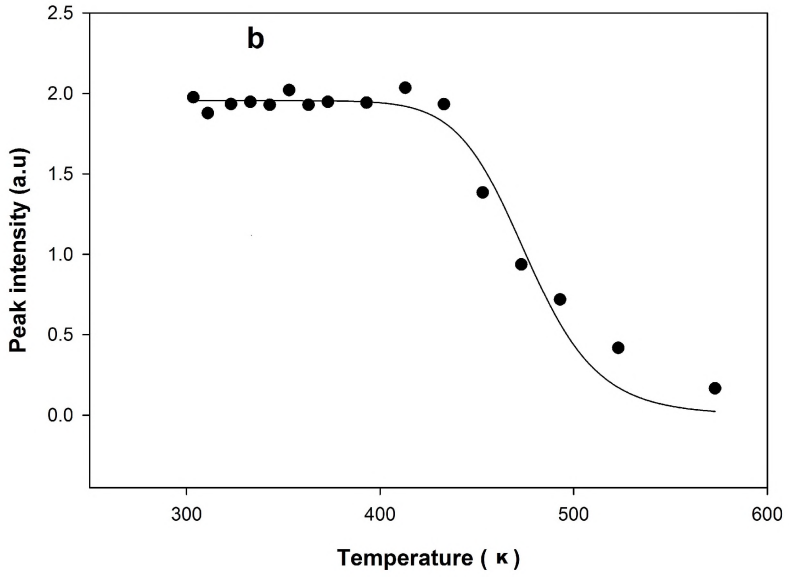

Figure 4.5: Evaluation of thermal quenching parameters using the thermal quenching equation (Equation 4.2). The thermal quenching parameters are $W = 1.07$ eV and $C = 2.1 \times 10^{11}$ obtained at $R^2 = 0.99$.

of Figure 4.6 i.e between 30-120 °C has been captured in the diagram.

The result of the Arrhenius fit gives an activation energy of thermal assistance equal to 0.008 ± 0.001 eV. We postpone the discussion on thermal assistance to Chapter 5 where it has been comprehensively covered.

4.3 Sensitivity changes of XERL emissions with repeated measurements

The aim of this exercise was to investigate any changes in the sensitivity of the F-centre and Cr^{3+} R-line emissions during repeated XERL measurements. For this purpose, a sample was irradiated to X-ray dose at 1.8 Gy/min during RL measurement. These measurements were repeated sequentially for 20 times. Fig. 4.7 shows the plots of peak intensities (normalised to the initial intensity at run 1) for the F-centre and Cr^{3+} R-line emissions (a); Cr^{3+} emission bandshape as measured at different runs (b), emission wavelength vs. number of runs (c) and FWHM against number of runs (d).

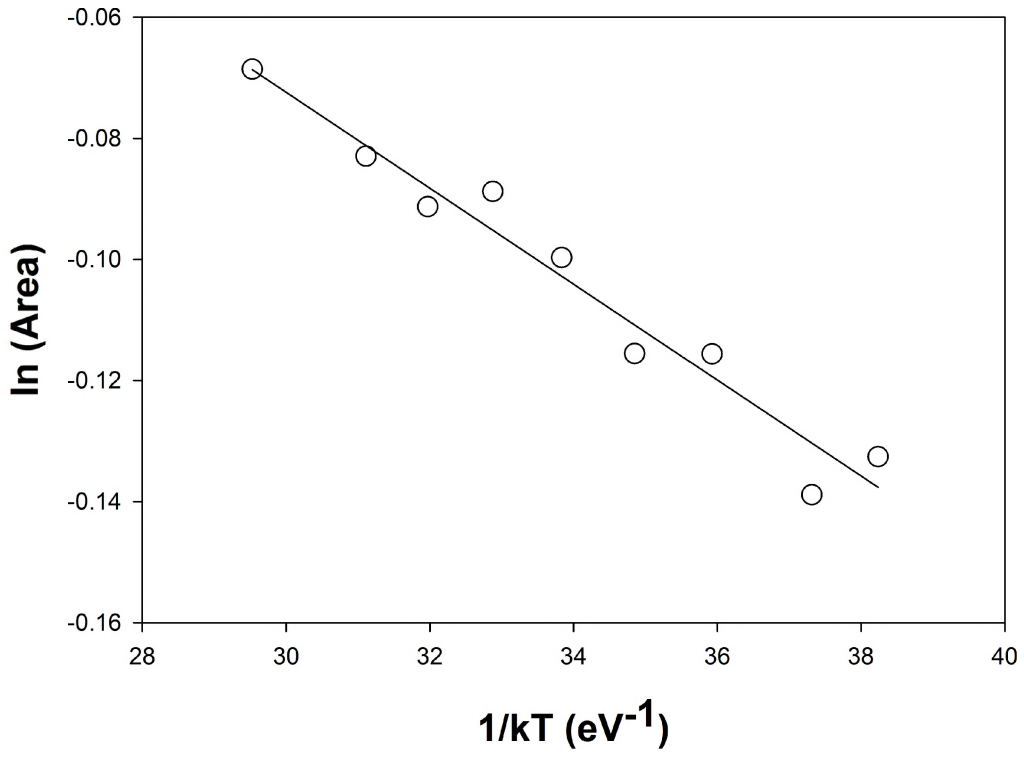

Figure 4.6: An Arrhenius plot of ln(Intensity) against 1/kT to obtain the activation energy of thermal assistance using the wavelength-resolved integrated area vs. temperature data between 30-120 °C. The activation energy obtained from the fit is 0.008 ± 0.001 eV at $R^2 = 0.99$.

It can be seen from Figure 4.7a that the peak intensity of the F-centre emission is almost constant, whereas that of the Cr^{3+} R-line emission generally decreases with repeated measurements. The peak intensity decrease is substantial in the Cr^{3+} R-line i.e. by the 20^{th} run the peak intensity has decreased by about 32% of its initial peak intensity at run 1. It is also important to note that this reduction in intensity observed in the Cr^{3+} R-line emission is not accompanied by any changes in its vibronic sidebands and/or the broad emission band at its base. This can be clearly seen from the emission band plots in Figure 4.6b.

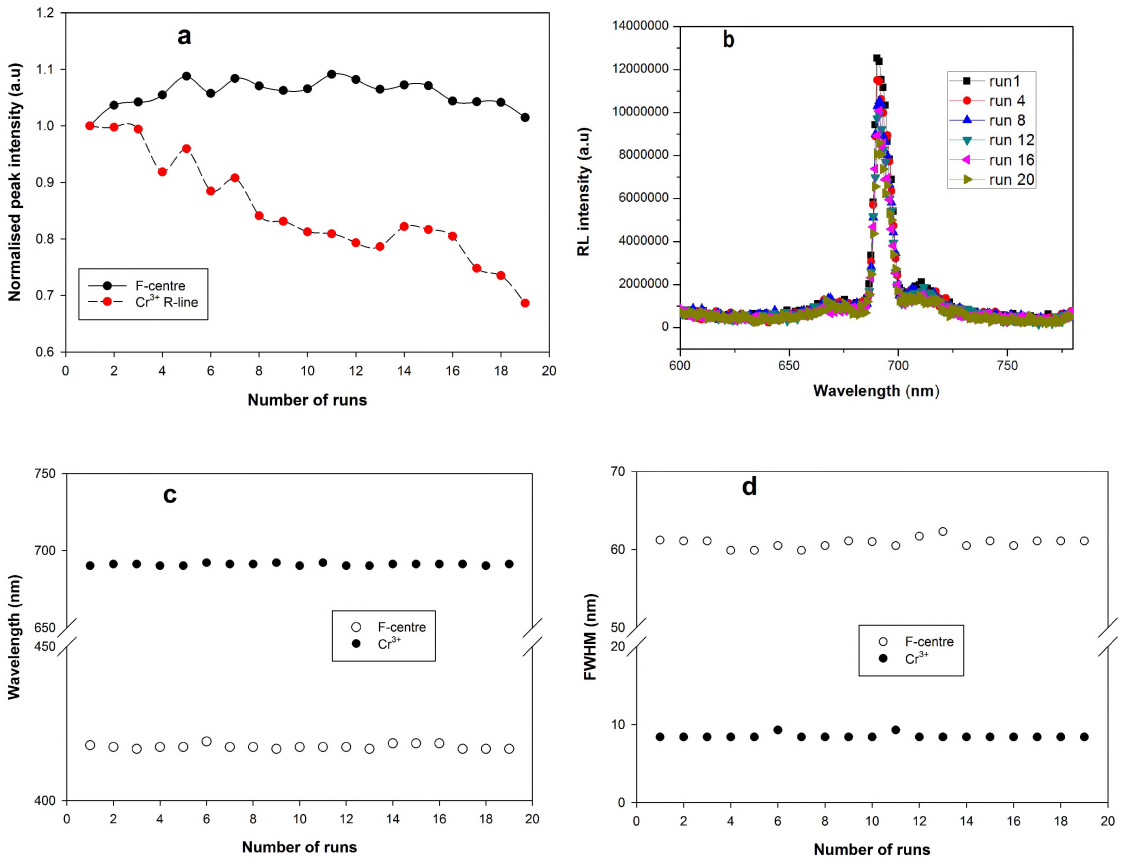

Figure 4.7: Plots of peak intensity (normalised to the initial intensity at run 1) vs. number of runs for the F-centre and Cr^{3+} R-line emissions (a); Cr^{3+} emission bandshape as measured at different runs (b), emission wavelength vs. number of runs (c) and FWHM against number of runs (d). For each run, a sample was irradiated to X-ray dose at the rate of 1.8 Gy/min during RL measurement. The lines through the datapoints in (a) are just for visual clarity.

It is also clear from Figures 4.7c and d that both the emission wavelength and FWHM of both the F-centre and Cr^{3+} R-line emissions did not change with repeated

RL measurements.

4.3.1 The XERL-TL emission spectrum

In this investigation, luminescence was recorded whilst a sample was simultaneously irradiated to X-rays and heated from room temperature to 400°C at 10°C/min. At this heating rate, it is expected that trapped charge will accumulate with time in the main trap and the higher temperature traps. Thus, the resulting spectrum is a combination of spontaneous emissions i.e. RL and thermally stimulated emissions i.e TL, hence the designation XERL-TL. Fig. 4.8 shows the isometric plot (a) and the corresponding contour plot (b) of the XERL-TL spectrum.

Figure 4.8 shows a main emission band ranging from 300-600 nm centred about 410-420 nm. The XERL-TL main emission increases slowly between 30-140°C; grows rapidly between 140-170°C forming a peak at 165°C; decays rapidly beyond the peak to assume a steady output between 250-350°C and finally decreases to another steady output between 350-400°C. The shape of the XERL-TL signal is similar to that of the intensity vs. temperature shown in Figures 4.3c and d. This similarity in shape indicates that the RL recorded at various temperatures has a phosphorescence (TL) component. The peak at 165°C corresponds to the main TL peak obtained from the sample at the heating rate used i.e. 10°C/min. The peak signifies a concentration of localized charge in the main trap. Thus, the peak is a TL feature and not an RL one. Apparently, the XERL-TL main emission band incorporates emissions from F^+ (334 nm), F (420 nm) and F_2^{2+} (559 nm) centres. The contour plot (Figure 4.8b) shows additional minor emissions in the short UV range (260-300 nm) and long wavelength range (690 nm).

4.3.2 The XERL-TL emission spectrum in specific temperature ranges

The XERL-TL emissions were monitored in specific temperature ranges i.e. 20-80, 80-120, 120-140, 140-160, 160-180, 180-200, 200-250 and 250-300°C. These temperature ranges were chosen because they coincide with peak I (30-80°C), peak II (90-250°C) and peak III (250-320°C) usually observed in the TL glow curve of the material (see

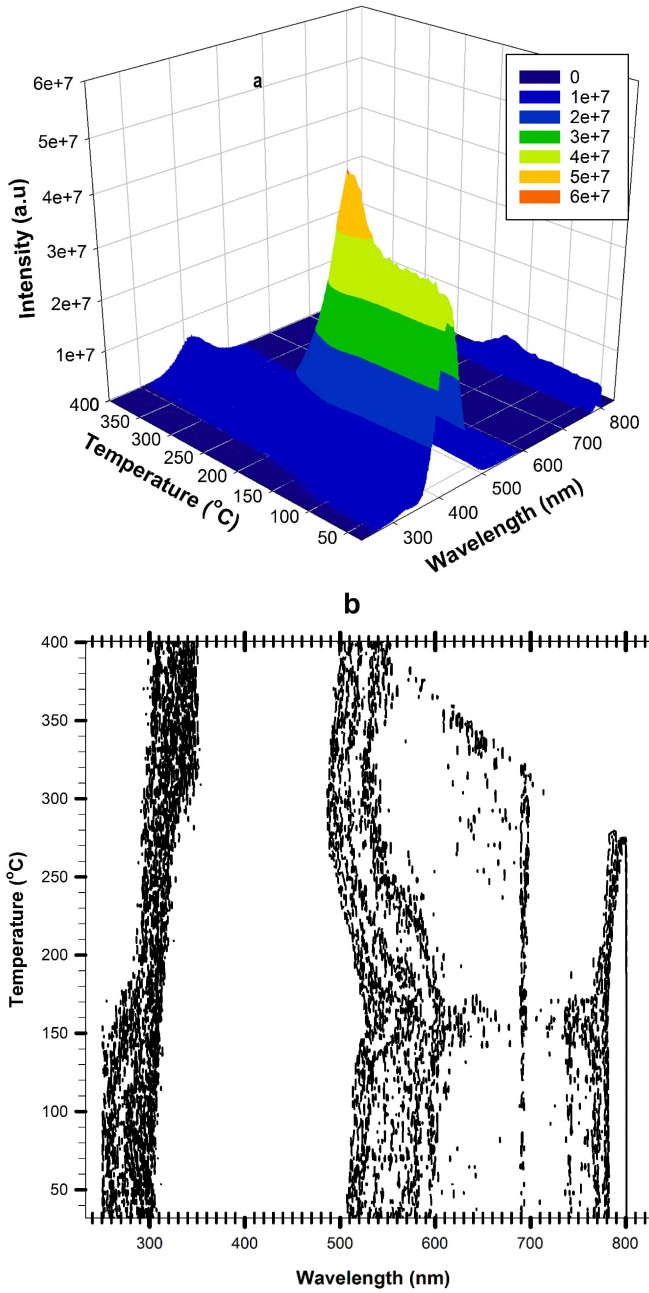

Figure 4.8: Isometric plot of XERL-TL emission spectrum (a) and its correspondig contour plot (b) showing a broad emission band (300-600 nm) in the UV-green region, a narrow emission in the red (695 nm) and an emission band in the short UV range.The peak is located at 418 nm and 165°. A heating rate of 10°C/min was used. The feature above 760 nm is an experimental artefact due to second order diffractions of the main emission band.

Figure 3.5). The aim of this piece of work was to monitor the trapping and recombination processes taking place simultaneously during prompt luminescence (RL) and thermally stimulated luminescence (TL). Figure 4.9 presents semi-log intensity plots of XERL-TL emission spectra obtained in the aforementioned temperature ranges.

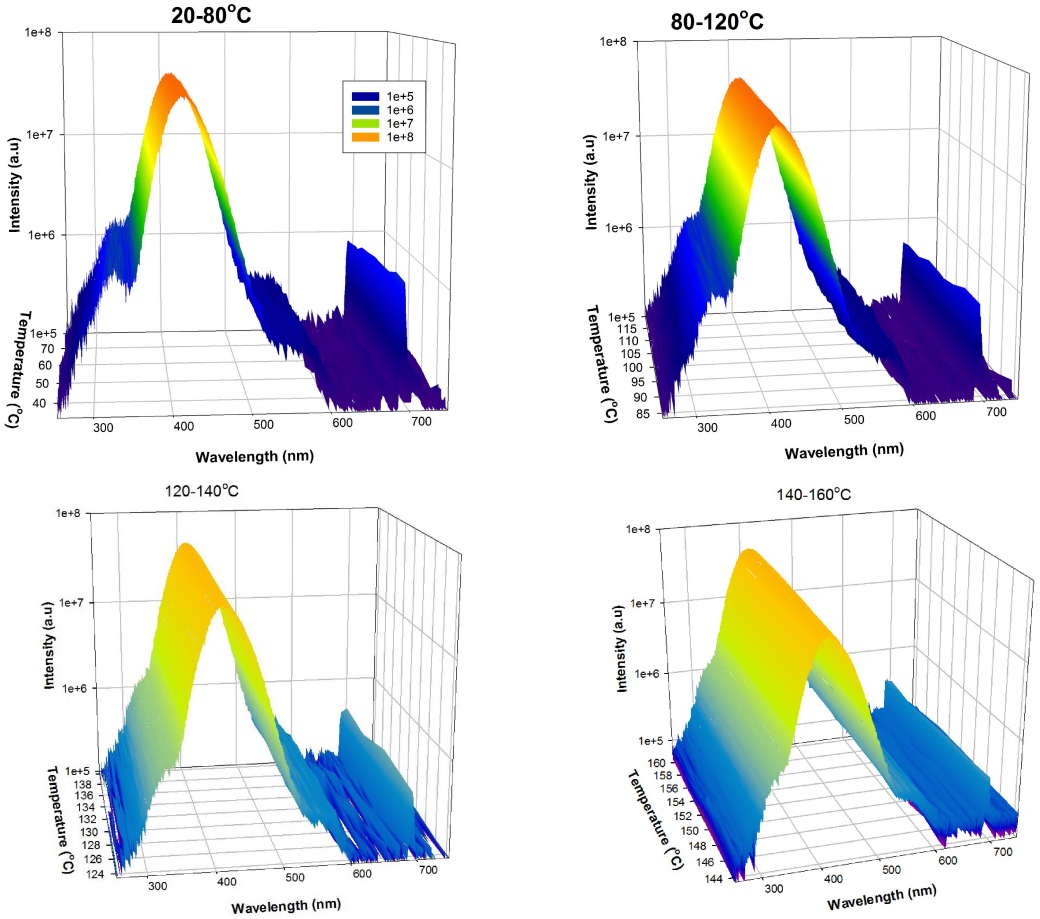

Figure 4.9: Semilogarithmic intensity plots of XERL-TL emission spectra recorded in various temperature ranges. A heating rate of 10°C/min was used.

As shown in Figure 4.9 and Figure 4.10, in all the temperature regions, the broad emission band of the XERL-TL spectra apparently incorporates emissions from F-centres (dominant), F^{+}-centres, F_2^{2+}, 690-nm R-line and the 260-300 nm emission. It should be noted that the 280-nm and 690-nm emissions get weaker and weaker in successive higher temperature regions i.e. the centres get thermally quenched. There is no visible emission from the 260-300 nm emission band beyond 150°C. In the higher temperature regions i.e. above 200°C, the F_2^{2+} is barely visible and the 660-750 nm broad emission band grows in importance over the R-line emission.

The following important points have been drawn from the results presented in

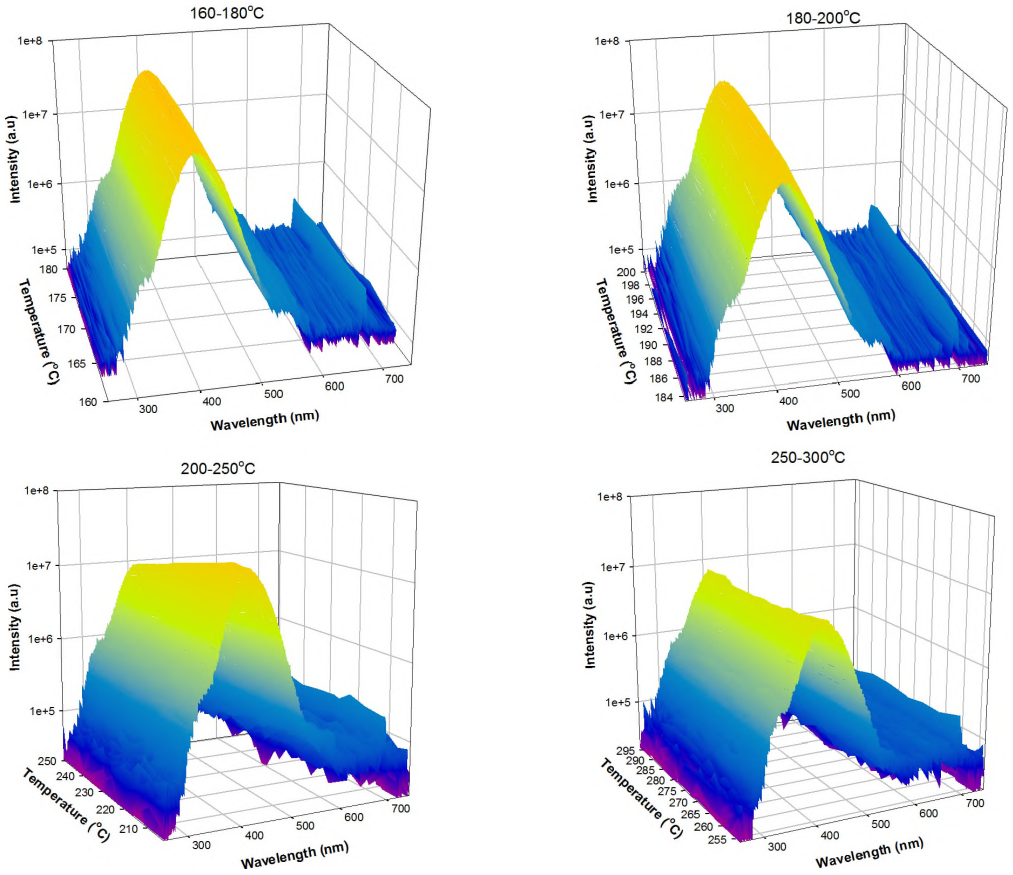

Figure 4.10: Semilogarithmic intensity plots of XERL-TL emission spectra recorded in various temperature ranges. A heating rate of 10°C/min was used.

Figures 4.9 and 4.10:

- at low temperatures (20-160°C), the XERL-TL spectrum is dominated by emissions from F-centres, F^+-centres, F_2^{2+}, 690-nm R-line and the 280-nm centre . However, at higher temperatures i.e. above 160°C , only the F-centres, F^+-centres, F_2^{2+} and the 690-nm emissions persist albeit relatively less intense. The emissions produce constant output (and not peaks) within a given temperature range.

- there is continuous generation of holes and electrons with simultaneous trapping and recombinations throughout the X-ray irradiation and heating period as evidenced from persistent emissions from e.g. both F-centres and F^+-centres. This is typical of radioluminescence.

- the 280-nm emission band is strongly quenched above 150°C.

4.4 The X-ray excited thermoluminescence

The X-ray excited thermoluminescence (XETL) is the thermoluminescence that is measured following exposure of a sample to X-ray irradiation. To obtain an XETL profile, a sample was irradiated to 5.0 Gy. A TL was then measured at a heating rate of 10°C/min to 400°C. Figure 4.11 shows an isometric plot of an XETL emission spectrum (a) and its corresponding contour plot (b) obtained from the sample. Significant blackbody radiation i.e. many orders of magnitude greater that the luminescence signals from a sample is observed at longer wavelengths with increasing temperature. As a result, the system automatically deletes the data where significant blackbody radiation is experienced. This is evident from Figure 4.11b for temperatures above 320°C and going from 800 nm towards 600 nm.

It is clear from Figure 4.11 that the XETL emission spectrum is dominated by the F-centre emission band centred at 417 nm and 170°C i.e. the location of the main TL peak of the material. The emission between 795-800 nm is merely an experimental artefact caused by second-order diffractions corresponding to the main emission. Figure 4.11b also shows a low temperature peak (peak I) between 30-70°C, a high temperature peak (peak III) between 250-320°C and the beginning of a new peak above $\sim$ 380°C. The XETL emission spectra presented in Figure 4.11a is similar to that reported by Chithambo, et al [25] for the same material following a 1.0-Gy X-ray dose.

4.4.1 Thermoluminescence emission spectra in specific temperature ranges

Clearly from Figure 4.11, the thermoluminescence emission features of the secondary peaks of α-Al_2O_3:C are suppressed by the intense 420-nm emission. To appreciate some spectral features from both the main and secondary TL peaks of the material, XETL spectra were recorded in different temperatures ranges using an X-ray irradiation dose of 1.8 Gy and a heating rate of 10°C/min. Particularly those temperature ranges that coincided with the TL peaks of the material were studied. Figures 4.12 and 4.13 show the recorded spectra for the various selected temperature ranges.

The following observations can be made based on the emission spectra presented

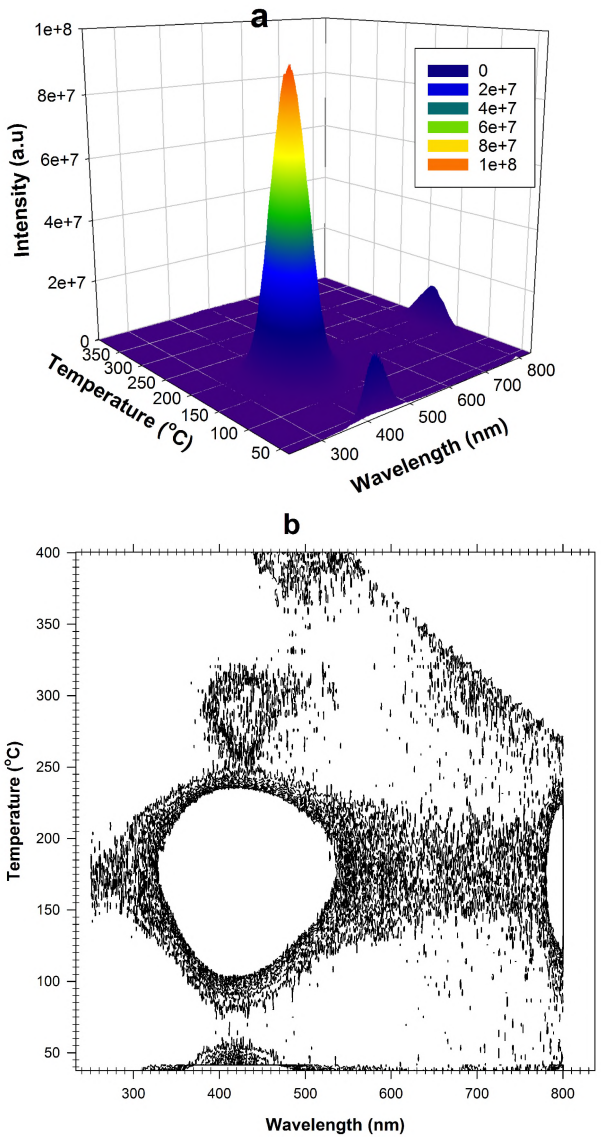

Figure 4.11: An isometric plot of XETL emission spectrum (a) and its corresponding contour plot (b) showing 3 TL peaks i.e. 30-70, 90-250 and 250-320°C (only visible in the contour plot). The main peak is centred at 417 nm and 170°C. The contour plot also shows the beginning of a new peak above $\sim$ 380°C. An XETL was measured at 10°C/min to 400°C following a 5.0-Gy X-ray irradiation dose. The emission between 795-800 nm is merely an experimental artefact caused by second-order diffractions corresponding to the main emission.

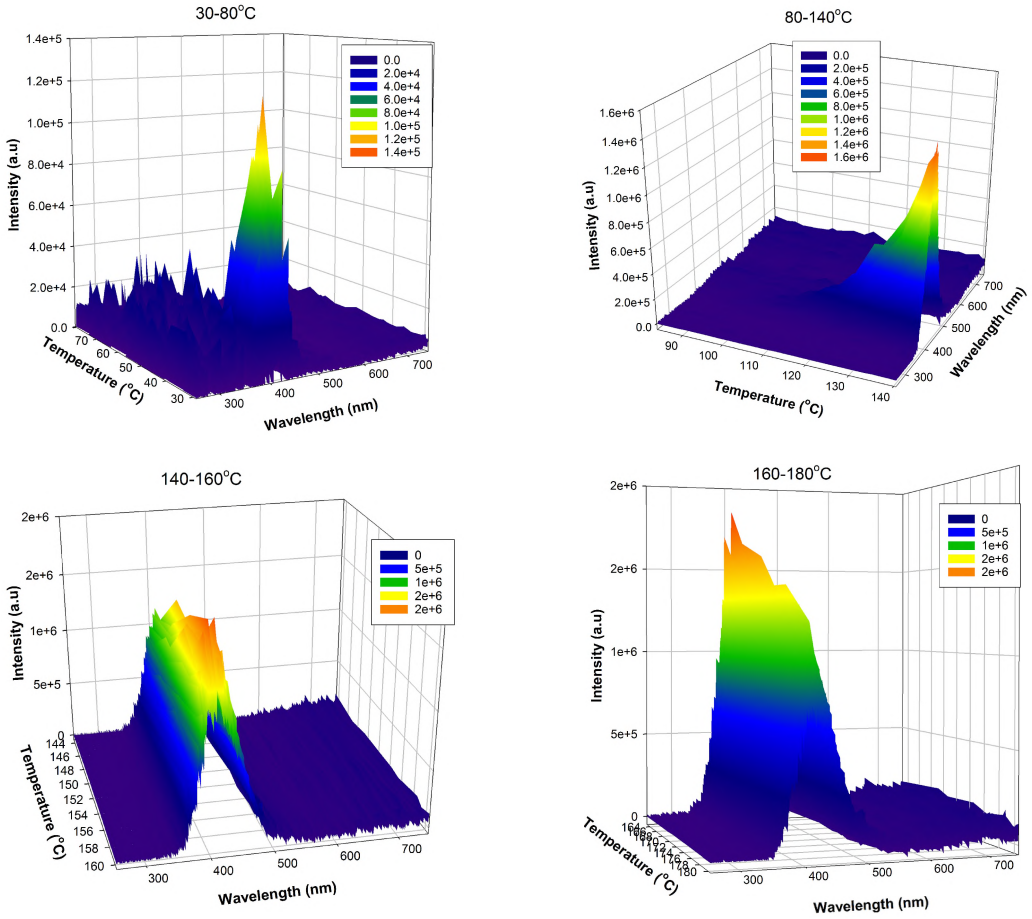

Figure 4.12: Isometric plots of XETL emission spectra recorded in various temperature regions following an X-ray irradiation dose of 1.8 Gy. A heating rate of 10°C/min was used.

in Figures 4.12 and 4.13:

- 30-80°C:

  this region coincides with the low temperature TL peak (peak I) and shows a broad emission from 410-450 nm peaking at 417 nm. There are no apparent emissions in the shorter and longer wavelength regions.

- 80-140°C:

  this region coincides with the low temperature region of the main peak (peak II) and shows a strong broad emission band (350-500 nm at 140°C) peaking at 417 nm. Both the emission band width and the intensity of the peak increase moving from 110-140°C.

- 140-160°C:

  this region coincides with the central region of the main peak (peak II) and

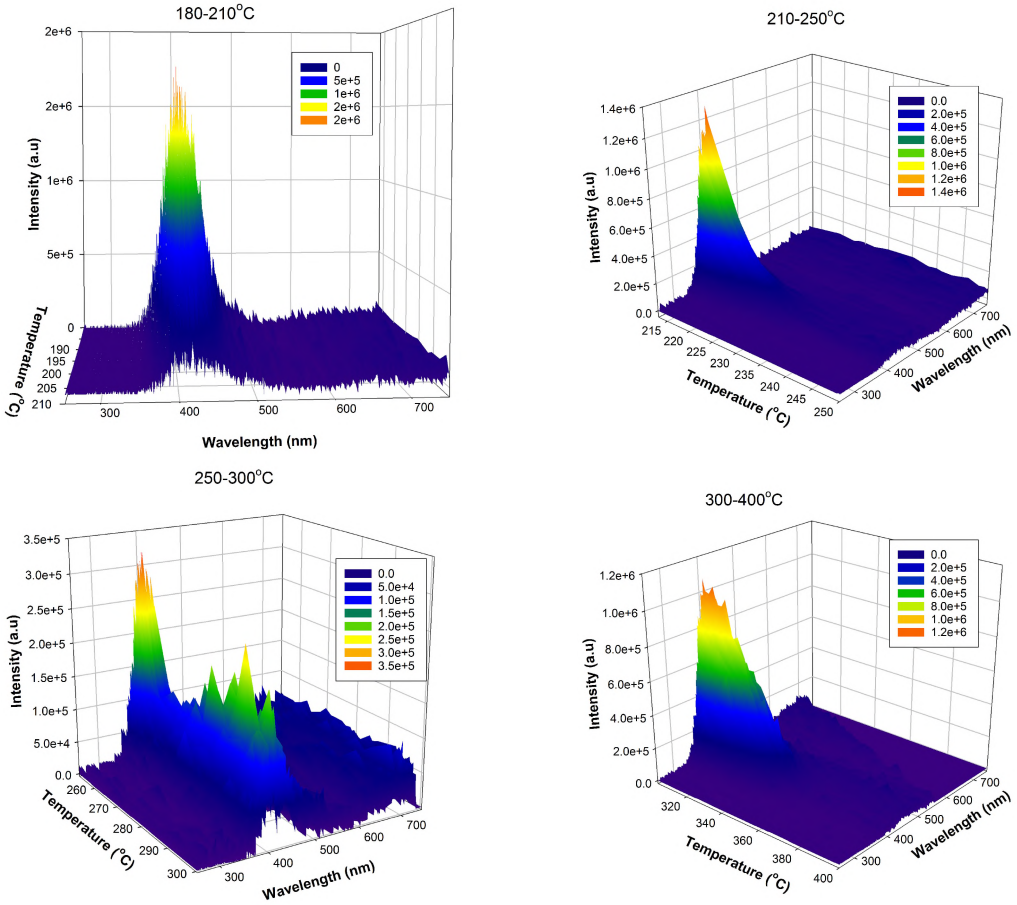

Figure 4.13: Isometric plots of XETL emission spectra recorded in various temperature regions following an X-ray irradiation dose of 1.8 Gy. A heating rate of 10°C/min was used.

shows a strong emission between 350-500 nm peaking at 417 nm.

- 160-180°C:

  this region coincides with the central region of the main peak (peak II) and shows a strong emission between 320-550 nm peaking at 412 nm. There is also a less intense broad emission between 600-750 nm.

- 180-210°C:

  this region coincides with the central part of the main peak (peak II) and shows a strong emission band between 350-550 nm peaking at 412 nm and a less intense broad emission band between 600-750 nm.

- 210-250°C:

  this region coincides with the higher temperature region of the main peak (peak II) and shows a strong emission band between 350-550 nm peaking at 417 nm.

- 250-300°C:

  this region coincides with the temperature region of the high temperature subsidiary peak (peak III) and shows a strong emission band between 350-550 nm peaking at 412 nm. There is also a broad emission band between 600-750 nm.

- 300-400°C:

  there is a relatively intense strong emission band (340-550 nm) between 300-340°C peaking at 411 nm and thereafter, a substantially reduced luminescence in the same emission range. The emission between between 300-340°C represents the high temperature part of the peak III and the beginning of peak IV. The data for longer wavelengths in this temperature range are deleted due to high blackbody radiation as pointed out earlier.

It is abundantly clear from the summary presented above that the F-centre emission band dominates in the TL recorded between room temperature and 400°C at a heating rate of 10°C/min following an X-ray dose of 1.8 Gy. This also means that the traps getting emptied during the TL measurement are (mostly) electron traps i.e. $F^+ + e^- \longrightarrow F^* \longrightarrow F + h\nu_{409-421nm}$. Clearly, hole recombination processes seem to be rare in the 30-400°C heating range for the 1.8 Gy X-ray irradiation dose.

4.4.2 Dose dependence of some TL emission centres

The effect of high dose on emissions of the TL peaks in the temperature regions 30-70 (peak I), 70-250 (peak II), 250-350 (peak III) and 350-400°C, was investigated. Doses used in this investigation were 10, 50 and 100 Gy. For a particular dose, a TL was recorded from 30-400°C at a rate of 10°C/min. Figure 4.14 shows the dose-dependence contour plots (adjusted to the same intensity scale) for X-ray irradiation doses of 10 Gy (a), 50 Gy (b) and 100 Gy (c).

The following observations can be made from dose-dependence XETL spectra presented in Figure 4.14:

- 10 Gy:

  the main peak (II) emits across the whole emission wavelength i.e 250-750 nm with the most intense emission (enclosed whitespace) between 310-600 nm region. The low temperature peak (peak I) shows a broad emission between

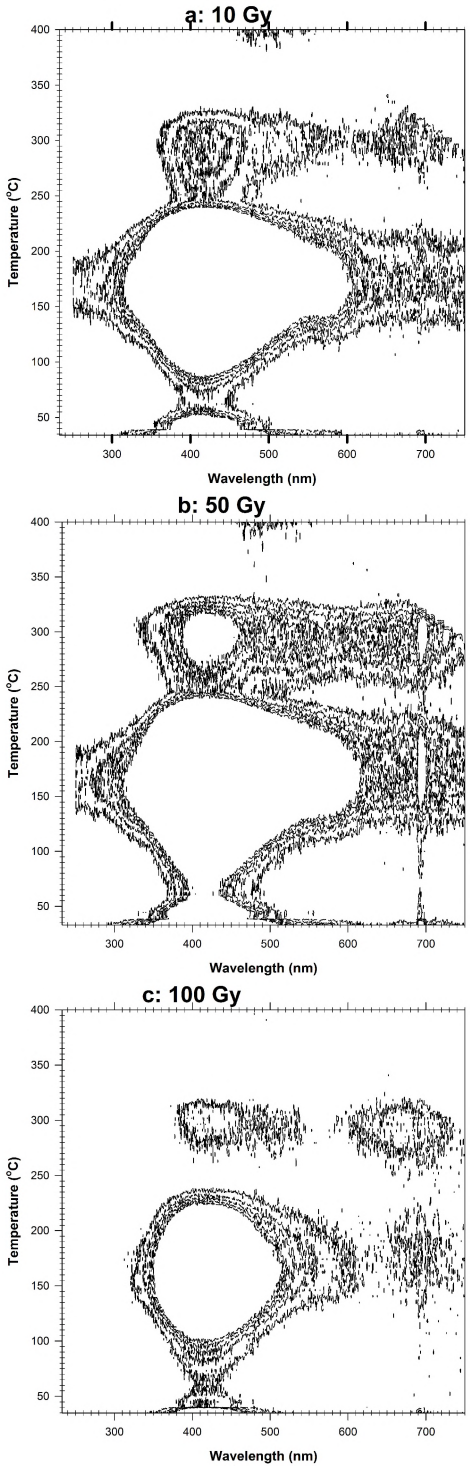

Figure 4.14: Contour plots of X-ray excited thermoluminescence spectra following an X-ray irradiation dose of 10 Gy (a), 50 Gy (b) and 100 Gy (c). The spectra were measured at a heating rate of 10°C/min. The plots have been drawn to the same contour scale in intensity for better comparison.

310-590 nm which gets more intense in the 350-500 nm region. An imperceptible Cr^{3+} emission also accompanies peak I emission. The high temperature subsidiary peak (peak III) emits strongly between 360-600 nm and relatively weak in the 620-750 nm range. The beginning of peak V at ~400°C is visible in the 450-550 nm emission range with apparently no emissions in the F-centre range. There is also considerable overlap in temperature between peak I and the main peak (peak II) whereas the overlap between the main peak and peak III is not apparent.

- 50 Gy:

  all peaks are relatively more intense than those obtained following 10 Gy of X-ray irradiation dose. An intense Cr^{3+} emission band (688-702 nm) is clearly visible alongside the main emission bands from peak I, the main peak (II) and peak III. The main peak emits strongly across the whole wavelength range getting more intense between 310-620 nm. The low temperature peak (peak I) emits between 300-620 nm then 650-750 nm and exhibits most intense emission in the 350-500 nm range. On the other hand, peak III emits strongly between 330-750 nm with the most intense emission in the 385-460 nm range. The small emission at ~400°C associated with peak V persists between 450-550 nm. There is also strong overlap in temperature between the main peak and peaks I and II.

- 100 Gy:

  all emissions are relatively less intense than in the previous two cases i.e. 10 and 50 Gy. There is weak overlap in temperature between peak I and the main peak whereas apparently no overlap is observed between the main peak and peak III. Peak emissions are not continuous across the emission wavelength range as is the case in 10 and 50 Gy. The main peak starts emitting from 330-600 nm then 650-750 nm with the most intense emission in the 350-515 nm range. The low temperature peak (peak I) shows a broad emission band from 350-500 nm. The high temperature peak emits strongly between 380-540 nm then 600-750 nm.

In addition to the observations summarised above, the following can be inferred from the dose-dependence spectra in Figure 4.14:

- There is substantial F^+-centre emission (320-340 nm) in the following temperature ranges: 115-220°C (10 Gy), 110-220 °C (50 Gy) and 135-190°C (100 Gy). These temperature ranges indicate that F^+-centre emission occurs for the most part of the main peak. The XETL spectra measured following 50 Gy shows the most intense F^+-centre emission band whereas the lowest is obtained following 100 Gy X-ray irradiation dose.

- The 550-560 nm emission band attributed to the F_2^{2+}-emission centre mirrors the behaviour of the F^+-centre emission i.e. it most intense where F^+-centre emission is most intense e.g. 50 Gy and least intense where F^+-centre emission is the least e.g. 100 Gy. This is a confirmation that F_2^{2+}-centre emission is due to holes recombining at the neutral F_2 aggregate centres [30].

- The unidentified 280-nm emission band also seems to follow the emission patterns of the F^+-centre with respect to the main peak. This suggests that hole-recombination may be responsible for this emission band. However, this remains inconclusive at this stage.

- For all the X-ray irradiation doses used i.e. 10, 50 and 100 Gy, both peak I and the main peak emit strongly in the F-centre emission band whereas peak III emits strongly in the F-centre emission band for an X-ray irradiation dose of 10 Gy, then in the Cr^{3+} emission band for X-ray irradiation doses of 50 and 100 Gy.

These results on dose-dependence measurements have implications on the well-known hypothesis that the low temperature component of the TL peak in this material is due to electron traps whereas the higher temperature component is due to hole traps [37, 38, 39, 40]. In his recent work in which 2 kGy of X-ray irradiation dose was used, Kortov et al [30] dispelled this hypothesis by showing that it is electron traps that are responsible for both the lower-temperature and high-temperature components of the main peak. Our results for XETL measured in specified temperature ranges for which an X-ray irradiation dose of 1.8 Gy was used do agree with the observation by Kortov et al [30]. However, our dose-dependence investigations reveal that the F^+-centres (and indeed F_2^{2+}-centres) contribute significantly to the main peak emission

especially for an X-ray irradiation dose of 50 Gy. These results show that, regardless of the temperature range of the main peak, both hole and electron traps contribute to the main peak emission band. The F-centre band is dominant at both low doses e.g 1.8 Gy used in our investigations, and at very high doses e.g 2 kGy used by Kortov et al [30]. The F^+-centre emission is too weak at low doses to be noticed, grows in importance with irradiation dose up to some optimal dose e.g. 50 Gy after which it starts deteriorating with dose e.g. 100 Gy such that at very high doses e.g 2 kGy its emission is unnoticeable again.

4.5 Time-resolved X-ray excited optical luminescence

Time-resolved X-ray excited optical luminescence (TR-XEOL) is a technique in which a previously X-ray irradiated material is exposed to a pulsed light source. The luminescence is often recorded after a pulse of light. Analysis of time-resolved spectra provides information on the luminescence lifetimes and allows for the study of recombination pathways during luminescence [10, 11].

Luminescence lifetimes and their temperature-dependence in α-Al_2O_3:C were studied in detail by Chithambo et al [25]. In this section, we report the spectral study of the detrapping and emission/recombination processes in the material underlying optically stimulated luminescence (OSL) measured isothermally in the temperatures between 30-400°C. The results of sample X-ray irradiation at elevated temperatures have also been presented. During our analyses, the data for the blue (250-500 nm) and red (350-750 nm) detectors were treated separately.

4.5.1 The emission spectrum

To obtain a TR-XEOL spectrum, a sample was X-ray irradiated to 1.8 Gy followed by a TR-XEOL measurement at room temperature for an integration time of 1000 s. The optical pulsewidth used was 10 ms. Figure 4.15 shows the energy-resolved spectra recorded using the blue and red detectors. These spectra will hereafter be referred to as Blue spectrum and Red spectrum, respectively. For the sake of visual

clarity, a semi-log plot of the Blue spectrum has been presented in the inset whereas we have zoomed on the low energy (long wavelength) region of the Red spectrum.

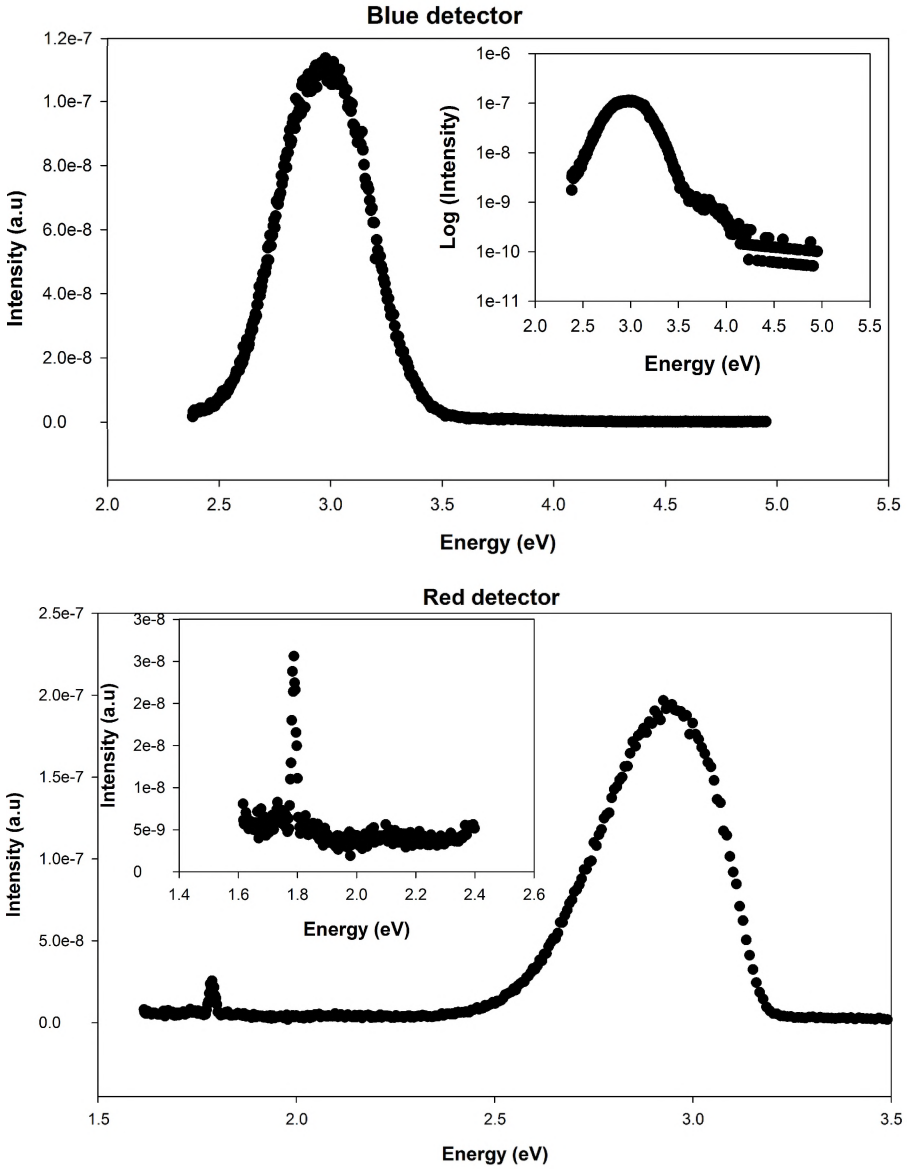

Figure 4.15: Plots of TR-XEOL spectra in energy space from the blue and red detectors obtained from a sample that was irradiated to 1.8 Gy at room temperature. TR-XEOL was measured at room temperature using 470-nm blue LEDs for an integration time of 1000 s. In the insets are the semi-log plot (blue detector) and low energy (long wavelength) plot (red detector) for visual clarity.

The Blue spectrum of Figure 4.15 shows an intense broad emission band (2.5-3.5 eV) centred at $\sim$ 3.0 eV which is attributed to F-centres [25]. In addition to the F-centre emission, the semi-log plot of the Blue spectrum also shows a weak emission centred at 3.72 eV (333.8 nm) that is ascribed to F^+-centre emission [25]. In the Red

spectrum, we see the dominant F-centre emission, a narrow R-line emission (1.79 eV) superimposed on a broad emission between 1.6-2.0 eV and an emission band in the green between 2.0-2.3 eV centred at 2.2 eV. These low-energy emissions are well captured in the inset. The 1.79-eV narrow emission is ascribed to the Cr^{3+} ions [25] whereas the 2.0-2.3 eV broad emission band is associated with F_2^{2+} aggregates [30].

The F-centre emission in the Red spectrum is redundant as it also appears in the Blue spectrum hence will not be included in further analyses of the Red spectra.

4.5.2 Temperature-dependence of time-resolved XEOL

In this investigation, our focus was mostly directed towards the dependence on temperature of the F-centre and Cr^{3+} emissions between 30-300°C with an aim of gaining further insights into luminescence processes taking place at these recombination sites during optical stimulation and for the sake of comparison with the results obtained using XERL.

Before use, a sample was annealed at 900°C for 15 minutes. Three sets of measurements were performed on the same sample. The same measurement temperatures were used in all the three sets. In the first set of measurements, a TR-XEOL spectrum was measured from an annealed and unirradiated sample at temperatures between 30-300°C (without any sample irradiation in between measurements). In the second set of measurements, the sample used in the previous set of measurements was first irradiated to 5.0 Gy of X-ray at room temperature (RT) followed by TR-XEOL spectral measurements at room temperature. This was repeated for measurement temperatures between 30-300°C. In the third set, the sample was irradiated at 400°C (i.e. high-temperature irradiation) then cooled to room temperature where a TR-XEOL spectrum was measured. This measurement was repeated, each time elevating the recording temperature. All the spectra were recorded at an integration time of 500 s. Figure 4.16 shows the spectra for these three sets of measurements for TR-XEOL specifically measured at room temperature (RT). The inset to the Blue spectrum of Figure 4.16 compares the normalized spectra obtained following a 5.0-Gy X-ray irradiation dose at room temperature (RT) against that obtained following 5.0 Gy X-ray irradiation dose at 400°C.

From the Blue spectrum of Figure 4.16, the following can be inferred:

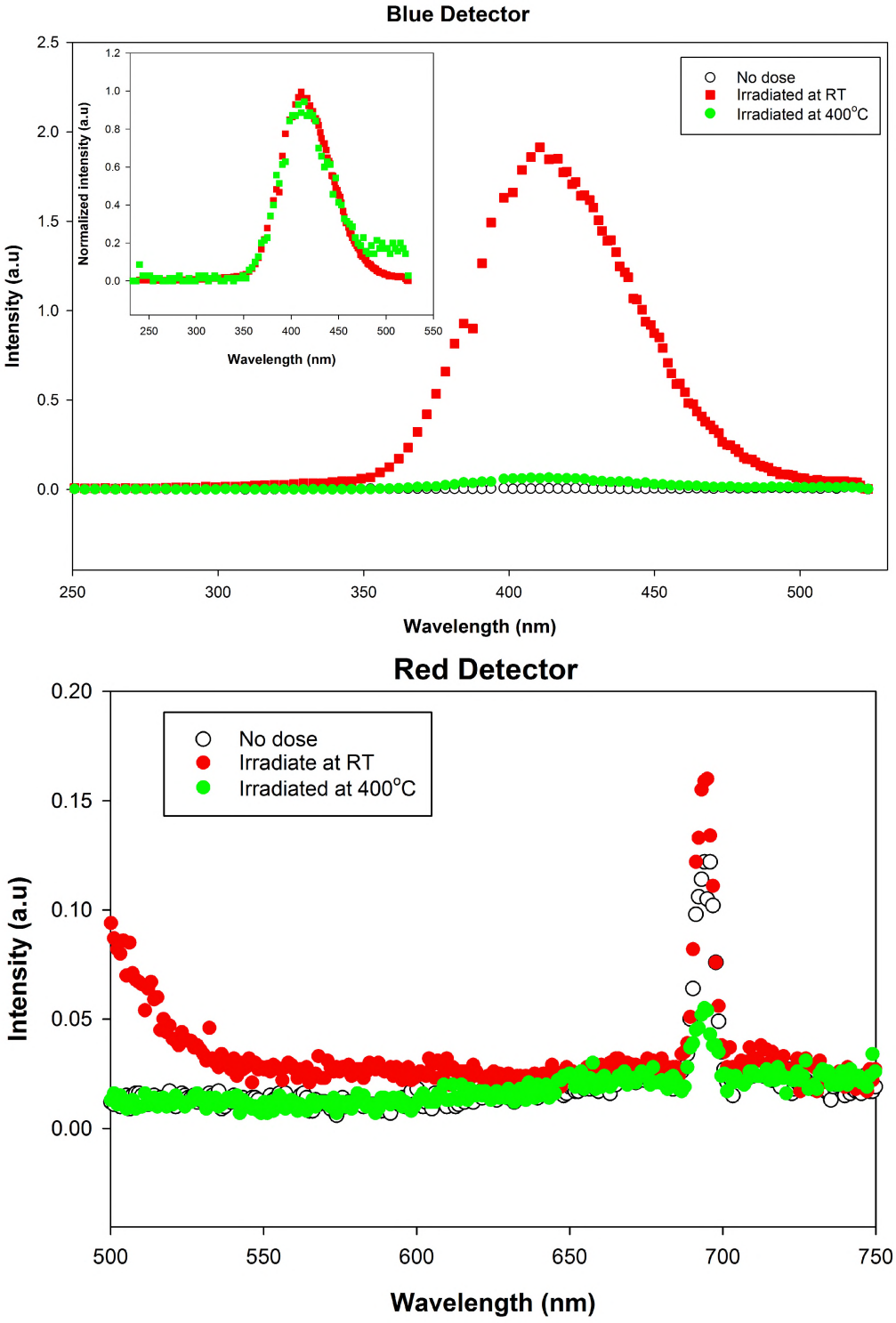

Figure 4.16: Plots of TR-XEOL spectra from the blue and red detectors obtained from a sample that received no dose, 5.0 Gy X-ray irradiation dose at room temperature (RT) and 5.0 Gy X-ray irradiation dose at 400°C. TR-XEOL was measured at room temperature using 470-nm blue LEDs pulsed at 10 ms for an integration time of 500 s. The inset to the Blue spectrum compares the normalised TR-XEOL spectra obtained following a 5.0-Gy X-ray irradiation dose at RT against that obtained following 5.0 Gy X-ray irradiation dose at 400°C.

- only background signal is recorded for the unirradiated sample. This is true for all the temperatures at which TR-XEOL spectrum was recorded for the unirradiated sample.

- an intense broad emission band (350-500 nm) centred about 417 nm is observed following sample X-ray irradiation at room temperature.

- when X-ray irradiation is done at 400°C, a relatively weak broad emission band (350-500 nm) is obtained. This emission band has the same bandshape as the one obtained when X-ray irradiation is done at room temperature. However, the emission band obtained following X-ray irradiation at 400°C decays slowly on the long wavelength region compared to the one obtained following X-ray irradiation at RT. This is evident from the inset.

On the other hand, the following observations can be made from the Red spectrum of Figure 4.16:

- a 694-nm narrow emision line is visible for all the three sets of measurements irrespective of X-ray irradiation dose and irradiation temperature.

- the 695-nm emission line is most intense in the spectrum obtained when the sample is irradiated at RT, whereas the least intense signal of the three sets of measurements is obtained when the sample is irradiated at 400°C. It is important to note the 694-nm emission with no X-ray irradiation dose is more intense than the emission corresponding to X-ray irradiation at 400°C.

- the spectrum recorded at room temperature following X-ray irradiation at room temperature shows a less conspicuous 550-600 nm emission band. This band can hardly be seen in the no-irradiation and 400°C-irradiation cases.

As has been seen from Figure 4.16, the 694-nm Cr^{3+} R-line emission is observed in measurements in which no X-ray irradiation dose was used. What this means therefore is that the blue light ($\lambda_p = 470$ nm) is capable of exciting a Cr^{3+} ion which then relaxes to the ground state radiatively. This kind of emission is technically called photoluminescence (PL) since both excitation and emission occur within the same centre. The excitation of Cr^{3+} in the blue light region has been previously reported by some researchers e.g. Bouman [33] and Singh et al [41].

To get further insight into the dynamics of the observed emissions with temperature, the shapes of the TR-XEOL spectra obtained at different temperatures were compared. Figure 4.17 presents a graphical comparison in terms of the shape of the spectra obtained at different temperatures following room-temperature X-ray irradiation of the sample to 5.0 Gy.

It is clear from the plots in Figure 4.17 that both the shape and intensity of the emission bands are affected by the temperature at which TR-XEOL is measured. The shape of the Blue spectrum is strongly influenced by temperature in the short-wavelength region. There seems to be an increasing contribution from the short-wavelength UV emissions with increasing temperature resulting into a clear distortion of the bandshape in the UV region. From the XERL results, we can identify these short-wavelength emissions as the 280-nm and 330-nm (F^+) emission bands. The greatest distortion in shape in the short-wavelength region is observed at 200°C. Beyond 200°C these UV emissions are reduced in intensity albeit still more intense than at temperatures between 30 to 80°C. It is also worthy to note that these short-wavelength UV emissions show strong temperature dependence i.e. emit strongly, in the temperature ranges of the main peak i.e (120-250°C) and peak III at 300°C. Note that these are the same temperatures regions in which F^+ emission band showed significant growth in strength in the XETL spectra of the main peak as presented in the previous section. This means that both holes and electrons are involved in the OSL processes, with holes recombination processes contributing significantly in the temperature ranges of the TL main peak.

Similarly, the Red spectrum in Figure 4.17 shows strong dependence of its emission bands on temperature. It is obvious from Figure 4.17 that the Cr^{3+} emission is completely quenched at 300°C. One also notices that the Cr^{3+} emission is lifted up in intensity with increasing temperature, with the maximum lifting happening between 140-160°C. It is also interesting to note that the Cr^{3+} emission seems to show signs of recuperation at 250°C. In addition, the F_2^{2+} emission band (550-600 nm) also grows in strength with temperature and shows significant emissions between 140-160°C (just like F^+ and Cr^{3+} emissions). The F_2^{2+} band shows reduced emission at 200°C followed by an apparent recuperation at 250 and 300°C.

Figure 4.18 and Figure 4.19 show the temperature dependence of the parameters

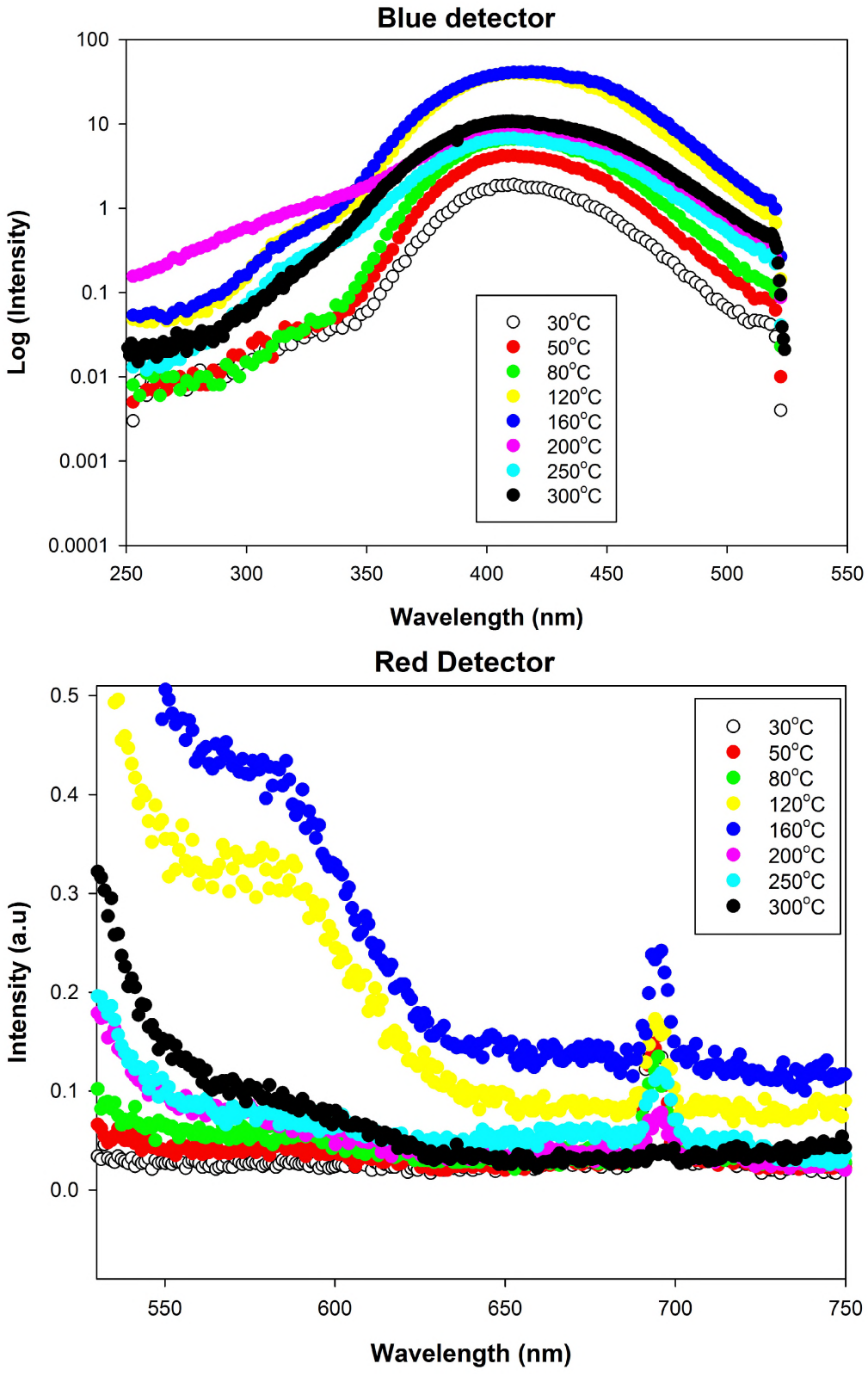

Figure 4.17: Plots of TR-XEOL spectra from the blue and red detectors obtained at various temperatures from a sample that received a 5.0 Gy X-ray irradiation dose at room temperature. TR-XEOL was measured at temperatures between 30-300°C using 470-nm blue LEDs for an integration time of 500 s.

i.e. intensity, FWHM and central emission energy of the Cr^{3+} and F-centre emission bands respectively, based on the three sets of measurements made on the sample.

We can infer the following from Figure 4.18 about the temperature dependence of the Cr^{3+} impurity ions emission:

- the peak intensity, in all the three sets of measurements, generally decrease with temperature, a result also shown by XERL. The intensities are generally highest for TR-OSL measured following X-ray irradiation at room temperature (RT) whereas as the lowest intensities are observed for measurements following X-ray irradiation at 400°C. There is no clear Cr^{3+} emission peak i.e. the emission is fuzzy, above (i) 80°C for the measurements following X-ray irradiation at 400°C, (ii) 200°C for the measurements from non-irradiated samples, and (iii) 250°C for the measurements following X-ray irradiation at room temperature.

- the FWHM of the Cr^{3+} emission band obtained following X-ray irradiation at 400°C are not well defined due to scatter hence were not featured in Figure 4.18b. However, the FWHM of the emission bands obtained following no irradiation and those following irradiation at room temperature are constant up to a measurement temperature of 100°C after which the behaviour becomes erratic. This erratic behaviour can be attributed to reduced intensities of the Cr^{3+} peaks with temperature coupled with increased scatter with temperature of the broad emission band at the base of the Cr^{3+} emission peaks.

- the central emission energy of the Cr^{3+} emission band is independent of temperature in all the three sets of measurements and lies between 1.78-1.79 eV. This is shown in Figure 4.18. This is consistent with the result presented in the section of XERL.

Similarly, the following points can be inferred from Figure 4.19 concerning the dependence of the main emission band (350-500 nm) on temperature:

- for the room-temperature X-ray irradiation measurements (a), the intensity of the main emission band shows a slow increase in peak intensity with temperature up to 100°C. This is followed by a rapid increase in its peak intensity between 100-140°C. Thereafter the intensity decays rapidly with temperature.

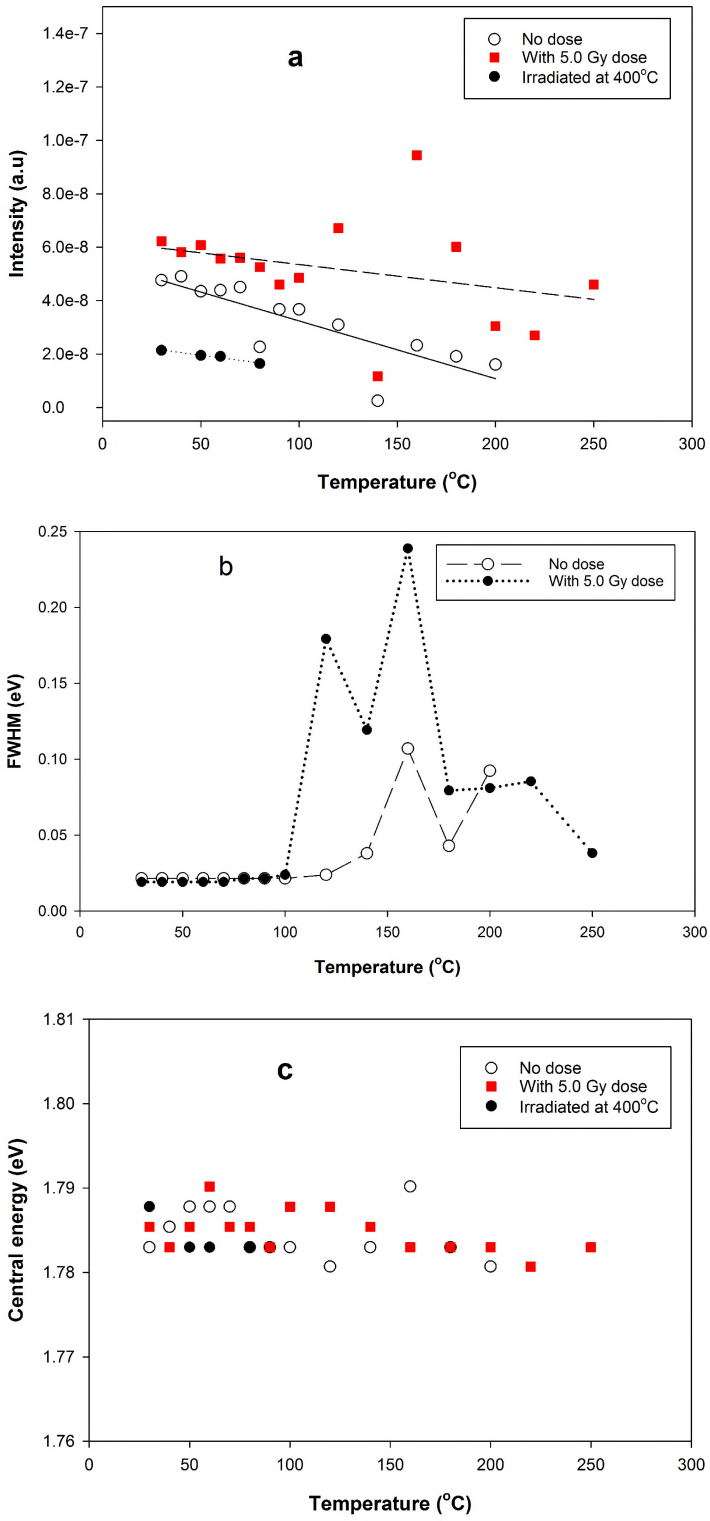

Figure 4.18: Plots of temperature dependence of Cr^{3+} emisssion: Intensity vs. temperature (a); the FWHM vs. temperature (b), and the central energy vs. temperature (c). TR-XEOL spectra were measured at an integration time of 500 s following room-temperature X-ray irradiation to 5.0 Gy.

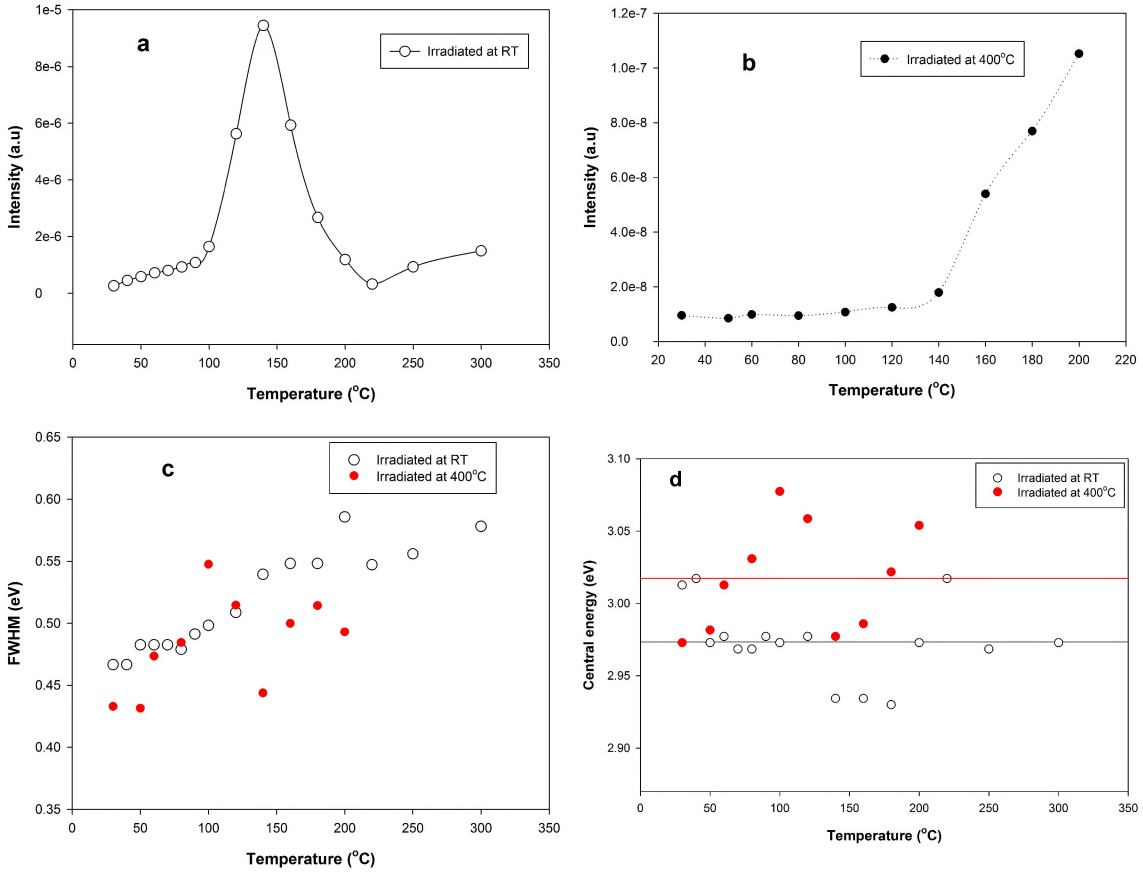

Figure 4.19: Plots of temperature dependence of F-centre emisssion: Intensity vs. temperature for the sample irradiated to 5.0 Gy at room temperature (a); Intensity vs. temperature for the sample irradiated to 5.0 Gy at 400°C (b); the FWHM vs. temperature (c) and the central energy vs. temperature (d). TR-XEOL spectra were measured at an integration time of 500 s.

We observe further increase in peak intensity with temperature between 200-300°C. The shape of the peak as depicted in Figure 4.19a closely resembles that of the main TL peak in the material. A similar shape was obtained by Chithambo and Costin [28] for the same material.

- for the 400°C-X-ray irradiation measurements (b), the peak intensity of the main emission band is fairly constant in magnitude up to about 80°C. Beyond 80°C, the peak intensity increases slowly with temperature up to 140°C. Between 140-200°C, a large increase in peak intensity with temperature is observed. This behaviour is strange because ideally one would expect a decrease in intensity with temperature between 140-200°C due to thermal quenching effects.

- despite the scatter, Figure 4.19c indicates that the FWHM of the main emission band generally increases with temperature for both sets of measurements i.e those following X-ray irradiation at room temperature and those following X-ray irradiation at 400°C. Furthermore, the FWHM of the main emission peak obtained following X-ray irradiation at room temperature is slightly larger than for those obtained following X-ray irradiation at 400°C. This indicates that the high-temperature X-ray irradiation eliminates and/or reduces the contribution from some emission centres.

- as shown in Figure 4.19d, the central emission energy of the main peak is fairly independent of temperature. The solid lines in Figure 4.19d represent mean energy values i.e. 2.98 eV for emission peaks obtained following X-ray irradiation at RT and 3.02 eV for those obtained following X-ray irradiation at 400°C. Thus, the high-temperature irradiation slightly shifts the mean central emission wavelength towards higher values i.e. short emission wavelength.

As before, the FWHM vs. temperature data of the F-centre band shown in Figure 4.19c were fitted using Equation 4.1 [32] to extract electron-lattice coupling parameters. The result of this fit yielded $S = 13 \pm 3$ and $E_p = 0.046 \pm 0.009$ eV. These values are consistent with those obtained using the XERL method i.e. $S = 5.0 \pm 0.9$ and $E_p = 0.079 \pm 0.008$ eV for the Huang-Rhys factor and phonon energy respectively.The

values of S are consistent in the sense that they both represent the strong coupling case.

Plots of ln(Intensity) against 1/kT corresponding to data presented in Figures 4.19a and b were plotted in order to obtain activation energy of thermal assistance. Table 4.2 gives a summary of these activation energies. The discussion on thermal assistance is postponed to Chapter 5 where its full treatment is covered.

Table 4.2: Activation energies evaluated from Arrhenius plots of peak intensity vs. temperature data of the main emission peak following sample X-ray irradiation at room temperature (RT) and 400°C.

Irradiation temperature	Temperature range°C	Activation energy (eV)
RT	30-80	0.15±0.01
	90-140	0.59±0.06
400°C	30-80	0
	100-140	0.082±0.006
	160-180	0.295±0.003

4.5.3 TR-XEOL spectrum obtained following high-temperature irradiation

The aim of this exercise was to monitor the OSL processes that take place when the high temperature traps (above 400°C) are selectively filled with dose then exposed to blue light.

A sample was irradiated to 5.0 Gy of X-rays at 400°C followed a measurement of the TR-XEOL spectrum at the same temperature i.e. 400°C. Irradiation at 400°C ensures that electron traps that are thermally unstable in the temperature range between room temperature and 400°C are presumably empty after X-ray irradiation and prior to optical stimulation. Figure 4.20 shows the spectra of the sample that was both irradiated and optically stimulated at 400°C. In the inset are the semi-log plots of the spectra obtained at relatively higher X-ray irradiation doses.

As it can be seen from Figure 4.20, the Blue spectrum shows the main emission peak centred at about 409 nm (3.03 eV). It is also clear from the inset that both

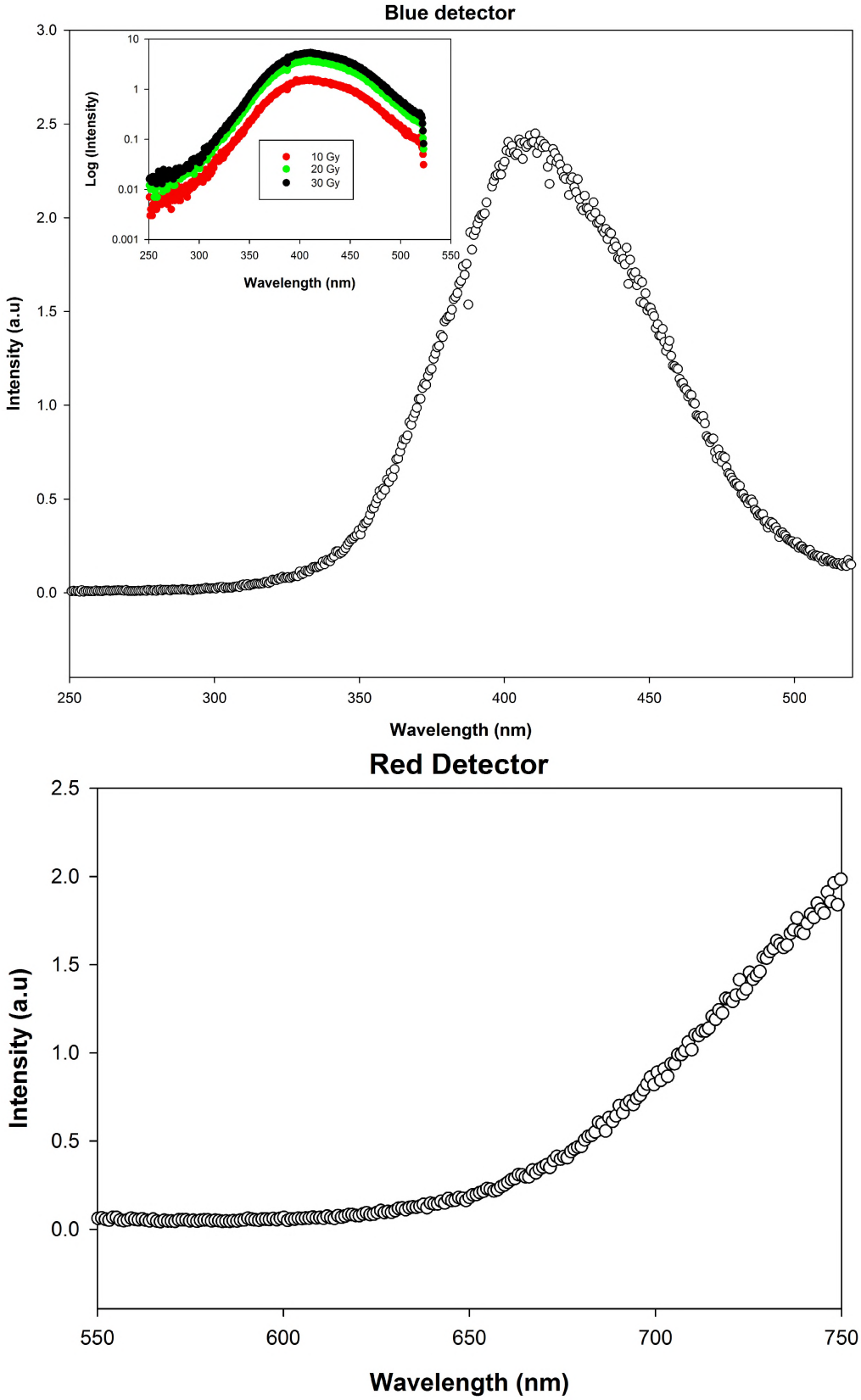

Figure 4.20: Plots of TR-XEOL spectra from the blue and red Detectors obtained from a sample that received a 5.0 Gy X-ray irradiation dose at 400°C. TR-XEOL was measured at 400°C using 470-nm blue LEDs at an integration time of 500 s.

the emission wavelength and the shape of peak are independent of dose. However, the peak gets slightly broader with dose. The red detector on the hand, shows a featureless spectrum. We suspect that this could be due to intense thermal irradiation produced at 400°C which obscures any relatively weak luminescence in the long wavelength range. This result shows that electron recombination at the F^+-centres is the dominant mechanism for the charges optically released from traps lying beyond 400°C.

In Figure 4.21, we present a graphical comparison of the normalised TR-XEOL UV-Blue spectra (from the blue detector) obtained from the same sample following (i) both X-ray irradiation and optical stimulation at room temperature, (ii) X-ray irradiation at 400°C then optical stimulation at room temperature, and (iii) both X-ray irradiation and optical stimulation at 400°C.

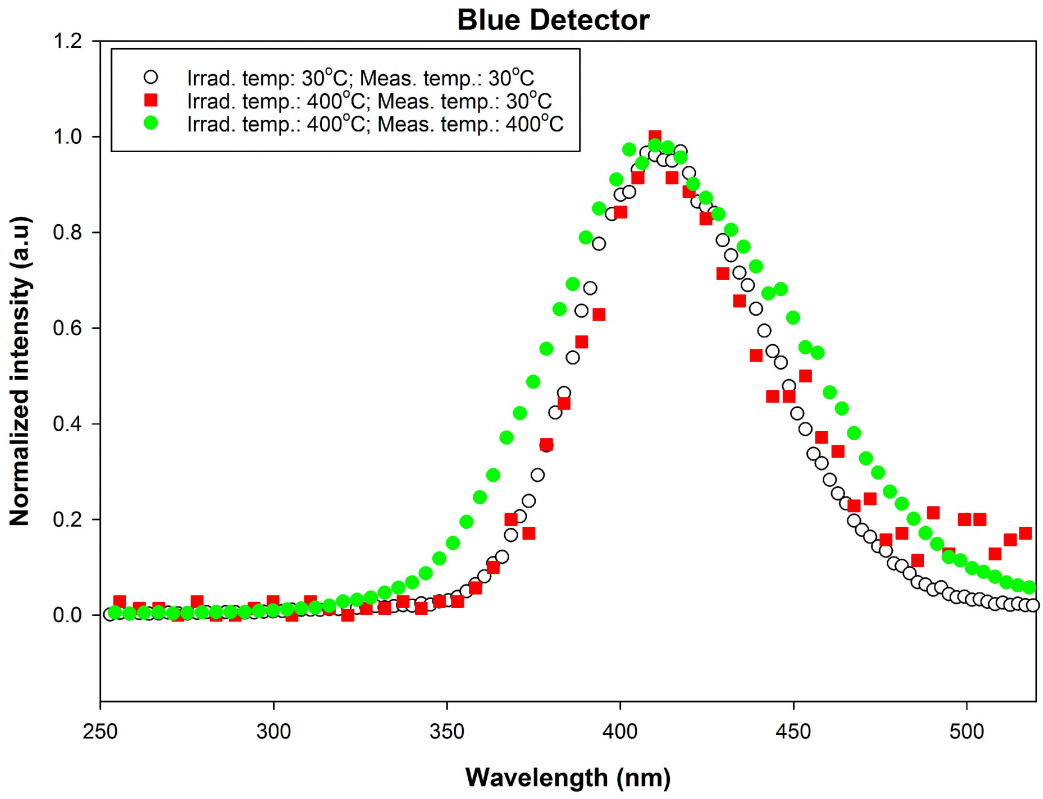

Figure 4.21: Comparison of the normalised TR-XEOL UV-Blue spectra obtained from the same sample following both X-ray irradiation and optical stimulation at room temperature; X-ray irradiation at 400°C then optical stimulation at room temperature and both X-ray irradiation and optical stimulation at 400°C.

It is clear from Figure 4.21 that the spectrum obtained following both irradiation and optical stimulation at room temperature is equivalent (in shape and position) to that obtained following irradiation at 400°C then optical stimulation at room temperature. However, despite sharing the same shape, the spectrum obtained following both irradiation and optical stimulation at 400°C is significantly broader than the two measured at room temperature as shown in Figure 4.21. It is clear from this result that the temperature of 400°C at which the TR-XEOL spectrum is measured, is responsible for the broadening of the peak. This broadening may be ascribed to increased vibronic transitions that occur at high temperatures of measurement. One also observes different decay rates on the longer wavelength side of the spectra presented in Figure 4.21.

4.6 Summary

In this chapter, we have looked at the XERL, XERL-TL, XETL and TR- XEOL spectra. An unidentified emission band (260-300 nm) has been observed in the XERL spectra. Our results strongly suggest that this unidentified band may be associated with hole recombinations at a luminescence centre. The other observed emission bands i.e. F (420 nm), F^+ (334 nm), F_2^{2+} (559 nm), Stoke's vibronic band of Cr^{3+} (671 nm), Cr^{3+} R-line emission (694 nm) and anti-Stokes vibronic band of Cr^{3+} (710 nm), are well documented.

The following recombination processes are assumed possible for the Cr^+ R-line emission:

1. Cr^{2+}+h$\longrightarrow Cr^{3+*} \longrightarrow Cr^{3+}$+694-nm luminescence

2. Cr^{4+}+e^- $\longrightarrow Cr^{3+*} \longrightarrow Cr^{3+}$+694-nm luminescence

3. Cr^{3+}+light ($\lambda_p = 400nm$)$\longrightarrow Cr^{3+*} \longrightarrow Cr^{3+}$+694-nm luminescence (PL)

Detailed analysis of the XERL-TL, XETL and TR-XEOL data has shown that luminescence dynamics of F^+ , F_2^{2+} and Cr^{3+} R-line emissions are the same i.e. they exhibit similar patterns regarding intensity changes, appearance/disappearance of the bands in a give spectrum. It is well known that both F^+ , F_2^{2+} emissions result from holes recombining with F and F_2 centres respectively. Our results therefore, support recombination process 1 in which holes recombine with Cr^{2+} impurity ions to produce the 694-nm R-line emission. There is no obvious evidence from our data to support recombination process 2. However, this does not mean that recombination process 2 does not occur in the material. The third process producing photoluminescence (PL) has been observed during TR-XEOL using an annealed and unirradiated sample.

We have also seen that with repeated XERL measurements, Cr^{3+} R-line emission decreases whereas that of the F-centre band gets slightly increased in intensity. Furthermore, we have established that there is strong electron-lattice coupling between the F-centre and the crystal lattice.

Results on the investigations of dose-dependence of XETL emission spectra have revealed that the most intense emission band associated with peak III in the material, shifts from F-centre to Cr^{3+} with X-ray irradiation dose.

Finally, it has been established that depending on the X-ray irradiation dose, both holes and electrons may take place in the emission process of peaks I, II and III during a TL readout.

Chapter 5

Stimulated phenomena associated with deep traps in α-Al_2O_3:C

Deep traps, on operational basis, refer to those traps that are thermally inaccessible when a luminescence material is heated from room temperature to a maximum temperature of 500°C. The number of reported studies emphasizing on the deep electron and hole traps in α-Al_2O_3:C, remains limited to date. In his investigation on the effects of deep trap population on the TL of Al_2O_3:C, Yukihara et al [42] identified deep hole and electron traps in the material located in the temperature range $\sim 527-602$°C and $\sim 827-927$°C, respectively. Yukihara et al [42] observed that depending on the level of deep trap filling, the features of the main peak i.e. width, area and height, are remarkably affected due to competing effects and multi-component nature of the peak. Previously, Akselrod and Gorelova [43] had reported the deep hole and electron traps in the range $\sim 450-550$°C and $\sim 800-900$°C, respectively. Polymeris et al [44] suggested an experimental method to measure OSL signal from deep traps in Al_2O_3:C using 470-nm blue LEDs without heating the samples to temperatures greater than 500°C. Polymeris et al [44] went further to investigate the influence of his method on some specific features of the main TL peak. Other similar literary pieces of work include that of Polymeris and Kitis [37], Bulur and Gøksu [17] and Colyott et al [40].

In this chapter, we present results of investigations on the OSL signal obtained by optical stimulation of the deep traps in α-Al_2O_3:C using 470-nm blue LEDs. We shall refer to the OSL obtained in this way as deep-traps OSL. The techniques used during these investigations include CW-OSL, TR-OSL and phototransferred thermo-

luminescence (PTTL). The temperature dependence of the deep-traps OSL signal has been thoroughly studied. A detailed analysis of the concept of thermal assistance in α-Al_2O_3:C has also been provided. For purposes of simplicity and consistency, we shall often refer to the traps emptied during the heating to 500°C as acceptor traps i.e. shallow, main and intermediate traps, whereas donor deep traps will apply to those traps lying beyond 500°C. In this chapter, PTTL and RTL for residual TL, will be used synonymously.

5.1 Continuous wave optically stimulated luminescence

In this section, we look at the trapping, retrapping, radiative and non-radiative recombination processes during constant-intensity blue light stimulation of the deep traps in α-Al_2O_3:C. It is very important to note that the CW-OSL signal is measured from a previously irradiated sample following heating to 500°C. The heating to 500°C empties the acceptor traps and leaves the donor deep traps intact with charge. Thus, the OSL will be referred to as deep-traps CW-OSL.

5.2 The profile of deep-traps continuous-wave OSL signal

To record a profile of a deep-traps continuous-wave OSL signal, the following procedure was used:

1. TL at 1 °C/s to 500°C in order to remove background dose from the acceptor traps i.e. shallow, main and intermediate traps.

2. Beta-irradiation to 5.0 Gy at room temperature to populate traps with charges

3. A preheat at 1 °C/s to 500°C to empty the acceptor traps.

4. Sample illumination using 470-nm blue LEDs for 500 s at 30°C to record deep-traps CW-OSL.

5. TL at 1 °C/s to 500°C to record residual TL (RTL).

Using this procedure, OSL was also measured at 100, 180 and 300°C. For purposes of comparison, the procedure above was repeated without the preheat at step 3 in order to record conventional or normal CW-OSL. Normal CW-OSL was also measured at 30, 100, 180 and 300°C. We shall refer to these temperatures as measurement temperatures. Figure 5.1 shows the plots of normal and deep-traps CW-OSL signals measured from α-Al_2O_3:C using 470-nm blue LEDs for a stimulation time of 500 s at 30, 100, 180 and 300°C.

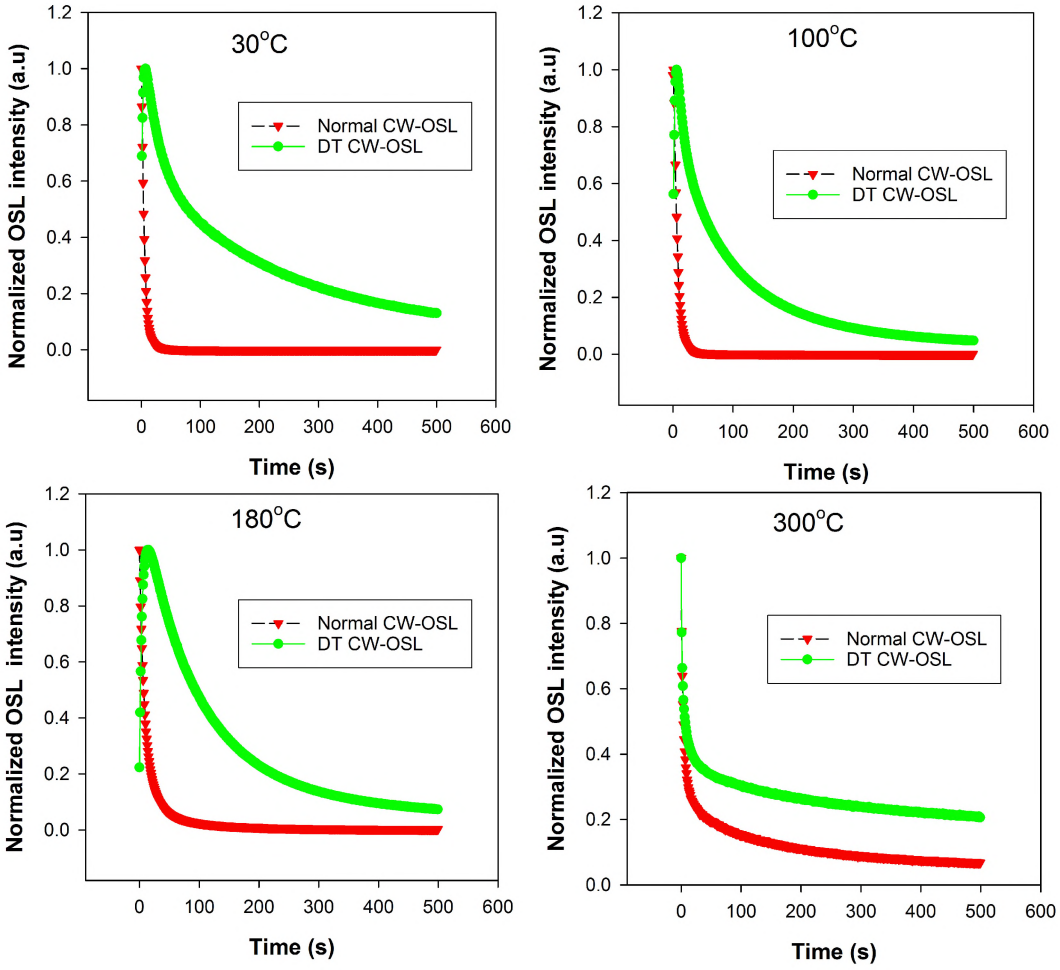

Figure 5.1: Plots of normal and deep-traps (DT) CW-OSL signals measured from α-Al_2O_3:C using 470-nm blue LEDs for a stimulation time of 500 s at 30, 100, 180 and 300°C. A beta irradiation dose of 5.0 Gy was used for this purpose.

It can be readily seen from Figure 5.1 that the deep-traps CW-OSL signal is different from the conventional one regardless of the temperature at which OSL is

measured. Whereas the normal CW-OSL signal is simply a decay at all the measurement temperatures, the deep-traps CW-OSL signal is peak-shaped at 30, 100, 180° and shows just a decay at 300°C similar to that of the normal signal. From visual inspection of Figure 5.1, it is obvious that a deep-traps CW-OSL signal decays slowly in time compared to the normal signal at all the measurement temperatures.

A similar result i.e. peak-shaped deep-traps CW-OSL signal at various temperatures, was reported by Polymeris et al [44] for α-Al_2O_3:C using 470-nm blue light stimulation following sample beta irradiation to 25.0 Gy of beta dose and post-irradiation heating to 500°C. A peak-shaped normal CW-OSL signal from α-Al_2O_3:C has also been previously reported e.g. McKeever et al [45] and Yukihara [9] who attributed it to trapping and thermal detrapping of charges at the shallow traps during optical stimulation of the sample. A full discussion on the peak-shape nature of the CW-OSL signal from the deep traps in α-Al_2O_3:C has been provided in a later section.

5.3 Identifying OSL traps

The objective of this exercise was to identify the trapping centres that are actively involved in the OSL processes of the material. A method of post-irradiation preheating was used for this purpose as follows:

1. TL at 1 °C/s to 500°C in order to remove background dose from the acceptor traps.

2. Beta-irradiation to 5.0 Gy at room temperature to populate traps with charges.

3. A preheat at 1 °C/s to a temperature T_i without hold.

4. CW-OSL measurement for 1000 s at 30°C.

5. TL at 1 °C/s to T_i to record phototransferred TL (PTTL).

The preheat temperatures, T_i, ranged from 30 to 700°. Note that the deep-traps CW-OSL signal was recorded at 30°C for all the preheat temperatures used. It is important to also note that the maximum temperature T_i to which PTTL was recorded (step 5) equals the preheat temperature (step 3). Step 5 ensures that all the traps beyond the current preheat temperature remain intact with their residual charge until the

next beta irradiation-preheat cycle. Figure 5.2 shows plots of the integrated OSL (a) and the normalized maximum intensities of the main PTTL peak (peak II) and low temperature PTTL peak (peak I) (b) against preheat temperature.

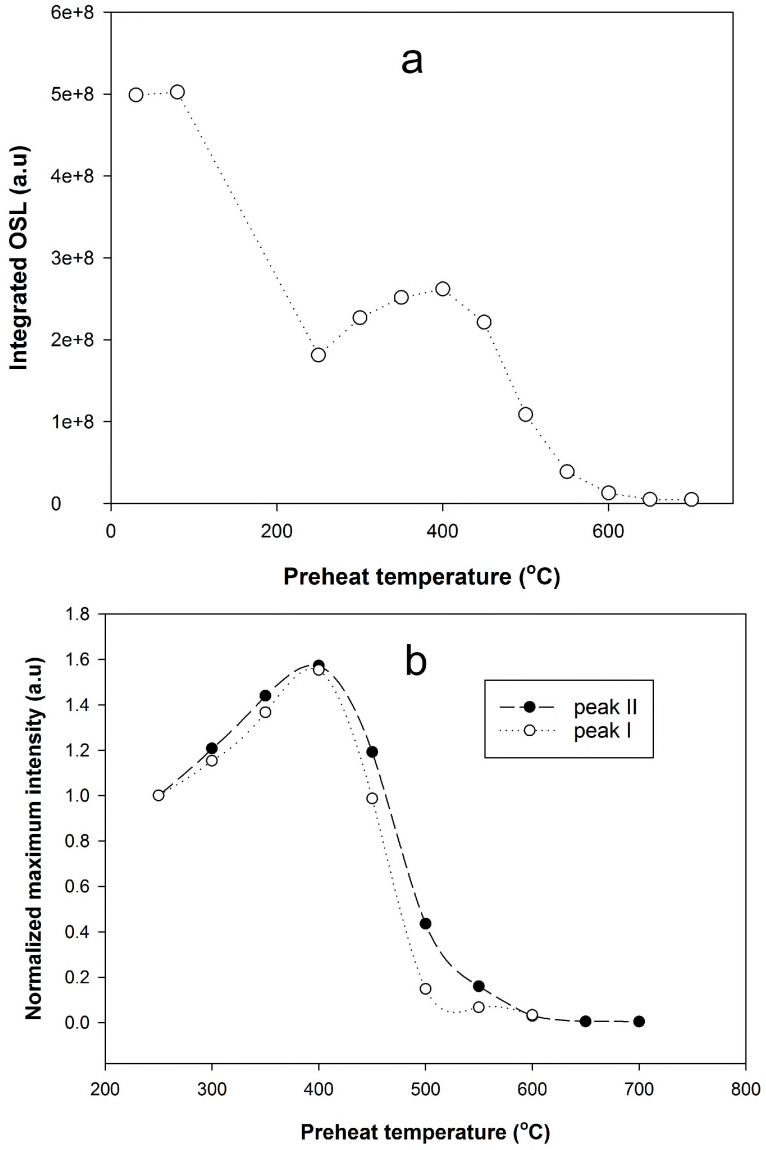

Figure 5.2: Plots of the integrated OSL (a) and the normalized maximum intensities of the main PTTL peak (peak II) and low temperature PTTL peak (peak I) (b) against preheat temperature. OSL was measured at 30°C using 470-nm blue LEDs for a stimulation time of 1000 s. A beta irradiation dose of 5.0 Gy was used for this purpose.

It can be seen from Figure 5.2a that the OSL yield decreases substantially (by $\sim$ 65%) between 80 and 250°C; increases between 250 and 400°C; significantly decreases (by $\sim$ 50%) between 400 and 600°C with major reduction following preheat

temperatures of 500 and 550°C; and is almost constant between 600 and 700°C. The intensities of the phototransferred peaks i.e. peaks I and II, simply simulate the behaviour of the OSL yield versus preheat temperature as shown in Figure 5.2b. It should be pointed out that peak III was also observed in the glow curve of the phototransferred TL for preheat temperatures between 350 and 500°C. This result contradicts Chithambo et al [18] who recently reported that no PTTL can be observed from peak III at all. However, there is a good agreement between our results and those of Chithambo et al [18] with respect to peak I which is reproduced under PTTL for preheat temperatures between 80 and 600°C as shown in Figure 5.2b.

From this result, we can conclude that the major OSL traps lie in the temperature ranges 80-250°C and 450-550°C associated with the main peak (peak II) and peak VI, respectively. These major OSL traps will be referred to as main OSL traps and secondary OSL traps, respectively. Note that there are also minor contributions from traps in the range 400-450°C and 550-600°C. The fact that roughly equal OSL yield is obtained for preheat temperatures of 650 and 700°C is enough proof that there are apparently no OSL traps in the 600-700°C range and that the OSL yield observed in this range is from much deeper traps lying beyond 700°C. To account for an increase in OSL yield observed in the 250-400°C range, it is important to recall from our experimental procedure that the preheat temperature and the maximum temperature to which PTTL is measured, are equal. Thus, for preheat temperatures of 300, 350 and 400°C, the residual charge following OSL readouts keeps on piling up in the secondary OSL traps between 400-600°C. The beta irradiation to 5.0 Gy that happens in the subsequent measurement cycle, further increases the trapped charge in the 400-600°C OSL traps. This causes an increase in the OSL yield. From this behaviour, we can infer that the TL traps lying in the temperature range 250-400°C associated with peaks III, IV and V, are apparently not optically active traps when deep-traps OSL is measured at 30°C. In other words, the traps in the 250-400°C range may be optically active at other measurement temperatures for OSL.

Another significance of this result is that the secondary OSL traps are also the major contributors to the phototransferred TL. This is an indication that charges stimulated from these secondary OSL traps are recaptured by the shallow and main traps before recombination takes place.

Larsen [46] identified the thermal depths of optically active trap centres in α-Al_2O_3:C at 142 (main peak), 300 (peak III), 500 and 642°C. Thus, our result contradicts that of Larsen on the 300 and 642°C traps.

Our results on the spectral study of luminescence from α-Al_2O_3:C presented in the previous chapter, showed that main trap in the material is predominantly an electron trap. This means that the main OSL trap is an electron trap. Recall that Akselrod and Gorelova [43] reported that the traps with thermal depth between 450-550°C are deep hole traps. This proposal has been widely accepted by most researchers working on the material. If this proposal is true, it implies that the secondary OSL traps are hole traps. This is the statement that requires scrutinizing. In the previous chapter, we recorded spectra of the TR-XEOL in three specific instances:

1. sample X-ray irradiation at 30°C then TR-XEOL measurement at 30°C,
2. sample X-ray irradiation at 400°C then TR-XEOL measurement at 30°C and
3. sample X-ray irradiation at 400°C then TR-XEOL measurement at 400°C.

You may wish to refer to Figure 4.21 for these spectra. As expected the spectrum measured at 30°C following X-ray irradiation at 30°C is dominated by the F-centre emission band. This confirms that the main trap, which happens to be the primary OSL trap in the material, is an electron trap. Irradiating a sample at 400°C keeps the main trap empty (presumably) but fills the secondary OSL traps and the donor deep traps. We expect the secondary OSL traps (400-550°C) to dominated either through retrapping at the main trap in the case of the spectrum measured at 30°C or direct recombinations in the case of the spectrum recorded at 400°C. However, in either case, the dominant emission remains the F-centre emission band, an indication that it is the electrons that are involved in the recombination process and that the traps involved are electron traps. If the secondary OSL traps were indeed hole traps, we would expect the emission to be dominated by recombination of holes and not otherwise. In addition, the fact that most of the retrapping occurring at the main trap during optical stimulation is due to charge carriers released from the secondary OSL traps, suggests that both the main OSL trap and the secondary OSL traps contain charge carriers of the same polarity. Based on the above arguments, we strongly feel that the traps between 400-550°C may be electron traps. Alternatively, hole traps and electrons traps coexist in this temperature range. This, however, is

open to discussion.

5.4 Concerning the peak-shape of the deep-traps OSL signal

We saw in Figure 5.1 that the deep-traps CW-OSL signal is peak-shaped when measured at temperatures of 30, 100 and 180°C but is simply a decay when measured at 300°C. In this section, we present factors that influence the peak-shape nature of the CW-OSL signal obtained using 470-nm blue light stimulation of the deep traps in α-Al_2O_3:C. Based on these factors, we offer an explanation for the peak observed in the deep-traps CW-OSL signal.

5.4.1 Irradiation dose

A sample was annealed once in a furnace at 900°C for 15 minutes to empty the traps. It was then irradiated to 1.0 Gy, heated linearly at 1.0°C/s to 500°C to clear the acceptor traps and then exposed to 470-nm blue LEDs for 1000 s at 30°C to record CW-OSL. This procedure was repeated for a beta irradiation dose of 5.0 Gy. Figure 5.3 shows normalized CW-OSL signals corresponding to the irradiation doses used.

It is clear from Figure 5.3 that a beta irradiation dose of 5.0 Gy produced a peak-shaped CW-OSL signal whereas a 1.0-Gy beta irradiation dose did not. It is important to remember that in both cases i.e. 1.0 Gy and 5.0 Gy, all the traps up to the thermal depth of 500°C, the main trap inclusive, were empty prior to optical stimulation.

5.4.2 Post-irradiation annealing temperature

A sample was beta irradiated to 1.0 Gy, annealed by heating at 1°C/s to 400°C, then cooled down to 30°C prior to OSL measurement. There was no holding time at 400°C. Thereafter, the sample was illuminated with 470-nm blue LEDs for 1000 s to record OSL. This procedure was repeated for annealing temperatures of 500°C, 600°C and 700°C. Figure 5.4 shows the deep-traps CW-OSL signal recorded for the specified annealing temperatures.

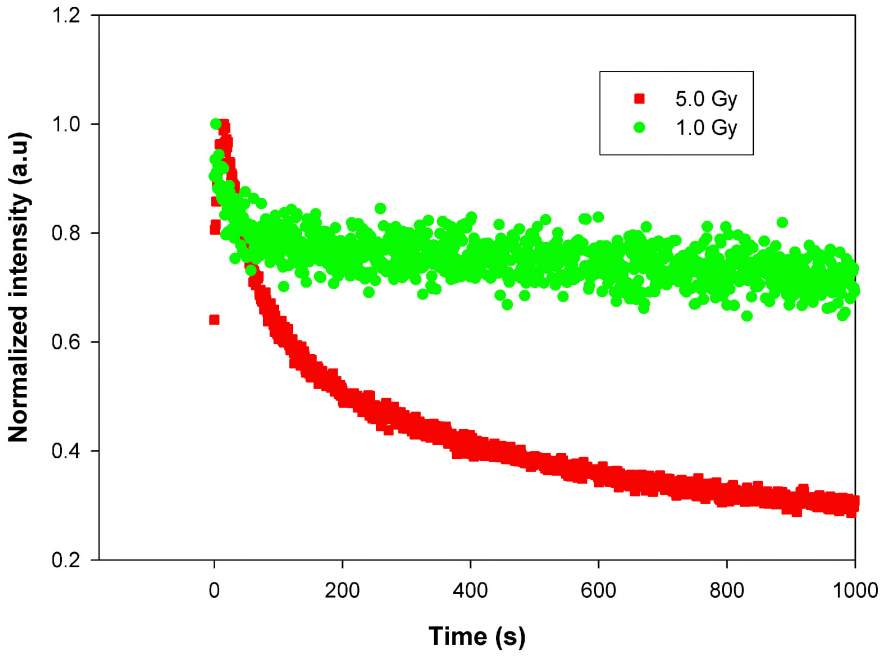

Figure 5.3: Plots of CW-OSL signal normalized to their maximum intensities as function of time for 1.0 Gy and 5.0 Gy beta irradiation doses. The sample was first irradiated then heated to 500°C at 1.0°C/s before exposing it to 470-nm blue LEDs. The signal was recorded at 30°C for a stimulation period of 1000 s.

Figure 5.4 shows a peak-shaped CW-OSL signal following a post-irradiation annealing temperature of 400°C. This profile is not observed for annealing temperatures of 500°C, 600°C and 700°C. Worthy noting are the signals obtained for the annealing temperatures of 600°C and 700°C i.e. there is an initial fast decay followed by slight evidence of an apparent peak-shaped OSL signal. The peak-shaped nature can be easily noticed in the signal corresponding to the annealing temperature of 700°C.

5.4.3 Illumination light

A sample was irradiated once to 5.0 Gy, heated at 1.0°C/s to 500°C to deplete the acceptor traps i.e. the acceptor traps. Thereafter, it was exposed to 470-nm blue LEDs for 1000 s at 30°C to record OSL. The OSL measurements were repeated several times without any further beta irradiation. Every OSL measurement was succeeded by heating to 500°C to empty the acceptor traps prior to the next OSL

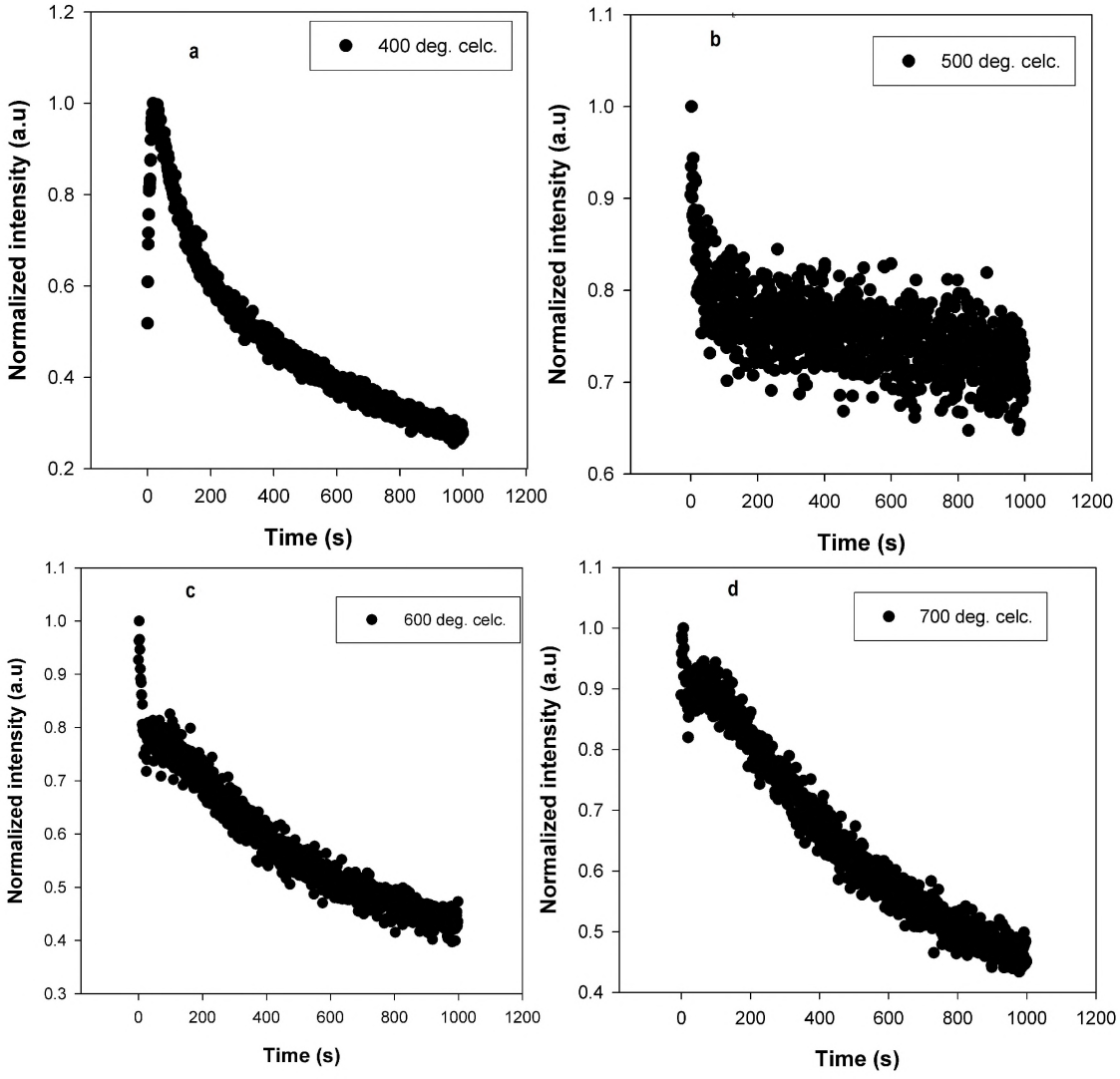

Figure 5.4: Plots of CW-OSL signal obtained following post-irradiation preheating to 400°C (a), 500°C (b), 600°C (c) and 700°C (d). The sample was beta irradiated to 1.0 Gy, preheated to a specific temperature, followed by 470-nm blue light stimulation for 1000 s at 30°C to record OSL. There was no holding time at the preheat temperature.

readout. Figure 5.5 presents plots of CW-OSL signal obtained during multiple OSL measurements. Figure 5.5 shows that the peak of the deep-traps CW-OSL signal diminishes with increasing number of OSL runs.

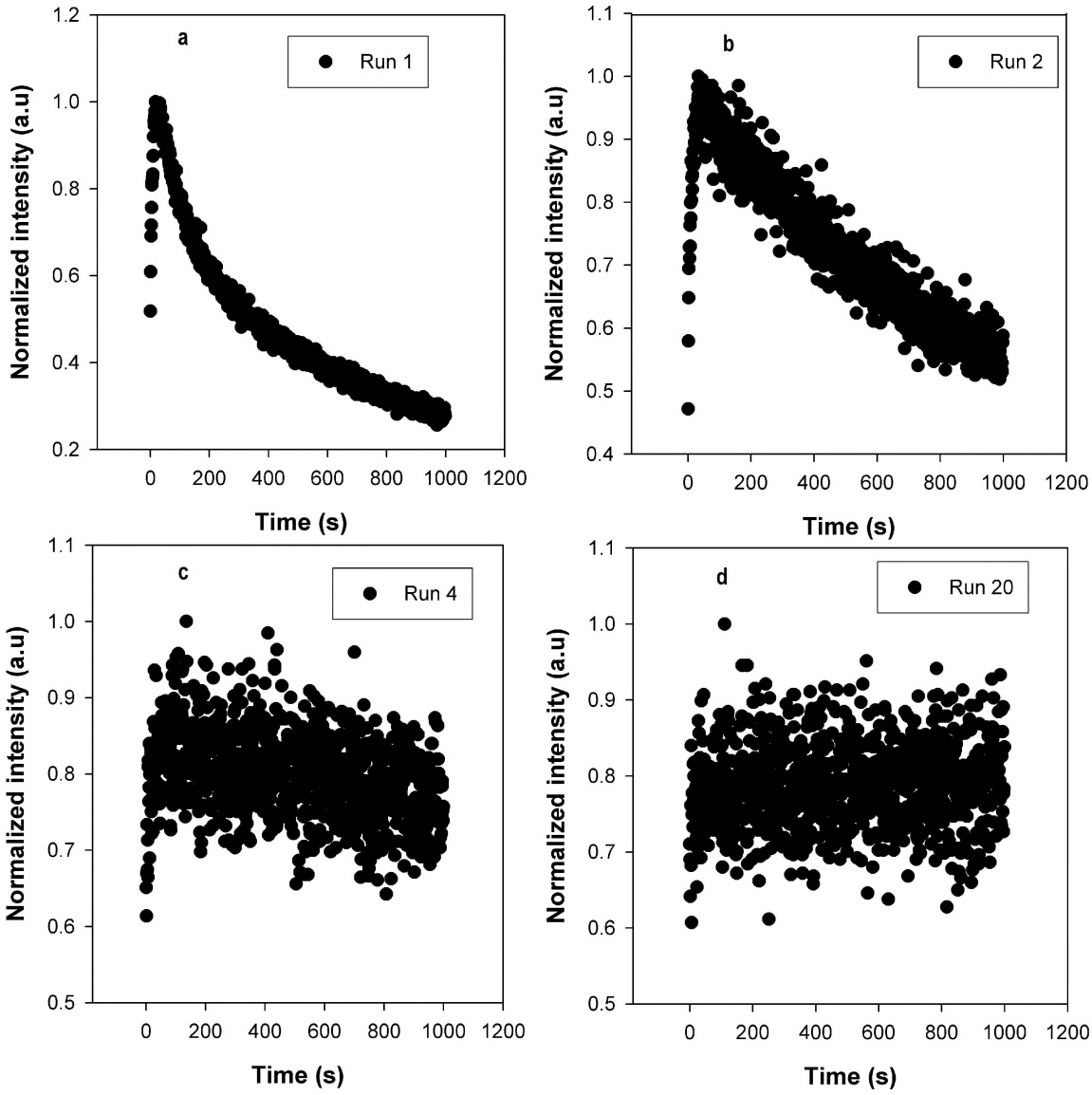

Figure 5.5: Plots of repeated CW-OSL measurements. The sample was irradiated to 1.0 Gy only once at the beginning and heated to 500°C at 1.0°C/s between OSL measurements. Blue LEDs (470 nm) were used for deep trap stimulation for a period of 1000 s at 30°C. The plot only shows the first, second, fourth and twentieth runs to illustrate change in shape with repeated stimulation.

5.4.4 Charge concentration in the main trap

In this investigation, we explore the effect of charge occupancy of the main trap i.e. the primary OSL trap, on the peak-shape of the deep-traps CW-OSL signal.

A sample was irradiated to 5.0 Gy, preheated to a temperature T_{max} at 1.0°C/s, followed by an OSL measurement at 30°C. T_{max} represents the maximum temperature during a preheat. The preheat was meant to depopulate the acceptor traps prior to OSL readout. The procedure was repeated for T_{max} values between 30-700°C. Figure 5.6 shows plots of CW-OSL signal for various preheat temperatures, T_{max}. It can be readily seen from Figure 5.6a that for preheat temperatures between 30-220°C, a decaying OSL signal (without a peak) is obtained.

The peak-shaped CW-OSL signal is observed for preheat temperatures between 250-540°C (Figures 5.6b and c). The observed OSL signals for preheat temperatures between 560-700°C do not show a peak and resemble those observed for preheat temperatures between 30-220°C. This suggests that the dominant charge transfer mechanism is the same between these two temperature ranges.

Comparison of CW-OSL signals in Figures 5.4c and d against Figure 5.6d for OSL recording temperatures between 600-700°C reveals that a beta irradiation dose i.e. 1.0 Gy and 5.0 Gy respectively, affects the shape of the deep-traps CW-OSL signal and the associated charge transfer mechanisms.

5.4.5 Measurement temperature

By measurement temperature, we refer to the temperature at which OSL is measured or recorded. During this investigation, a sample was irradiated to 5.0 Gy, heated at 1.0°C/s to 500°C to deplete the acceptor traps, then exposed to 470-nm blue LEDs for 1000 s at a temperature T_i to record OSL. T_i represents a measurement temperature. This procedure was repeated for T_i's between 30-560°C. The whole experiment was repeated using an empty sample holder to record noise in the OSL signal measured at a temperature, T_i. The recorded noise represents the unwanted signal due to sources external to the sample and the blackbody radiation produced at high measurement temperatures. The recorded noise was then subtracted from the actual data. Figure 5.7 presents the plots of the net CW-OSL signal obtained at various temperatures. It is clear in Figure 5.7 that peak-shaped OSL signal is obtained for measurement temperatures between 30-240°C. Measurement temperatures above 240°C (Figures 5.7c and d) did not produce a peak-shaped OSL signal.

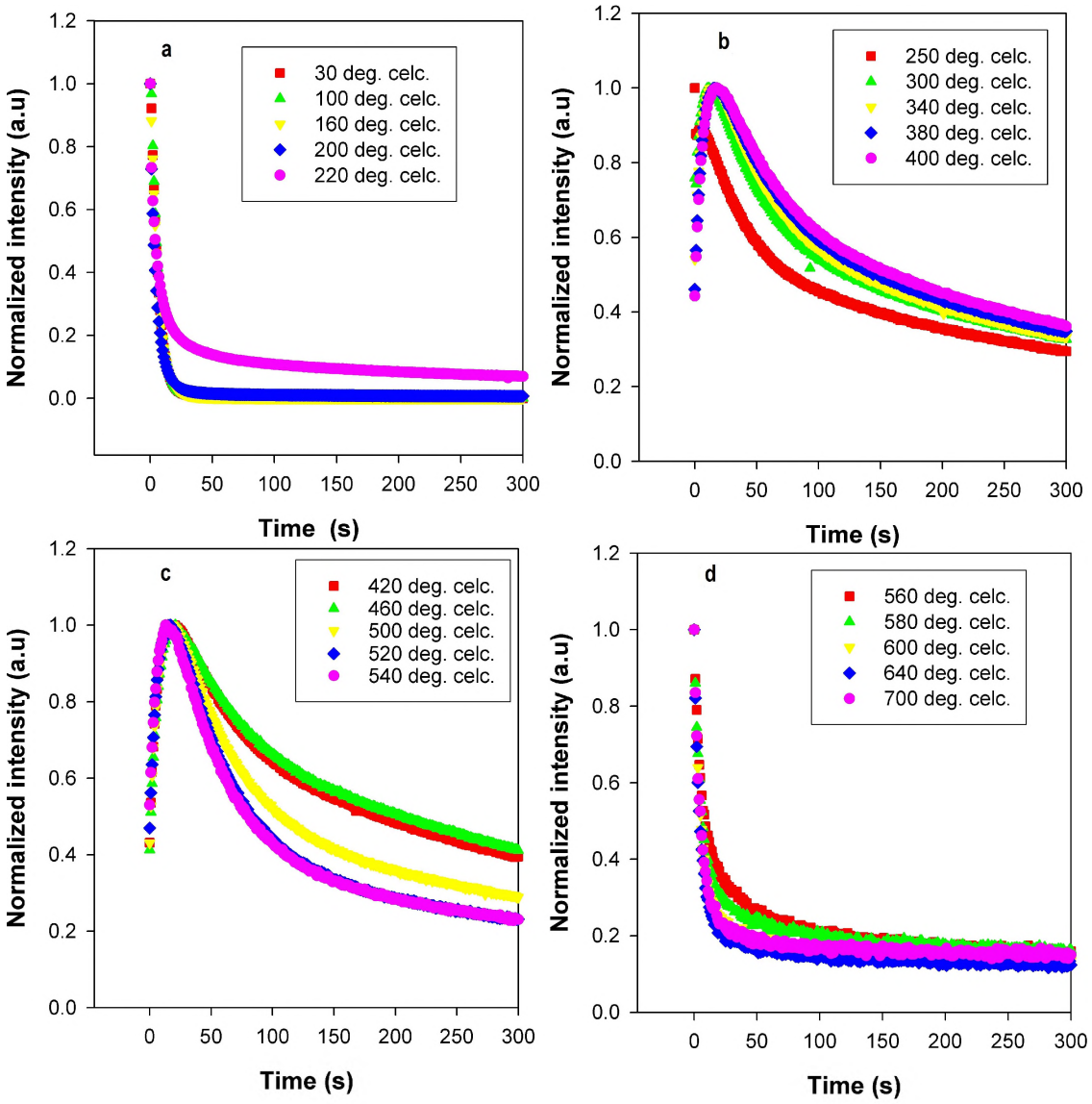

Figure 5.6: Plots of CW-OSL signal for various post-irradiation preheat temperatures. For a given preheat temperature, the sample was irradiated to 5.0 Gy, heated to a specified maximum temperature at 1.0°C/s then illuminated by 470-nm blue light for 1000 s at 30°C to record OSL. The plots show the signal for the first 300 s only.

Discussion

In investigating the influence of beta irradiation dose on the peak-shape of the deep-traps CW-OSL signal, we observed a peak for the 5.0-Gy beta irradiation dose and none for the 1.0 Gy dose. Obviously, the high dose (5.0 Gy) sufficiently fills both the

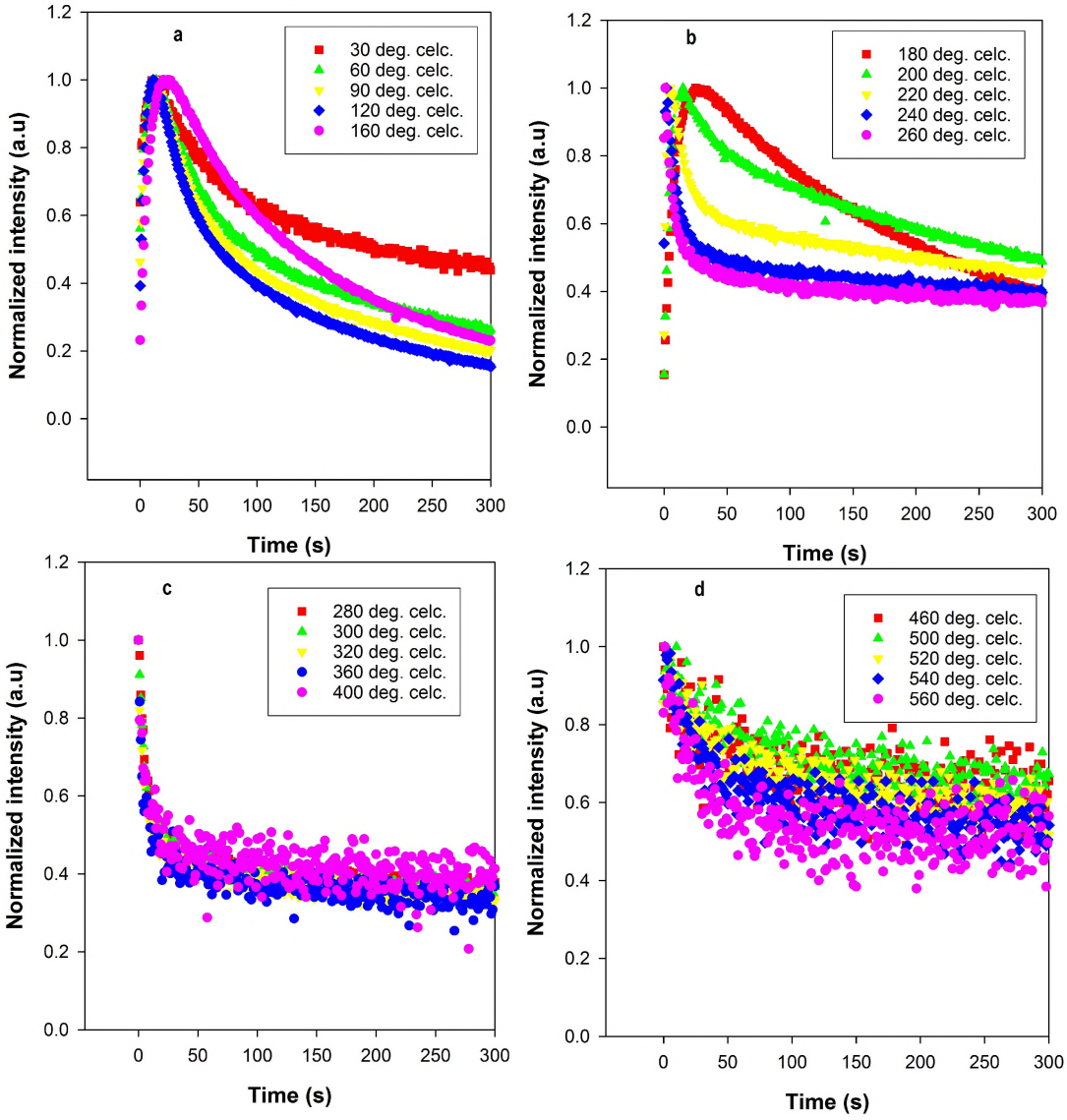

Figure 5.7: Plots of CW-OSL signal recorded isothermally at various temperatures. For a given recording temperature, the sample was first irradiated to 5.0 Gy, heated to 500°C at 1.0°C/s, followed by 470-nm blue light stimulation for 1000 s to record OSL. The plots show the signal for the first 300 s only.

acceptor traps i.e. shallow, main and intermediate traps, and the donor deep traps compared to 1.0 Gy. For both beta irradiation doses the acceptor traps are empty prior to OSL readout due to a preheat to 500°C whereas the donor deep traps are substantially occupied following 5.0 Gy beta irradiation dose and less occupied for the 1.0 Gy dose. Note that the sample was irradiated to 1.0 Gy then 5.0 Gy and not

vice versa.

We have seen in the previous sections that the second major contributors to the OSL signal in α-Al_2O_3:C, besides the main trap, are the traps lying in the temperature region between 400-550°C i.e. the secondary OSL traps (see Figure 5.2a). We have also seen from Figure 5.2b that charges optically released from the secondary OSL traps are largely involved in the retrapping process at the main trap. Annealing at 400°C therefore leaves the secondary OSL traps sufficiently occupied. Annealing to 500°C on the other hand substantially depletes the secondary OSL traps i.e. occupancy of the donor traps is significantly reduced with concomitant disappearance of the peak in the OSL signal (see Figure 5.4). Annealing at 600°C and 700°C depletes charges from both the main and secondary OSL traps. Thus, prior to OSL readout, charge is available in the very deep traps (VDTs) only. The rate of charge detrapping from VDTs by optical means is usually very low owing to the small photoionization cross-section of the VDTs. Consequently, retrapping and recombination rates are both low.

In the case of repeated OSL measurements without further beta irradiation, the occupancy of donor deep traps diminishes with the number of OSL runs. Note that prior to OSL readout, the acceptor traps are empty of charge.

Further, we have seen that preheat temperatures between 30-220°C produce a decaying OSL signal (without a peak). The peak-shaped CW-OSL signal is observed for preheat temperatures between 250-540°C (Figures 5.6b and c). The observed OSL signals for preheat temperatures between 560-700°C do not show a peak and resemble those observed for preheat temperatures between 30-220°C. It is clear that preheat temperatures between 30-220°C do not completely empty the main trap. On the other hand, preheat temperatures between 250-540°C completely depopulate the main trap, whereas the preheat temperatures between 560-700°C (Figure 5.6d) deplete the main and secondary OSL traps and substantially depopulate the occupied donor deep traps.

In the case of the measurement temperature investigations, the acceptor traps are empty prior to OSL readout. In addition, the measurement temperature itself restricts the level of retrapping in OSL active traps i.e. the higher the measurement temperature, the less the retrapping levels. The peak-shaped OSL signal is obtained

for measurement temperatures between 30-240°C. In this temperature range, charge retrapping at the main OSL trap during optical stimulation is still possible. However, beyond 240°C, retrapping at the main peak is almost impossible hence the main trap is presumably empty during optical stimulation.

Thus, from the observations listed above, the major deciding factor for the presence of the peak in the deep-traps CW-OSL signal is the relative concentration of charges in the main trap, the secondary OSL traps and the donor deep traps. The OSL signal shows a peak when both the secondary OSL traps and deep traps collectively are substantially filled and the main trap is substantially empty. The difference in charge population between the main trap in one hand, and the secondary and deep traps on the other hand, determines levels of retrapping during optical stimulation which in turn determines the shape of the OSL signal. The greater the difference in charge population, the greater the retrapping at the main trap, and the greater the likelihood of getting a peak-shaped OSL signal.

5.5 Further results on the measurement temperature dependence of the deep-traps CW-OSL signal

The results reported here are based on the data acquired during the investigations on the influence of measurement temperature on the shape of the deep-traps CW-OSL signal, presented in previous sections. The data for the OSL signals were, where necessary, digitally separated into the rising component and decay component. The rising component was fitted by a single saturating exponential for the measurement temperatures between 30-220°C that produced a peak-shaped OSL signal i.e.

$$y = y_0 + a\,[1 - \exp(-bt)]$$

where b is a decay rate, y_0 and a are scaling parameters. It is important to recall that the peak-shape disappears at 240°C and above. The decay component on the other hand was fitted by a single exponential and a constant i.e. $y = y_0 + a\exp(-bt)$ for temperatures between 30°C and 220°C and two exponentials plus a constant i.e.

$y = y_0 + \exp(-bt) + c\exp(-dt)$ for measurement temperatures between 240°C and 400°C where a and c are scaling parameters, b and d are decay rates and other parameters as previously defined. Figure 5.8 shows plots of decay rates of the rising component (a) and for the decay component (b and c) as a function of measurement temperature.

The following observations can be made from Figure 5.8:

- the decay rates for the rising component (a) are approximately 15 times larger than the corresponding decay rates for the medium component (b). However, the two decay rates exhibit similar dependence on measurement temperature up to 180°C above which the decay rate for the rising component increases dramatically. The decay rates for both the rising and decay components start decreasing beyond 120°C.

- the behaviour of the decay rates for both the rising and decay components between 30°C and 180°C resembles the thermal quenching curve.

- Figure 5.8c shows a fast decaying component and a slowly decaying component for measurement temperatures above 240°C where the peak-shape in the OSL signal is no longer observed.

To aid in our interpretation of the decay results, we have presented Figure 5.9 which shows a plot of the peak intensity against measurement temperature for the main residual TL peak. It is clear from Figure 5.9 that the main RTL peak is no longer reproduced for measurement temperatures of 240°C and above. Recall that these are the same temperatures at which the peak-shaped OSL disappears. The disappearance of both the main RTL peak and the peak-shape of the OSL signal is an indication of negligible retrapping at the main trap. Coincidentally, the medium component of the OSL decay also disapppears at 240°C as shown in Figure 5.8b. Thus, we may attribute the medium component to the OSL component that is associated with charge retrapping at the main trap. Similarly, we expect the rate of direct recombinations to increase with negligible retrapping at the main trap. We observe this behaviour in the decay rate of the rising component i.e. it increases rapidly above 200°C. Thus, we may attribute the rising component to the OSL component

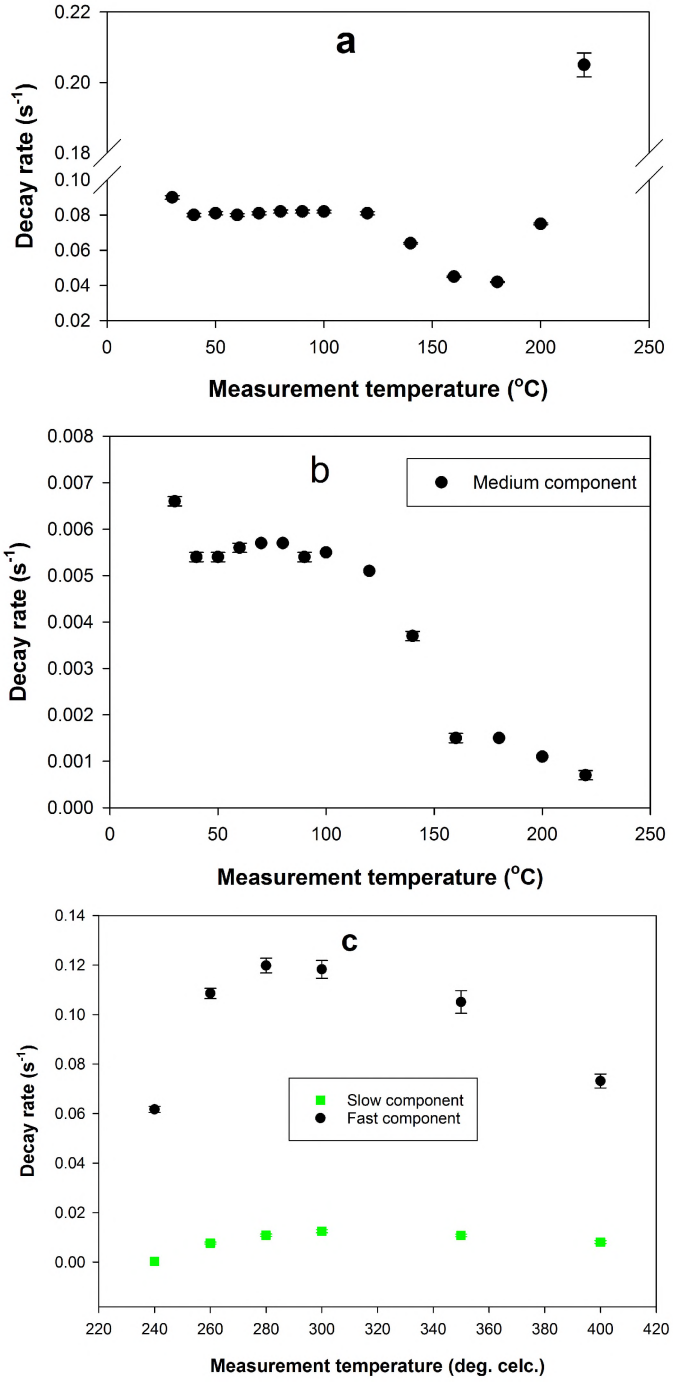

Figure 5.8: Plots of the decay rates of the rising component (a) and for the decay component (b and c) as a function of measurement temperature. A sample was first irradiated to 5.0 Gy, heated to 500°C then illuminated with 470-nm blue LEDs at a specified measurement temperature.

associated with direct recombinations. In a similar manner, the fast component, which

is apparently dominant at higher measurement temperatures, may be attributed to direct recombinations from secondary OSL traps (lying between 500-600°C) which are not erased in heating to 500°C prior to OSL readout. On the other hand, an almost steady slow component may be associated with the OSL from very deep traps with very low photoionization cross-section lying beyond 700°C.

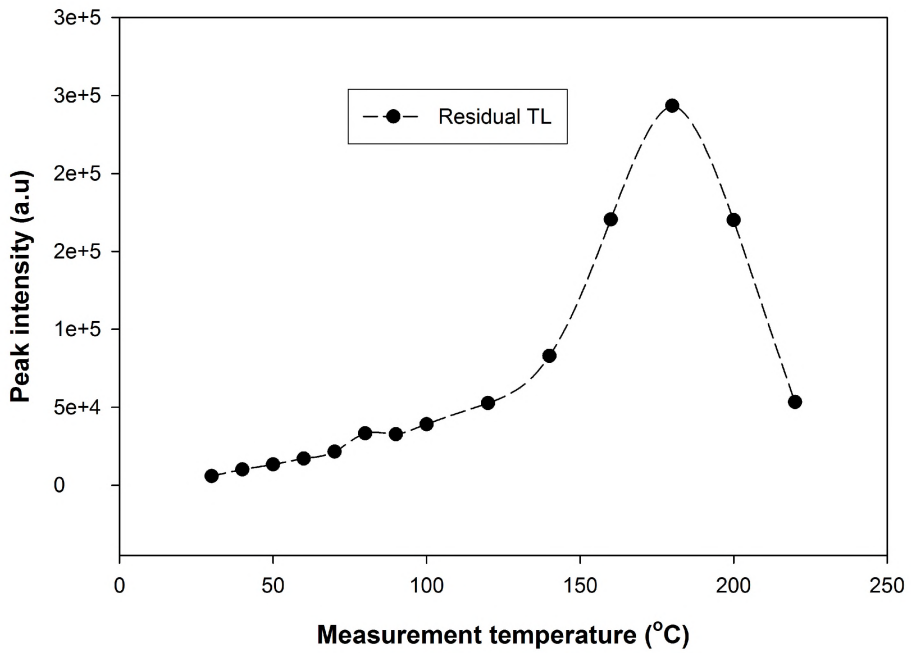

Figure 5.9: Plot of the peak intensity of the main residual TL peak as a function of measurement temperature.

5.6 Time-resolved optically stimulated luminescence

In this section, a study of transfer mechanisms of charges stimulated optically from the deep traps in α-Al_2O_3:C is reported. The investigations were carried out using thermally assisted time-resolved optical stimulation (TA-TR-OSL), thermoluminescence (TL) and residual thermoluminescence (RTL).

Before use, samples were annealed in a furnace at a nominal temperature of 900°C followed by rapid cooling in air. The annealing was meant to empty the traps. All TL measurements were carried out in the Risø TL/OSL DA-20 Reader. For TR-OSL

measurements, the pulsing system [21, 22] was used. The 470-nm blue LEDs of the pulsing system were set at a pulse width of 18±2 ms. The TR-OSL signal was recorded at a dynamic range of 500 ms. The Oven AO 500 (MBE-Komponenten GmbH, Germany) provided the platform for controlling and setting the sample temperature during TR-OSL measurements. The following procedure was followed during this investigation:

1. A preheat at 1°C/s to 500°C to remove background dose.
2. Beta-irradiation to 100 Gy to fill the traps.
3. TL at 1°C/s to 500°C in order to empty charges in acceptor traps i.e shallow, main and intermediate traps.
4. TR-OSL measured at a temperature T_i
5. TL at 1°C/s to 500°C to record Residual TL (RTL).

Step 1 was necessary only during the first measurement, whereas the rest of the steps were repeated for measurement temperatures, T_i's between 30-220°C. Note that a high beta irradiation dose was required in order to get an analyzable OSL signal from the deep traps.

5.6.1 TR-OSL profile following deep-traps stimulation

Figure 5.10 shows a TR-OSL signal measured at 70°C following light stimulation of the deep traps by the 470-nm blue LEDs. The rising component of the TR-OSL signal is recorded with the light pulse on, whereas the decay component is recorded with the light pulse off. The deep-traps TR-OSL signal shown in Figure 5.10 resembles a conventional TR-OSL signal obtained from the same material [25].

5.6.2 Dependence of the luminescence lifetime on measurement temperature of the deep-traps TR-OSL

Here we look at how the measurement temperature influences the luminescence lifetime of the TR-OSL signal due to deep-traps stimulation.

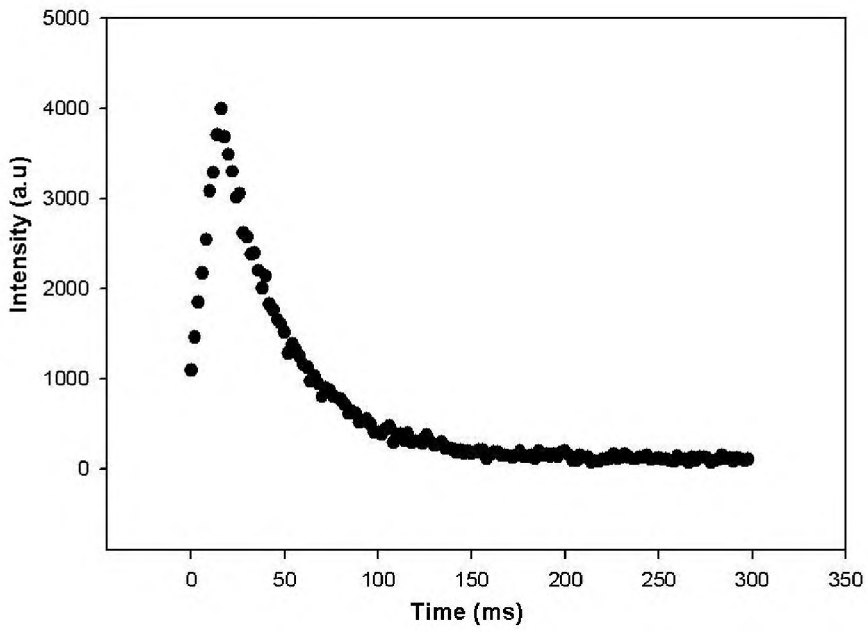

Figure 5.10: A TR-OSL spectrum obtained at 70°C using an 18 ms pulse width following sample beta irradiation to 100 Gy (step 2) and a TL to 500°C (step 3).

The luminescence lifetimes were evaluated by fitting the decay component of the TR-OSL signal with a single exponential plus a temperature dependent term, C, i.e. $A\exp(-t/\tau) + C$, where τ is the luminescence lifetime and A is a scaling parameter. Figure 5.11 shows a plot of luminescence lifetimes as a function of measurement temperature.

The plot shown in Figure 5.11 resembles that reported by Chithambo et al. [25] for the same material and using the same TR-OSL technique. However, Chithambo et al [25] did not involve a preheat to 500°C (like in our case) immediately after beta irradiation in order to get rid of charges in the acceptor traps i.e. shallow, main and intermediate traps.

The similarity between the deep-traps TR-OSL and the conventional TR-OSL strongly suggests that the traps and recombination centres involved in the conventional TR-OSL are not different from those involved in the TR-OSL due to deep traps. Furthermore, a charge carrier of the same polarity is involved in both cases. It was observed under CW-OSL investigations that the conventional OSL is primarily associated with the main trap in α-Al_2O_3:C which happens to be an electron trap.

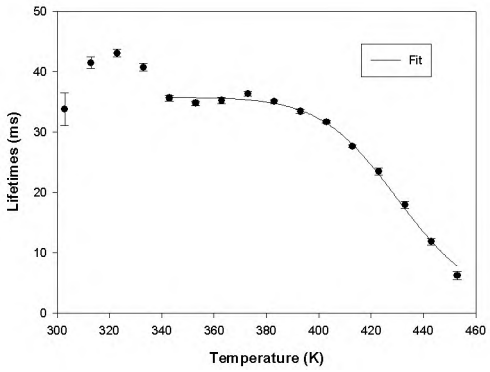

Figure 5.11: A plot of luminescence lifetimes against measurement temperature for a TR-OSL signal associated with the deep traps. The solid line represents the best-fit regression line using Equation 5.1 of thermal quenching.

From this behaviour, we can suggest that when charges i.e. electrons, are optically stimulated from the deep traps, they are redistributed via the conduction band to particularly the main trap and shallow traps, followed by optical release from the main trap and subsequent recombination at the luminescence centres. It is important therefore that caution should be exercised when using OSL from deep traps for deep trap characterization. Except for measurement temperatures beyond the position of the main electron trap i.e. 250°C and above, the trapping parameters obtained from the OSL due to the deep traps may not necessarily be characteristic of the deep traps but rather of the main trap.

It is clear from Figure 5.11 that the luminescence lifetimes get increasingly shorter with measurement temperature. This behaviour is a well known effect of thermal quenching in the material [25]. The behaviour of luminescence lifetime against measurement temperature shown in Figure 5.11 is expected to follow the well-known thermal quenching model:

$$\tau(T) = \frac{\tau_0}{1 + C\exp(-\frac{W}{kT})} \tag{5.1}$$

where $\tau(T)$ is the lifetime at measurement temperature T , τ_0 is the mean radiative lifetime evaluated at 0 K and is equal to 35 ms for α-Al_2O_3:C and other parameters as previously defined. The solid line in Figure 5.11 represents the best-fit regression line based on Equation 5.1 from which: $W = 1.028 \pm 0.002$ eV and $C = 9.8 \times 10^{11}$ which

gives the Debye frequency, ν, equal to 2.8×10^{13} s^{-1}. These values are consistent with those obtained by Chithambo, et al [25] ($W = 1.025 \pm 0.002$ eV and $\nu = 6.00 \times 10^{12}$ s^{-1}), Nyirenda [23] (1.045 ± 0.002 eV and $\nu = 2.1 \times 10^{11}$ s^{-1}) and Akserlod, et al ($W = 1.08 \pm 0.03$ eV and $\nu = 1.02 \times 10^{14}$ s^{-1}).

5.6.3 Comparison of the residual and normal TL with respect to measurement temperature

The comparison is made between parameters of the main peak obtained solely due to residual charge at the main electron trap following optical stimulation of the deep traps i.e. RTL, against the conventionally obtained TL. The comparison has been made at all the temperatures at which deep-traps TR-OSL was measured. The aim is to assess if the measurement temperature has any influence on the parameters of the main peak of the residual TL. The parameters of interest are the position, height and the full-width at half-maximum (FWHM) of the peak.

Figure 5.12 shows plots of the position (a), FWHM (b) and height (c) of both the normal main TL peak and the main RTL peak against the measurement temperature. It is evident from Figure 5.12a that the position for the main RTL peak has considerably shifted towards higher temperatures and that this behaviour is independent of the temperature at which TR-OSL is measured. It is well known that the main peak in the TL glow curve of the material has a high temperature component [47] which is less bleachable by light than its corresponding low temperature component [38]. During optical stimulation of the deep traps, charges get recaptured at the main trap. However, the low temperature traps are effectively emptied by light compared to the hard-to-bleach high temperature traps. Thus, in the TL following the TR-OSL i.e. RTL, the main peak is mostly due to thermal release of the charges in the high-temperature traps hence the shifting of the peak towards higher temperatures.

Besides the shifting of peak position to higher temperatures, the main peak in the residual TL glow curve also broadens i.e. FWHM increases irrespective of the TR-OSL measurement temperature as can be seen in Figure 5.12b. This increase in FWHM may be attributed to the collocation of the lower temperature component peak (which does not get completely bleached during light exposure) with the high

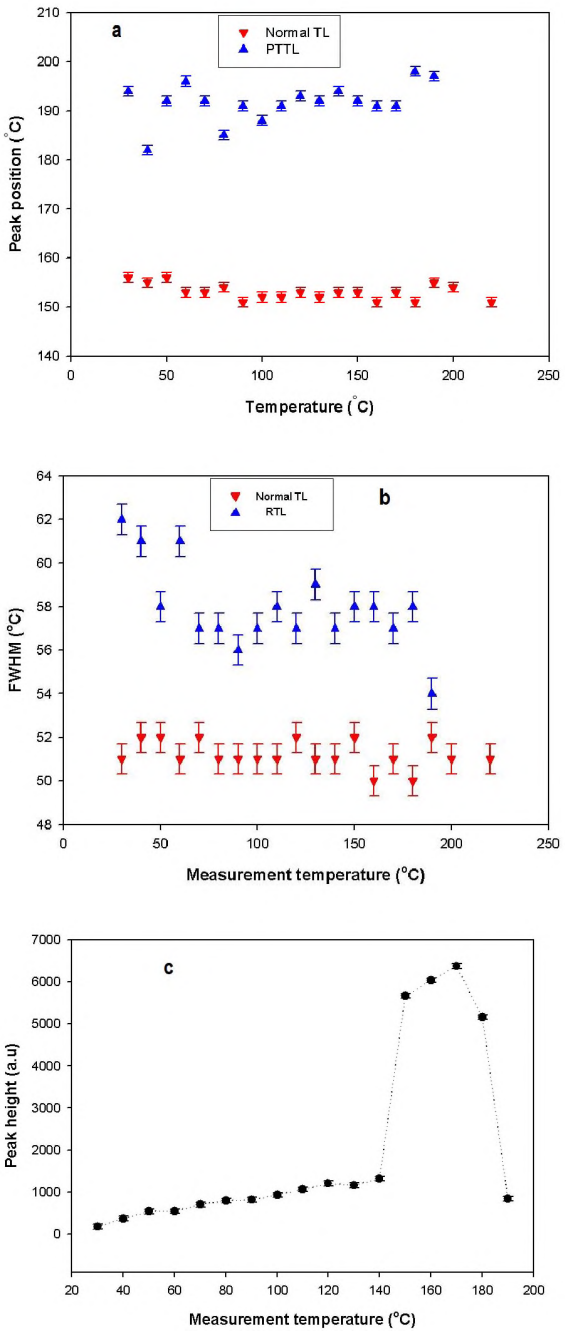

Figure 5.12: Comparative plots of the residual and normal TL in terms of peak position (a), FWHM (b) and peak intensity (c) against the measurement temperature of the TR-OSL from the deep traps.

temperature component peak. Polymeris and Kitis [37] also observed an increase in FWHM of the main RTL peak using CW-OSL light stimulation modality.

Figure 5.12c shows that the peak height of the main RTL peak increases slowly for measurement temperatures between 30-140°C, thereafter increases rapidly peaking at 170°C followed by a decline. The increase in peak height of the main RTL peak with measurement temperature between 30-170°C is as a result of thermal assistance mechanisms during the OSL readout stage. The decrease beyond 170°C may be due to a combined effect of thermal quenching and less retrapping at the main trap. In the next section, we explore the concept of thermal assistance in a greater detail.

5.7 Thermal assistance

Thermal assistance is a phenomenon that is associated with the increase in the integrated OSL observed when OSL is measured at elevated temperatures. Markey, et al [48] ascribes the phenomenon to two possible effects:

1. shallow traps recapture charges from the deep traps during optical stimulation. Raising the measurement temperature reduces the lifetime of these captured charges in the shallow traps and increases the probability of direct recombinations at the luminescence centres. This effect is realised by an observed reduction in the decay time.

2. a thermally activated process at the wavelengths used for optical stimulation. For example, an optical transition raises charge to an intermediate excited state just below a delocalized band where thermal stimulation is sufficient to raise the charge into the band.

In the case of α-Al_2O_3:C, Markey, et al [48] concedes that "it is difficult to separate the temperature dependence of the OSL due to the deep traps from that of the OSL due to the dosimetric traps". It is the aforementioned statement that motivated us to make a detailed investigation into this phenomenon. Different methods of investigations were employed e.g different annealing temperatures prior to OSL readout, high dose, low dose and different stimulation times. In this section we present the results of these

investigations which have been compared against the results obtained elsewhere in this work and those by other researchers.

All the activation energies of thermal assistance presented in this section were obtained using the Arrhenius analysis of the integrated OSL signal in which a straight line fit of the ln(Integrated OSL) vs. 1/kT yields the activation energy of the thermally assisted OSL process. Except for the sample used, all investigations were independent of each other.

5.7.1 Investigations based on the normal OSL

A sample was first heated to 500°C at 1°C/s to clear background charge from the acceptor traps. It was then irradiated to 5.0 Gy followed by a CW-OSL measurement at temperature T_i for 500 s and finally heated to 500°C at 1°C/s to clear residual charge from the acceptor traps. This was repeated for measurement temperature T_i between 30-300°C. The whole exercise was repeated using an empty sample holder to record the noise signal at each measurement temperature which was subtracted from the total OSL signal. It should be made clear that noise signal obtained at all the measurement temperatures was negligible and had no impact on the original data. Figure 5.13 shows integrated OSL plotted against measurement temperature (a) and the corresponding Arrhenius plot (b).

As expected, the integrated OSL increases with measurement temperature between 30-160°C, thereafter it decreases monotonically. The increase in the OSL yield between 30-160°C is what is associated with the phenomenon of thermal assistance. The decrease beyond 160°C may be a combined effect of less retrapping at the main trap of the charges stimulated from the deep traps and thermal quenching of the recombination sites at these higher temperatures. The activation energy of thermal assistance as evaluated from the Arrhenius plot between 30-160°C is $E_a = 0.066 \pm 0.002$ eV .

5.7.2 Investigations based on the annealing temperature

In this investigation, we were interested in finding out if the maximum temperature i.e. the annealing temperature to which a sample is heated after beta irradiation and

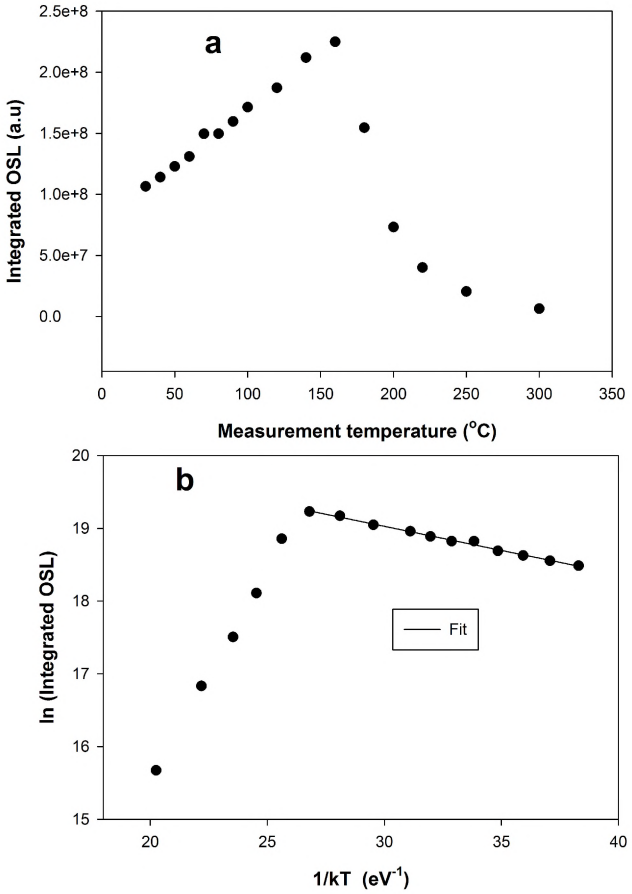

Figure 5.13: The integrated OSL plotted against measurement temperature (a) and the corresponding Arrhenius plot (b). The activation energy of thermal assistance, $E_a = 0.066 \pm 0.002$ eV.

prior to OSL readout has an effect on the activation energies of thermal assistance. For this purpose, we carried out the following procedure:

1. A preheat at 1°C/s to 500°C to remove background dose.

2. Irradiated once to 1.0 Gy.

3. Heating at 1°C/s to a preset annealing temperature, T_{max}.

4. CW-OSL measured at 30°C for 1000 s.

   Steps 3-4 were repeated until the total OSL yield was (almost) constant.

5. Heating at 1°C/s to a preset annealing temperature, T_{max}.

6. CW-OSL at a measurement temperature T_i for 1000 s, for T_i's between 30-300°C.

This procedure was carried out for the thermal annealing temperatures, T_{max} of 400, 500, 600 and 700°C. For a given thermal annealing temperature T_{max}, the whole procedure was repeated with an inclusion of a 120-s pause between the heating to a preset annealing temperature and the CW-OSL readout. The pause was meant to allow the sample to cool down properly to a preset measurement temperature T_i before commencing the CW-OSL measurement. These two sets of measurements will also be referred to as "Without pause" and "With 120 s pause", respectively. Figure 5.14 shows plots of the normalized integrated OSL against the number of runs. Figure 5.15 presents the plots of the integrated OSL as a function of measurement temperature for all the annealing temperatures used and Figure 5.16 shows the corresponding Arrhenius plots.

Note that Figure 5.14 has been presented here just to show that the OSL yield became steady after a certain number of repeated OSL measurements and will not be discussed further.

It is clear from Figure 5.15 that both the annealing temperature and the 120-s pause have a remarkable effect on the curves of the integrated OSL against measurement temperature. Firstly, all the plots of the integrated OSL vs. measurement temperature go through a peak between 180-220°C. Secondly, they all show a decrease in the integrated OSL for measurement temperatures between 30-60°C. Thirdly, the integrated OSL for the measurements made without a pause are generally higher than their corresponding integrated OSL obtained with a 120-s pause. Furthermore, all the measurements made in the presence of the 120-s pause show an increase with measurement temperature beyond 240°C, something that is apparently absent in the measurements made without a pause.

According to the Arrhenius plots presented in Figure 5.16, there are two activation energies of thermal assistance for the low temperature region (70-100°C) and intermediate temperature region (120-180°C), respectively. Hereafter, we will call the activation energy of thermal assistance for the low temperature region E_{a1} and that for the intermediate temperature region, E_{a2}. The results of the analysis have been summarised in Table 5.1.

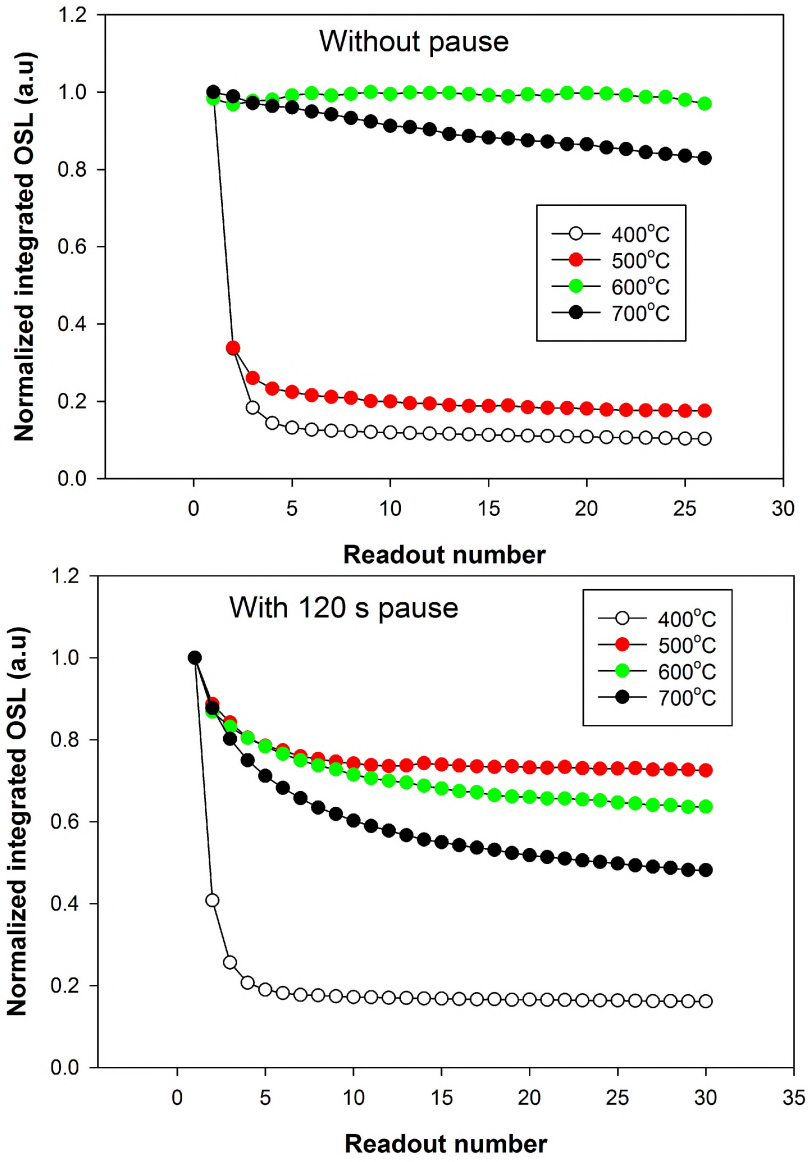

Figure 5.14: Plots of the normalized integrated OSL against the number of runs. The sample was irradiated once at the beginning to 1.0 Gy and then illuminated repeatedly with 470-nm blue LEDs at 30°C until the OSL output was constant.

It is clear from Table 5.1 that for all the annealing temperatures, the activation energy of thermal assistance evaluated from the measuments made without pause is generally higher that from the corresponding measurement made with a 120-s pause. The activation energies, E_{a1} and E_{a2} evaluated from measurements made without a pause are separately consistent with each other. Likewise, E_{a1} and E_{a2} evaluated from measurements made with a 120-s pause are separately consistent with each

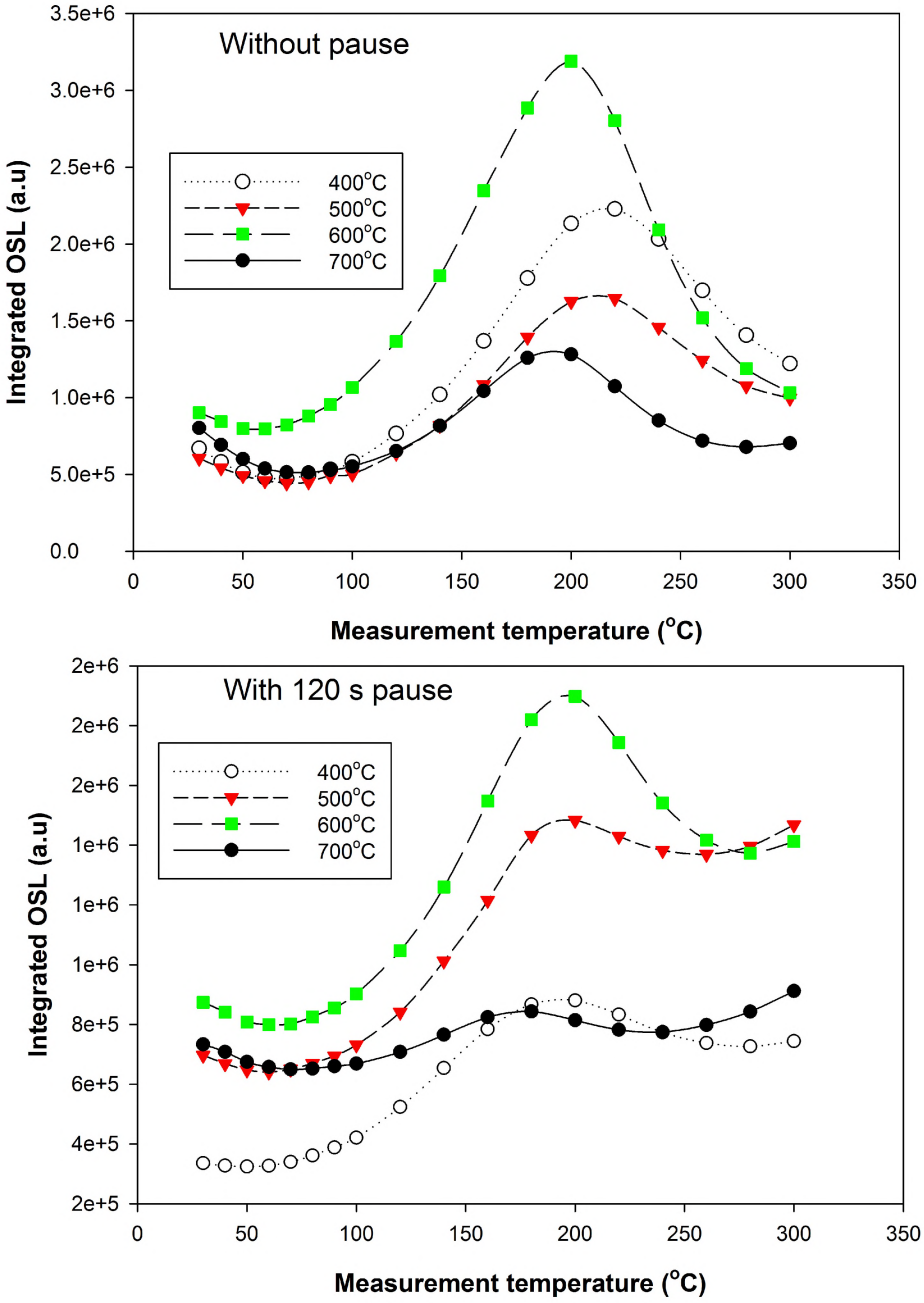

Figure 5.15: Plots of the integrated OSL as a function of measurement temperature for various thermal annealing temperatures. The sample was irradiated once to 1.0 Gy, illuminated repeatedly with 470-nm blue LEDs at 30°C until the OSL output was constant as shown in Figure 5.14 followed by CW-OSL measurements at elevated temperatures.

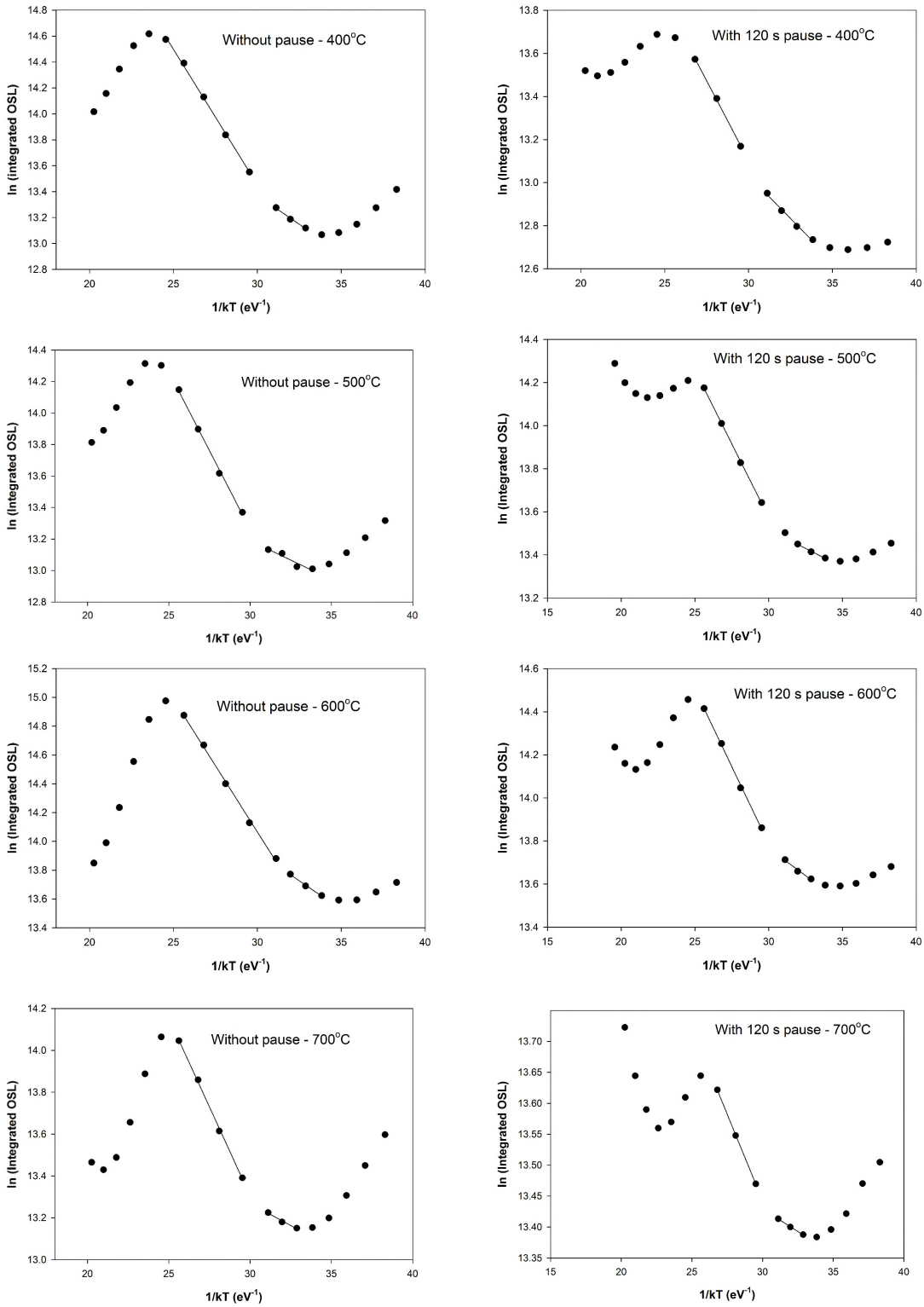

Figure 5.16: Arrhenius analysis of the plots presented in Figure 5.15. See Table 5.1 for results.

Table 5.1: A summary of activation energies for the Arrhenius plots presented in Figure 5.16. E_{a1} and E_{a2} are the activation energies of thermal assistance for the low temperature region (70-100°C) and intermediate temperature region (120-180°C), respectively.

Annealing temperature(°C)	Pause (s)	E_{a1} (eV)	E_{a2} (eV)
400	0	0.089±0.008	0.209±0.005
	120	0.079±0.005	0.148±0.004
500	0	0.05±0.01	0.200±0.007
	120	0.035±0.003	0.137±0.002
600	0	0.080±0.006	0.184±0.005
	120	0.051±0.006	0.143±0.004
700	0	0.042±0.006	0.170±0.004
	120	0.015±0.006	0.056±0.006

other except for the annealing temperature of 700°C which yields relatively very low activation energies for both E_{a1} and E_{a2}. These low activation energies will not be included in our further analyses. The mean values of E_{a1} and E_{a2} as presented in Table 5.1 are:

without pause: $E_{a1} = 0.065 \pm 0.008$ eV and $E_{a2} = 0.192 \pm 0.005$ eV;

with 120-s pause: $E_{a1} = 0.055 \pm 0.005$ eV and $E_{a2} = 0.143 \pm 0.003$ eV.

We will use these mean energy values hereafter to refer to the activation energies in Table 5.1.

5.7.3 Investigations based on different illumination times

A sample was first heated to 500°C at 1°C/s to clear background charge from the acceptor traps. It was then irradiated to 5.0 Gy followed by a CW-OSL measurement at a temperature T_i for an illumination time of 300 s and finally heated to 500°C at 1°C/s to clear residual charge from the acceptor traps. This was repeated for measurement temperature T_i between 30-300°C. The whole exercise was repeated for illumination times of 1000 s and 1500 s. Figure 5.17 shows the plots of the integrated OSL against measurement temperature and their corresponding Arrhenius plots for the various illumination times used.

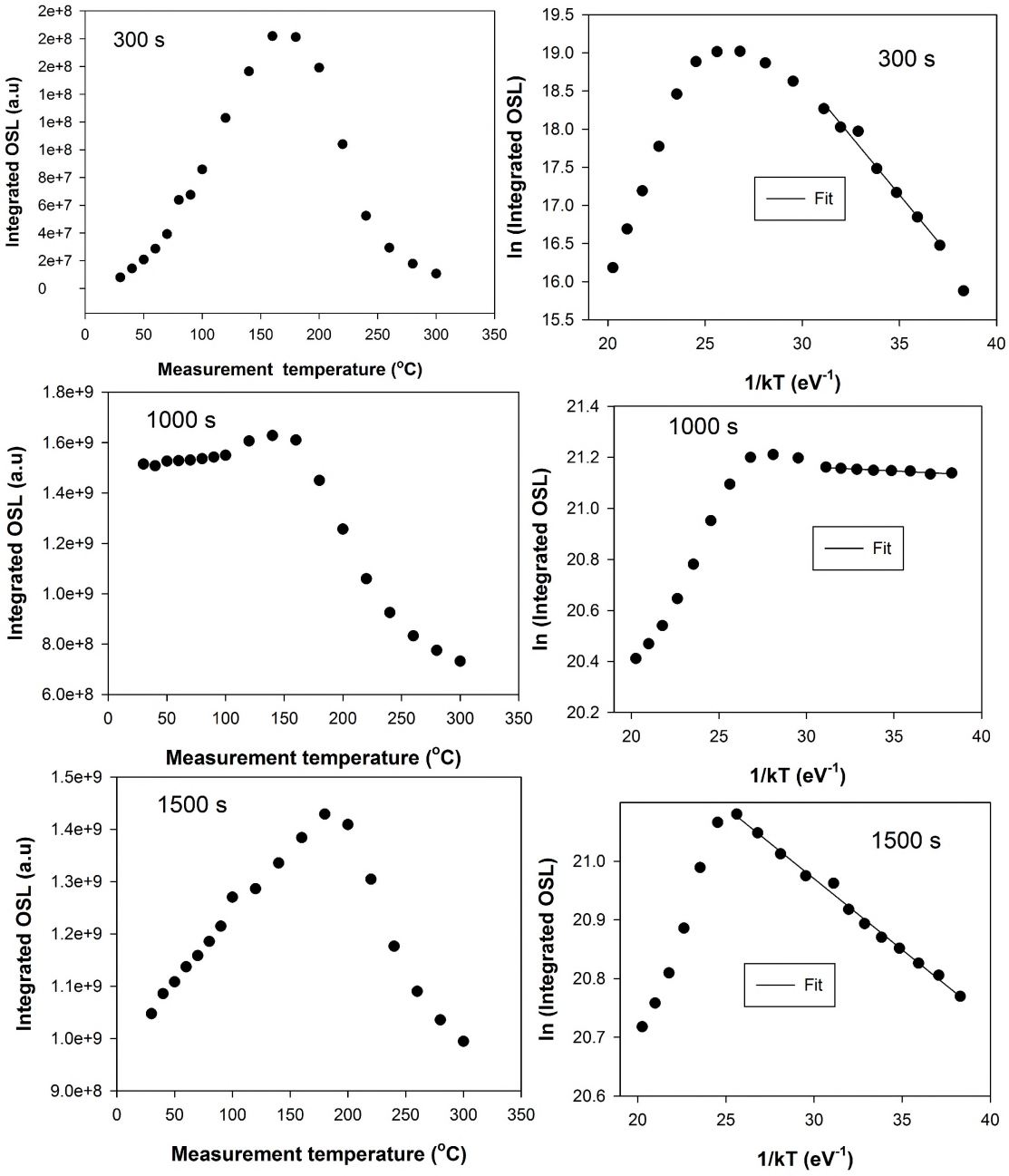

Figure 5.17: Plots of the integrated OSL against measurement temperature and their corresponding Arrhenius plots for the various illumination times of 300, 1000 and 1500 s. For 300 s, $E_a = 0.31 \pm 0.02$ eV (40-100°C); for 1000 s, $E_a = 0.0030 \pm 0.0005$ eV (30-100°C) and for 1500 s, $E_a = 0.024 \pm 0.006$ eV (30-180°C).

The activation energy of thermal assistance for the illumination times used are as follows:

300 s, $E_a = 0.31 \pm 0.02$ eV evaluated between 40-100°C;

1000 s, $E_a = 0.0030 \pm 0.0005$ eV, 30-100°C and

1500 s, $E_a = 0.024 \pm 0.006$ eV, 30-180°C.

It is readily seen that the activation energy of thermal assistance is much higher for the 300-s illumination time, intermediate for the 1500-s and lowest for the illumination time of 1000 s. The cause of such a wide variation requires further investigations.

Table 5.2 provides a comparison of the activation energies of thermal assistance as reported in this work against those reported by other researchers using various techniques of investigation. Note that the activation energies reported by Polymeris, et al [44, 37] are both much higher and incomparable to any of our results. One can

Table 5.2: A summary of activation energies of thermal assistance in α-Al_2O_3:C. ET represents exposure or illumination time in seconds; IT is irradiation temperature in °C; E_{a1} and E_{a2} are activation energies in eV as evaluated in a given temperature region (Range in °C). Pause represents the pause time between a preheat and a subsequent OSL readout.

Researcher	Method	Pause	ET	IT	E_{a1}	Range	E_{a2}	Range
This work	DT CW-OSL	0			0.065±0.008	70-100	0.192±0.005	120-180
		120			0.055±0.005	70-100	0.143±0.003	120-180
			300		0.31±0.02	40-100		
			1000		0.0030±0.0005	30-100		
			1500		0.024±0.006	30-80		
	CW-OSL				0.066±0.002	30-160		
	TR-XEOL			RT	0.15±0.01	30-80	0.59±0.06	90-140
				400	0.082±0.006	100-140	0.295±0.003	160-180
	XERL				0.008±0.001	30-120		
Polymeris, et al [44]	TA-OSL				1.21±0.16	80-180		
Polymeris, et al [37]	TA-OSL				3.07±0.23			
Chithambo and Costin [28]	TR-OSL				0.054±0.001	40-90	0.53±0.03	110-150

appreciate from Table 5.2 that, despite some activation energies being similar, it is generally extremely difficult to interpret the activation energies presented. It may not be possible to say in confidence that a particular activation energy is associated with a particular trap. The results of this investigation suggest that thermal assistance is a more complex phenomenon than usually treated and that deliberate efforts are required to systematically study the phenomenon in the material.

5.8 Summary

In this chapter, we have presented the results of investigating the OSL obtained by stimulation of deep traps in α-Al_2O_3:C. We have identified the optically active traps as the main trap i.e. main OSL trap, and the traps in the temperature range between 400-550°C i.e. the secondary OSL traps. We have argued that the secondary OSL traps may necessarily be electron traps and not hole traps as is generally accepted.

Under CW-OSL technique, we have seen that the deep-traps CW-OSL exhibits a peak-shaped signal, the presence/absence of which depends on the beta irradiation dose, post-irradiation annealing temperature, illumination light, concentration of charges in the main trap and the measurement temperature. The necessary condition for the deep-traps CW-OSL signal to exhibit a peak is that the secondary OSL traps and the donor deep traps should be sufficiently occupied with charge and that the main trap be sufficiently empty.

Our results have also indicated that in deep-traps CW-OSL, most of the charges released from donor deep traps during optical stimulation get recaptured by the main trap before undergoing recombination at the luminescence centres. Furthermore, the secondary OSL traps are the major contributors of the charges that undergo retrapping at the main trap during optical stimulation. The most probable route by which charges stimulated from the deep traps get recaptured at the acceptor traps is via the delocalized bands. The aforementioned results were also confirmed using the TR-OSL technique.

In the investigations using TR-OSL due to deep-traps stimulation, a plot of the lifetimes against measurement temperature is a replica of the plot derived using conventional TR-OSL. The lifetimes exhibit thermal quenching effects at higher temperatures with an activation energy of 1.028 ± 0.002 eV.

Finally, the phenomenon of thermal assistance has been studied using Arrhenius analysis to extract the activation energies. The results of this exercise are far from conclusive. It is a challenge to interpret the values of the activation energies obtained. A systematic study is needed in order to make sense of the activation energies of thermal assistance in α-Al_2O_3:C.

Chapter 6

Radiation induced defects in α-Al_2O_3:C

It is known that exposing Al_2O_3 to heavy irradiation by particles e.g. neutrons, not only modifies the structure of the material but also induces new defects in the material [49, 50]. The common radiation-induced defects that have been reported for oxides i.e. α-Al_2O_3:C include complex aggregates of F_2 centres in different charged states i.e. F_2^+ and F_2^{2+} [51, 52]. The F_2, F_2^+ and F_2^{2+} are aggregates of two oxygen vacancies that have captured four, three and two electrons, respectively.

In this chapter, we present and discuss results on the influence of radiation-induced defects in α-Al_2O_3:C on the TL and OSL measured after high-dose beta irradiation. The effects of a 1000-Gy beta irradiation dose on the TL properties of the main peak and on the overall OSL response of the material, is presented first. Secondly, the effect of the 1000-Gy beta irradiation dose on the OSL properties of the material are described. Finally, we report on the dynamics of the radiation-induced defects with dose by monitoring the TL response of the main peak and the low-temperature peak (peak I) for beta irradiation doses ranging from 5.0 Gy to 1500 Gy.

6.1 The thermoluminescence glow curve following heavy beta-irradiation

An annealed sample was irradiated to 1000 Gy then heated to 300°C at 1°C/s (in the presence of a neutral density filter) to record a TL glow curve. The sample was immediately thereafter heated again from room temperature to 700°C at 1°C/s to record a second TL glow curve. A third TL glow curve was then measured from room temperature to 700°C at 1°C/s following beta irradiation to 1.0 Gy. The three TL glow curves are shown in Figure 6.1.

Figure 6.1a shows a semi-log plot of the TL glow-curve measured to 300°C showing peaks centred at 48, 78, 149, and 282°C. This is denoted as Run 1. The dominant peak at 149°C is generally referred to as the main peak. This peak is well known for its dosimetric applications. Figure 6.1b shows the TL glow curve measured immediately after Run 1 (denoted as Run 2) and the TL glow curve measured after Run 2 following a 1.0-Gy beta irradiation dose (denoted as Run 3). In the inset of Figure 6.1b are the corresponding TL glow curves (Run2 and Run 3) in semi-log scale. The glow curve from Run 2 shows peaks centred at 198, 281, 560°C and a relatively less intense broad peak between 330-490°C. The TL glow curve from Run 3 shows peaks centred at 45, 175 and 281°C as well as a broad peak between 330-520°C. The peak at 175°C is the dosimetric peak.

It is noted that the main peak is centred at 149°C in Run 1 corresponding to 1000 Gy and at 175°C in Run 3 for 1.0 Gy . This change in position of the main peak with dose is expected since it is known that the main peak shifts towards lower temperatures at high beta irradiation doses [53, 54].

It is also expected that heating the sample at a rate of 1°C/s to 300°C following 1000 Gy beta irradiation should completely clear the main peak which covers the 90-250°C temperature range. However, as shown in Run 2 of Figure 6.1b, the main peak is obviously visible albeit less intense and shifted towards higher temperatures. This indicates presence of charge in the main trap without any irradiation. It is only reasonable to suggest that charge carriers leak away from those traps that are not destabilized by heating to 300°C. The mechanism through which the main trap gets repopulated with charge carriers in the presence of filled higher temperature traps

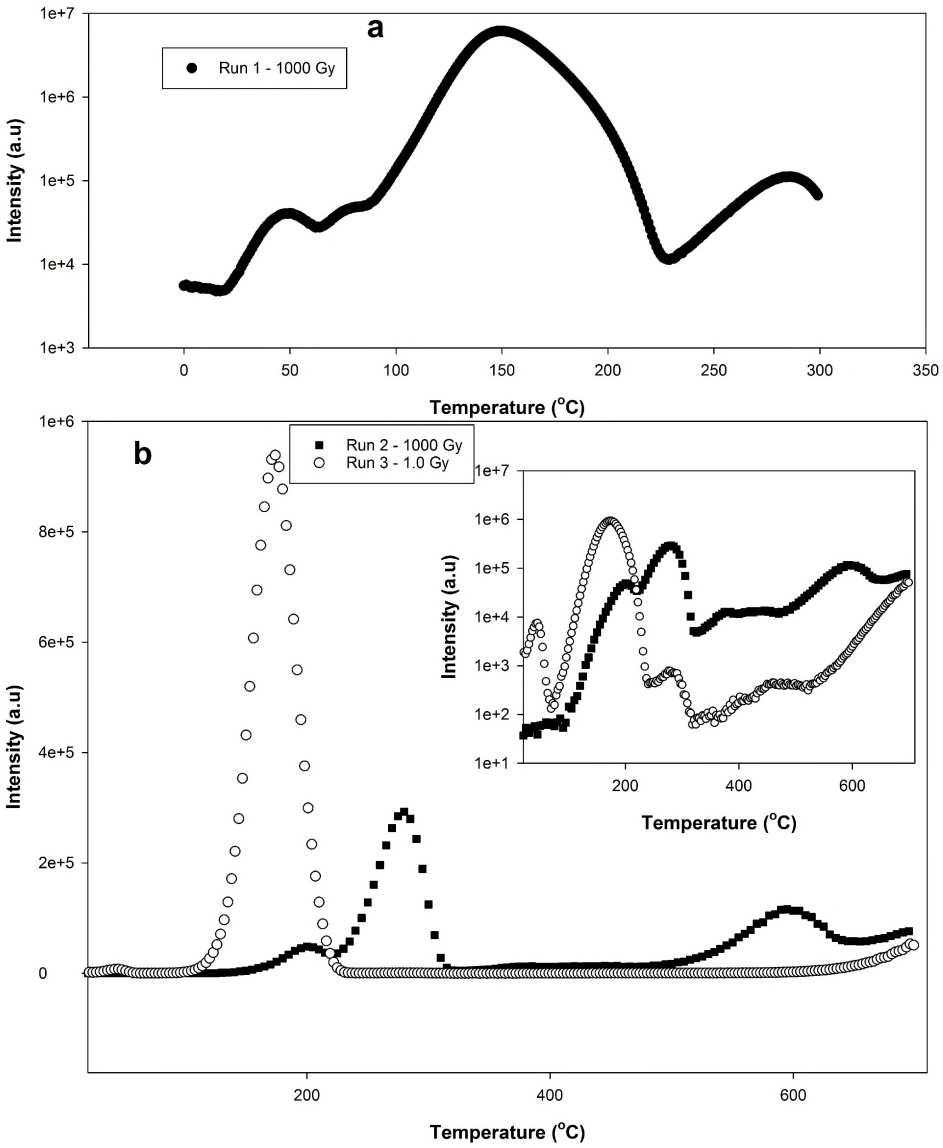

Figure 6.1: Plots of TL glow curves recorded at 1°C/s. Run 1 (whose plot is shown in a semi-log scale) was measured from room temperature to 300°C following 1000 Gy beta irradiation (a); Run 2, from room temperature to 700°C without further irradiation measured immediately after Run 1 whereas Run 3 was measured from room temperature to 700°C following a 1.0 Gy beta irradiation dose (b). The inset in (b) shows glow curves from Run 2 and Run 3 in a semi-log plot for visual clarity.

without any irradiation requires further investigation.

It is also clear that the TL peaks centred at 78°C in Run 1 of Figure 6.1a, and 560°C in Run 2 of Figure 6.1b were only observed in the TL glow curve measured fol-

lowing a 1000-Gy beta irradiation dose. The presence of these two peaks can therefore be attributed to new defects which act as charge trapping sites, presumably created by the heavy beta irradiation dose i.e. 1000 Gy. In addition, heating the sample to 700°C (Run 2) after the 1000 Gy beta irradiation apparently destroys the induced defects and their associated traps as evident from absence of these 78°C and 560°C peaks in the TL glow-curve from Run 3 in Figure 6.1b that was measured following beta irradiation to 1.0 Gy. The thermal destruction of the irradiation induced defects due to annealing at 700°C was also reported by Harutyunyan et al [55] for the same material.

It is also possible that the assumed radiation-induced defects are always present in the material except that they are less effective at low beta irradiation doses. As will be seen in the subsequent sections, the radiation-induced defects have a profound effect on the TL response of particularly the main peak. If these defects were 'naturally' present in the material, there would be no observable significant changes in the parameters of the main peak.

The fact that the radiation-induced trapping centres produce TL peaks without further beta irradiation proves that these newly created trapping centres are filled with charge carriers during the high-dose irradiation. In other words, the new trapping centres are simultaneously created and populated with charge during the high-dose irradiation.

In this study, we focus on the radiation-induced defects that produce TL peak(s) in the range 480-650°C and centred at 560°C (see Run 2).

6.2 Stability of the TL peaks associated with the radiation-induced defects under sunlight exposure

In this experiment, a sample was irradiated to 1000 Gy then immediately thereafter exposed to direct sunlight for 9 hours. The temperatures of the day ranged from 7-16°C. Considering that α-Al_2O_3:C is well-known for its sensitivity to light, the motivation of the study was to investigate the behaviour of the radiation-induced

defects in the presence of light.

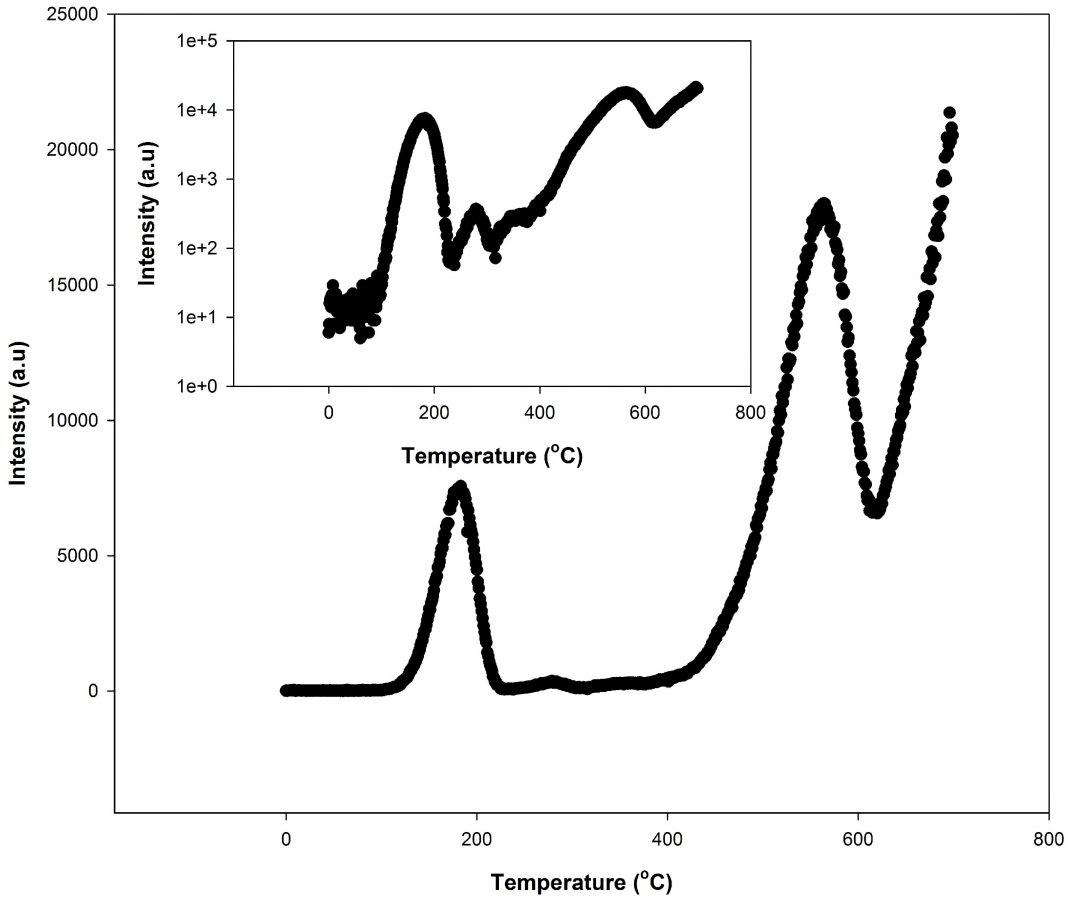

Figure 6.2: A TL glow curve recorded at 1°C/s after 9 hours of sunlight exposure of the sample previously irradiated to 1000 Gy. The inset shows the same plot in a semilog plot for visual clarity.

Figure 6.2 shows the measured TL glow curve, and in the inset, the same data on a semi-logarithmic scale. It can be seen in Figure 6.2 that the peak at 45°C and the additional peak at 78°C produced by the heavy beta irradiation dose of 1000 Gy (see Figure 6.1) are completely removed by sunlight exposure. The main peak is centred at 183°C whereas the high temperature peak produced by the radiation-induced defects is still at 564°C. In addition, the intensities of all the peaks are significantly less than those of peaks obtained immediately after 1000-Gy beta irradiation, that is, without exposure to sunlight (see Figure 6.1). Comparatively, the dosimetric peak decreased substantially whereas the peak at 564°C was apparently the least affected. This result indicates that under light exposure, specifically sunlight, the radiation-induced

defects are more stable than the shallow (peak I), main (peak II) and subsidiary traps (peaks III, IV, V and VI). This stability suggests that the radiation-induced defects may in fact be complex. The stability of the induced defects as seen means that they are amenable to being adapted for high radiation dose TL dosimetry.

6.3 Effects of the radiation-induced defects on the thermoluminescence response of the main peak

The samples used in this investigation were annealed once at 900°C for 15 minutes before use. The following protocols, namely, Protocol 1 and the Modified Protocol 1, were used to investigate the effects of heavy beta irradiation dose (1000 Gy) on the TL response of the main peak. A beta irradiation dose of 1000 Gy was used for this purpose. The same sample was used throughout the investigation.

Protocol 1

Stage 1

1. A preheat at 1°C/s to 700°C to remove any residual dose
2. Beta-irradiation to a test dose of 1.0 Gy (for monitoring changes in the TL response of the main peak)
3. TL at 1°C/s to 400°C

   Steps 2-3 were repeated 10 times. The TL measurements in step 3 shall be referred to as **TL A**.

Stage 2

4. Beta-irradiation to 1000 Gy (intended to induce defects)
5. A preheat at 1°C/s to 400°C (to clear the main peak)
6. Beta-rradiation to a test dose of 1.0 Gy (used to monitor changes in TL)
7. TL at 1°C/s to 400°C

   Steps 6-7 were repeated 10 times. The TL measurements in step 7 shall be referred to as **TL B**.

Stage 3

8. A preheat at 1°C/s to 700°C (intended to remove radiation-induced defects)

9. Beta-irradiation to a test dose of 1.0 Gy (used to monitor changes in TL)

10. TL at 1°C/s to 400°C

    Steps 9-10 were repeated 10 times. The TL measurements in step 10 shall be referred to as **TL C**.

Each irradiation was preceded by a 120-s pause to ensure that the sample was irradiated at room temperature.

In order to isolate the influence of the 1000-Gy beta irradiation dose and its associated radiation-induced defects on the TL main peak, *Stage 2* of Protocol 1 was modified by preheating the sample to 700°C instead of 400°C (step 5) immediately after 1000 Gy irradiation i.e. the modified protocol involves two separate preheats to 700°C, the other being at the beginning of *Stage 3*. This modified version of Protocol 1 shall be referred to as Modified Protocol 1. Both Protocol 1 and Modified Protocol 1 were repeated for TL glow curves measured to 500°C instead of 400°C.

The influence of the high-dose beta irradiation is assessed by monitoring changes in behaviour of the position, FWHM, maximum intensity and consequently the trap depth of the main peak. It is only necessary at this stage to summarize the important terminology used in our results.

For Protocol 1:

TL A represents the 10 TL measurements made before sample beta irradiation to 1000 Gy.

TL B are the 10 TL measurements recorded after the 1000 Gy beta irradiation and before the preheat to 700°C.

TL C are the 10 TL measurements carried out after the preheat to 700°C.

For Modified Protocol 1:

TL A represents the 10 TL measurements made before beta 1000 Gy irradiation.

TL B represents the 10 TL glow curves measured after 1000 Gy beta irradiation then a preheat to 700°C.

TL C represents the 10 TL measurements carried out after a preheat to 700°C following **TL B** measurements.

6.3.1 Influence of heavy beta irradiation dose on the position of the main peak

Figure 6.3 presents the plots of peak position of the main peak obtained in **TL A**, **TL B** and **TL C** using Protocol 1 and Modified Protocol 1 for TL glow curves measured to a maximum temperature of 400°C (a nd b) and 500°C (c and d).

It can be seen from Figure 6.3a that the positions of the main peak in the TL glow curves obtained in **TL A** (166-170°C) are equivalent to those obtained in **TL C** (170-173°C) albeit slightly higher in **TL C**. Figure 6.3a also shows that the position of the main peak shifts towards higher temperatures (182-184°C) in the TL glow-curves obtained in **TL B**. This result strongly suggests that the defects induced in the sample following the 1000-Gy beta irradiation dose are responsible for the shift of the main peak towards higher temperatures. The result also attests to the earlier observation that heating the sample to 700°C obliterates the radiation induced point-defects and resets the sample.

Figure 6.3b shows that the position of the main peak is unaffected when the sample is preheated to 700°C immediately following the heavy beta irradiation (**TL B**). This result confirms the role of the radiation-induced defects in the shift of the peak position observed in Figure 6.3a. As expected, the second preheat of the sample to 700°C does not affect the position of the main peak (**TL C**). This result suggests that merely heating the sample to 700°C does not affect the position of the peak.

Figure 6.3c shows that the positions of the main peak in the TL glow curves obtained in **TL A** (172-173°C) are equivalent to those obtained in **TL C** (172-175°C). In addition, Figure 6.3c indicates that the position of the main peak shifts towards higher temperatures (182-183°C) in the TL glow-curves obtained in **TL B**. On the other hand, Figure 6.3d shows that the position of the main peak remains unaffected when the sample is preheated to 700°C immediately following the heavy beta irradiation (**TL B**).

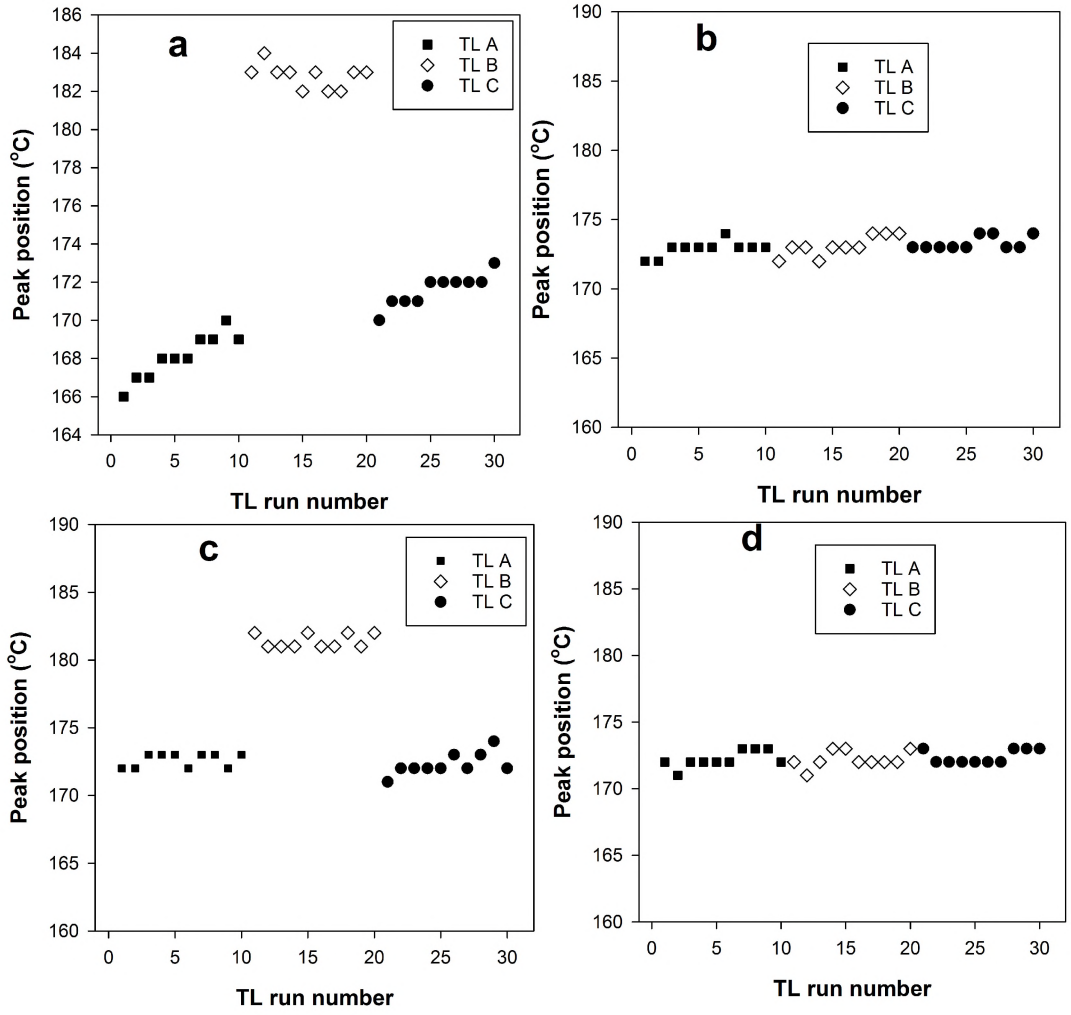

Figure 6.3: Behaviour of the position of the main peak when TL is measured at 1°C/s to 400°C using Protocol 1 (a); 400°C using Modified Protocol 1 (b); 500°C using Protocol 1 (c) and 500°C using modified Protocol 1 (d). The sample was given a test dose of 1.0 Gy prior to each TL measurement.

The behaviour of the peak position as shown in Figure 6.3c and Figure 6.3d for the TL glow curves measured to 500°C is similar to that shown in Figure 6.3a and Figure 6.3b, respectively. Hence, the explanations given above for Figure 6.3a and Figure 6.3b also apply to Figure 6.3c and Figure 6.3d. This result signifies that measuring the TL glow curve to a maximum temperature of 400°C or 500°C is immaterial in this case since the behaviour of the peak position is identical in either case.

6.3.2 Influence of heavy beta irradiation dose on the width of the main peak

Figure 6.4 presents the plots of FWHM of the main peak obtained in **TL A**, **TL B** and **TL C** using Protocol 1 and Modified Protocol 1 for TL glow curves measured to a maximum temperature of 400°C (a nd b) and 500°C (c and d).

It can be seen from Figure 6.4a that the values of the FWHM of the main peak in the TL glow curves obtained in **TL A** i.e. 31-35°C are equivalent to those obtained in **TL C** i.e 32-33°C. However, according to Figure 6.4a, the FWHM of the main peak increases to 36-39°C in the TL glow curves obtained in **TL B**. As was the case with the shifting of the peak position, this broadening of the main peak is ascribed to the radiation-induced defects in the sample due to the 1000-Gy beta irradiation dose. Essentially, this means that new emission components that contribute to the already existing main peak emissions, are created by the high beta irradiation dose.

Figure 6.4b shows that the FWHM of the main peak does not change when the sample is preheated to 700°C immediately following the 1000 Gy beta irradiation (**TL B**). This result simply confirms that radiation-induced point-defects are responsible for the broadening of the main peak. We again notice that the second preheating to 700°C does not affect the width of the main peak.

As expected, the behaviour of the FWHM of the main peak as shown in Figure 6.4c and Figure 6.4d for the TL glow curves measured to 500°C using Protocol 1 and Modified Protocol 1 respectively, is equivalent to that presented in Figure 6.4a and Figure 6.4b, respectively. This result implies that measuring the TL glow curve to a maximum temperature of 400°C or 500°C has no effect on the width of the main peak. Furthermore, this result means that merely preheating to 700°C is not enough

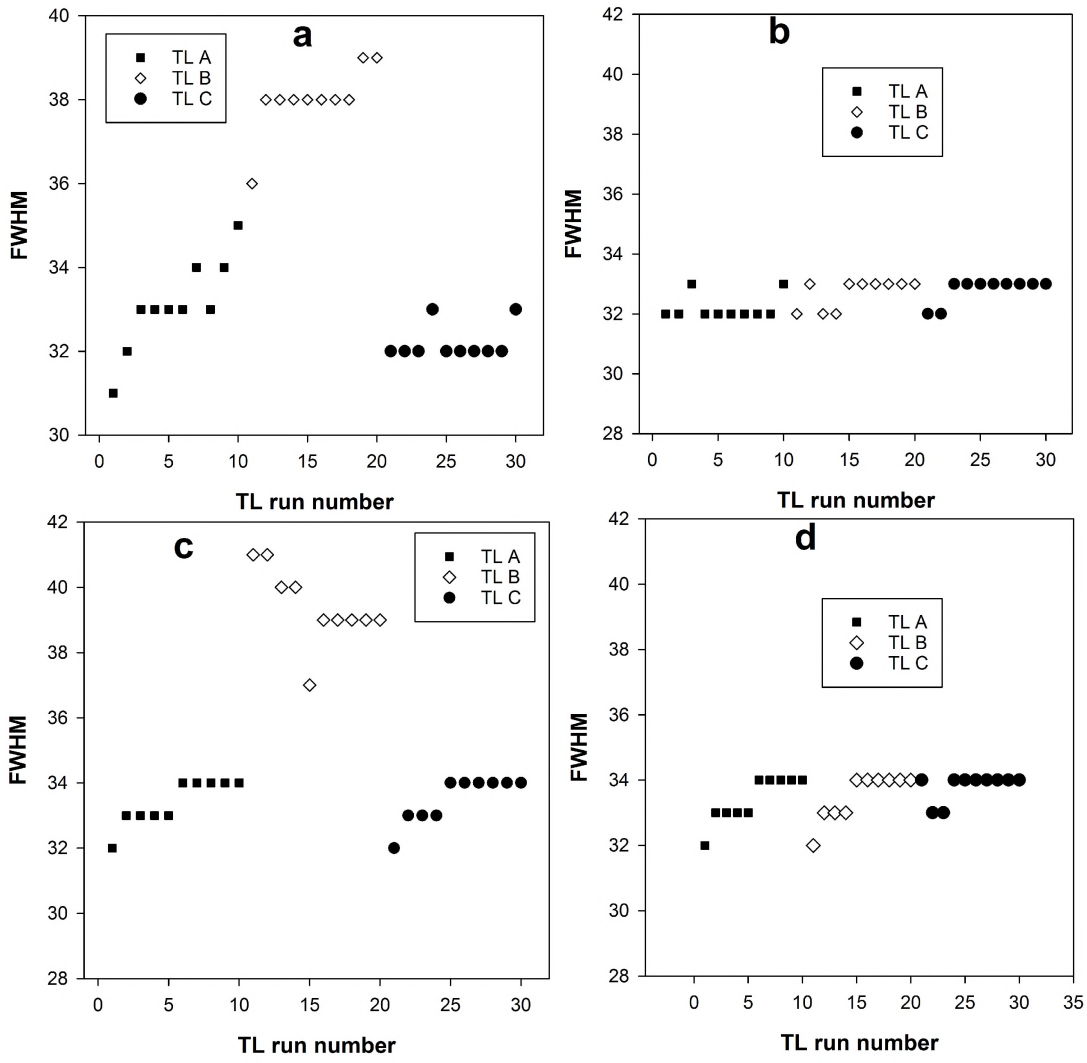

Figure 6.4: Behaviour of the FWHM of the main peak when TL is measured at 1°C/s to 400°C using Protocol 1 (a); 400°C using Modified Protocol 1 (b); 500°C using Protocol 1 (c) and 500°C using modified Protocol 1 (d). The sample was given a test dose of 1.0 Gy prior to each TL measurement.

to affect the width of the main peak.

6.3.3 Influence of heavy beta irradiation dose on the maximum intensity of the main peak

Figure 6.4 presents the plots of maximum intensity of the main peak obtained in **TL A**, **TL B** and **TL C** using Protocol 1 and Modified Protocol 1 for TL glow curves measured to a maximum temperature of 400°C (a nd b) and 500°C (c and d).

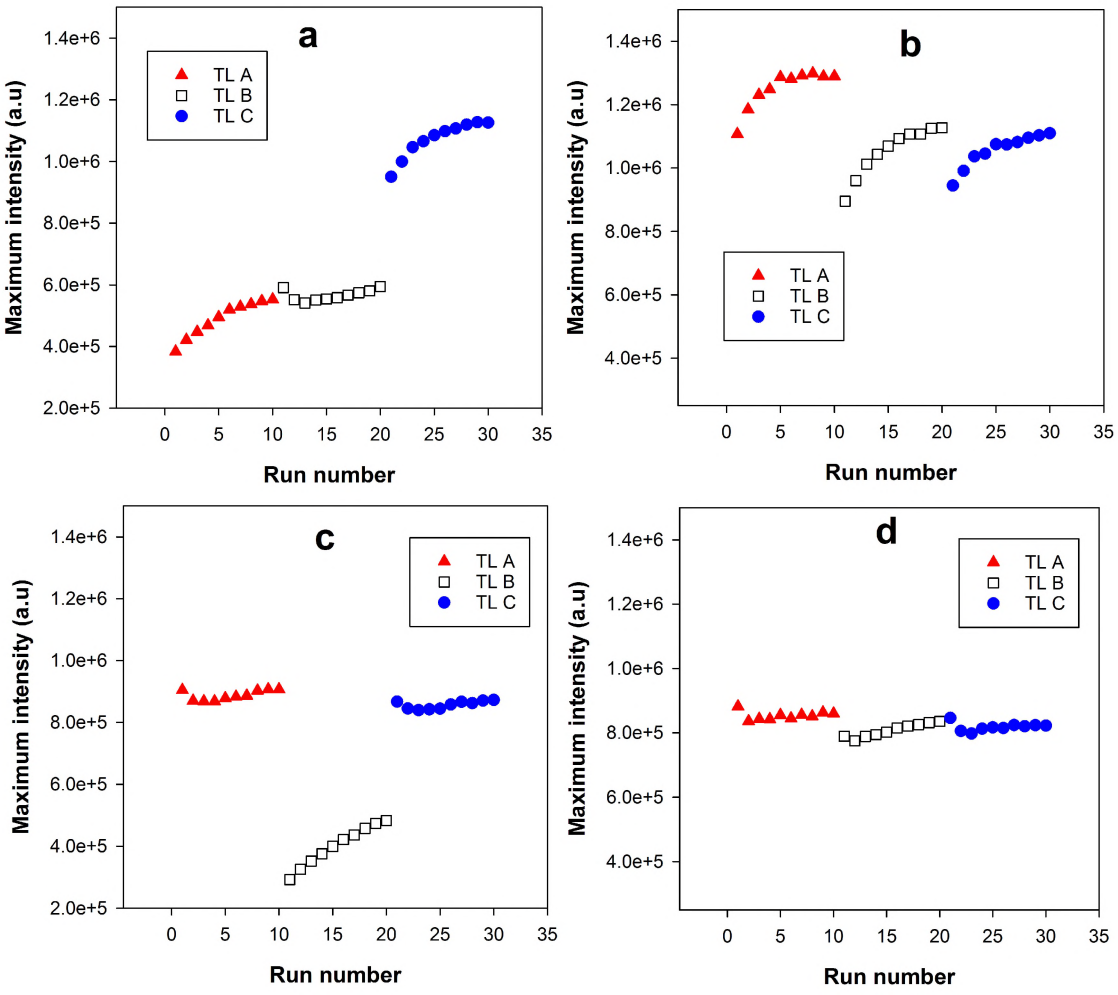

Figure 6.5: Behaviour of the maximum intensity of the main peak when TL is measured at 1°C/s to 400°C using Protocol 1 (a); 400°C using Modified Protocol 1 (b); 500°C using Protocol 1 (c) and 500°C using modified Protocol 1 (d). The sample was given a test dose of 1.0 Gy prior to each TL measurement. For better comparison, all the graphs have been drawn using the same range of intensities.

It is clear from Figure 6.5a that the maximum intensity of the main peak for TL glow curves obtained in **TL A** increases gradually with number of TL runs. This trend is maintained in **TL B** after the heavy beta irradiation dose. However, after preheating to 700°C, the maximum intensities obtained in **TL C** are significantly higher (by greater than 30 %) compared to those in either **TL A** or **TL B**. This shows an increased TL sensitivity of the sample to the test dose of 1.0 Gy . Basically, the results in Figure 6.5a show that the 1000 Gy and the radiation-induced defects associated with it, does not affect the behaviour of the maximum intensities of the main peak. However, the heating of the sample to 700°C coupled with the thermal obliteration of the radiation-induced defects at the onset of *Stage 3*, does affect the maximum intensities of the main peak in **TL C**. The increase of the maximum intensity with repeated irradiation-TL cycles within each stage can be attributed to deep trap filling which in turn reduces competition for charge between the main and deep traps during beta irradiation.

Figure 6.5b shows that the maximum intensity has the same behaviour in all the three stages of the Modified Protocol 1 i.e the maximum intensity gradually increases with number of TL readouts. However, the maximum intensity following each 700-°C preheat is reduced compared to the final maximum intensity in the preceding stage. This is because the preheats partially empty the deep traps consequently increasing the competition for charge between the main traps and deep traps in the subsequent irradiation cycle.

If the sample sensitization observed in **TL C** of Figure 6.5a is solely due to the heating to 700°C and the thermal destruction of the radiation-induced defects associated with it, then one would expect sample sensitization to occur in **TL B** of the Modified Protocol 1. However, this is not clearly the case as seen in Figure 6.5b. Thus, a different mechanism may be responsible for the observed sensitization.

Figure 6.5c shows that the maximum intensities obtained before the 1000-Gy beta irradiation dose (**TL A**) and those obtained post-700°C preheating (**TL C**), are equivalent in both magnitude and behaviour. In addition, we observe a major decrease (more than 40 %) in the maximum intensities of the main peak following the 1000 Gy beta irradiation (**TL B**). This indicates that preheating the sample to 700°C following heavy beta irradiation restores the sensitivity of the sample. This

behaviour is in sharp contrast to that observed when TL glow curves were measured to a maximum temperature of 400°C where the sensitivity of the sample seems not affected by heavy irradiation and preheating to 700°C significantly sensitizes the sample (see Figure 6.5a).

Figure 6.5d shows that the corresponding maximum intensities obtained in **TL A**, **TL B** and **TL C** are roughly equal. This result implies that the 1000 Gy beta irradiation causes desensitization of the sample when TL glow-curves are measured to 500°C. Secondly, it demonstrates that preheating to 700°C alone has little effect on the sensitivity of the sample.

In order to account for the actual effect i.e. sensitization or desensitization, of the radiation-induced defects on the maximum intensities of the main peak, we make the following observations from the detailed analysis of the data presented in Figure 6.5:

- the maximum intensities of the main peak in **TL A** from TL glow curves measured to 500°C are generally much greater than their corresponding intensities in **TL A** from TL glow curves measured to 400°C. This difference has nothing to do with the presence/absence of the radiation-induced defects in the material.

- the maximum intensities of the main peak in **TL B** from TL glow curves measured to 500°C are generally equivalent in magnitude to their corresponding intensities in **TL B** from TL glow curves measured to 400°C. These intensities are much lower than those obtained in **TL C** for either case.

- the maximum intensities of the main peak in **TL C** from TL glow curves measured to 500°C are generally equivalent in magnitude to their corresponding intensities in **TL C** from TL glow curves measured to 400°C.

Based on the three points above, we can conclude that the presence of the radiation-induced defects in the sample produces low maximum intensities of the main peak i.e. causes sample desensitization as is the case in **TL B**. The removal of these radiation-induced defects following the 700°C heating, simply restores the samples sensitivity as evidenced from comparable intensities in **TL C** for either case i.e. 400°C or 500°C.

6.3.4 Effect of the heavy beta irradiation dose on the activation energy of the main peak

It is now quite obvious that the heavy beta irradiation dose of 1000 Gy significantly alters the shape, position and intensities of the main peak due to the induced defects. It is only necessary therefore, to assess whether and how the activation energy of the main peak is affected. The analysis was done using Chen's peak shape [4] and computer glow curve deconvolution (CGCD) methods. In the CGCD method, the TL data were fitted using the general order equation (Equation 2.9). For this exercise, three glow curves were randomly chosen, one from each stage of Protocol 1.

Using the CGCD method, the following results were obtained:

For **TL A**: activation energy, $E = 1.71 \pm 0.01$ eV and order of kinetics, $b = 1.87 \pm 0.01$.

For **TL B**: $E = 1.23 \pm 0.01$ eV and $b = 1.33 \pm 0.01$.

For **TL C**: $E = 1.71 \pm 0.01$ eV and $b = 1.86 \pm 0.01$.

We note that the values of the activation energy of the main peak (1.71 eV) and its order of kinetics (1.87) for **TL A** and **TL C** are equal and higher in value than those obtained in **TL B** i.e. 1.23 eV and 1.33, respectively. These values indicate that the main peak can be approximated by general-order kinetics characterized by less charge retrapping in the presence of the radiation-induced defects and more charge retrapping in the absence of these radiation-induced defects.

Table 6.1 provides a summary of the results obtained by the Chen's peak-shape method [4]. It is worth noting that the parameters of the TL main peak in **TL A** and **TL C** are identical. This indicates that thermal destruction of radiation-induced defects restores the original state of the sample. The value of the geometrical factor suggests that in the presence of radiation-induced defects, the TL main peak follows general-order kinetics ($\mu = 0.44 \pm 0.02$) characterized by less retrapping whereas in the absence of these induced defects, the peak follows general-order kinetics ($\mu = 0.50 \pm 0.02$) that is characterized by more retrapping. In addition, the activation energy obtained in **TL A** and **TL C** for the main peak is significantly higher than that obtained in **TL B**. It is important to note that results obtained by these two methods of kinetic analysis are consistent within experimental errors.

Table 6.1: Activation energy of the main peak evaluated using Chen's peak shape method [4]. TL glow curves were measured to 500°C following a 1.0 Gy test dose. **TL A** represents the TL measurements made before sample beta irradiation to 1000 Gy; **TL B**, the TL measurements made after the 1000 Gy beta irradiation and before the preheat to 700°C and **TL C**, the TL measurements carried out after the preheat to 700°C as outlined in Protocol 1.

	μ	E_τ (eV)	E_σ (eV)	E_ω (eV)
TL A	0.50±0.02	1.7±0.1	1.7±0.2	1.7±0.1
TL B	0.44 ± 0.02	1.1±0.1	1.1±0.2	1.1±0.1
TL C	0.50±0.02	1.7±0.1	1.7±0.2	1.7±0.1

It is known that in BeO, thermal quenching of the TL data results in the underestimation of both the activation energy and the order of kinetics [56]. We have seen that the main peak in α-Al_2O_3:C gets significantly shifted to a higher temperature position in the presence of the radiation-induced defects. We conclude that at the higher temperature position, the main peak becomes affected by thermal quenching. Consequently, this significantly affects the kinetic parameters of the main peak just like in BeO i.e. the lowering of the activation energy and the order of kinetics in the presence of the radiation-induced defects as revealed by CGCD and Chen's peak-shape methods. Thus, the low values of the activation energy and the order of kinetics of the main peak in **TL B**, are as a result of thermal quenching effects due to the shifting of the peak to high temperatures in the presence of radiation-induced defects.

6.4 Effect of radiation-induced defects on optically stimulated luminescence

In the previous section, the influence of the radiation-induced defects on the thermoluminescence (TL) response of the main peak in the material was presented. In this section, we present the results of investigating the influence of the radiation-induced

defects on the properties of the optically stimulated luminescence (OSL) produced by the material. The following protocol, namely, Protocol 2, was used during these investigations.

Protocol 2

Stage 1

1. A preheat at 1°C/s to 700°C (to remove any residual dose in the material)
2. Beta-irradiation to a test dose of 1.0 Gy (for monitoring changes in OSL)
3. OSL at 30°C for 200 s using 470-nm blue LEDs set at 90% optical power
4. TL at 1°C/s to 500°C (to record residual phototransferred TL (RPTTL))
   Steps 2-4 were repeated 10 times. The OSL measurements at step 3 and RPTTL measurements at step 4 shall be referred to as **OSL A** and **RPTTL A**, respectively.

Stage 2

5. Beta-irradiation to 1000 Gy (intended to induce defects)
6. A preheat at 1°C/s to 500°C (to clear the main peak)
7. Beta-irradiation to a test dose of 1.0 Gy (for monitoring changes in OSL)
8. OSL at 30°C for 200 s using 470-nm blue LEDs set at 90% optical power
9. TL at 1°C/s to 500°C (intended to record RPTTL)
   Steps 7-9 were repeated 10 times.The OSL measurements at step 8 and RPTTL measurements at step 9 shall be referred to as **OSL B** and **RPTTL B**, respectively.

Stage 3

10. A preheat at 1°C/s to 700°C (intended to remove radiation-induced defects)
11. Beta-irradiation to a test dose of 1.0 Gy (for monitoring changes in OSL)
12. OSL at 30°C for 200 s using 470-nm blue LEDs set at 90% optical power

13. TL at 1°C/s to 500°C (intended to record residual RPTTL)

Steps 11-13 were repeated 10 times. The OSL measurements at step 12 and RPTTL measurements at step 13 shall be referred to as **OSL C** and **RPTTL C**, respectively. Each irradiation was preceded by a 120-s pause to ensure that the sample was irradiated at room temperature.

Figure 6.6 shows the shapes of the randomly chosen OSL signals obtained in **OSL A**, **OSL B** and **OSL C**. It is clear from Figure 6.6 that the measured OSL signals are all peak-shaped. This is an indication of substantial retrapping at the main trap os the optically stimulated charges from the deep traps [57]. Secondly, the OSL signals in **OSL A** and **OSL C** coincide with each other but not with the OSL signal in **OSL B**. This shows that the radiation-induced defects cause the OSL signal to be altered. Furthermore, the initial intensities for the signal in **OSL B** are significantly higher than those in **OSL A** and **OSL C**.

A more complete peak in observed in **OSL A** and **OSL C** compared to **OSL B** is an indication of higher levels of charge retrapping in **OSL A** and **OSL C** than in **OSL B**. This is similar to the more retrapping case in **TL A** and **TL C** than in **TL B** observed in the previous sections. Consequently, we might say that in both TL and OSL, the role of the radiation-induced effects is to minimize the retrapping levels during heating as well as optical stimulation of a previously irradiated sample.

Figure 6.7a shows a plot of the peak position of the OSL signal with respect to the number of OSL runs. It can be seen from Figure 6.7a that the peak position for the OSL signal in **OSL B** shifts towards earlier times. This shift of the peak to earlier times when OSL is measured in the presence of the radiation-induced defects suggests that direct recombination quickly dominates over retrapping of charge carriers during optical stimulation. This result is in good agreement with our earlier findings that in the presence of these radiation-induced defects, the sample follows general-order kinetics characterized by less retrapping i.e. b decreases from 1.87 to 1.33.

Figure 6.7b shows a plot of the integrated OSL intensity with respect to the number of OSL runs. According to Figure 6.7b the integrated OSL intensities in **OSL A** and **OSL C** are equivalent. In addition, the intensities are higher for OSL measured in **OSL B** compared to those measured in **OSL A** and **OSL C**. This result

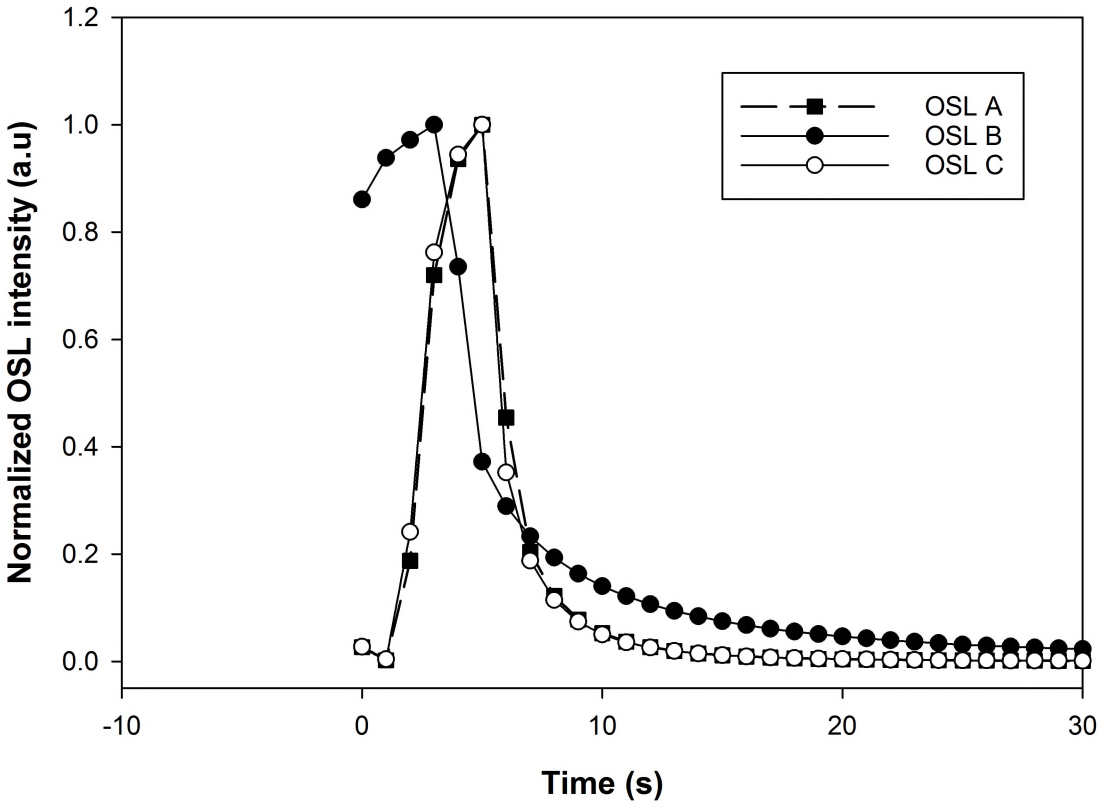

Figure 6.6: OSL signals measured using Protocol 2. The samples were stimulated by 470-nm blue LEDs for 200 s following beta irradiation to 1.0 Gy. **OSL A** represents the OSL measurements made before sample beta irradiation to 1000 Gy; **OSL B**, the OSL measurements made after the 1000 Gy beta irradiation and before the preheat to 700°C and **OSL C**, the OSL measurements carried out after the preheat to 700°C. Note that only the first 30 s have been shown for visual clarity.

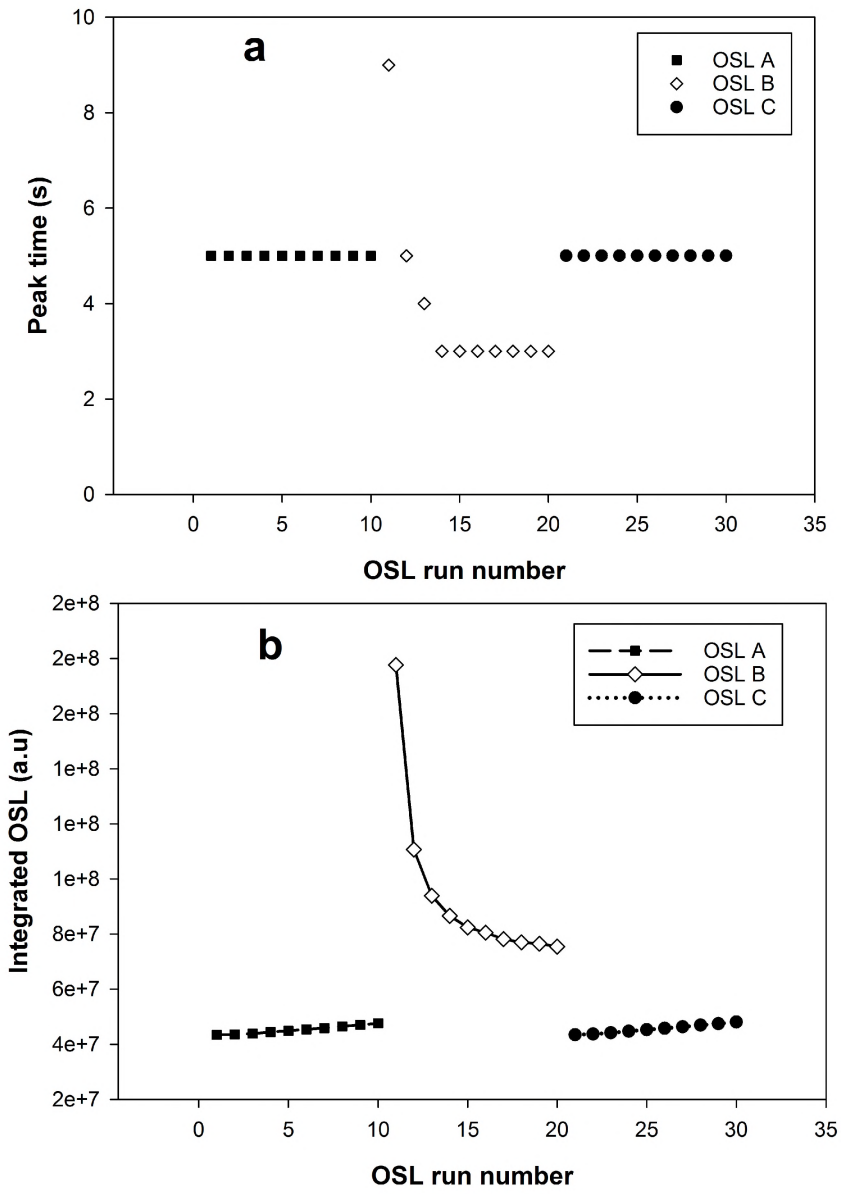

Figure 6.7: Behaviour of the peak position (a) and the integrated OSL intensities (b) of the OSL signals measured after 1.0 Gy beta irradiation then 470-nm blue LEDs stimulation for 200 s. **OSL A** represents the OSL measurements made before sample irradiation to 1000 Gy; **OSL B**, the OSL measurements made after the 1000 Gy beta irradiation and before the preheat to 700°C and **OSL C**, the OSL measurements carried out after the preheat to 700°C.

shows that the radiation-induced defects significantly change the OSL sensitivity of the sample. Further to that, the result confirms the role of heating to 700°C in restoring the sample's initial sensitivity.

The high OSL yield in **OSL B** compared to both **OSL A** and **OSL C** suggests that the high-irradiation dose of 1000 Gy creates new defect centres that are optically active. These contribute significantly to the overall OSL yield.

6.4.1 Effect of the heavy beta irradiation dose on the residual phototransferred thermoluminescence

The main peak observed in the TL glow-curve recorded after OSL measurement as indicated in Protocol 2, is due to residual charge carriers in the main trap plus the phototransferred charge carriers from deep traps into main trap, hence the designation residual phototransferred thermoluminescence (RPTTL). In this investigation, which is based on Protocol 2, we focused on the effect of the high beta irradiation dose on the main RPTTL peak. Recall that **RPTTL A** represents the 10 RPTTL measurements made before sample beta irradiation to 1000 Gy; **RPTTL B** are the 10 RPTTL measurements recorded after the 1000 Gy beta irradiation and before the preheat to 700°C and **RPTTL C** are the 10 RPTTL measurements carried out after the preheat to 700°C.

Figure 6.8a shows semi-log plots of normalized TL glow curves measured in **RPTTL A**, **RPTTL B** and **RPPTL C**. The TL glow-curves of **RPTTL A** and **RPTTL C** coincide and show a relatively intense main peak centred at 177°C (main peak) and a high temperature secondary peak (peak III) whereas that of**RPTTL B** shows an intense main peak centred at 190°C alongside low temperature (peak I) and high temperature (peak III) secondary peaks. This dominant peak at 177°C or 190°C will be referred to as the main RPTTL peak.

Figure 6.8b shows a plot of the position of the main RPTTL peak with respect to number of OSL runs for TL measurements in **RPTTL A**, **RPTTL B** and **RPTTL C**. The positions of the main peak lie in the range of 173-181°C for TL glow curves in **RPTTL A**; 187-195°C for those in **RPTTL B** and 172-180°C for those in **RPTTL C**. This indicates that the position of the main RPTTL peak is shifted towards higher

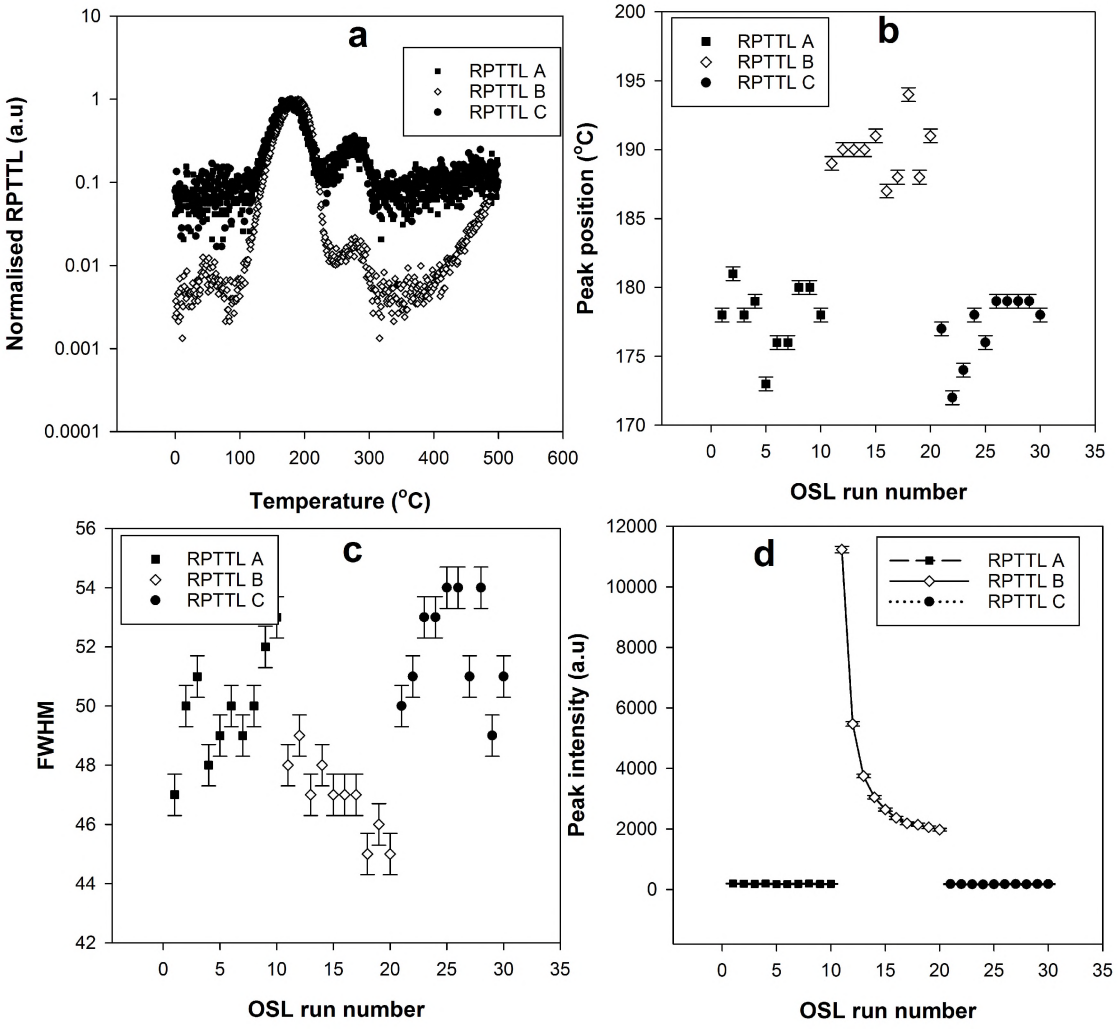

Figure 6.8: The RPTTL glow curves measured at 1°C/s to 500°C following 470-nm blue LEDs stimulation for 200 s of a sample that was irradiated to 1.0 Gy (a). The behaviour of the position (b), the FWHM (c) and the maximum intensity (d) of the main RPTTL peak against OSL run numbers. **RPTTL A** represents the RPTTL measurements made before sample beta irradiation to 1000 Gy; **RPTTL B**, the RPTTL measurements made after the 1000 Gy beta irradiation and before the preheat to 700°C and **RPTTL C**, the RPTTL measurements carried out after the preheat to 700°C.

temperatures when RPTTL is measured in the presence of radiation-induced defects. Note that the average temperatures of the position for the main RPTTL peak i.e. 177°C for **RPTTL A** and **RPTTL C** and 190°C **RPTTL B** are in general higher than those obtained for conventional TL i.e. 172°C for **TL A** and **TL C** and 182°C **TL B** as shown in Figure 6.3. This shift in position of the main peak in conventional TL towards higher temperatures in phototransferred TL has already been reported [58].

Figure 6.8c shows a plot of the FWHM of the main RPTTL peak with respect to number of OSL runs for TL measurements in **RPTTL A**, **RPTTL B** and **RPPTL C**. In general the FWHM of the main RPTTL peak is slightly reduced when the RPTTL is measured in the presence of radiation-induced defects. This is in sharp contrast to the behaviour of the FWHM for conventional TL in which the FWHM increases for TL measured when the radiation-induced defects are present. It is also important to note that the average FWHM of the the main RPTTL peak i.e. 51°C for **RPTTL A** and **RPTTL C** and 47°C for **RPTTL B** as shown in Figure 6.8 are in general higher than those obtained for conventional TL i.e. 33°C for **TL A** and **TL C** and 38.5°C for **TL B** as shown in Figure 6.4.

Figure 6.8d is a plot of the maximum intensity of the main RPTTL peak with respect to number of OSL runs.The maximum intensities in **RPTTL A** and **RPTTL C** are equivalent and considerably lower than than those obtained in **RPTTL B**. Note that this plot is a complete replica of Figure 6.7b in which the total OSL yield is plotted against OSL run number. This indicates a strong dependence of the intensities of the main RPTTL peak on the preceding OSL measurement.

6.5 The effect of irradiation beta dose on the evolution of radiation induced defects

We have seen previously that an beta irradiation dose of 1000 Gy introduces defects that have remarkable effect on the TL response of the material i.e. the shape, position and maximum intensity of the main peak are significantly affected.

In the work presented in this section, we investigated the evolution of the radiation-induced defects from a beta irradiation dose as low as 5 Gy to a high beta irradiation

dose of 1500 Gy. The level of concentration of these radiation-induced defects for a given irradiation dose was assessed by their degree of influence on the parameters of both the main peak (peak II) and the low temperature peak (peak I). For purposes of comparison, analysis was performed on both the raw data and the thermal-quenching-corrected data using some published values i.e. $W = 1.028$ eV and $C = 9.8 \times 10^{11}$ [58].

For this investigation, a sample was annealed once at 900°C for 15 minutes before use. The following procedure, equivalent to Protocol 1, was followed:

Stage 1

1. A preheat at 1°C/s to 700°C to erase any residual dose
2. Beta-irradiation to a test dose of 1.0 Gy (for monitoring changes in TL)
3. TL at 1°C/s to 500°C

   Steps 2-3 were repeated 10 times. The TL measurements in step 3 shall be referred to as **TL A**.

Stage 2

4. Beta-irradiation to dose D_i (intended to induce point-defects)
5. A preheat at 1°C/s to 500°C (to erase the main peak)
6. Beta-irradiation to a test dose of 1.0 Gy (for monitoring changes in TL)
7. TL at 1°C/s to 500°C

   Steps 6-7 were repeated 10 times. The TL measurements in step 7 shall be referred to as **TL B**.

Stage 3

8. A preheat at 1°C/s to 700°C (intended to remove radiation-induced defects)
9. Beta-irradiation to a test dose of 1.0 Gy (for monitoring changes in TL)
10. TL at 1°C/s to 500°C

    Steps 9-10 were repeated 10 times. The TL measurements in step 10 shall be referred to as **TL C**.

The whole procedure was repeated for doses D_i=5, 10, 30, 80, 100, 200, 300, 500, 800, 1000, 1200 and 1500 Gy. Each irradiation was preceded by a 120-s pause to ensure that the sample was irradiated at room temperature. To minimize random errors, the peak parameters were averaged over the 10 repeated measurements at each stage for each irradiation dose under investigation. Thus, for a given parameter, x, the measured value, x_m is given by:

$$x_m = \bar{x} \pm s$$

where $\bar{x} = \frac{\Sigma_i^n x_i}{n}$ is the arithmetic mean and $s = \sqrt{\frac{(x_i - \bar{x})^2}{n-1}}$ is the standard deviation representing the estimate of an uncertainty in the measured value. Note that n is the number of repeated measurements at each stage and is equal to 10 in this particular case, and x_i is a parameter value obtained from the i^{th} TL glow curve.

6.5.1 The dose profile of the high-temperature peak associated with the radiation-induced defects

Figure 6.9a shows the plots of the TL peak arising from the radiation-induced defects for different high beta irradiation doses. The behaviour of the position for this peak with beta irradiation dose is shown in Figure 6.9b whereas 6.9 shows the behaviour of its peak intensity with respect to high doses.

It is clear from Figure 6.9c that the position of the radiation-induced peak, albeit erratic, generally shifts towards lower temperatures with increasing beta irradiation doses. This behaviour is also typical of the main peak [53]. The peak intensity, on the other hand, increases with beta irradiation doses, saturating between 800-1500 Gy.

6.5.2 Dose dependence of the radiation-induced defects based on the position of the TL peaks

Figure 6.10 presents the behaviour of the peak position against the defect-inducing irradiation doses for the main peak before thermal quenching corrections (a), the main peak after thermal quenching corrections (b) and the low temperature peak (peak I) (c). Note that for peak I, there was no difference between peak position

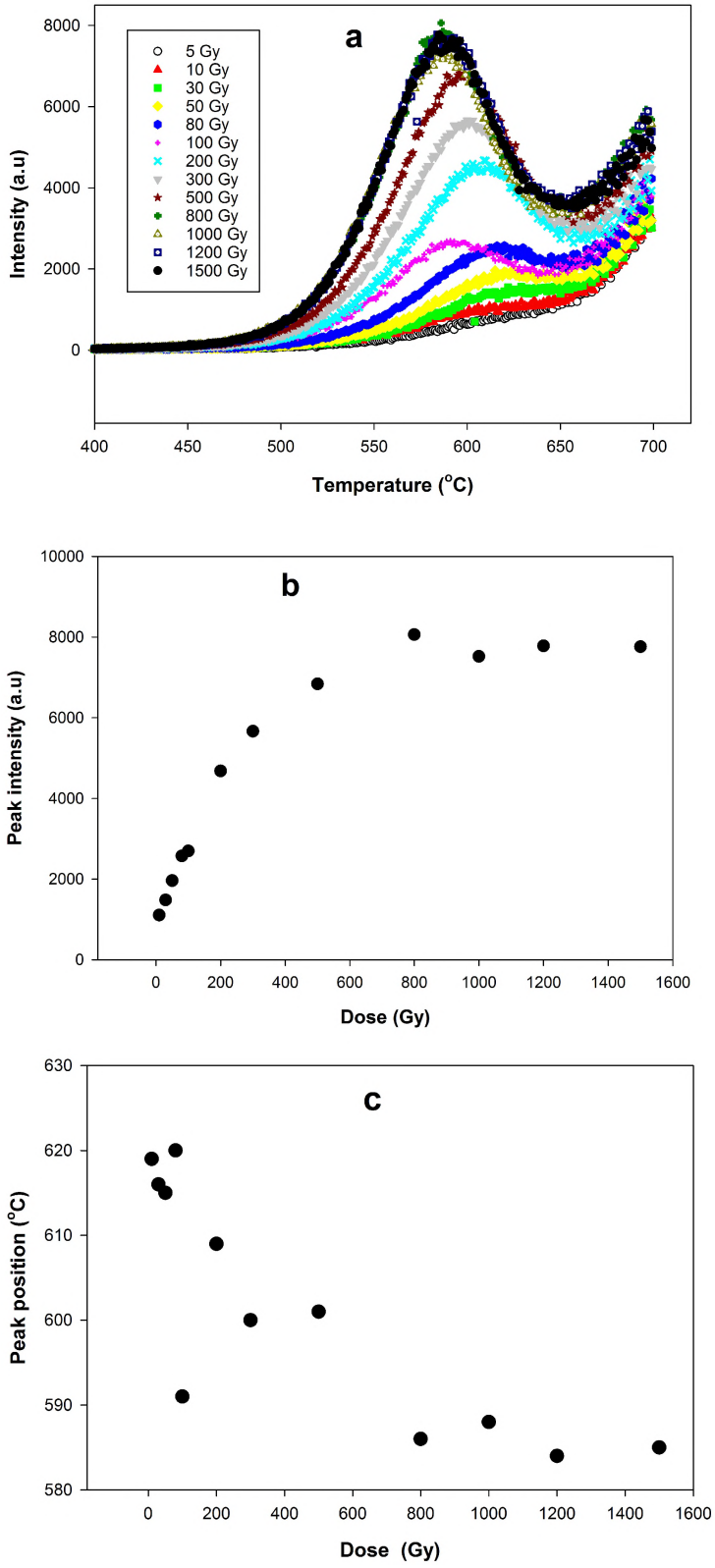

Figure 6.9: Plots of the radiation-induced peak for different beta irradiation doses. Note that only the high temperature section of the TL glow curve has been presented. TL was measured at 1°C/s to 700°C.

values obtained from the raw data and those from the corresponding data following thermal-quenching corrections.

It is clear from both Figures 6.10a and b that when TL is measured in the presence of the radiation induced defects (**TL B**), the main peak is significantly shifted towards higher temperatures. At 5.0 Gy, the position of the main peak in **TL B** is equivalent to that obtained in **TL A** and **TL C** i.e. the radiation damage caused by a 5.0 Gy beta irradiation dose is not significant enough to affect the TL response of the main peak. However, from 10 Gy and above, the position of the main peak due to a 1.0-Gy test dose, shifts towards higher temperatures following high beta irradiation doses. The main peak is stable for high beta irradiation doses between 200-1500 Gy. Note that the effect of thermal quenching is to down-shift the position of the main peak from 203±2°C and 187±2°C to 186±2°C and 173±2°C in **TL B** and **TL A/ TL C**, respectively. In other words, thermal quenching shifts the position of the main peak from higher temperatures towards low temperatures. The position of the low temperature peak (peak I) is not affected by the presence of the irradiation-induced defects for all the high-irradiation doses used as shown in Figure 6.10c.

It is important for the reader to note that the peak positions plotted in Figure 6.10 are average values obtained from the 1.0-Gy test dose and NOT for the high-irradiation doses shown in the abscissa.

6.5.3 Dose dependence of the radiation-induced defects based on the shape of the TL peaks

Figure 6.10 shows the behaviour of the FWHM against the defect-inducing irradiation doses for the main peak before thermal quenching corrections (a), the main peak after thermal quenching corrections (b) and the low temperature peak (peak I) (c). Just like in the case of peak position, there was no difference between FWHM values obtained from the raw data and those from the corresponding data following thermal-quenching corrections for peak I.

The FWHM values plotted in Figure 6.11 are average values obtained from the 1.0-Gy test dose and NOT for the high-irradiation doses shown in the abscissa.

As shown in Figure 6.11a, the FWHM in **TL B** is higher than those observed

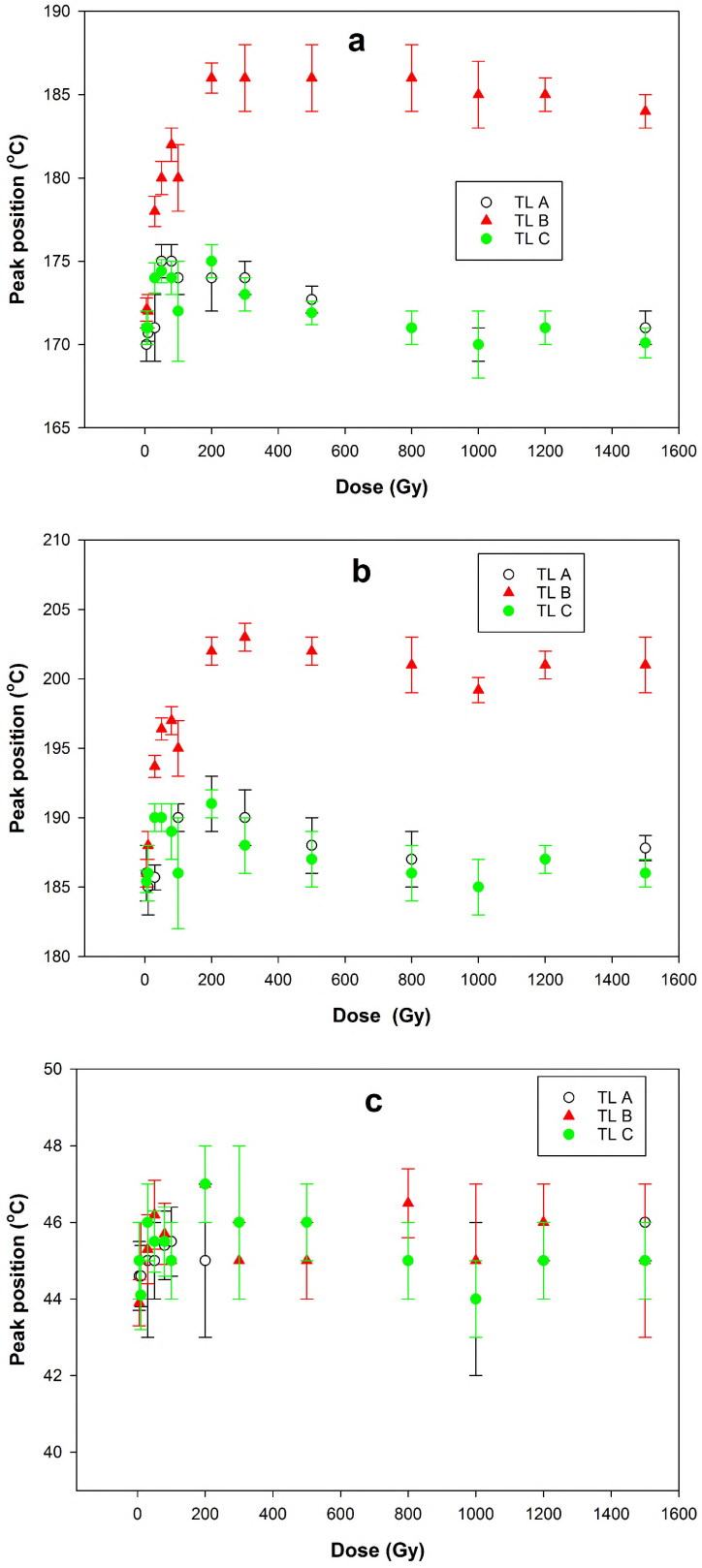

Figure 6.10: Plots of the peak position against the defect-inducing irradiation doses for the main peak before thermal quenching corrections (a), the main peak after thermal quenching corrections (b) and the low temperature peak (peak I) (c). TL was measured at 1°C/s to 500°C following a test dose of 1.0 Gy.

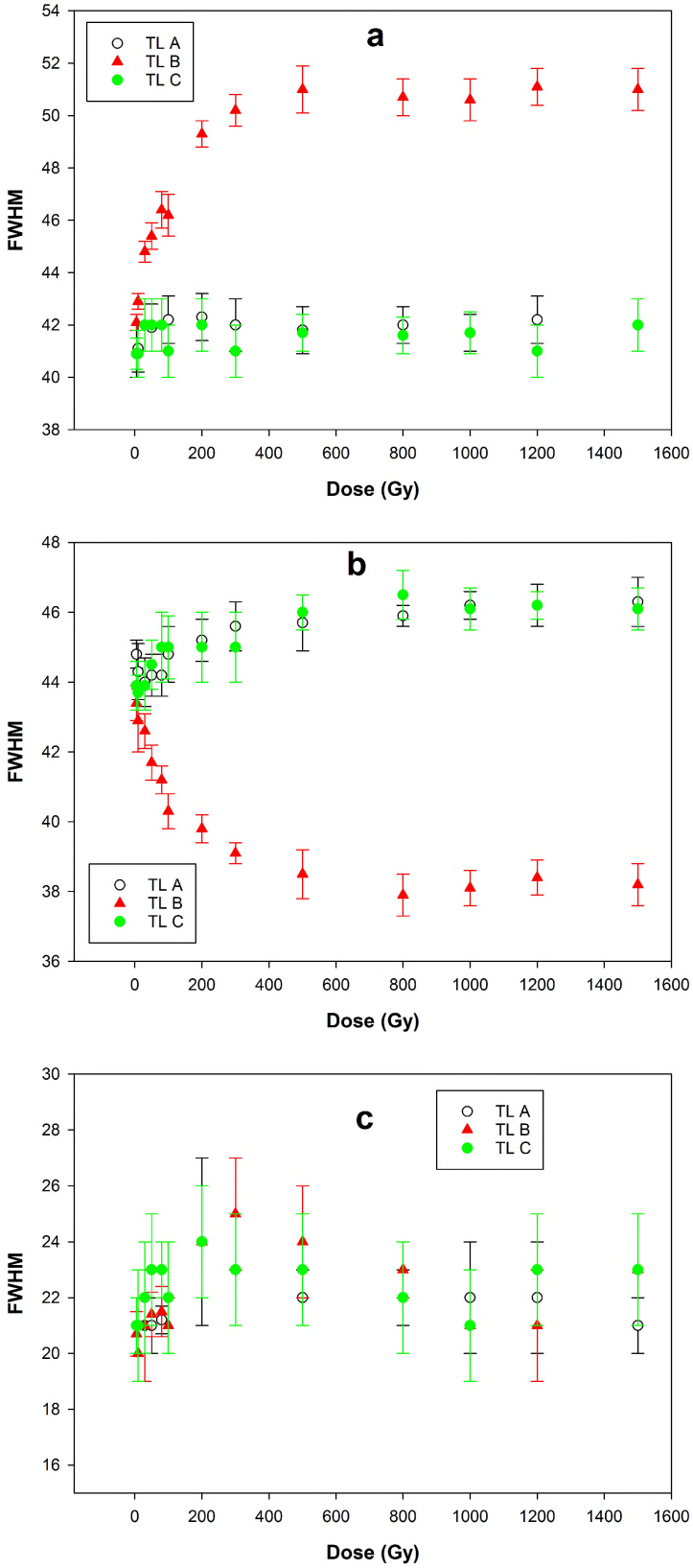

Figure 6.11: Plots of the FWHM against the defect-inducing irradiation doses for the main peak before thermal quenching corrections (a), the main peak after thermal quenching corrections (b) and the low temperature peak (peak I) (c). TL was measured at 1°C/s to 500°C following a test dose of 1.0 Gy.

in both **TL A** and **TL C**. The FWHM of the main peak due to a 1.0 Gy test dose, is not affected for beta irradiation doses of 5 and 10 Gy. However, it increases between 30 and 300 Gy. Beyond 300 Gy, the FWHM of the main peak is stable i.e. does not change with the applied high-irradiation doses. Following thermal quenching corrections as shown in Figure 6.11b, the FWHM of the main peak has slightly increased from 42°C to 45°C in both **TL A** and **TL C**. In the case of **TL B**, the FWHM of the main peak gets smaller and smaller with the applied high-irradiation doses then stabilizes between 800-1500 Gy. It is interesting to note that whereas thermal quenching causes substantial broadening of the main peak in **TL B** i.e. in the presence of the radiation-induced defects, the same thermal quenching decreases the FWHM of the main peak in absence of the radiation-induced defects i.e. in **TL A** and **TL C**. In addition, we notice that the FWHM values in **TL B** before and after thermal-quenching corrections, are inversely related. It is known that thermal quenching causes peak broadening [4] which is consistent with the results in **TL B**. The peak broadening observed in the thermal-quenching-corrected data of **TL A** and **TL C** contradicts with this observation. The FWHM of the low temperature peak (peak I) is apparently not affected by the presence of the irradiation-induced defects for all the applied high-irradiation doses as shown in Figure 6.11c.

6.5.4 Dose dependence of the radiation-induced defects based on the maximum intensity of the TL peaks

Figure 6.12 shows the behaviour of the peak intensity against the applied high-irradiation doses, for the main peak before thermal quenching corrections (a), the main peak after thermal quenching corrections (b) and the low temperature peak (peak I) (c). Here too, there was no difference between peak intensity values obtained from the raw data and those from the corresponding data following thermal quenching corrections for peak I. The peak intensities plotted in Figure 6.12 are average values obtained from the 1.0-Gy test dose and NOT for the high-irradiation doses shown in the abscissa.

It can be clearly seen from Figure 6.12a that for the TL measured in **TL A**, **TL B** and **TL C**, the intensity of the main peak decreases with applied high-beta irradi-

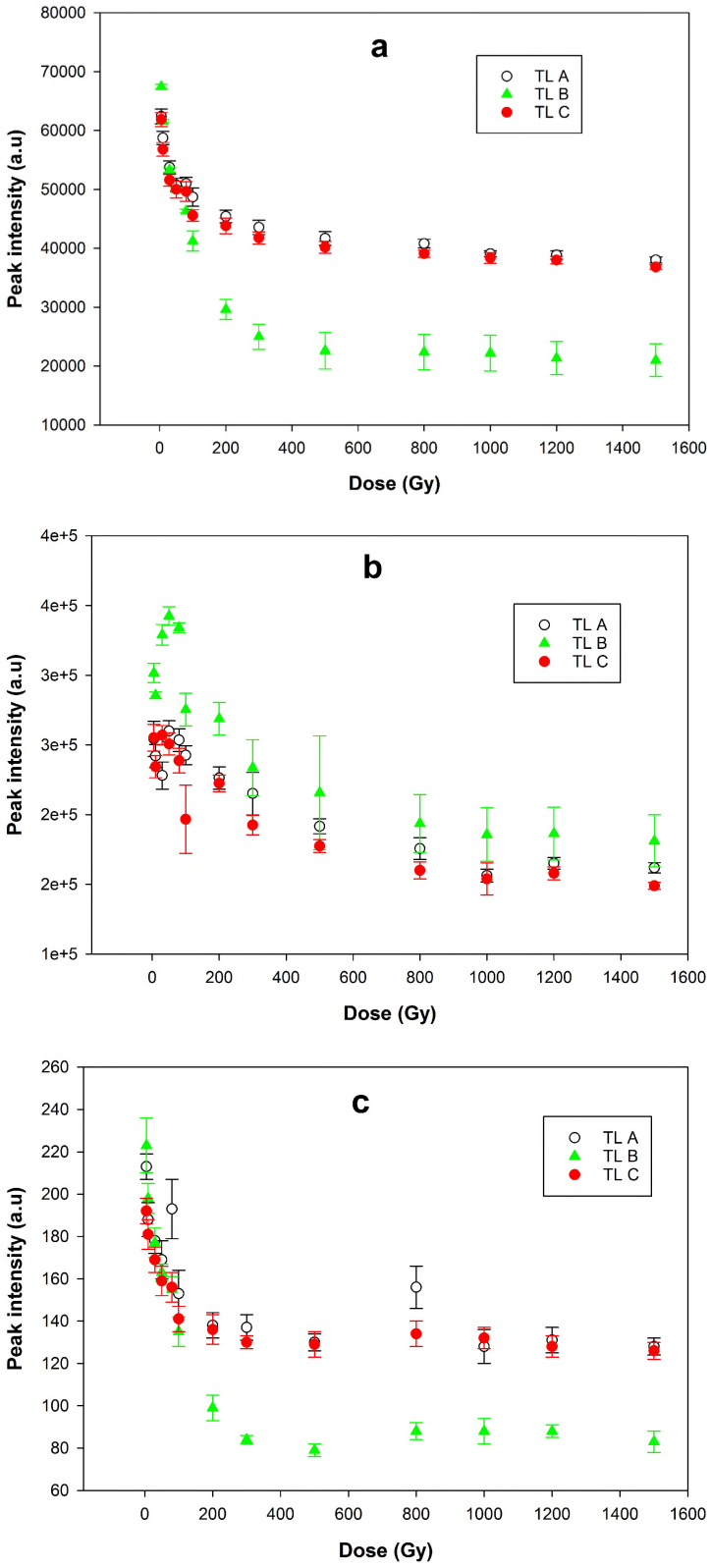

Figure 6.12: Plots of the peak intensity against the defect-inducing beta irradiation doses for the main peak before thermal quenching corrections (a), the main peak after thermal quenching corrections (b) and the low temperature peak (peak I) (c). TL was measured at 1°C/s to 500°C following a test dose of 1.0 Gy.

ation doses. However high-irradiation doses between 100-1500 Gy show a remarkable difference in peak intensity between TL measured in **TL A** and **TL C** i.e. in the absence of radiation-induced defects, and those measured in **TL B** i.e. in the presence of the radiation-induced defects. The peak intensities measured in the presence of the radiation-induced defects (**TL B**) are considerably lower than those obtained in their absence in **TL A** and **TL C** for high-irradiation doses between 100-1500 Gy. We can therefore say that the high-irradiation doses between 100-1500 Gy cause sample desensitization as a result of the induced defects. Following thermal-quenching corrections, the peak intensities presented in Figure 6.12b show a decrease in magnitude with applied high-irradiation doses, just like in the case of raw data. However, the intensities of the main peak in **TL A** and **TL C** are roughly equal to those obtained in **TL B** albeit slightly lower in magnitude. Apparently, thermal-quenching-corrected data do not show sample desensitization (or sensitization) in the 100-1500 Gy dose range as is the case with the raw data. The intensities of the low temperature peak (peak I) as shown in Figure 6.12c mirror the behaviour of the intensities of the main peak for the raw data as shown in Figure 6.12a. Thus, the behavoiur of the intensities of peak I also suggest sample desensitization. Whereas thermal-quenching corrections produce relatively high peak intensities of the main peak, the peak intensities of peak I are unaffected.

As observed in the previous chapter, the emission bands of the main peak and low temperature peak (peak I) overlap i.e. the same emission bands or recombination sites are involved in the luminescence processes involving both the main peak and peak I. F-centre emission band is dominant for both peaks. It is therefore expected that the behaviour of their peak intensities be the same as observed in Figure 6.12a (main peak) and Figure 6.12c (peak I). Thus, the observed sample desensitization can be attributed to defect transformation of the recombination centres i.e. F^+ to aggregate centres thereby reducing emissions from the dominant band. Equivalently, the high-irradiation doses reduce the concentration of the traps responsible for these peaks by transforming them into aggregate trapping centres consequently reducing the peak intensities. The peak observed at above 500°C following a high-irradiation dose can be attributed to these aggregate trapping centres. Another possibility is that both transformation processes do take place simultaneously during the high-dose beta

irradiation.

With regard to the desensitization observed in the intensities of the main peak, the thermal-quenching corrected data shown in Figure 6.12c may provide an alternative explanation for the perceived desensitization. Since the intensities of the main peak in the presence/absence of the radiation-induced defects are roughly equal following thermal-quenching corrections, we could attribute the observed low intensities in **TL B** of Figure 6.12a to thermal quenching effects. We have already seen that the effect of the radiation-induced defects is to substantially shift the position of the peak towards higher temperatures. At these high temperature positions, we expect the intensities to be significantly reduced by thermal quenching hence the observed low intensities. Note that this latter explanation suggests that the radiation-induced defects are indirectly responsible for the sample desensitization.

6.6 Summary

In this chapter, we have seen that high-beta irradiation beta-doses can produce remarkable effects on the luminescence response of the α-Al_2O_3:C samples. This is because of the new aggregate defects that are induced by the high-irradiation doses. These radiation-induced defects are responsible for a high-temperature peak observed above 500°C in the TL glow curve of the material measured following a high-dose irradiation. The effect of these radiation-induced defects can be reversed by heating a sample to 700°C following a high-dose irradiation i.e. heating to 700°C completely restores the luminescence response of the sample. This means that the radiation-induced defects are transformed back to original defects by thermally induced processes. This thermal transformation restores the original concentrations of defects responsible for luminescence.

In the presence of the radiation-induced defects, the position of the main peak shifts towards higher temperatures, the peak gets broader, its maximum intensities are decreased, both the activation energy and the kinetic order of the peak are underestimated. All the aforementioned effects have been attributed to thermal quenching as a result of shifting of the peak to a higher temperature position. The position and FWHM of the low temperature peak (peak I) are unaffected by the radiation-induced

defects whereas its peak intensities are reduced.

The OSL yield recorded in the presence of the radiation-induced defects is significantly higher than that recorded under similar circumstances in the absence of the radiation-induced defects. Thus, the OSL response of the sample is increased following a high-irradiation dose.

Finally, the filled radiation-induced traps have shown to be relatively more stable under sunlight exposure of the sample compared to the main traps. This could be due to the complex nature of these radiation-induced defects.

Chapter 7

Transfer of charges from deep traps to the main and intermediate traps during storage

In this chapter, we present experimental evidence of transfer of charges from the deep traps to the main and subsidiary traps in α-Al_2O_3:C during sample storage at ambient temperature. The study was carried out using thermoluminescence and optically stimulated luminescence techniques. OSL signal recuperation i.e. luminescence signal regrowth during storage, observed in α-Al_2O_3:C [23] has been attributed to this charge transfer phenomenon.

7.1 Dynamics of the charges in the deep traps during sample storage

The aim of this experiment was to investigate the movements, during storage, of the charges localised in the deep traps. All the samples used in this investigation were first annealed at 900°C for 15 minutes followed by rapid cooling in open air prior to use. The first set of the samples was irradiated, one sample at a time, to 1000 Gy of beta dose, preheated at 1°C/s to 500°C to empty the shallow, main and intermediate traps then placed in a light-tight storage container. This is denoted as set 1. The preheat to 500°C ensured that deep traps were left occupied. The second

set (denoted as set 2) of the samples was, immediately after annealing, placed in the same light-tight storage container without any irradiation or preheating. This second set of samples was used as a control. In each case, the storage container was kept in the dark at ambient temperature. After 25 days of storage, a TL measurement at 1°C/s to 500°C was performed on all the samples, one sample at a time, followed by a CW-OSL measurement. Figure 7.1 shows plots of the TL glow curves that were obtained from samples in set 1 following storage in the dark at ambient temperature for 25 days. In the inset are the corresponding semi-log plots of the same data. On the other hand, Figure 7.2 shows plots of the TL glow-curves measured from samples in set 2 i.e. annealed and unirradiated.

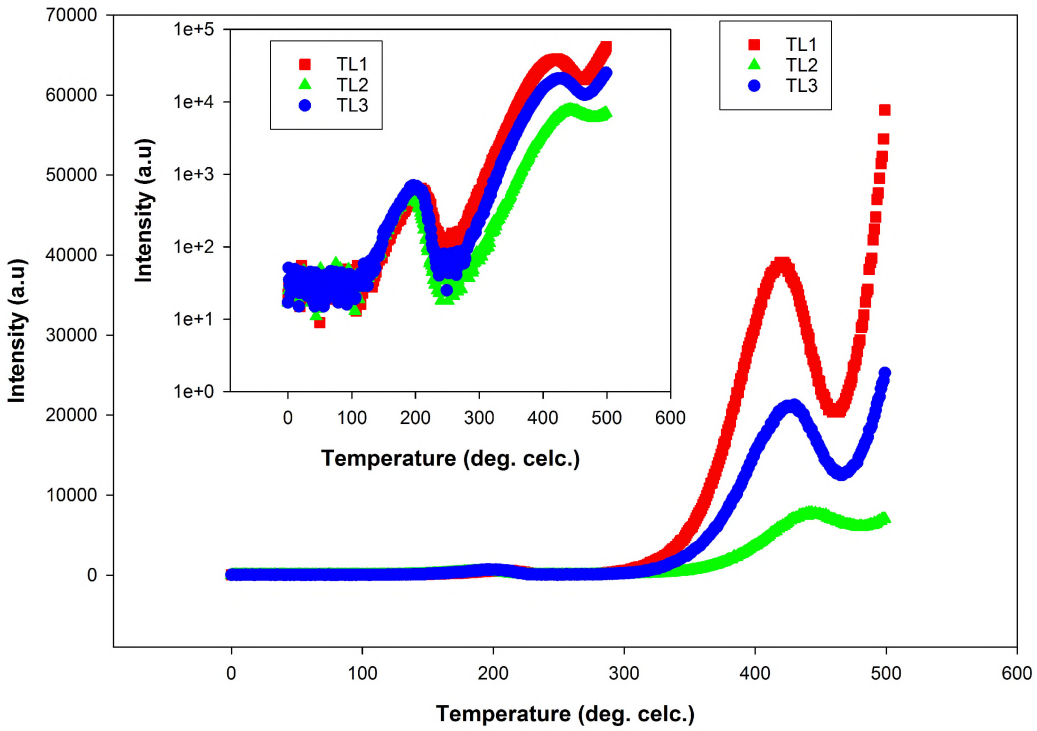

Figure 7.1: TL glow curves obtained after a 25-day storage period at ambient temperature from three separate samples of set 1 that were first annealed at 900°C for 15 minutes, thereafter irradiated to 1000 Gy followed by a preheat to 500°C before being kept in the dark. The inset shows the corresponding TL glow-curves in semi-log scale.

It can be seen from Figure 7.1 that all the TL glow-curves show a less intense main

peak and a relatively high intense intermediate peak. On the other hand, Figure 7.2 shows the presence of a less intense main peak only. The main peak is centred at $\sim$ 209°C, $\sim$ 191°C and $\sim$ 197°C in TL1, TL2 and TL3 respectively for set 1 samples and at $\sim$ 165°C, $\sim$ 169°C and $\sim$ 163°C in TL1, TL2 and TL3 respectively for set 2 samples. It is evident from Figure 7.1 that there is transfer of charges into the main and intermediary traps during storage with intermediate traps receiving substantial amount of charges compared to the main trap. Similarly, Figure 7.2 shows evidence of charge transfer into the main trap only. Samples in set 2 had no charges in all their traps prior to storage due to the annealing procedure and storage without irradiation. Thus, the presence of charges in the main trap following storage suggests that the samples received a beta irradiation dose from an external source. Since there was no deliberate exposure of these samples to an external irradiation dose, we ascribe the charges captured at the main trap of samples in set 2 to background radiation. The average background for 25 days was calculated and subtracted from TL data in set 1. The inset in Figure 7.2 shows the net TL glow-curves of samples in set 1 following background subtraction.

It is only reasonable to suggest that the charges available in the main and intermediate traps of samples in set 1 following storage, migrated from the deep traps, since the deep traps were the only occupied electron traps prior to storage. This charge migration from the deep traps seems to be happening in cascade fashion i.e. from deep traps into intermediate traps then into the main trap. This is evidenced from the large intensities for peak VI and decreasing intensities going towards the main peak.

Figure 7.3 shows plots of the CW-OSL signal for the annealed-irradiated-preheated then stored samples of set 1 (a) and for the annealed-unirradiated then stored samples of set 2 (b) measured immediately after a TL readout following 25 days of storage. In each case, the OSL was measured at 30°C. The shape of the CW-OSL signals shown in Figure 7.3a are typical of the CW-OSL signals obtained from α-Al_2O_3:C upon blue light stimulation of deep traps following a preheat to 500°C [57]. On the other hand, the random intensities shown in Figure 7.3b are typical of the CW-OSL signals obtained from annealed and unirradiated α-Al_2O_3:C samples. The CW-OSL plots provide proof of presence of charges in the deep traps for set 1 samples as well

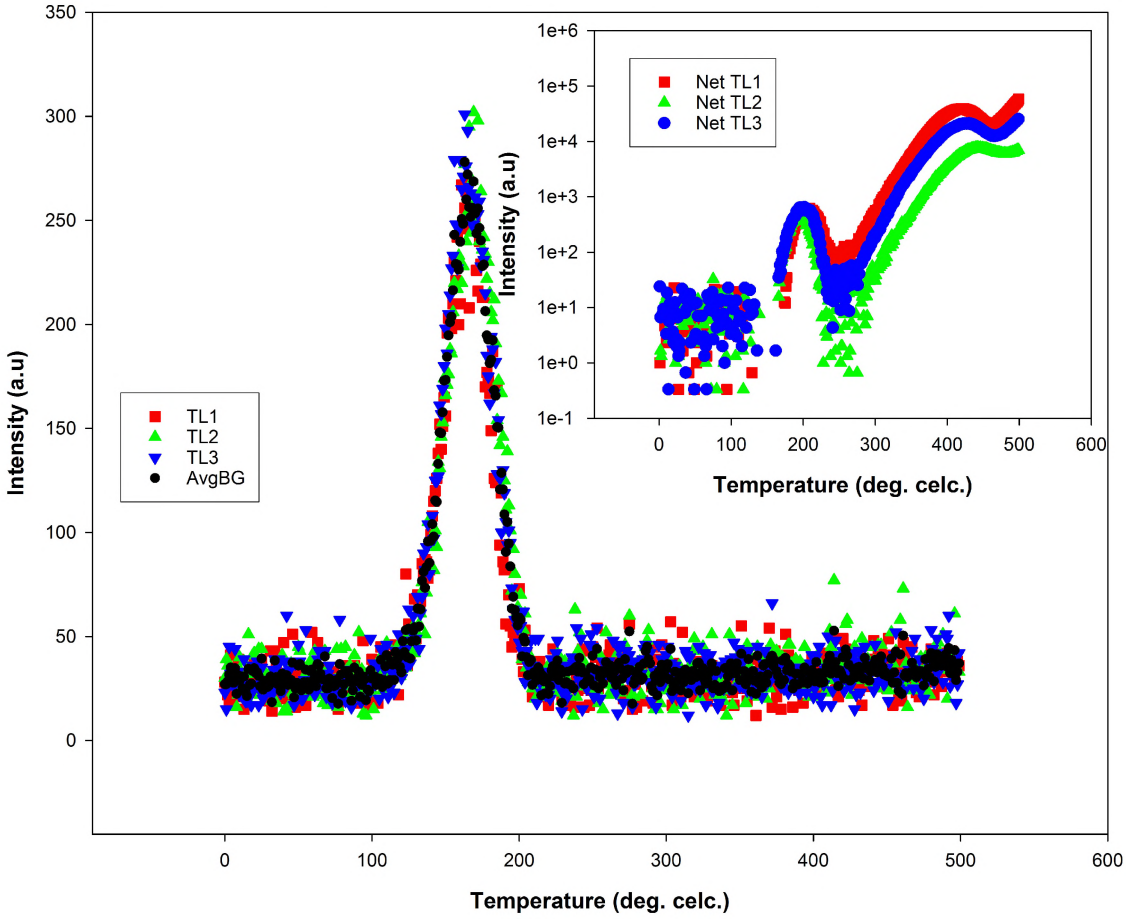

Figure 7.2: TL glow curves obtained after a 25-day storage period from three separate samples of set 2 that were annealed at 900°C for 15 minutes then immediately kept in the dark at ambient temperature without both irradiation and a preheat. The glow-curves have been attributed to background irradiation. The inset shows the semi-log plots of TL glow curves for samples in set 1 after background subtraction.

as proof of apparently empty traps (even deep traps) for set 2 samples.

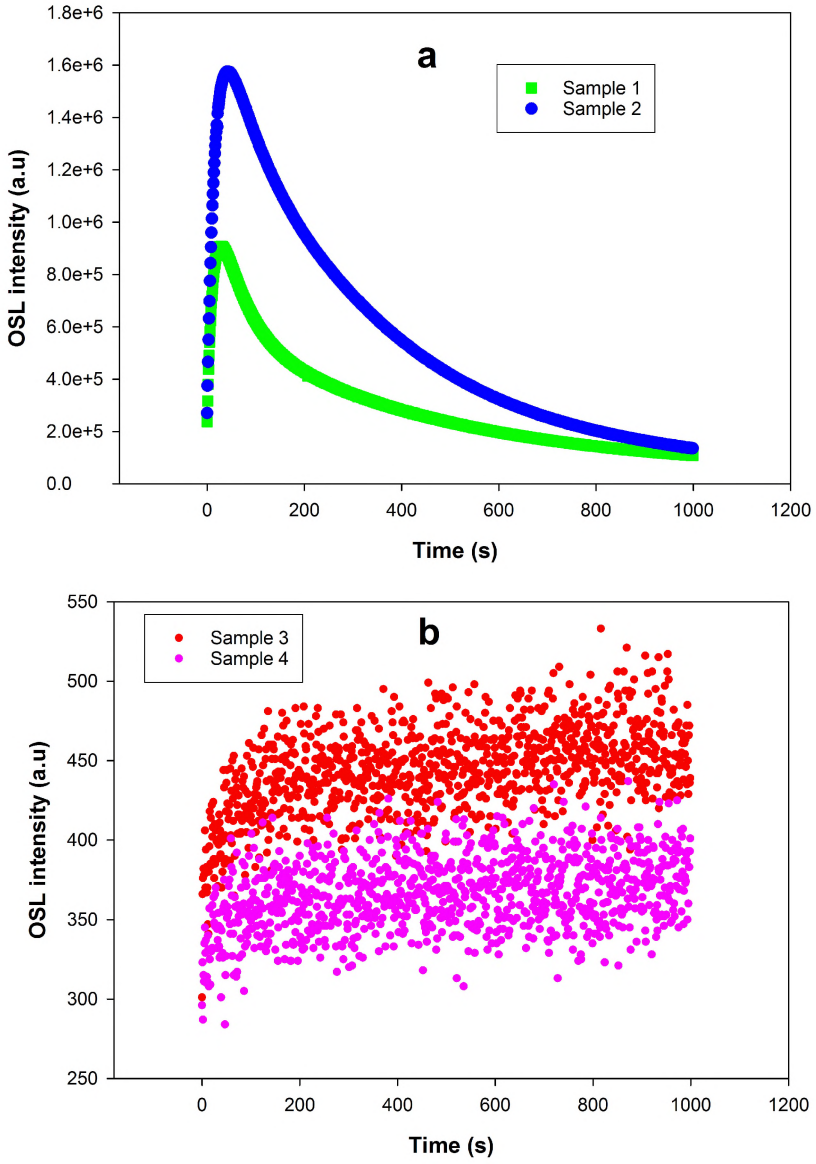

Figure 7.3: Plots of a CW-OSL signal for the annealed-irradiated-preheated then stored samples of set 1 (a) and annealed-unirradiated then stored samples of set 2 (b) measured immediately after a TL readout following a storage period of 25 days. The signals were obtained from two arbitrarily selected samples from each set. 470-nm blue light was used for optical stimulation at 30°C.

.

7.2 The influence of storage period on the TL glow curves of the annealed, irradiated and pre-heated samples

A total of eight (8) samples (labelled a1-a8) were irradiated once (without prior annealing) to 1000 Gy of beta dose followed by a TL at 1.0°C/s to 500°C to empty shallow, main and intermediate traps. This TL measurement was necessary to provide the parameters i.e. maximum position and FWHM, of the main peak. Upon completion of TL measurements, samples were stored in a light-tight container in the dark at ambient temperature. Periodic TL measurements were carried out on each sample without any further irradiation in between TL measurements. For example, in the case of sample a1, TL measurements were made on the 8th, 20th, 80th and 120th day from the first day of storage. The samples were exposed to diffuse red light only during sample transfer between the storage container and the Risø Reader. The minimum storage period before the first TL readout, was 8 hours (sample a5) and the maximum storage period prior to the first TL readout, was 52 days (sample a8). Figure 7.4 shows semi-log plots of the TL glow-curves recorded after various storage periods for the samples used. Note that no subtraction of background signal from TL data was made for these plots.

What is evident in all the plots of Figure 7.4 is that there is always significant charge transfer from the deep traps (donors) to the intermediate traps (acceptors) for all storage times. However, to some extent, the population of charges in the main trap seems to depend on the storage period. It is also important to note, that the filling of the main and intermediate traps is not systematic with respect to storage period. This may suggest that the transfer mechanism is a random one. Some samples i.e. a3, a7 and a8, exhibit an apparent double-component nature of the main peak. The non-uniformity of the samples is clear from the different responses shown by the samples i.e. varying intensities, peak positions and shapes of the TL peaks with storage.

Table 7.1 provides a summary of the main peak parameters before and after storage, for samples a1-a4. It is worthwhile to point out the samples a1-a4 were arbitrarily chosen and that their behaviour is representative of the whole sample

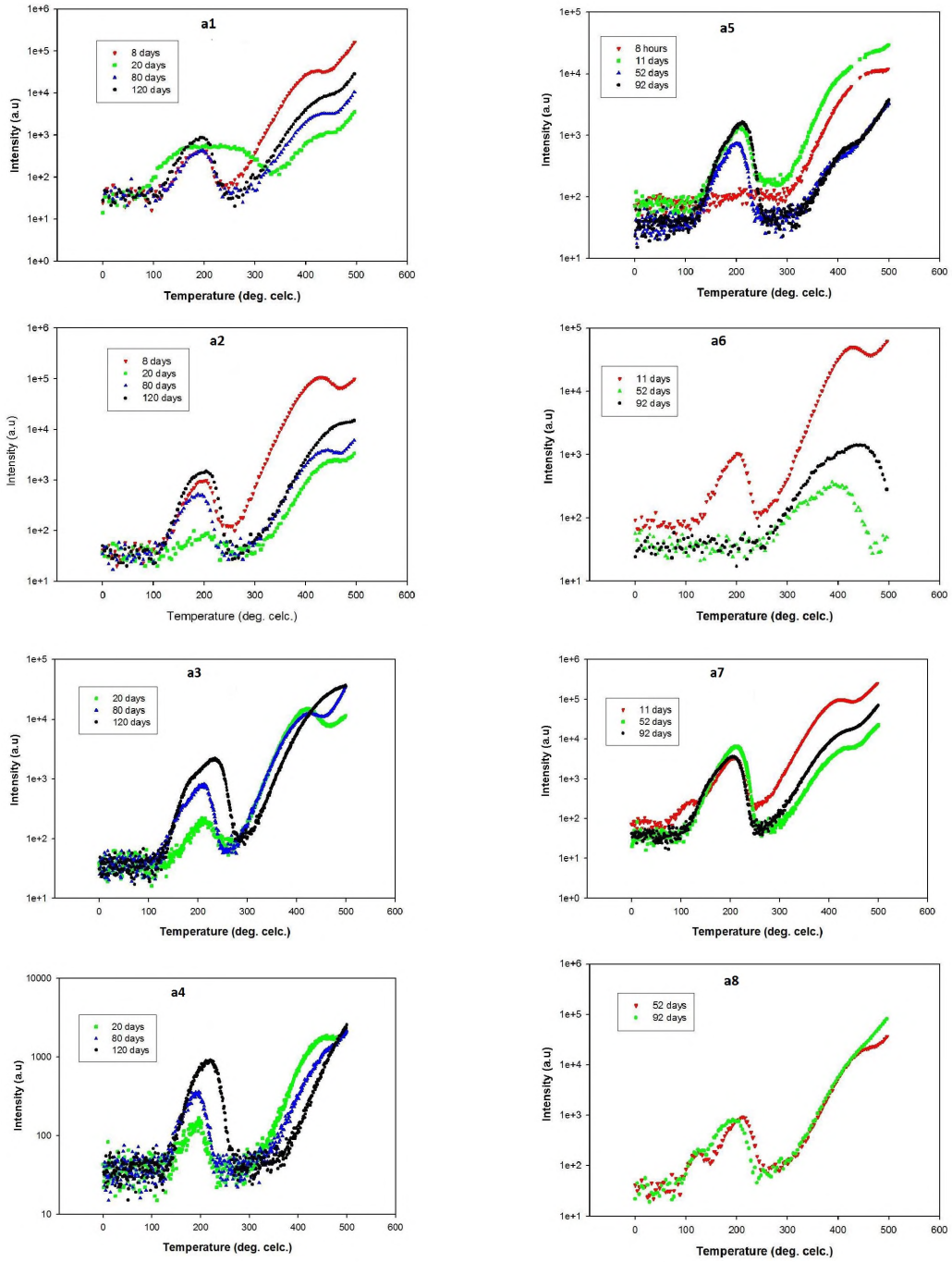

Figure 7.4: Semi-log plots of TL glow curves obtained from 8 different samples for different storage periods in the dark at ambient temperature. Samples were irradiated once to 1000 Gy, then heated to 500°C at 1°C/s to empty the shallow, main and intermediate traps. All TL data were obtained at 1°C/s and are plotted without background subtraction.

population.

From Table 7.1, it is observed that the position of the main peak shifts to higher

Table 7.1: Comparison of the main peak parameters for samples a1-a4 as observed before and after storage.

Sample number	Readout Day	Peak position (°C)	FWHM	Peak Area(a.u)
a1	0	172	48	
	8	193	47	31244
	20	indeterminate		
	80	197	53	29749
	120	201	53	53089
a2	0	154	44	
	8	199	45	59380
	20	indeterminate		
	80	204	55	34042
	120	204	55	90276
a3	0	164	48	
	20	indeterminate		
	80	212	49	51050
	120	234	61	144120
a4	0	146	44	
	20	indeterminate		
	80	195	45	25001
	120	220	56	59691

temperatures with increasing number of storage days, an indication that the higher temperature components become more and more dominant. This agrees with the observation that the charge transfer mechanism occurs in a cascade fashion i.e from deep traps to intermediate traps then to the main trap. The main peak also widens with storage days i.e. FWHM increases. This could be a result of more and more closely related traps getting filled up with charges and contributing to the resultant peak. Except for sample a2, the area under the main peak also increases with storage time.

7.3 Effect of background radiation on charge occupancy of the traps

All samples used in this investigation were first annealed at 900°C for 15 minutes then cooled quickly in open air. The samples were randomly selected. Immediately after the annealing procedure, three of the samples were placed in a light-tight container and stored in the dark at ambient temperature. These samples were labelled c1, c2 and c3. Two other samples, labelled s1 and s2, were stored at two separate sites in th open (not in a container) and subject to conditions of the storage room. The room was kept dark throughout the storage period. A TL measurement was carried out on all the samples after 66 days of storage. The choice of 66 days was arbitrary. Figure 7.5 shows TL glow curves due to background radiation after 66 days of storage. All the glow curves show the presence of the main TL peak only.

It is clear from Figure 7.5 that all the samples recorded comparable amount of TL intensity since the differences in their peak intensities are minor. This is plausible since all the samples were stored in the same room meaning they were exposed to the same background radiation regardless of the storage conditions. The presence of the main TL peak only indicates that background irradiation dose fills the stable main trap. The main peak is centred at $\sim$ 175°C, $\sim$ 169°C, $\sim$ 171°C, $\sim$ 171°C and $\sim$ 168°C for s1, s2, c1, c2 and c3, respectively. This result further demonstrates that background irradiation preferentially fills the low-temperature components of the main peak. On the other hand, the charge transfer mechanism responsible for charge migration from deep traps to the main and intermediate traps, seems to preferentially fill the high-temperature components of the main peak.

There is no evidence of availability of charge in the intermediate traps after 66 days of storage. This is expected since deep traps (donors) are empty. Our evidence has shown that it is the occupied deep traps that donate charges most preferably to intermediate traps. In other words, this result is consistent with the fact that charges in occupied deep traps leak away to unoccupied intermediate traps.

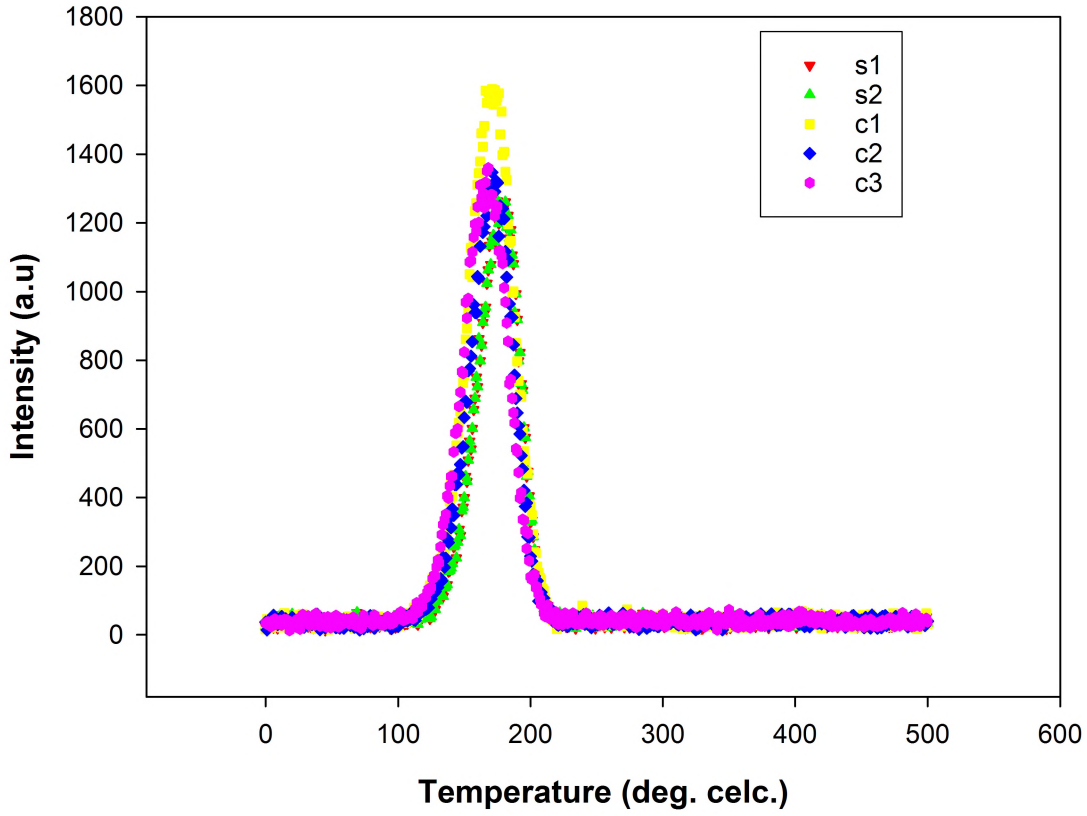

Figure 7.5: TL glow curves measured after 66 days of storage from samples that were annealed at 900°C for 15 minutes then stored in the dark at ambient temperatures in the same room without artificial irradiation. Samples c1, c2 and c3 were stored in a light-tight container, whereas samples s1 and s2 were stored at two separate sites in an open space.

7.4 Effect of post-irradiation preheat temperature on charge occupancy of the main and intermediate traps during sample storage

We investigated how a post-irradiation preheat temperature affects the rate of charge transfer from the deep traps into the main and intermediate traps during storage. Three samples, labelled e1, e2 and e3, of approximately similar TL sensitivity, were annealed at 900°C for 15 minutes then irradiated to 1000 Gy of beta dose followed by a preheat to 400°C, 500°C and 600°C respectively. All the three samples were

thereafter stored at ambient temperature in a light-tight container which was kept in the dark. The samples were stored for 25 days. Figure 7.6 shows the recorded TL glow curves (after background substraction) for the three samples and in the inset are same glow curves on semi-log scale.

The TL glow curves of Figure 7.6 show that the main peak and intermediate peaks appeared in the samples annealed at 400°C and 500°C. However, there is apparently no TL peak for a preheat temperature of 600°C.

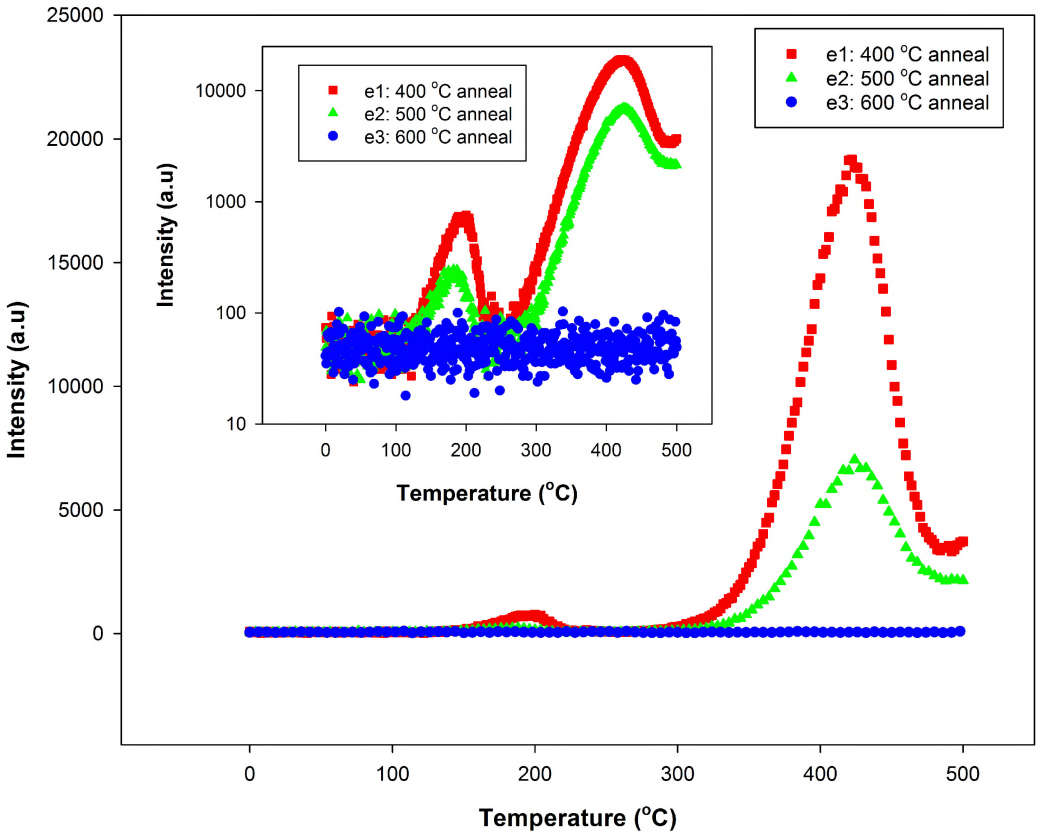

Figure 7.6: TL glow curves measured at 1°C/s for samples that were preheated to 400°C, 500°C and 600°C following 1000 Gy beta irradiation and stored at ambient temperature in the dark for 25 days before TL readout. The inset shows the corresponding plots in a semi-log scale.

It is evident from Figure 7.6 that both the main trap and intermediate traps for samples e1 and e2 contain charges prior to TL readout following storage. Since the preheat temperature of sample e1 i.e. 400°C, does not erase all the intermedi-

ate traps, the presence of the intermediate peaks is to be expected. However, the presence of charges in the main peak of e1 indicates migration of charges from the occupied intermediate traps and deep traps. Furthermore, the intermediate peak in e1 begins at temperatures around 300°C which indicates the presence of charges in the low-temperature intermediate traps which were otherwise supposed to be empty due to the post-irradiation preheat treatment before storage. As observed in sample e2, preheating to 500°C decreases charge population in both the main traps and subsidiary traps as evidenced from reduced intensities of both the main peak and intermediate peaks. Preheating to 500°C after irradiation, empties the shallow, main and intermediate traps all together but leaves the deep traps intact. The presence of charge in the main and subsidiary traps, is therefore, due to charge leakage from deep traps as explained in the previous sections. Preheating to 600°C on the other hand, causes the possibility of getting charges into either the main or intermediate traps to be less likely. This is evident from apparent absence of charges in both the main and subsidiary peaks. This suggests that annealing to 600°C completely empties those deep traps that donate charge to the main and intermediate traps. Probably, the preheat to 600°C increases the spatial separation between acceptor traps (main and intermediate traps) and donor traps (deep traps).

7.4.1 Possible explanation of OSL signal recuperation observed in α-Al_2O_3:C

Ideally, when a luminescent material is irradiated and stored at ambient temperature, every subsequent OSL readout without further irradiation is expected to yield less and less luminescence due to depopulation of OSL active traps at each readout stage. However, there are other mechanisms by which charge depopulation at the OSL traps may occur without external influences such as light and heat. One such mechanism is anomalous fading. Anomalous fading has been widely reported for luminescent materials such as feldspar [59, 60, 61]. Investigations on fading in α-Al_2O_3:C carried out by Nyirenda [23] revealed that there is a possibility of getting more OSL yield after some storage period than the OSL yield obtained during the preceding OSL measurement. This signal re-growth following storage is what has been termed as signal

recuperation. Signal recuperation has also been previously reported for luminescent materials such as quartz [62, 63, 64] and α-Al_2O_3:C [23].

It has been shown in the previous chaptes that, in α-Al_2O_3:C, the main trap is the primary OSL trap whereas the intermediate traps (V and VI) constitute the secondary contributors to the OSL. Thus, charge population in these intermediate traps has remarkable effect on the OSL yield. It has also been shown in the previous sections that intermediate traps are capable of accepting charges from deep traps. Consequently, the population of charges in these intermediate traps depends on the concentration of filled donor traps and storage time before the next OSL readout. Therefore, a significant degree of charge migration from deep traps to the intermediate traps during storage is likely to result into an increased OSL yield in the succeeding OSL readout i.e. recuperation.

7.5 Summary

It has been successfully demonstrated using experimental data that charges do migrate from the deep traps (donors) to the main and intermediate traps (acceptors) during sample storage in the dark at ambient temperature. The intermediate peaks recorded due to this charge migration, evolve into a single TL peak. On the other hand, the main peak shifts towards higher temperatures and its FWHM increases with storage time. During storage, the background radiation selectively fills the low-temperature components, whereas the charges from deep traps and/or intermediate traps preferentially occupy the high-temperature components of the main trap. Pre-heating to 600°C following beta irradiation seems to extremely minimize occurrences of charge transfer between the donor traps and acceptor traps. This indicates that the major donor traps lie between 500-600°C. The fact that the intermediate peaks are relatively more intense than the main peak indicates that the mechanism of charge transfer is donor-acceptor proximity dependent i.e. the intermediate traps lie close to the major donor traps between 500 and 600°C. However, the actual mechanism by which charges move from the deep traps to the main and intermediate traps requires further investigations.

Chapter 8

Conclusions

The emission spectra and stimulated luminescence processes in α-Al_2O_3:C have been studied. The radioluminescence (RL) emission spectra produce 7 peaks, one of which, situated in the 260-300 nm range, remains unidentified. This unidentified emission band, according to our results, may be associated with hole recombinations at a luminescence centre. The 694-nm R-line emission from Cr^{3+} impurity ions is most likely due to hole recombination at Cr^{2+} during stimulated luminescence and as a result of an intracentre excitation of Cr^{3+} due to photon absorption in photoluminescence (PL). Furthermore, the Cr^{3+} emission decreases in intensity with repeated RL measurements, an occurrence that requires further investigations.

It has also been noted that with increasing X-ray irradiation doses, the dominant emission associated with the TL peak III (250-320°C), shifts from the F-centre emission band to the Cr^{3+} emission band. In addition, it has been established that depending on the amount of X-ray irradiation dose imparted to a sample, both holes and/or electrons may be involved in the recombination processes during the thermal emptying of the traps associated with TL peaks I, II and III. This revelation contradicts the fact that the main trap generally consists of a low-temperature electron trap and a high-temperature hole trap.

We have seen that deep-traps CW-OSL produces a peak-shaped signal. The presence/absence of the peak depends upon the radiation dose used, illumination light, post-irradiation annealing temperature, concentration of charges in the main trap and the measurement temperature of OSL. The major requirement to obtained a peak-shaped signal is that the secondary OSL traps and deep traps collectively, be

sufficiently filled relative to the main trap.

Both TR-OSL and CW-OSL have shown evidence of strong retrapping at the main trap during optical stimulation of charges from the secondary OSL traps and the deep traps and that the retrapping occurs via the delocalized bands. A detailed study of the phenomenon of thermal assistance in the material using CW-OSL method under different conditions has revealed that the phenomenon is a complex one and requires a more systematic approach.

The first challenge in studying the deep traps in the material is the high temperatures at which they occur, which makes them unattainable using the commercially available TL/OSL Readers. Secondly, the high-levels of retrapping in the material make it difficult to characterize the deep traps based on the OSL produced since the main trap plays a big role in the production of OSL.

We have also observed that a high-beta irradiation dose induces aggregate defect centres in the material which remarkably affect the TL and OSL properties of the material. The induced aggregate centres get completely destroyed by heating a sample to 700°C, an effect that restores the initial TL and OSL properties of the material. The radiation-induced defects cause the main TL peak to shift towards higher temperatures, increase its FWHM, reduce its maximum intensity and cause an underestimation of both the activation energy and order of kinetics of the peak. On the other hand, the OSL response of the material is increased following a high-beta irradiation dose.

Finally, we have successfully demonstrated using experimental means that charges do migrate from the deep traps (donors) to the main and intermediate traps (acceptors) during sample storage in the dark at ambient temperature. In addition, the major donor traps during this charge transfer phenomenon lie between 500-600°C.

8.1 Potential areas for further research

- The details of deep traps in the material remain sketch due to equipment limitations and high retrapping rates at the main trap during OSL. The traps in the temperature range 400-600°C have shown to have greater influence on both TL and OSL characteristics of the material. It would be interesting to carry out

a spectral study of these traps i.e. using TL that can be measured up to 600°C. This study would also reveal the real nature of the traps in terms of whether they are hole traps or electron traps.

- It has been demonstrated in Chapter 5, that the phenomenon of thermal assistance in the material is a complex one. It is difficult to interpret the activation energies of thermal assistance obtained using the Arrhenius plots. However, to enhance our understanding of the luminescence processes that take place at elevated temperatures leading to thermal assistance, it is imperative that the mechanisms underlying thermal assistance get uncovered.

- More spectral studies are required to understand the nature and identities of the radiation-induced defects in the material. This will assist in understanding the actual mechanisms by which these defects influence the TL and OSL characteristics of the material.

- Under TR-XEOL investigations on temperature dependence of some emission features, it was discovered that for a sample that was irradiated at 400° then TR-XEOL spectra measured at various temperatures from 30-300°C, the peak intensity of the F-centre emission band increased with measurement temperature. Furthermore, the increase is rapid beyond 140°C where you would expect the F-centre emission to be considerably affected by thermal quenching. This behaviour warrants further investigation.

- The decrease in 694-nm Cr^{3+} emission with repeated RL measurements also requires further investigation.

8.2 List of publications

1. Nyirenda, A.N., Chithambo, M.L., (2017) Factors influencing the shape of CW-OSL signal obtained by stimulation of very deep traps in carbon-doped aluminium oxide: An experimental study, J. Lumin, 192:436-442

2. Nyirenda, A.N., Chithambo, M.L., (2017) The influence of radiation-induced

defects on thermoluminescence and optically stimulated luminescence of α-Al_2O_3:C. Nucl. Instr. Meth. B, 397:92-100

3. Nyirenda, A.N., Chithambo, M.L., Polymeris, G.S., (2016) On luminescence stimulated from the deep traps using thermally-assisted time-resolved optical stimulation in α-Al_2O_3:C, Radiat. Meas., pp 1-4

4. Nyirenda, A.N., Chithambo, M.L., (2016) Dependence of the photoionization cross-section of α-Al_2O_3:C on the measurement temperature. Proceedings of SAIP2015, ISBN: 978-0-620-70714-5

5. Nyirenda, A.N., Chithambo, M.L., (2015) Kinetic analysis of the main glow peak of α-Al_2O_3:C exposed to high irradiation dose. Nucl. Journal of Nuclear Sciences, 2:23-30

6. Chithambo, M.L., Nyirenda, A.N., Finch, A.A., Rawat, N.S., (2015) Time-resolved optically stimulated luminescence and spectral emission features of α-Al_2O_3:C. Phys. B. 473:62-71

Submitted

1. Nyirenda, A.N., Chithambo, M.L., Spectral study of X-ray excited radioluminescence in carbon-doped aluminium oxide. Radiation Measurements.

References

[1] M.S. Akselrod, V.S. Kortov, and E.A. Gorelova. Preparation and properties of α-Al_2O_3:C. *Radiat. Prot. Dos.*, 47:159–164, 1993.

[2] M.S. Akselrod, V.S. Kortov, D.J. Kravetsky, and V.I. Gotlib. Highly sensitive thermoluminescent anion defective α-Al_2O_3:C single crystal detectors. *Rad. Prot. Dos.*, 32:15–20, 1990.

[3] Y. Kirsh. Kinetic analysis of thermoluminescence. *Phy. Stat. Sol.*, 129:15, 1992.

[4] V. Pagonis, G. Kitis, and C. Furreta. *Numerical and Practical Exercises in Thermoluminescence.* Springer, 2006.

[5] R. Chen and V. Pagonis. *Thermally and Optically stimulated luminescence.* John Wiley and Sons Ltd, 2011.

[6] M.L. Chithambo. A method for kinetic analysis and study of thermal quenching in thermoluminescence based on the area under an isothermal decay-curve. *J. Lumin.*, 151:235–243, 2014.

[7] L. Bøtter-Jensen, S.W.S. McKeever, and A.G. Wintle. *Optically Stimulated Luminescence Dosimetry.* Elsevier, Amsterdam, 2003.

[8] E. Bulur. An alternative technique for optically stimulated luminescence (OSL) experiment. *Radiat. Meas.*, 26:701–709, 1996.

[9] E.G. Yukihara and S.W.S. McKeever. *Optically stimulated luminescence: Fundamentals and applications.* John Wiley and Sons, Ltd, 2011.

[10] M.L. Chithambo. The analysis of time-resolved optically stimulated luminescence: II. computer simulations and experimental results. *J. Phys. D: Appl. Phys.*, 40:1880–1889, 2007.

[11] V. Pagonis, J. Lawless, R. Chen, and M.L. Chithambo. Analytical expressions for time-resolved optically stimulated luminescence experiments in quartz. *J. Lumin.*, 131:1827–1835, 2011.

[12] M.L. Chithambo. The analysis of time-resolved optically stimulated luminescence: I. theoretical considerations. *J. Phys. D: Appl. Phys.*, 40:1874–1879, 2007.

[13] V. Pagonis, R. Chen, J.W. Maddrey, and B. Sapp. Simulations of time-resolved photoluminescence experiments in α-Al_2O_3:C. *J. Lumin.*, 131:1086–1094, 2011.

[14] S.W.S. McKeever. *Thermoluminescence of solids.* Cambridge University Press, 1985.

[15] I.K. Bailif, S.G.E. Bowman, S.F. Mobbs, and M.J. Aitken. The phototransfer technique and its use in thermoluminescence dating. *J. Electrostat.*, 3:269–280, 1977.

[16] C.S. Alexander and S.W.S. McKeever. Phototransferred thermoluminescence. *J.Phys. D: Appl. Phys.*, 31:2908–2920, 1998.

[17] E. Bulur and H.Y. Gøksu. Phototransferred thermoluminescence from α-Al_2O_3:C using blue light emitting diodes. *Radiat. Meas.*, 30:203–206, 1999.

[18] M.L. Chithambo, C. Seneza, and J.M. Kalita. Phototransferred thermoluminescence of α-Al_2O_3:C: Experimental results and empirical models. *Radiat. Meas.*, pages 1–10, 2017.

[19] J.G. Solé, L.E. Bausá, and D. Jaque. *An introduction to the optical spectroscopy of inorganic solids.* John Wiley and Sons, Ltd, 2005.

[20] M. Gaft, R. Reisfield, and G. Panczer. *Modern luminescence spectroscopy of minerals and materials.* Springer, 2015.

[21] M.L. Chithambo and R.B. Galloway. A pulsed light-emitting-diode system for stimulation of luminescence. *Meas. Sci. Technol.*, 11:418, 2000.

[22] M.L. Chithambo. A time-correlated photon counting system for measurement of pulsed optically stimulated luminescence. *J. Lumin.*, 131:92–98, 2011.

[23] A.N. Nyirenda. Mechanisms of luminescence in α-Al_2O_3:C: Investigations using time-resolved optical stimulation and thermoluminescence techniques. *Unpublished MSc thesis*, 2013.

[24] B.J. Luff and P.D. Townsend. High sensitivity thermoluminescence spectrometer. *Measurement Science and Technology*, 4:65–71, 1993.

[25] M.L. Chithambo, A.N. Nyirenda, A.A. Finch, and N.S. Rawat. Time-resolved optically stimulated luminescence and spectral emission features of α-Al_2O_3:C. *Physica B*, 473:62–71, 2015.

[26] A.A. Finch, Y. Wang, P.D. Townsend, and M. Ingle. High Sensitivity Luminescence Measurements of materials - the St Andrews Luminescence Facility. *Unpublished manuscript.*

[27] S.W.S. McKeever, M. Moscovitch, and P.D. Townsend. *Thermoluminescence dosimetry of materials: properties and uses.* Nuclear Technology Publishing, Ashford, Kent TN23 1YW, England, 1995.

[28] M.L. Chithambo and G. Costin. Temperature-dependence of time-resolved optically stimulated luminescence of synthetic α-Al_2O_3:C. *J. Lumin.*, 182:252–262, 2017.

[29] S.M.S. Damkjær, C.E. Andersen, and M.C. Aznar. Improved real-time dosimetry using the radioluminescence signal from Al_2O_3:C. *Radiat. Meas.*, 32:893–897, 2008.

[30] V. Kortov, A. Lushchik, V. Nagirnyi, D. Anancheko, and I. Romet. Spectrally resolved thermally stimulated luminescence of irradiated anion-defective alumina single crystals. *J. Lumin.*, 186:189–193, 2017.

[31] K.H. Lee and Jr. J.H. Crawford. Luminescence of the F centre in sapphire. *Physical Review B*, 19:3217–3221, 1979.

[32] B. Henderson and G.F. Imbusch. *Optical spectroscopy of Inorganic solids.* Oxford University Press, New York, 1989.

[33] J. Bouman. On the deep-red luminescence of Cr^{3+} in $Y_3Al_{5-x}Ga_xO_{12}$:Cr^{3+}. *MSc thesis*, 2016.

[34] G. Blasse and B.C. Grabmaier. *Luminescent Materials.* Springer-Verlag, New York, 1994.

[35] S.V. Nikiforov, I.I. Milman, and V.S. Kortov. Thermal and optical ionization of F-centers in the luminescence mechanism of anion-defective corundum crystals. *Radiat. Meas.*, 33:547–551, 2001.

[36] M.S. Akselrod, N.A. Larsen, V. Whitley, and S.W.S. McKeever. Thermal quenching of F-centre luminescence in Al_2O_3:C. *J. Lumin.*, 84, 1998.

[37] G.S. Polymeris and G. Kitis. Thermally assisted photo transfer OSL from deep traps in Al_2O_3:C exhibiting different TL peaks. *Applied Radiation and Isotopes*, 70:2478–2487, 2012.

[38] A.E. Akselrod and M.S. Akselrod. Correlation between OSL and the distribution of TL traps in Al_2O_3:C. *Rad. Prot. Dos.*, 100:217–220, 2002.

[39] S.V. Nikiforov, V.S. Kortov, A.A. Nosal, and E.V. Moiseikin. On the role of hole trapping centres in the interactive mechanism of the trap interaction in anion-defect alumina single crystals. *Physics of the solid state*, 53:2141–2146, 2011.

[40] L.E. Colyott, M.S. Akselrod, and S.W.S. McKeever. Phototransferred thermoluminescence in α-Al_2O_3:C. *Radiat. Prot. Dos.*, 65:263–266, 1996.

[41] V. Singh, R.P.S. Chakradhar, J.L. Rao, J.L. Al-Shamery, M. Haase, and Y.-D. Jho. Electron paramagnetic resonance and photoluminescence properties of α-Al_2O_3:Cr^{3+}. *Appl. Phys. B*, 107:489–495, 2012.

[42] E.G. Yukihara, V.H. Whitley, J.C. Polf, D.M. Klein, S.W.S. McKeever, A.E. Akselrod, and M.S. Akselrod. The effects of deep traps on the thermoluminescence of Al_2O_3:C. *Radiat. Meas.*, 37:627–638, 2003.

[43] M.S. Akselrod and E.A. Gorelova. Deep traps in highly sensitive α-Al_2O_3:C. *Nucl. Tracks Radiat. Meas.*, 21:143–146, 1993.

[44] G.S. Polymeris, S. Raptis, D. Afouxenidis, N.C. Tsirliganis, and G. Kitis. Thermally assisted OSL from deep traps in Al_2O_3:C. *Radiat. Meas.*, 45:519–522, 2010.

[45] S.W.S. McKeever, L. Bøtter-Jensen, N. Agersnap Larsen, and G.A.T. Duller. Temperature dependence of OSL decay curves: Experimental and theoretical aspects. *Radiat. Meas.*, 27:161–170, 1997.

[46] N.A. Larsen. *Dosimetry based on thermally and optically stimulated luminescence, PhD Dissertation.* Niels Bohr Inst., Univ. of Copenhagen, 1997.

[47] M.L. Chithambo, C. Seneza, and F.O. Ogundare. Kinetic analysis of the high temperature secondary thermoluminescence glow peaks in α-Al_2O_3:C:. *Radiat. Meas.*, 66:21–30, 2014.

[48] B.G. Markey, M.S. McKeever, S.W.S.and Akselrod, L. Bøtter-Jensen, N. Agersnap Larsen, and L.E. Colyott. The temperature dependence of optically stimulated luminescence from α-Al_2O_3:C. *Radiat. Prot. Dos.*, 65:185–189, 1996.

[49] A.I. Surdo, V.S. Kortov, and I.I. Milman. Creation of aggregate F-centres in corundum irradiated with fast electrons. *Technol. Phys. Lett.*, 11:943–947, 1985.

[50] M. Izerrouken and T. Banyahioa. Adsorption and photoluminescence study of Al_2O_3 single crystal irradiated with fast neutrons. *Nucl. Instru. Meth. B*, 268:2087–2090, 2010.

[51] V.S. Kortov, V.A. Pustovarov, S.V. Zvonarev, and Shtang T.V. Luminescence and radiation-induced color centres in anion-defective alumina crystals after high-dose irradiation. *Radiat. Meas.*, pages 1–4, 2016.

[52] E.A. Kotomin and A.I. Popov. Radiation-induced point defects in simple oxides. *Nuclear Instrum. Methods B*, 141:1–15, 1998.

[53] A.N. Nyirenda and M.L. Chithambo. Kinetic analysis of the main glow peak of α-Al_2O_3:C exposed to high irradiation dose. *Journal of Nuclear Sciences*, 2:23–30, 2015.

[54] M.L. Chithambo. Concerning secondary peaks in α-Al_2O_3:C. *South African J. Sci.*, 100:524–527, 2004.

[55] V.V et al Haratyunyan. Radiation-induced effects in corundum single crystals. *Armenian Journal of Physics*, 8:129–139, 2015.

[56] E. Aşlar, E. Şahiner, G.S. Polymeris, and N. Meriç. Determination of trapping parameters in BeO ceramics in both quenched as well as reconstructed thermoluminescence glow curves using various analysis methods. *Appl. Radiat. Isot.*, 129:142–151, 2017.

[57] A.N. Nyirenda and M.L. Chithambo. Factors influencing the shape of CW-OSL signal obtained by stimulation of very deep traps in carbon-doped aluminium oxide: An experimental study. *J. of Lumin.*, 19:436–442, 2017.

[58] A.N. Nyirenda, M.L. Chithambo, and G.S. Polymeris. On luminescence stimulated from deep traps using thermally-assisted time-resolved optical stimulation in α-Al_2O_3:C. *Radiat. Meas.*, pages 1–4, 2016.

[59] R. Visocekas, V. Tale, A. Zink, N.A. Spooner, and I. Tale. Trap spectroscopy and TSL in feldspar. *Rad. Prot. Dosim.*, 66:391–394, 1996.

[60] A. Molodkov, I. Jaek, and V. Vasichenko. Anomalous fading of IR-stimulated luminescence from feldspar minerals: some results of the study. *Geochronometria*, 26:11–17, 2007.

[61] N.K. Meisl and D.J. Huntley. Anomalous fading parameters and activation energies of feldspar. *Ancient TL*, 23, 2005.

[62] F. Preusser, M.L. Chithambo, T. Gotte, M. Martini, K. Ramseyer, J.E. Sendezera, J.G. Susino, and G.A. Wintle. Quartz as a natural luminescence dosimeter. *Earth-Science Reviews*, 97:196–226, 2009.

[63] G. Kitis, G.S. Polymeris, and N.G. Kiyak. Component resolved thermal stability and recuperation study of the LM-OSL curves of four sedimentary quartz samples. *Radiat. Meas.*, 42:1273–1279, 2007.

[64] R. Chen and V. Pagonis. *Thermally and optically stimulated luminescence: A simulation approach.* John Wiley and Sons, Ltd, 2011.

Appendix

Part of the work presented in this thesis was published in some international journals. Attached below are the published papers.

Radiation Measurements xxx (2016) 1–4

Contents lists available at ScienceDirect

Radiation Measurements

journal homepage: www.elsevier.com/locate/radmeas

On luminescence stimulated from deep traps using thermally-assisted time-resolved optical stimulation in α-Al_2O_3:C

A.N. Nyirenda [a], M.L. Chithambo [a, b, *], G.S. Polymeris [b]

[a] Department of Physics and Electronics, Rhodes University, PO BOX 94, Grahamstown 6140, South Africa
[b] Institute of Nuclear Sciences, Ankara University, Beşevler, 06100 Ankara, Turkey

HIGHLIGHTS

- The transfer mechanisms of electrons from deep traps in cα-Al_2O_3:C is reported.
- Electrons from deep traps are redistributed to the main and shallow trap before recombination.
- The luminescence from deep traps is affected by thermal quenching showing that the F-centre is key in the process.
- W = 1.028 ± 0.002 eV and $\nu = 2.8 \times 10^{13}$ s^{-1}.

ARTICLE INFO

Article history:
Received 25 October 2015
Received in revised form
7 December 2015
Accepted 9 January 2016
Available online xxx

Keywords:
Deep traps
Time-resolved luminescence
Photo-transfer
Thermal assistance
Thermoluminescence
Lifetimes

ABSTRACT

We report a study of charge transfer mechanisms of electrons stimulated optically from very deep traps, also known as donor traps, in α-Al_2O_3:C. The investigations were carried out using thermally-assisted time-resolved optical stimulation, thermoluminescence and by way of residual thermoluminescence from the main electron trap. When the charges are optically stimulated from the deep traps, they are redistributed via the conduction band to the main electron trap and the shallow trap from where they are optically or thermally released for recombination at luminescence centres. The luminescence is strongly quenched at high measurement temperature as evident by very short luminescence lifetimes at these temperatures. The main peak due to residual thermoluminescence is located at a higher temperature than the conventional main peak.

1. Introduction

α-Al_2O_3:C is a well-known UV and ionizing radiation detector whose high sensitivity is attributed to a large concentration of F^+-centres (oxygen vacancy with one trapped electron) and F-centres (oxygen vacancy with two trapped electrons) which act as luminescence sites in the material (Akselrod et al., 1990). As with most luminescence materials, α-Al_2O_3:C has a wide energy-band gap with localised energy levels within this region. This report is concerned with time-resolved optically stimulated luminescence and thermoluminescence (TL) associated with localized energy levels lying well within the band gap which will be referred to as very deep traps (VDT) hereafter. For pragmatic reasons, we identify VDTs as those traps that are thermally inaccessible when a luminescent material is heated from room temperature to 500 °C, as is usual, with archetypical TL measurement systems.

Due to a number of reasons including loss of luminescence caused by increase in measurement temperature (thermal quenching), interference from blackbody radiation, large thermal depth in conjunction with low photo-ionization cross section and instrumental limitations, the signal from VDTs is rather difficult to measure directly. Polymeris et al. (2010) developed an alternative experimental method on α-Al_2O_3:C aimed at measuring the signal from VDTs without any need to heat a sample to greater than 500 °C. In this method, which they referred to as thermally-assisted optically stimulated luminescence (TA-OSL), an irradiated sample is first heated to 500 °C in order to deplete the main TL dosimetric trap and all other subsidiary electron traps. Subsequently, photo-transferred OSL is then measured at elevated temperatures

* Corresponding author. Department of Physics and Electronics, Rhodes University, PO BOX 94, Grahamstown 6140, South Africa.
E-mail address: m.chithambo@ru.ac.za (M.L. Chithambo).

http://dx.doi.org/10.1016/j.radmeas.2016.01.016
1350-4487/

(180–190 °C) using 470 nm blue LEDs for optical stimulation. The methodology is similar to that proposed by Bulur and Göksu (1999) for measurement of phototransferred thermoluminescence (PTTL).

The presence of VDTs in a number of other materials including CaF_2:N (Polymeris et al., 2006) and apatite (Kitis et al., 2013; Polymeris et al., 2014) has been experimentally verified by measuring the corresponding TA-OSL. Indeed, TA-OSL has proven to be a promising tool in quartz dosimetry (Kitis et al., 2010; Polymeris et al., 2015). Nevertheless, all aforementioned experimental studies on TA-OSL stimulating VDTs have revealed several experimental features which need further exploration. Among these, the most important feature deals with the shape of the TA-OSL curve. For naturally occurring luminescent phosphors such as, for example, quartz or apatite, the shape of the TA-OSL decay curve resembles a conventional continuous-wave OSL (CW-OSL) decay curve. In contrast, the signal from CaF_2:N and α-Al_2O_3:C resembles the shape of a linearly modulated OSL (LM-OSL) curve. It is interesting to note that the maximum position in the latter is shifted towards higher stimulation times as the stimulation temperature is increased. For the case of CaF_2:N, the model adopted to describe the photo-transfer effect assumes the presence one deep trap from which the charge is excited, a shallow trap into which the charge is transferred and a recombination centre. The corresponding data (Figs. 11 and 15 of Polymeris et al., 2006) were successfully fitted using the simplified analytical expression given by Chen and McKeever (1997) to describe the transfer mechanism, implying that the electrons go through the conduction band after eviction from the VDTs.

The aim of the present work is to verify this hypothesis for the case of crystalline anion deficient alumina doped with carbon (α-Al_2O_3:C) by using time resolved optically stimulated luminescence (TR-OSL).

Time-resolved optical stimulation is a key method for measurement of OSL whose aim is to separate temporally the stimulation and emission of luminescence. The stimulation is done using a brief light pulse during which the resultant luminescence builds up over a background of photomultiplier noise and constant scatter from the stimulating light. After the pulse, the luminescence is measured over photomultiplier noise only. In this way, time resolved luminescence spectra can be recorded and resolved into components each associated with a distinct mean lifetime denoting the delay between stimulation and emission of luminescence. The measured lifetime consists of the time required to stimulate an electron from a trap, the transit time through the conduction band and the lifetime of the excited state at the recombination centre but in most cases, the dominant component is the relaxation time at the luminescence centre (Chithambo and Galloway, 2001). The lifetimes are associated with charge transfer processes and as such help to explain dynamics of luminescence. The mathematical basis of TR-OSL was described by Chithambo (2007a,b) and its theory and applications have been reviewed by Chithambo et al. (2016).

2. Experimental details

Samples used were aluminium oxide disks of 5 mm diameter and 1 mm thickness (Rexon TLD Systems, Ohio, USA). Before use, samples were annealed in a furnace at 900 °C followed by rapid cooling in air. All TL measurements were carried out in a Risø TL/OSL DA-20 Reader. The luminescence was detected by an EMI 9235QB photomultiplier tube through a 7-mm thick Hoya U-340 filter (transmission band 270–380 mm FWHM). Samples were irradiated using a $^{90}Sr/^{90}Y$ beta-source at a dose rate of 0.10 Gy s^{-1}.

Time-resolved luminescence was measured using a pulsing system described elsewhere (Chithambo and Galloway, 2000; Chithambo, 2005, 2011). In the set-up, an ORTEC MCS-plus multichannel scaler is used to trigger a set of 470 nm blue LEDs (Nichia NSPB-500) while simultaneously processing luminescence photon counts from an EMI 9635QA photomultiplier to produce time-resolved luminescence spectra. Luminescence was stimulated at a pulse width of 18 ms and each spectrum obtained using a dwell time of 1 ms, 1000 sweeps and a dynamic range of 500 ms. The sample temperature was controlled by an AO500 sample heater (MBE-Komponenten GmbH, Germany).

Time-resolved luminescence spectra discussed in this paper should not be confused with similarly named ones found in either optical absorption or photoluminescence and fluorescence spectrometry where the luminescence intensity is recorded as a function of the emission wavelength or the photon energy (Becker, 2005).

All samples were subjected to the same procedure as follows:

1. TL at 1 °C s^{-1} to 500 °C in order to remove background dose
2. Irradiation to 100 Gy
3. TL at 1 °C s^{-1} to 500 °C in order to empty charges in shallow and intermediate traps. This measurement was also used for checking changes in sample sensitivity
4. TR-OSL measurement
5. TL at 1 °C s^{-1} to 500 °C to record PTTL

Step 1 was necessary only during the first measurement whereas the rest of the steps were repeated for measurement temperatures of TR-OSL ranging from 30 to 220 °C at intervals of 10 °C. Unless otherwise stated, all samples were beta irradiated to 100 Gy. To avoid damage to the photomultiplier due to excessive intensities at high dose (i.e. 100 Gy), an absorptive neutral density filter, a Hoya ND-03 (1\% transmission, 400–700 nm) was used in combination with a Hoya U-340 at step 3.

3. Results and discussion

3.1. General characteristics of VDT signals

Fig. 1 shows a TL glow curve obtained at 1 °C/s from α-Al_2O_3:C after irradiation to 5.0 Gy. Step 3 in the procedure above erases all the peaks visible in Fig. 1 except for the charge in VDTs. Pulsed light from 470 nm blue LEDs is able to stimulate charges from the VDTs resulting into a TR-OSL signal an example of which is shown in Fig. 2. The rising component of the TR-OSL signal is obtained with the light pulse on whereas the decay component is obtained with

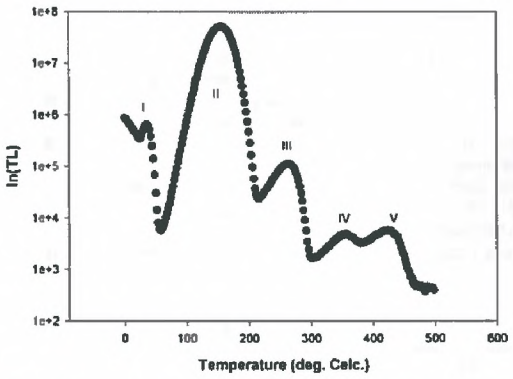

Fig. 1. TL from α-Al_2O_3:C obtained at 1 °C s^{-1} following irradiation to 5.0 Gy showing peaks at 37 °C (I), 155 °C (II), 280 °C (III), 340 °C (IV) and 420 °C (V).

Please cite this article in press as: Nyirenda, A.N., et al., On luminescence stimulated from deep traps using thermally-assisted time-resolved optical stimulation in α-Al_2O_3:C, Radiation Measurements (2016), http://dx.doi.org/10.1016/j.radmeas.2016.01.016

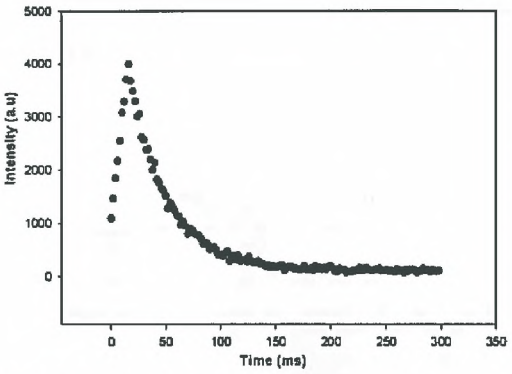

Fig. 2. A TR-OSL spectrum obtained at 70 °C using an 18 ms pulse following sample irradiation to 100 Gy (step 2) and a TL run to 500 °C (step 3).

the light pulse off. OSL from VDTs in α-Al_2O_3:C was observed at all measurement temperatures, room temperature inclusive. In contrast, α-Al_2O_3:C single crystal grains (Landauer Inc., Oklahoma, USA) produce OSL from deep traps only at elevated temperatures (Polymeris et al., 2010).

Fig. 3 shows a glow curve of the residual thermoluminescence (RTL) plotted alongside the normal TL glow curve. The intensities have been normalized to aid visual clarity. There is a clear shift in the position of the residual TL peak relative to that of the normal TL peak. It has previously been shown (Chithambo and Seneza, 2014) that the apparently single main peak in α-Al_2O_3:C is collocated with a weaker-intensity peak on its higher temperature end. The latter peak only becomes visible after the preceding main peak has been removed. Our investigations suggest that it is possibly this high temperature subsidiary component that is observed and recorded during a residual TL following optical stimulation. This explains the peak shift to higher temperatures for the residual TL peak.

3.2. The dependence of luminescence lifetimes on measurement temperature

Luminescence lifetimes were evaluated by fitting the decay component of the TR-OSL signal with the function $Ae\exp(-t/\tau) + C$,

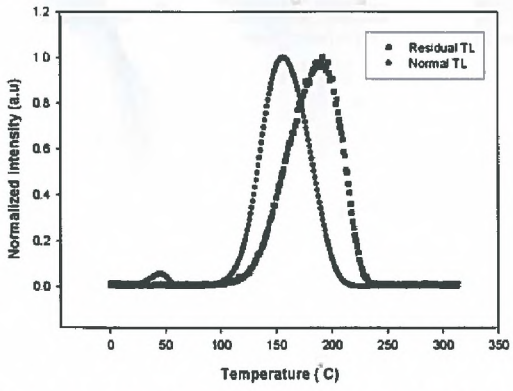

Fig. 3. Normal TL and residual TL glow curves normalized to their respective peak intensities. Both glow-curves were obtained at 1 °C s^{-1}.

where t is time, τ is the luminescence lifetime, A is a scaling parameter and C is a temperature dependent term. Fig. 4 shows the plot of luminescence lifetimes against measurement temperature.

As expected, the lifetimes get increasingly shorter with measurement temperature due to thermal quenching (Chithambo et al., 2015). Interestingly, the plot in Fig. 4 resembles that obtained by Chithambo et al. (2015) and Nyirenda (2013) for the influence of measurement temperature on luminescence lifetimes in α-Al_2O_3:C using the same TR-OSL technique. Chithambo et al. (2015) showed that lifetimes increase in the vicinity of both the shallow and main electron trap although to different extent.

Fig. 5 (from Nyirenda, 2013) shows plots of lifetime against measurement temperature for two types of samples labelled Samples 1 and 2. The thermoluminescence of both types of samples has been discussed by Chithambo et al. (2015). The thermoluminescence glow-curve of sample 1 shows the main peak with a number of weaker intensity peaks on its either end. Sample 2 shows similar features except the shallow trap. Therefore Fig. 5 compares the result of Fig. 4 with that from a sample with a

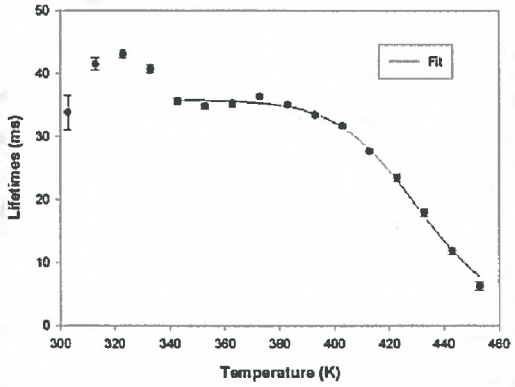

Fig. 4. A plot of luminescence lifetimes against measurement temperature for a signal associated with deep traps. The solid line represents the best-fit regression line for thermal quenching.

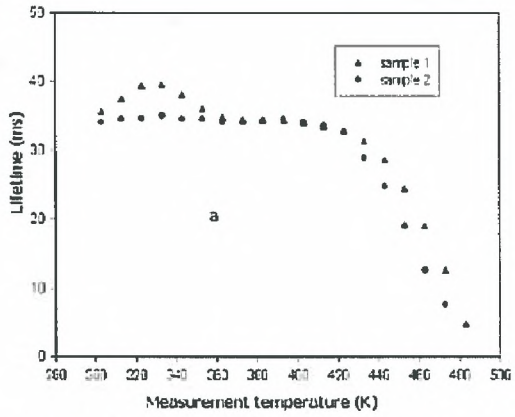

Fig. 5. A graph of luminescence lifetime against measurement temperature adapted from Nyirenda (2013). Sample 1 produced a TL glow curve that had a low temperature peak I, unlike sample 2.

Please cite this article in press as: Nyirenda, A.N., et al., On luminescence stimulated from deep traps using thermally-assisted time-resolved optical stimulation in α-Al_2O_3:C, Radiation Measurements (2016), http://dx.doi.org/10.1016/j.radmeas.2016.01.016

shallow trap, that is, sample 1.

However, both Chithambo et al. (2015) and Nyirenda (2013) recorded TR-OSL immediately after irradiation, that is, without any preheat to remove charges in shallow and intermediate traps. This similarity strongly suggests that the traps involved in the conventional TR-OSL are the same ones responsible for the TR-OSL due to the VDTs. Since the normal OSL is usually associated with the main electron trap in α-Al_2O_3:C, the similarity suggests that when charges are optically stimulated from VDTs, they are redistributed via the conduction band to the main electron trap and the shallow trap (labelled 1 in Fig. 1) followed by optical release from the main trap and subsequent recombination at luminescence centres. Therefore, caution needs to be exercised when using OSL from VDTs for deep trap characterization. Except for measurement temperatures beyond the position of the main electron trap i.e. 250 °C and above, the trapping parameters obtained from the OSL due to VDTs may not necessarily be characteristic of the VDTs but rather of the main electron trap.

The change of luminescence lifetimes with temperature (beyond the shallow trap) as shown in Fig. 4, for signal from deep traps, is expected to follow the usual thermal quenching model, $\tau(T) = \tau_{rad}/(\mathrm{Cexp}(-W/kT)$ where τ(T) is the lifetime at measurement temperature T in Kelvin, τ_{rad} is the mean radiative lifetime at 0 K and is equal to 35 ms for α-Al_2O_3:C, W is the activation energy for thermal quenching, k is the Boltzmann's constant and $C = \nu\tau_{rad}$ is a dimensionless constant where ν is the frequency factor applicable to the non-radiative process (Chithambo, 2007b). The solid line in Fig. 4 represents the best-fit regression line using the thermal quenching model from which $W = 1.028 \pm 0.002$ eV and $C = 9.8 \times 10^{11}$ which gives ν equal to 2.8×10^{13} s^{-1}. These values are consistent with those obtained by Chithambo et al. (2015) namely $W = 1.025 \pm 0.002$ eV and $\nu = 6.00 \times 10^{12}$ s^{-1}; $W = 1.08 \pm 0.03$ eV and $\nu = 1.02 \times 10^{14}$ s^{-1} (Akselrod et al., 1998) and 1.045 ± 0.002 eV and $\nu = 2.1 \times 10^{11}$ s^{-1} (Nyirenda, 2013).

4. Conclusion

The thermally assisted TR-OSL from very deep traps in α-Al_2O_3:C has been studied. The results strongly agree with the proposition that following optical stimulation from VDTs, electrons redistribute, via the conduction band to the shallow and intermediate energy electron traps. Evidence has been presented of strong retrapping of optically stimulated charges from the VDTs at the dosimetric trap. Luminescence lifetimes associated with signal from deep traps decreases with measurement temperature as a result of thermal quenching. The parameters describing thermal quenching have been evaluated and are consistent with others in the literature.

Acknowledgements

We acknowledge with gratitude financial assistance the National Research Foundation of South Africa (Grant 91546) and Rhodes University.

References

Akselrod, M.S., Larsen, N.A., Whitley, V., McKeever, S.W.S., 1998. Thermal quenching of F-center luminescence in Al_2O_3:C. J. Appl. Phys. 84, 3364–3373.
Akselrod, M.S., Kortov, V.S., Kravetsky, D.J., Gotlib, V.I., 1990. Highly sensitive thermoluminescent anion-defect α-Al_2O_3:C single crystal detectors. Radiat. Prot. Dosim. 33, 119–122.
Becker, W., 2005. Advanced Time-correlated Single Photon Counting Techniques. Springer, Berlin.
Bulur, E., Göksu, H.Y., 1999. Phototransferred thermoluminescence from α-Al_2O_3:C using blue light emitting diodes. Radiat. Meas. 30, 203–206.
Chen, R., McKeever, S.W.S., 1997. Theory of Thermoluminescence and Related Phenomena. World Scientific, Singapore.
Chithambo, M.L., 2005. Procedures preparatory to setting up a luminescence pulsing system. Ancient TL 23, 39–42.
Chithambo, M.L., 2011. A time-correlated photon counting system for measurement of pulsed optically stimulated luminescence. J. Lumin. 131, 92–98.
Chithambo, M.L., Ankjærgaard, C., Pagonis, V., 2016. Time-resolved luminescence from quartz: an overview of contemporary developments and applications. Phys. B Condens. Matter 481, 8–18.
Chithambo, M.L., Galloway, R.B., 2001. On the slow component of luminescence stimulated from quartz by pulsed blue light emitting diodes. Nucl. Instrum. Methods B 183, 358–368.
Chithambo, M.L., Galloway, R.B., 2000. A pulsed light emitting diode system for stimulation of luminescence. Meas. Sci. Technol. 11, 418–424.
Chithambo, M.L., 2007a. The analysis of time-resolved optically stimulated luminescence I: theoretical considerations. J. Lumin. 40, 1874–1879.
Chithambo, M.L., 2007b. The analysis of time-resolved optically stimulated luminescence. II: computer simulations and experimental results. J. Phys. D: Appl. Phys. 40, 1880–1889.
Chithambo, M.L., Nyirenda, A.N., Finch, A.A., Rawat, N.S., 2015. Time-resolved optically stimulated luminescence and spectral emission features of α-Al_2O_3:C. Phys. B Condens. Matter 473, 62–71.
Kitis, G., Kiyak, N.G., Polymeris, G.S., Pagonis, V., 2010. Investigation of OSL signals from very deep traps in unfired and fired quartz samples. Nucl. Instrum. Methods B 268, 592–598.
Kitis, G., Polymeris, G.S., Pagonis, V., Tsirliganis, N.C., 2013. Anomalous fading of OSL signals originating from very deep traps in Durango apatite. Radiat. Meas. 49, 73–81.
Nyirenda, A.N., 2013. Mechanisms of Luminescence in α-Al_2O_3:C: Investigations Using Time-resolved Optical Stimulation and Thermoluminescence Techniques (Unpublished MSc thesis).
Polymeris, G.S., Sahiner, E., MeriÃ¶, N., Kitis, G., 2015. Experimental features of natural thermally assisted OSL (NTA-OSL) signal in various quartz samples; preliminary results. Nucl. Instrum. Methods B 349, 24–30.
Polymeris, G.S., Giannoulatou, V., Sfampa, I.K., Tsirliganis, N.C., Kitis, G., 2014. Search for stable energy levels in materials exhibiting strong anomalous fading: the case of apatites. J. Lumin. 153, 245–251.
Polymeris, G.S., Kitis, G., Tsirliganis, N.C., 2006. Correlation between TL and OSL properties of CaF_2:N. Nucl. Instrum. Methods B 251, 133–142.
Polymeris, G.S., Raptis, S., Afouxenidis, D., Tsirliganis, N.C., Kitis, G., 2010. Thermally assisted OSL from deep traps in Al_2O_3:C. Radiat. Meas. 45, 519–522.

Please cite this article in press as: Nyirenda, A.N., et al., On luminescence stimulated from deep traps using thermally-assisted time-resolved optical stimulation in α-Al_2O_3:C, Radiation Measurements (2016), http://dx.doi.org/10.1016/j.radmeas.2016.01.016

Journal of Luminescence 192 (2017) 436–442

Contents lists available at ScienceDirect

Journal of Luminescence

journal homepage: www.elsevier.com/locate/jlumin

Factors influencing the shape of CW-OSL signal obtained by stimulation of very deep traps in carbon-doped aluminium oxide: An experimental study

A.N. Nyirenda*, M.L. Chithambo

Department of Physics and Electronics, Rhodes University, P.O Box 94, Grahamstown 6140, South Africa

ARTICLE INFO

Keywords:
Retrapping
Recombination
Trap
Donor
Acceptor
Peak-like
Radiative

ABSTRACT

The optically stimulated luminescence from carbon-doped aluminium oxide (α-Al2O3:C) displays a peak with time under certain measurement conditions. In this paper, we present factors that influence the peak-like shape of continuous-wave optically stimulated luminescence (CW-OSL) signal. The report is based on the experimental study of OSL signals obtained by stimulation of very deep traps in α-Al2O3:C. Methods exploiting post-irradiation annealing, variable dose and temperature dependent OSL measurements were used in the investigation. It is found that the rising part of the CW-OSL peak is obtained when the rate of retrapping at the most optically active trap (main trap) exceeds the rate of direct radiative recombination following optical release of charges from all optically active traps. This is possible if, during optical stimulation, the primary trap responsible for OSL i.e. the main trap, is substantially unoccupied and the very deep, donor traps are substantially filled up. The rate of charge retrapping itself is deduced to depend on the occupancy of the acceptor traps i.e. shallow, main and secondary traps; concentration of charge carriers in the very deep, donor traps; the post-irradiation annealing temperature and the temperature at which the OSL is measured.

1. Introduction

Continuous-wave optically stimulated luminescence (CW-OSL) is a steady-state method for measuring OSL whereby the intensity of the stimulation light is held constant throughout the stimulation period while the OSL signal is continuously monitored. Conventionally, the observed luminescence decays monotonically with optical stimulation time due to emptying of charges from traps and their subsequent recombination at luminescence centres. For first order kinetics i.e. no retrapping, the time-dependence of a CW-OSL decay curve can be approximated by a simple exponential or a summation of simple exponentials. Quartz, for example, produces a CW-OSL decay curve that can be deconvolved into three exponential components termed as fast, medium and slow components [1,2].

Depending on the experimental conditions, a peak-like CW-OSL signal, rather than a monotonically decaying one, is observed in some materials, for example, Al2O3:C [3,4], CaF2:N [5], BeO [6], quartz and feldspar [7]. Results of simulations based on the OSL model devised by Yukihara and McKeever [8] and McKeever, et al. [7] demonstrated that a peak observed in the CW-OSL curve can be attributed to trapping and thermal detrapping of charge from the shallow traps during optical stimulation. Poolton et al. [9] used the presence of the peak in the infrared (IR)-stimulated OSL curve obtained from feldspars after long green light exposure of an irradiated sample as evidence of localized, donor-acceptor type recombinations. Furthermore, McKeever [7] successfully used simulations and experimental measurements on quartz and feldspar at high dose, low optical stimulation intensity, and intermediate measurement temperatures to show that the OSL in these cases are capable of producing a peak-shaped OSL curve. The theoretical model used by Mckeever et al. [7] was based on the assumption that optical stimulation releases charges from traps into the conduction band from where they get recaptured by the traps or recombine radiatively or non-radiatively at recombination centres.

In the present work, we use an experimental approach to explore some factors that influence the peak-shaped nature of CW-OSL signal obtained by optical stimulation of very deep traps in α-Al2O3:C. Blue light and not green light was used during the study since blue light is more effective in releasing charge from deep traps in Al2O3:C [10].

* Corresponding author.
E-mail address: anyirenda@gmail.com (A.N. Nyirenda).

http://dx.doi.org/10.1016/j.jlumin.2017.07.016
Received 22 November 2016; Received in revised form 27 April 2017; Accepted 12 July 2017
Available online 13 July 2017

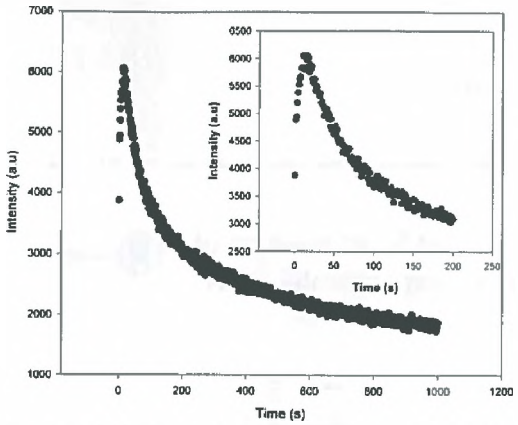

Fig. 1. A plot of CW-OSL signal obtained from blue light stimulation of very deep traps for 1000 s at 30 °C. The sample was first irradiated to 5.0 Gy followed by heating to 500 °C at 1.0 °C/s before exposing it to 470-nm blue LEDs. The inset shows the same plot for the first 200 s to provide a clearer view of the peak.

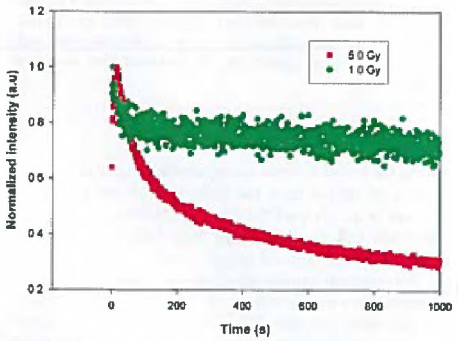

Fig. 2. Plots of CW-OSL signal for 1.0 Gy and 5.0 Gy irradiation doses. The sample was first irradiated then heated to 500 °C at 1.0 °C/s before exposing it to 470-nm blue LEDs. The signal was recorded at 30 °C for a stimulation period of 1000 s.

This work is intended to provide further insight into the charge transfer mechanisms during stimulated luminescence processes in α-Al2O3:C.

2. Experimental details

Samples used were carbon-doped aluminium oxide disks (Rexon TLD Systems, Ohio, USA) measuring 5 mm in diameter by 1 mm in thickness. All measurements were carried out in the Risø TL/OSL-DA-20 Reader. The irradiation unit is a built-in $^{90}Sr/^{90}Y$ source that delivers beta dose at a nominal rate of 0.1028 Gy/s. The luminescence detection unit consists of an EMI 9235 QB photomultiplier tube and a 7-mm thick Hoya U-340 filter (transmission 270–380 nm FWHM). The luminescence stimulation unit is comprised of 470-nm blue LEDs that delivers a maximum power intensity of 80 mW cm^2 at the sample position. Unless otherwise stated, optical power for the LEDs was set at 90% for a total stimulation time of 1000 s. All samples were annealed only once at 900 °C for 15 min before use to erase their irradiation history.

3. Results and discussion

3.1. The shape of the CW-OSL signal relative to optical stimulation of very deep traps

A previously annealed sample was irradiated to 5.0 Gy, heated linearly at 1.0 °C/s to 500 °C, and then optically stimulated for 1000 s using 470-nm blue LEDs at 30 °C to record OSL. Heating to 500 °C ensures that charge trapped during irradiation period is only available in very deep traps i.e. traps thermally accessible beyond 500 °C. Fig. 1 presents a plot of the OSL intensity versus stimulation time and, in the inset, the same feature for the first 200 s intended to better illustrate the peak-like profile. Fig. 1 shows that the CW-OSL signal obtained by optical stimulation of charge captured in very deep traps of α-Al2O3:C (following an irradiation dose of 5.0 Gy), is peak-shaped. Polymeris et al. [4] reported a similar result for α-Al2O3:C under 470-nm blue light stimulation following beta irradiation to 25.0 Gy and post-irradiation heating to 500 °C. The rising part of the curve represents the period during which the rate of charge retrapping into the most optically active traps i.e. main trap, is greater than the rate of detrapping from the optically active traps and subsequent recombination at the radiative luminescence centres. At the peak maximum, the retrapping rate is approximately equal to the rate of detrapping and subsequent direct recombination. Beyond the peak, the rate of detrapping and subsequent direct recombination exceeds charge retrapping.

We expect the retrapping rate to be more than the detrapping rate and subsequent direct recombinations if the most optically active trap is relatively less occupied and the very deep traps filled. What is relevant in Fig. 1 is that prior to optical stimulation, the main trap, that is, the most optically active trap in α-Al2O3:C, is unoccupied due to post-irradiation heating whereas the donor traps are significantly occupied due to the 5.0-Gy irradiation. We expect that the radiation history of the sample will influence the occupancy of the very deep traps. In the subsequent sections, we examine this proposal in greater detail.

3.2. Influence of charge concentration in very deep traps on the peak shape of the CW-OSL signal

The concentration of charges in very deep traps can be altered by irradiation dose, illumination light and post-irradiation annealing temperature. We now show how each one of these external influences affects the peak-shaped CW-OSL signal.

3.2.1. Effect of irradiation dose on the peak shape of the CW-OSL signal

For this study, a sample was irradiated to 1.0 Gy, heated at 1.0 °C/s to 500 °C to deplete the acceptor traps, then exposed to 470-nm blue LEDs for 1000 s at 30 °C. This procedure was repeated for 5.0 Gy irradiation dose. Fig. 2 shows the CW-OSL signals corresponding to the irradiation doses used.

Fig. 2 shows that an irradiation dose of 5.0 Gy produced a peak-shaped CW-OSL signal as expected (see Fig. 1) whereas a 1.0 Gy irradiation dose did not. In both cases i.e. 1.0 Gy and Gy, the main trap is unoccupied prior to optical stimulation. However, the occupancy of the very deep traps is greater for 5.0 Gy irradiation dose compared to 1.0 Gy irradiation dose. This is consistent with our earlier statement

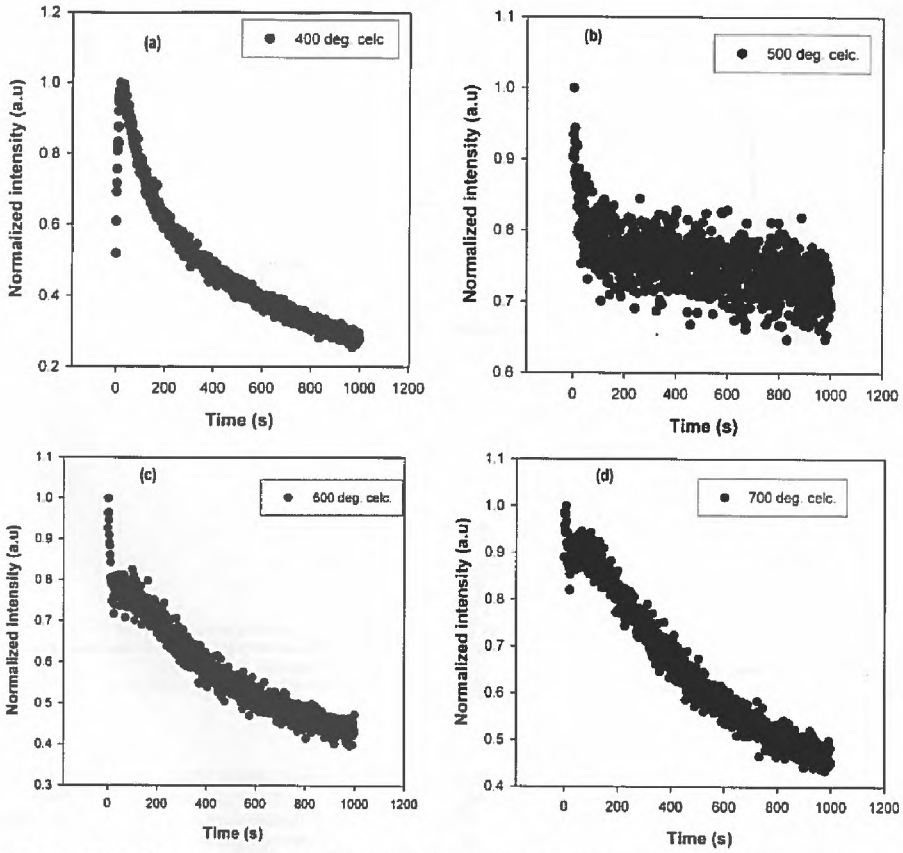

Fig. 3. Plots of CW-OSL signal obtained for annealing at 400 °C (a), 500 °C (b), 600 °C (c) and 700 °C (d). The sample was irradiated to 1.0 Gy, then annealed to a specific temperature, followed by 470-nm blue light stimulation for 1000 s at 30 °C to record OSL. There was no holding time at the annealing temperature.

that this behaviour should result when the very deep traps are significantly occupied.

3.2.2. Effect of post-irradiation annealing temperature on the peak shape of the CW-OSL signal

A sample was irradiated to 1.0 Gy, heated to 400 °C, then cooled down to 30 °C prior to OSL measurement. The sample was considered as having been annealed at 400 °C. The sample was then illuminated with 470-nm blue LEDs for 1000 s to record OSL. This procedure was repeated for annealing at 500 °C, 600 °C and 700 °C. Fig. 3 shows the CW-OSL signal recorded for the specified annealing temperatures.

Fig. 3 shows that a peak-shaped CW-OSL signal is observed after post-irradiation annealing at 400 °C. This profile is not observed for annealing at 500 °C, 600 °C and 700 °C. Scenarios observed for annealing temperatures of 600 °C and 700 °C are notable. In both cases (600 °C and 700 °C), there is an initial fast decaying component followed by slight evidence of an apparent peak-shaped OSL signal. The peak-shaped nature is more pronounced in the measurement corresponding to 700 °C than to 600 °C.

Relevant to this discussion are results of pulse annealing investigations on optically active trapping centres in α-Al2O3:C which indicate that the second major contributor to the OSL signal, besides the main trap, are the traps lying in the temperature region of 400–500 °C (see Fig. 4(a)). These traps will be referred to hereafter as secondary OSL traps. Furthermore, Fig. 4(b), a similar study by phototransfer, indicates that charges optically released from the secondary OSL traps are largely involved in the retrapping process at the main trap. Details of the investigations have been captured in the caption of Fig. 4. It is expected therefore to observe a peak-shaped OSL signal following annealing at 400 °C since the secondary OSL traps, which are the major contributor in the retrapping of charge at the main trap, are sufficiently occupied. Annealing to 500 °C on the other hand substantially depletes

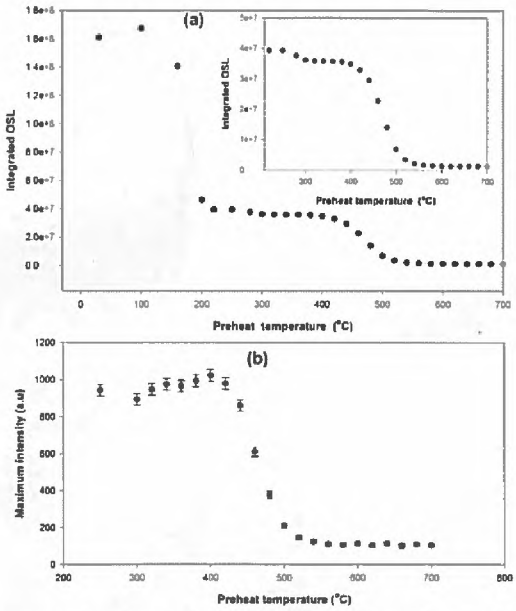

Fig. 4. (a) A Plot of integrated OSL vs. preheat temperature. A sample was irradiated to 5.0 Gy, preheated, then exposed to 470-nm blue light stimulation for 1000 s at 30 °C to record OSL. Preheat temperatures ranged from 30 to 700 °C. In the inset is the same plot for preheat temperatures between 200 and 700 °C. (b) A plot of the phototransferred TL (PTTL) maximum intensity of the main peak against preheat temperature. A sample was irradiated to 5.0 Gy, preheated to clear the main peak, illuminated with 470-nm blue LEDs for 1000 s at 30 °C followed by a TL measurement at 1.0 °C/s to 700 °C. Preheat temperatures ranged from 250 to 700 °C. A TL measurement recorded PTTL and cleared charge from the secondary traps prior to the next irradiation cycle.

the secondary OSL traps i.e. occupancy of the donor traps is significantly reduced with concomitant disappearance of the peak in the OSL signal (see Fig. 3(b)).

Annealing at 600 °C and 700 °C depletes charges from both the main and secondary OSL traps. Thus, prior to OSL readout, charge is available in the very deep traps (VDTs) only. The rate of charge detrapping from VDTs by optical means is usually very low owing to the small photoionization cross-section of the VDTs. Consequently, retrapping and recombination rates are both low. However, at the beginning of optical stimulation, the rate of direct recombination can be dominant due to competition between the main trap and secondary OSL traps to recapture charge optically released from VDTs. This may be responsible for the initial fast decay of the OSL signal seen in Fig. 3(c) for example. However, this behaviour is transient and is reversed as the main trap starts recapturing charge released from the secondary OSL traps besides that from the VDTs. It is probably for this reason that the peak starts to appear after an initial fast decay of the OSL signal (see Fig. 3(d)).

3.2.3. *Effect of illumination light on the peak shape of the CW-OSL signal*

In this test, a sample was irradiated once to 5.0 Gy, heated at 1.0 °C/s to 500 °C to deplete the main and secondary traps, then exposed to 470-nm blue LEDs for 1000 s at 30 °C to record OSL. The OSL measurements were repeated several times without any further irradiation. Every OSL measurement was succeeded by heating to 500 °C to empty the main and secondary traps prior to the next OSL cycle. Fig. 5 presents plots of CW-OSL signal obtained during multiple OSL measurements. Fig. 5 shows that the peak of CW-OSL signal diminishes with increasing number of OSL runs. Understandably, the occupancy of very deep traps (VDTs) diminishes with the number of repeated measurements hence the observed behaviour.

3.3. *Influence of charge concentration in acceptor traps on the peak shape of the CW-OSL signal*

As discussed earlier, the requirement to get the rising portion of the CW-OSL signal is that the main trap be substantially unoccupied and very deep traps substantially filled. In this investigation, we explore how the occupancy of the main trap affects the peak shape of the CW-OSL signal.

A sample was irradiated to 5.0 Gy, preheated to a temperature Tmax at 1.0 C/s, followed by an OSL measurement at 30 °C. Tmax represents a maximum temperature during a preheat. The procedure was repeated for Tmax values between 30 and 700 °C. Fig. 6 presents plots of CW-OSL signal for various maximum temperatures, Tmax. According to Fig. 6(a), for preheat temperatures between 30 and 220 °C, a decaying OSL signal (without a peak) is obtained. This indicates that these preheat temperatures do not substantially empty the main trap. As a consequence, direct radiative recombination of optically released charges from OSL active traps i.e. main trap, secondary traps and very deep traps, becomes a dominant mechanism. Under these circumstances, no peak can be observed in the time dependence of the OSL signal.

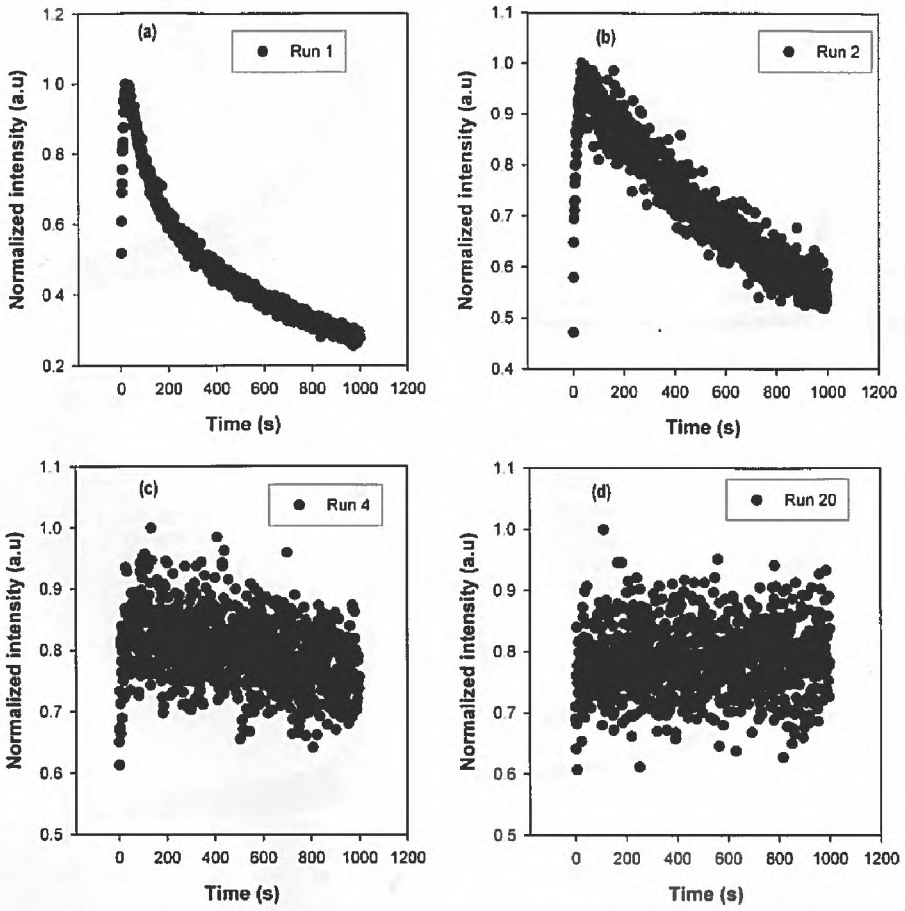

Fig. 5. Plots of repeated CW-OSL measurements. The sample was irradiated to 1.0 Gy only once at the beginning and heated to 500 °C at 1.0 °C/s between OSL measurements. Blue LEDs (470 nm) were used for very deep traps stimulation for a period of 1000 s at 30 °C. The plot only shows the first, second, fourth and twentieth runs to illustrate change in shape with repeated stimulation.

The peak-shaped CW-OSL signal is observed for preheat temperatures between 250 and 540 °C (Fig. 6(b) and (c)), an indication that the main trap is significantly unoccupied at these temperatures. As explained earlier, this the primary requirement for the time dependence of the OSL signal to show a peak profile.

Preheat temperatures between 560 and 700 °C (Fig. 6(d)) deplete the main and secondary OSL traps and substantially depopulate occupied very deep, donor traps. The observed OSL signals for preheat temperatures between 560 and 700 °C, resemble those observed for preheat temperatures between 30 and 220 °C. This suggests that the dominant charge transfer mechanism is the same between these two temperature ranges. Thus, at this temperature range, the rate of radiative recombination far exceeds the rate of retrapping in the main and secondary traps.

Comparison of CW-OSL signals in Fig. 3 ((c), (d)) and Fig. 4(d) for OSL recording temperatures between 600 and 700 °C, did show also that an irradiation dose i.e. 1.0 Gy and 5.0 Gy respectively, affects the shape of the CW-OSL signal and the associated charge transfer mechanisms.

3.4. Influence of measurement temperature on the peak shape of the CW-OSL signal

For this measurement, a sample was irradiated to 5.0 Gy, heated at 1.0 °C/s to 500 °C to deplete the main and secondary traps, then exposed to 470-nm blue LEDs for 1000 s at a temperature Ti to record OSL. Ti represents a temperature at which OSL is measured. This procedure was repeated for Ti's between 30 and 560 °C. The whole

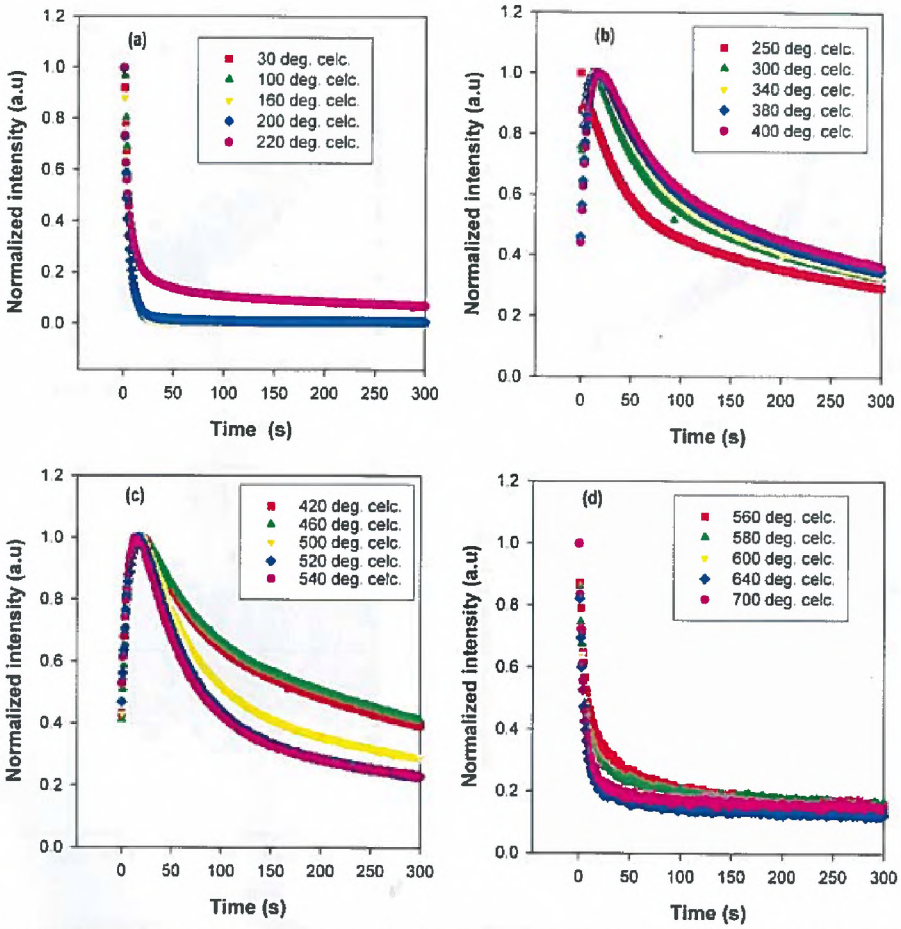

Fig. 6. Plots of CW-OSL signal for various post-irradiation preheat temperatures. For a given preheat temperature, the sample was irradiated to 5.0 Gy, preheated to a specified maximum temperature at 1.0 °C/s then illuminated by 470-nm blue light for 1000 s at 30 °C to record OSL. The plots show the signal for the first 300 s only.

experiment was repeated using an empty sample holder to record noise in the OSL signal measured at a temperature, Ti. The recorded noise represents the unwanted signal due to sources external to the sample. The recorded noise was then subtracted from the actual data. Fig. 7 presents the plots of the net CW-OSL signal obtained at various recording temperatures. It is clear in Fig. 7 that peak-shaped OSL signal is obtained for OSL recording temperatures between 30 and 240 °C. This shows that there is substantial retrapping at the main trap of charges optically released from very deep traps at these temperatures. On the other hand, temperatures above 240 °C (Fig. 7(c) and (d)) render the main trap less effective at charge retrapping. As a result, a direct recombination route becomes dominant and a decaying OSL signal is thus observed.

4. Conclusion

Factors influencing the peak-shaped nature of the luminescence signal obtained from α-Al2O3:C through optical stimulation of very deep traps at constant intensity have been presented. Irradiation dose, post-irradiation annealing temperature, charge occupancy in both the main and very deep traps and the OSL recording temperature, all have shown to have an effect on the shape of the CW-OSL signal. We have shown that the rising part of the CW-OSL signal can only be obtained if the most optically active trapping centre i.e. main trap in α-Al2O3:C is substantially empty and the donor traps i.e. very deep traps, are substantially filled.

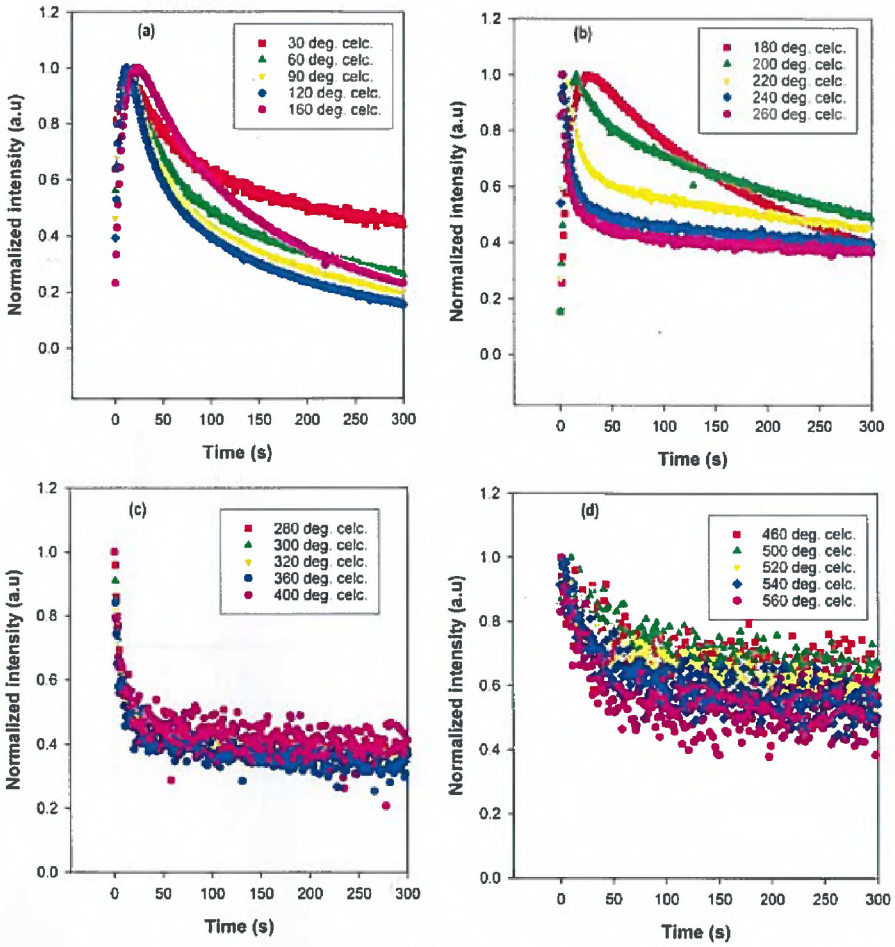

Fig. 7. Plots of CW-OSL signal recorded isothermally at various temperatures. For a given recording temperature, the sample was first irradiated to 5.0 Gy, heated to 500 °C at 1.0 °C/s, followed by 470-nm blue light stimulation for 1000 s to record OSL. The plots show the signal for the first 300 s only.

References

[1] M.L. Chithambo, R.B. Galloway, On the slow component of luminescence stimulated from quartz by pulsed blue light-emitting diodes, Nucl. Instrum. Methods B 183 (2001) 358–368.

[2] R.M. Bailey, B.W. Smith, E.J. Rhodes, Partial bleaching and the decay characteristics of quartz OSL, Radiat. Meas. 27 (1997) 123–136.

[3] R.H. Biswas, B.C. Bhatt, A.K. Singhvi, Effect of optical bleaching on the dosimetric TL peak in Al2O3:C for blue and UV emissions, Radiat. Meas. 59 (2013) 37–43.

[4] G.S. Polymeris, S. Raptis, D. Afouxenidis, N.C. Tsirliganis, G. Kitis, Thermally assisted OSL from deep traps in Al2O3:C, Nucl. Instrum. Methods Phys. Res. B 45 (2010) 519–522.

[5] G.S. Polymeris, G. Kitis, N.C. Tsirliganis, Correlation between TL and OSL properties of CaF2:N, Nucl. Instrum. Methods Phys. Res. B 251 (2006) 133–142.

[6] G.S. Polymeris, Thermally assisted OSL (TA-OSL) from various luminescence phosphors; an overview, Radiat. Meas. (2016) 1–8.

[7] S.W.S. McKeever, L. Botter-Jensen, N. Agersnap Larsen, G.A.T. Duller, Temperature dependence of OSL decay curves: experimental and theoretical aspects, Radiat. Meas. 27 (1997) 161–170.

[8] E.G. Yukihara, S.W.S. McKeever, Optically Stimulated Luminescence Fundamentals and Applications, John Wiley and Sons, Ltd, 2011.

[9] N.R.J. Poolton, L. Botter-Jensen, P.J.M. Ypma, O. Johnsen, Influence of crystal structure on the optically stimulated luminescence properties of feldspars, Radiat. Meas. (1994) 551–554.

[10] N.K. Umisedo, E.M. Yoshimura, B.R. Gasparian, E.G. Yukihara, Comparison between blue and green stimulated luminescence of Al2O3:C, Radiat. Meas. 45 (2010) 151–156.

Nuclear Instruments and Methods in Physics Research B 397 (2017) 92–100

Contents lists available at ScienceDirect

Nuclear Instruments and Methods in Physics Research B

journal homepage: www.elsevier.com/locate/nimb

The influence of radiation-induced defects on thermoluminescence and optically stimulated luminescence of α-Al_2O_3:C

A.N. Nyirenda *, M.L. Chithambo

Department of Physics and Electronics, Rhodes University, P.O Box 94, Grahamstown 6140, South Africa

ARTICLE INFO

Article history:
Received 1 December 2016
Received in revised form 10 February 2017
Accepted 27 February 2017

Keywords:
Radiation-induced
Defects
Thermoluminescence
Optically stimulated luminescence
Phototransferred
Residual

ABSTRACT

It is known that when α-Al_2O_3:C is exposed to excessive amounts of ionising radiation, defects are induced within its matrix. We report the influence of radiation-induced defects on the thermoluminescence (TL) and optically stimulated luminescence (OSL) measured from α-Al_2O_3:C after irradiation to 1000 Gy. These radiation-induced defects are thermally unstable in the region 450–650 °C and result in TL peaks in this range when the TL is measured at 1 °C/s. Heating a sample to 700 °C obliterates the radiation-induced defects, that is, the TL peaks corresponding to the radiation induced defects are no longer observed in the subsequent TL measurements when moderate irradiation doses below 10 Gy are used. The charge traps associated with these radiation-induced defects are more stable than the dosimetric trap when the sample is exposed to either sunlight or 470-nm blue light from LEDs. TL glow curves measured following the defect-inducing irradiation produce a dosimetric peak that is broader and positioned at a higher temperature than observed in glow curves obtained before the heavy irradiation. In addition, sample sensitization/desensitization occurs due to the presence of these radiation-induced defects. Furthermore, both the activation energy and the kinetic order of the dosimetric peak evaluated when the radiation-induced defects are present in the sample are significantly lower in value than those obtained when these defects are absent. The radiation-induced defects also affect the shape and total light sum of the OSL signal as well as the position and width of the resultant residual phototransferred thermoluminescence main peak.

1. Introduction

α-Al_2O_3:C is a material of great dosimetric importance due to its high sensitivity to ionising radiation, low detectable dose threshold, wide range of linear dose response, low fading rate, low background noise, simple annealing procedure and high resistance to radiation [1–4]. Its extreme sensitivity to ionising radiation is ascribed to high concentration of luminescence-active point defects consisting mainly of an oxygen vacancy localizing an electron (F^+ centre, emission wavelength, λ_{em} = 330 nm) and oxygen vacancy with two electrons trapped nearby (F centre, λ_{em} = 420 - nm). Both F^+ and F centres are intrinsic in as-grown α-Al_2O_3 and their concentration is enhanced when α-Al_2O_3:C is doped with carbon [1]. When Al_2O_3 is exposed to heavy irradiation of say energetic electrons or neutrons, its structure may not only change but defects may also be induced as a result [2,3]. Some previously reported radiation-induced defects in α-Al_2O_3:C and its precursor α-Al_2O_3 include complex aggregates of F_2 centres in different charged states as F_2, F^{+2} and F_2^{2+} [4,5]. F_2, F^{+2} and F_2^{2+} are aggregates of two oxygen vacancies that have trapped four, three and two electrons, respectively. Kortov et al. [4] go further to claim that it is the F^+ centres and not the F centres that are involved in the formation of these aggregates.

In this paper, we present the influence of radiation-induced defects in α-Al_2O_3:C on the TL and OSL measured after the defect-inducing irradiation.

2. Experimental details

Samples were aluminium oxide disks measuring 5 mm in diameter and 1 mm in thickness (Rexon

TLD Systems, Ohio, USA) and were annealed once at 900 °C for 15 min before use. All measurements were carried out in the Risø TL/OSL DA-20 Reader that measures both TL and OSL.

The luminescence detection unit consists of an EMI 9235QB photomultiplier tube (PMT) and a 7-mm thick Hoya U-340 detection filter (transmission 270–380 nm FWHM). However, to attenuate excessive luminescence intensities hazardous to the PMT at very high doses, we used an absorptive neutral density filter

* Corresponding author.
E-mail address: anyirenda@gmail.com (A.N. Nyirenda).

http://dx.doi.org/10.1016/j.nimb.2017.02.077
0168-583X/

(NDF), a Hoya ND-03 of 1% transmission and a transmission wavelength of 400–700 nm. The irradiation unit is a built-in $^{90}Sr/^{90}Y$ β-source with a nominal dose rate of 0.1028 Gy/s. For CW-OSL measurements, a set of blue LEDs (peak wavelength, λ_p = 470 nm, FWHM = 20 nm) that delivers a maximum power density of 80 mWcm^2 at the sample position was used.

The following protocols, labelled Protocol 1 and Protocol 2, were used to investigate the effects of the heavy irradiation on TL and OSL, respectively. For this, samples were irradiated to 1000 Gy.

2.1. Protocol 1

This protocol was used to investigate the effects of heavy irradiation on TL.

Stage 1

1. A preheat at 1 °C/s to 700 °C to remove any background dose
2. Irradiation to a test dose of 1.0 Gy (used to monitor changes in TL)
3. TL at 1 °C/s to 400 °C

Steps 2–3 were repeated 10 times to monitor sensitivity changes. The TL measurements in step 3 shall be referred to as **TL A**.

Stage 2

4. Irradiation to 1000 Gy (intended to induce defects)
5. A preheat at 1 °C/s to 400 °C (to clear the main peak)
6. Irradiation to a test dose of 1.0 Gy (used to monitor changes in TL)
7. TL at 1 °C/s to 400 °C

Steps 6–7 were repeated 10 times to monitor sensitivity changes. The TL measurements in step 7 shall be referred to as **TL B**.

Stage 3

8. A preheat at 1 °C/s to 700 °C (intended to remove radiation induced defects)
9. Irradiation to a test dose of 1.0 Gy (used to monitor changes in TL)
10. TL at 1 °C/s to 400 °C

Steps 9–10 were repeated 10 times to monitor sensitivity changes. The TL measurements in step 10 shall be referred to as **TL C**.

Each irradiation was preceded by a 120-s pause to ensure that the sample was irradiated at room temperature.

To isolate the influence of the radiation induced defects on TL, Stage 2 of Protocol 1 was modified by preheating the sample to 700 °C instead of 400 °C (step 5) immediately after 1000 Gy irradiation i.e. the modified protocol involves two separate preheats to 700 °C, the other being at the beginning of Stage 3. This modified version of Protocol 1 shall be referred to as modified Protocol 1. Both Protocol 1 and modified Protocol 1 were repeated for TL readouts measuring to 500 °C.

2.2. Protocol 2

This protocol was used to investigate the influence of radiation-induced defects on OSL measured following the defect-inducing irradiation:

Stage 1

1. A preheat at 1 °C/s to 700 °C (intended to remove any background dose)
2. Irradiation to a test dose of 1.0 Gy (to monitor changes in OSL)
3. OSL at 30 °C for 200 s using 470-nm blue LEDs set at 90% optical power
4. TL at 1 °C/s to 500 °C (intended to record residual phototransferred TL (RPTTL))

Steps 2–4 were repeated 10 times to monitor sensitivity changes. The OSL measurements at step 3 and RPTTL measurements at step 4 shall be referred to as **OSL A** and **RPTTL A**, respectively.

Stage 2

5. Irradiation to 1000 Gy (intended to induce defects)
6. A preheat at 1 °C/s to 500 °C (intended to clear the main peak)
7. Irradiation to a test dose of 1.0 Gy (to monitor changes in OSL)
8. OSL at 30 °C for 200 s using 470-nm blue LEDs set at 90% optical power
9. TL at 1 °C/s to 500 °C (intended to record RPTTL)

Steps 7–9 were repeated 10 times to monitor sensitivity changes. The OSL measurements at step 8 and RPTTL measurements at step 9 shall be referred to as **OSL B** and **RPTTL B**, respectively.

Stage 3

10. A preheat at 1 °C/s to 700 °C (intended to remove radiation-induced defects)
11. Irradiation to a test dose of 1.0 Gy (to monitor changes in OSL)
12. OSL at 30 °C for 200 s using 470-nm blue LEDs set at 90% optical power
13. TL at 1 °C/s to 500C (intended to record residual RPTTL)

Steps 11–13 were repeated 10 times to monitor sensitivity changes. The OSL measurements at step 12 and RPTTL measurements at step 13 shall be referred to as **OSL C** and **RPTTL C**, respectively.

Every irradiation in Protocol 2 was also preceded by a 120-s pause to ensure that irradiation took place at room temperature.

3. Results and discussion

3.1. Thermoluminescence peaks following heavy beta-irradiation

An annealed sample was beta-irradiated to 1000 Gy then heated to 300 °C at 1 °C/s to record a TL glow curve. The sample was thereafter reheated from room temperature to 700 °C at 1 °C/s to record another TL glow curve. A third TL measurement from room temperature to 700 °C at 1 °C/s was made following irradiation to 1.0 Gy. The results are shown in Fig. 1.

Fig. 1(a) shows a semi-logarithmic plot of the TL glow-curve measured to 300 °C. This is denoted as Run 1. There are peaks at 48, 78, 149, and 282 °C. The prominent peak at 149 °C is the one used for dosimetry. Fig. 1(b) shows results for the second set of measurements made immediately after that shown in Fig. 1(a). The glow curve, labelled Run 2, was measured immediately after Run 1 shown in Fig. 1(a). This glow curve shows obvious peaks at 45, 198, 281 and 560 °C. There is also a broad peak between 330 and 490 °C. The third measurement, shown as Run 3 in Fig. 1(b),

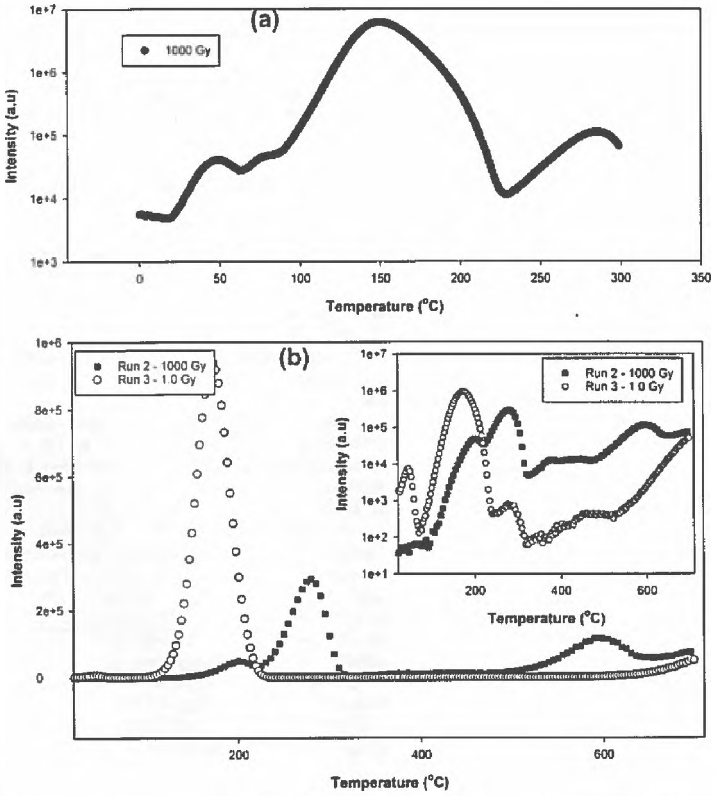

Fig. 1. (a) A semi-log plot of the TL glow curve measured to 300 °C following 1000 Gy irradiation.(b) The glow curve measured from room temperature to 700 °C immediately after Run 1 in (a) without further irradiation (Run 2) and following a 1.0 irradiation (Run 3). The inset in (b) shows the two glow curves i.e. Run 2 and Run 3 in a semi-log plot for visual clarity. TL glow curves were recorded at 1 °C/s.

was made after Run 2 but with the sample having been irradiated to 1.0 Gy. The latter has glow peaks at 175 °C (the dosimetric peak) and 281 °C as well as a broad peak between 330 and 520 °C. It should be noted that whereas the TL in Run 1 was measured to 300 °C, the glow curves in Runs 2 and 3 were made to 700 °C.

We expect the dosimetric peak to be centred at 175 °C (Run 3) for a 1.0 Gy irradiation. The shift of the dosimetric peak from 175 °C to 149 °C following irradiation to 1000 Gy is to be expected since the position of the dosimetric peak shifts towards lower temperatures at high irradiation doses [6,7].

We also expect the heating of the sample to 300 °C following 1000 Gy irradiation to clear the main peak. However, as is shown in Run 2 of Fig. 1(b), the dosimetric peak is palpably visible, albeit less intense. This indicates presence of charge in the main trap without any irradiation. It is reasonable to suggest that charge carriers leak away, possibly through a tunneling mechanism, from the filled higher temperature secondary traps to the main trap.

The TL peaks centred at 78 °C in Run 1, Fig. 1(a), and 560 °C in Run 2 of Fig. 1(b) were only observed when the sample was irradiated to 1000 Gy. We ascribe the presence of these two peaks to defects induced by the heavy irradiation dose i.e. 1000 Gy. Furthermore, heating the sample to 700 °C (Run 2) after the 1000 Gy irradiation removes the induced defects as evident from absence of these radiation-induced peaks in the TL glow-curve of Run 3 in Fig. 1(b). The removal of the heavy-irradiation induced defects due to annealing at 700 °C was also reported by Harutyunyan et al. [8] for the same material.

At this stage of our study, we can only speculate that these radiation-induced defects may be complex self-aggregates of as grown defect centres such as F^+ and F centres or complexities with radiation-induced oxygen interstitials (O^{2-}) and vacancies (V_O^{2+}) as well as aluminium interstitials (Al^{3+}) and vacancies (V_{Al}^{3-}). More insightful information about these radiation-induced defects can be obtained from spectral and electron spin resonance (ESR) measurements. It was not the aim of this work to unequivocally identify the defects. Recent studies by Kortov et al. [4] provide more information on the nature and identity of these radiation-induced defects in the material.

The current study focuses on the radiation-induced defects that produce TL peak(s) in the range 480–650 °C and centred at 560 °C (see Run 2). The influence of these radiation-induced defects on TL and OSL measured after the defects-inducing irradiation have been presented in later sections.

3.2. Stability of the radiation-induced peaks under exposure to sunlight

In this simple experiment, a sample was irradiated to 1000 Gy then immediately exposed to direct sunlight for about 9 h. The temperatures of the day ranged from 7 to 16 °C. The motivation

for this study was that since luminescence in α-Al_2O_3:C is sensitive to light, the question about how radiation-induced defects are affected by light needed to be addressed. The study only used sunlight as an exemplar.

Fig. 2 shows the measured TL glow curve, and in the inset, the same data on a semi-logarithmic scale. It can be seen in Fig. 2 that the peak at 45 °C and the additional peak at 78 °C produced by heavy irradiation (see Fig. 1) are completely removed by sunlight exposure. The dosimetric peak is centred at 183 °C whereas the high temperature peak produced by radiation-induced defects is still at 564 °C. In addition, the intensities of all the peaks are significantly less than those of peaks obtained immediately after 1000-Gy irradiation, that is, without exposure to sunlight (see Fig. 1). The dosimetric peak decreased substantially whereas the peak at 564 °C was the least affected. This result indicates that under light exposure, specifically sunlight, the radiation-induced defects are more stable than the shallow, main and subsidiary traps. This stability suggests that the radiation-induced defects may indeed be complex as reported by other researchers [2,4,5]. The stability of these defects under sunlight exposure, as seen, means that they are amenable to being adapted for high radiation dose TL dosimetry. Comparison of the position of the dosimetric peak obtained immediately after 1000 Gy irradiation i.e. 149 °C (see previous section) and that obtained after 9 h of sunlight exposure i.e. 183 °C indicates that the lower temperature components of the dosimetric peak are more bleached than the higher temperature components.

3.3. Influence of heavy irradiation dose on the post-heavy-irradiation TL

We now present effects, based on Protocol 1, of a heavy irradiation dose on TL measured after the heavy irradiation. All the reported effects are based on the behaviour of the position, FWHM, maximum intensity and consequently the trap depth of the main peak. Please recall the terminology where **TL A** represents the 10 TL measurements made before sample irradiation to 1000 Gy; **TL B** are the 10 TL measurements recorded after the 1000 Gy irradiation and before the preheat to 700 °C and **TL C** are the 10 TL measurements carried out after the preheat to 700 °C. For the modified Protocol 1, **TL A** represents the 10 TL measurements made before 1000 Gy irradiation; **TL B** represents the 10 TL glow curves measured after 1000 Gy irradiation followed by a preheat to 700 °C and **TL C** represents the 10 TL measurements done after the second preheat to 700 °C.

3.3.1. Influence of heavy irradiation dose on the position of the main peak

Fig. 3(a) shows the behaviour of the peak position obtained using Protocol 1 for TL glow curves measured to 400 °C whereas Fig. 3(b) shows the behaviour of the peak position for TL glow curves measured to 400 °C corresponding to the modified Protocol 1 in which the sample is preheated to 700 °C twice as earlier explained.

It can be seen from Fig. 3(a) that the positions of the main peak in the TL glow curves obtained in **TL A** (168 °C) are equivalent to those obtained in **TL C** (172 °C) albeit slightly higher in **TL C**. In addition, Fig. 3(a) indicates that the position of the main peak shifts towards higher temperatures (183 °C) in the TL glow-curves obtained in **TL B**. This result suggests that the defects induced in the sample following the 1000 Gy irradiation are responsible for the shift of the main peak towards higher temperatures. One possibility could be that the formation of radiation-induced defects decreases the concentration of the traps responsible for lower temperature components through transformation of colour centres into aggregate centres [2,4]. The result also attests to the earlier observation that heating the sample to 700 °C removes the radiation induced defects and resets the sample.

Fig. 3(b) shows that the position of the main peak does not change when the sample is preheated to 700 °C immediately fol-

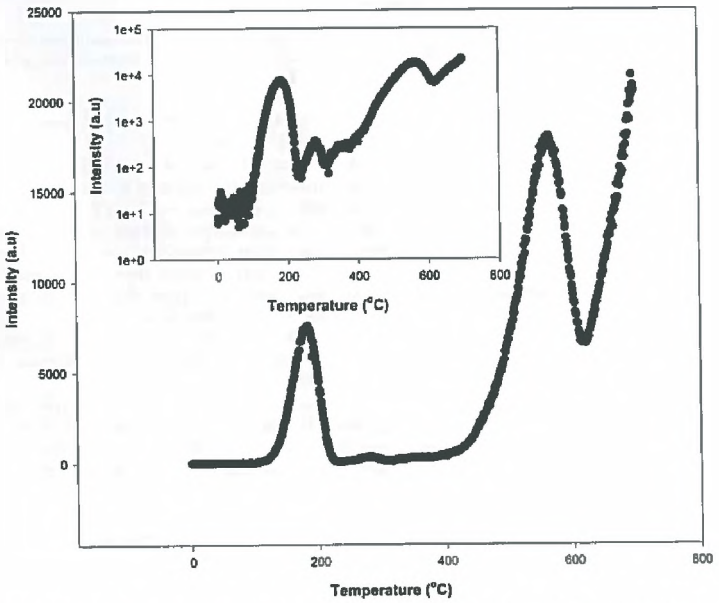

Fig. 2. A TL glow curve recorded at 1 °C/s after 9 h of sunlight exposure of the sample previously irradiated to 1000 Gy. The inset shows the same plot in a semi-log plot for visual clarity.

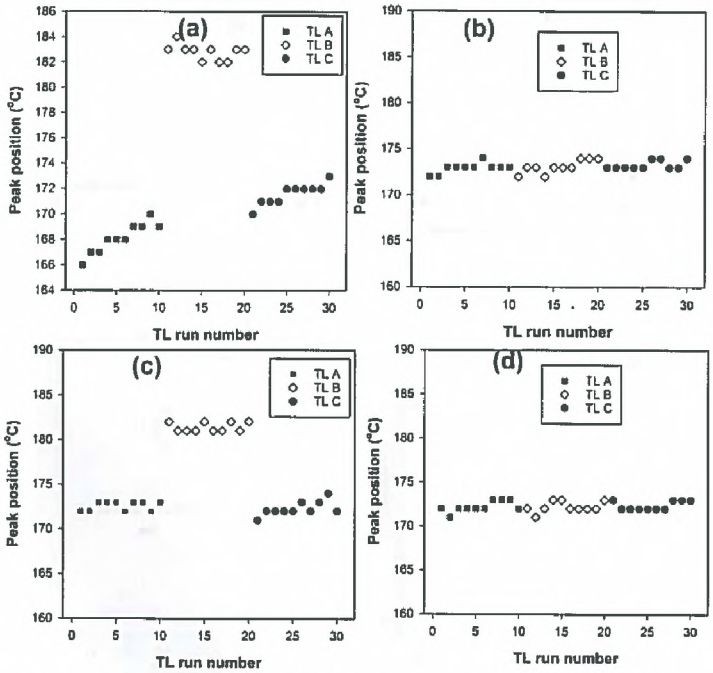

Fig. 3. Behaviour of the position of the main peak when TL is measured at 1 °C/s to (a) 400 °C using Protocol 1; (b) 400 °C using modified Protocol 1; (c) 500 °C using Protocol 1; and (d) 500 °C using modified Protocol 1. The sample was given a test dose of 1.0 Gy prior to each TL measurement. In Protocol 1, **TL A** represents the TL measurements made before sample irradiation to 1000 Gy; **TL B**, the TL measurements made after the 1000 Gy irradiation and before the preheat to 700 °C and **TL C**, the TL measurements carried out after the preheat to 700 °C. In the modified Protocol 1, **TL A** represents the TL measurements made before 1000 Gy irradiation; **TL B**, the TL glow curves measured after 1000 Gy irradiation followed by a preheat to 700 °C and **TL C**, the TL measurements done after the second preheat to 700 °C.

lowing the heavy irradiation (**TL B**). This result confirms the role of the radiation-induced defects in the shift of the peak position as shown in Fig. 3(a). We also notice that the second preheat of the sample to 700 °C does not affect the position of the main peak (**TL C**). This result suggests that merely heating the sample to 700 °C does not affect the position of the peak.

Fig. 3(c) shows that the positions of the main peak in the TL glow curves obtained in **TL A** (172 °C) are equivalent to those obtained in **TL C** (172 °C). In addition, Fig. 3(c) indicates that the position of the main peak shifts towards higher temperatures (182 °C) in the TL glow-curves obtained in **TL B**. On the other hand, Fig. 3(d) shows that the position of the main peak does not change when the sample is preheated to 700 °C immediately following the heavy irradiation (**TL B**).

The behaviour of the peak position as shown in Fig. 3(c) and (d) for the TL glow curves measured to 500 °C is similar to that shown in Fig. 3(a) and (b), respectively. Hence, the explanations given above for Fig. 3(a) and (b) also apply to Fig. 3(c) and (d). This result signifies that measuring the TL glow curve to a maximum temperature of 400 °C or 500 °C, does not affect the position of the main peak.

3.3.2. Influence of heavy irradiation dose on the width of the main peak

Fig. 4(a) shows the behaviour of the full width at half-maximum (FWHM) obtained using Protocol 1 for TL glow curves measured to 400 °C whereas Fig. 4(b) shows the behaviour of the FWHM for those measured to 400 °C corresponding to the modified Protocol 1.

It can be seen from Fig. 4(a) that values of the FWHM of the main peak in the TL glow curves obtained in **TL A** i.e. 33 °C is equivalent to those obtained in **TL C** i.e. 32 °C. Fig. 4(a) also indicates that the FWHM of the main peak increased to 38 °C in the TL glow curves obtained in **TL B**. This result suggests that the defects induced in the sample following the 1000 Gy irradiation are responsible for the observed broadening of the main peak. The peak broadening suggests that the radiation-induced defects give rise to additional components within the main TL peak.

Fig. 4(b) shows that the FWHM of the main peak does not change when the sample is preheated to 700 °C immediately following the 1000 Gy irradiation (**TL B**). This result simply confirms that radiation-induced defects are responsible for the broadening of the main peak. We again notice that the second preheating to 700 °C does not affect the width of the main peak.

The behaviour of the width of the main peak as shown in Fig. 4 (c) and (d) for the TL glow curves measured to 500 °C is equivalent to that presented in Fig. 4(a) and (b), respectively. This result implies that measuring the TL glow curve to a maximum temperature of 400 °C or 500 °C has no effect on the width of the main peak. In addition, this result means that merely preheating to 700 °C does not affect the width of the main peak.

3.3.3. Influence of heavy irradiation dose on the maximum intensity of the main peak

Fig. 5(a) shows the behaviour of the maximum intensity of the main peak for TL glow curves measured to 400 °C using Protocol 1. Fig. 5(b), on the other hand, shows the behaviour of the maximum

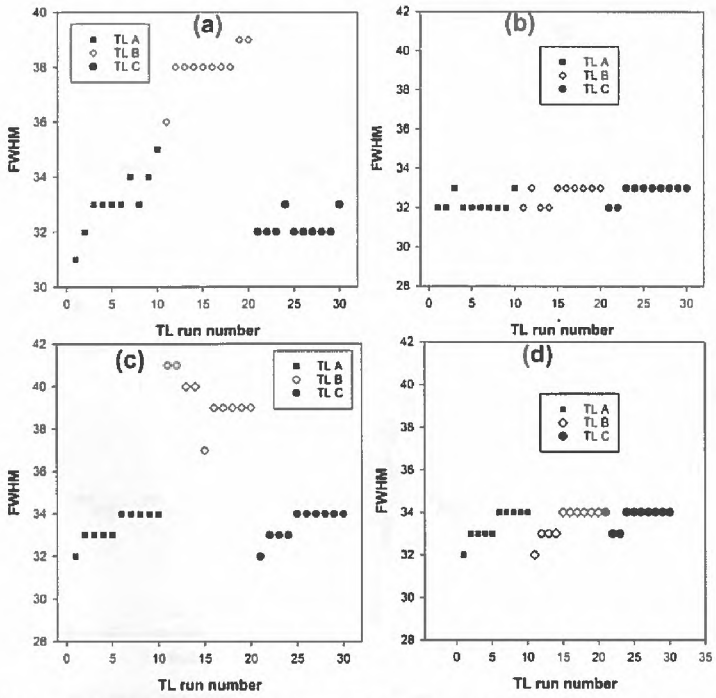

Fig. 4. Behaviour of the FWHM of the main peak when TL is measured at 1 °C/s to (a) 400 °C using Protocol 1; (b) 400 °C using modified Protocol 1; (c) 500 °C using Protocol; and (d) 500 °C using modified Protocol 1. The sample was given a test dose of 1.0 Gy prior to each TL measurement. In Protocol 1, **TL A** represents the TL measurements made before sample irradiation to 1000 Gy; **TL B**, the TL measurements made after the 1000 Gy irradiation and before the preheat to 700 °C and **TL C**, the TL measurements carried out after the preheat to 700 °C. In the modified Protocol 1, **TL A** represents the TL measurements made before 1000 Gy irradiation; **TL B**, the TL glow curves measured after 1000 Gy irradiation followed by a preheat to 700 °C and **TL C**, the TL measurements done after the second preheat to 700 °C.

intensity for TL glow curves measured to 400 °C corresponding to the modified Protocol 1.

In Fig. 5(a), the maximum intensity of the main peak for TL glow curves obtained in **TL A** increases gradually with number of TL runs. This trend is maintained in **TL B** after the heavy irradiation dose. However, after preheating to 700 °C, the maximum intensities obtained in **TL C** are significantly higher compared to those obtained in either **TL A** or **TL B**. This shows an increased sensitivity of the sample to irradiation. Further research is required to understand the cause of this sensitization since one would expect charge trapping competition, during irradiation, between the main traps and deep traps to increase after preheating to 700 °C with consequent decrease in the maximum intensity of the main peak. The increase of the maximum intensity with repeated irradiation-TL cycles within each stage can be attributed to deep trap filling which in turn reduces competition for charge between the main traps and deep traps during irradiation.

Fig. 5(b) shows that the maximum intensity gradually increases with number of TL readouts in all the three stages. However, both the first and second preheating to 700 °C result into a lower maximum intensity in the next TL measurement than that obtained in the previous TL. This indicates that the preheat lowers the charge concentration in the deep traps making them efficient charge competitors against the main trap in the subsequent irradiation.

Fig. 5(c), on the other hand, shows a major decrease in the maximum intensity of the main peak following the 1000 Gy irradiation (**TL B**) and a corresponding major increase in **TL C** after preheating to 700 °C. It is worthwhile noting that the maximum intensities obtained before the 1000 Gy irradiation (**TL A**) and those obtained post-700 °C preheating (**TL C**), are equivalent. This indicates that preheating the sample to 700 °C following heavy irradiation restores the sensitivity of the sample. This behaviour is in sharp contrast to that observed when TL glow curves were measured to a maximum temperature of 400 °C where the sensitivity of the sample seems not affected by heavy irradiation and preheating to 700 °C significantly sensitizes the sample (see Fig. 5(a)).

Fig. 5(d) shows that the maximum intensities obtained in **TL B** and **TL C** are almost equivalent and are lower than those obtained in **TL A**. This result implies that the 1000 Gy irradiation causes desensitization of the sample when TL glow-curves are measured to 500 °C. Secondly, it demonstrates that preheating to 700 °C alone has little effect on the sensitivity of the sample.

Overall, results presented in Fig. 5 have shown that the sensitivity of the sample is affected by the heavy irradiation dose and/or the maximum temperature to which the TL glow curve is measured.

3.3.4. Effect of the heavy irradiation dose on the activation energy of the main peak

We have seen in the previous sections how heavy irradiation i.e. 1000 Gy significantly affects the shape, position and intensities of the main peak due to the induced defects. It is only instructive therefore, to assess whether and how the activation energy of

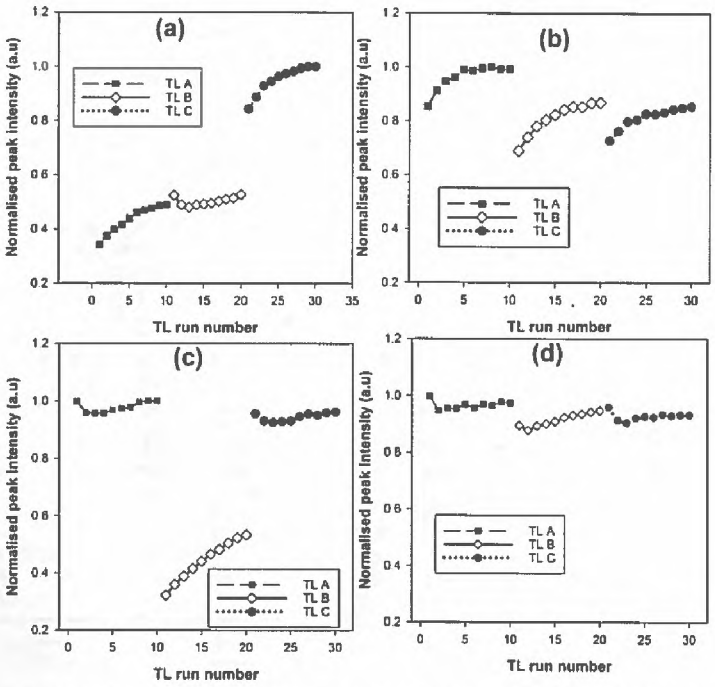

Fig. 5. Behaviour of the maximum intensity of the main peak when TL is measured at 1 °C/s to(a) 400 °C using Protocol 1; (b) 400 °C using modified Protocol 1; (c) 500 °C using Protocol 1; and (d) 500 °C using modified Protocol 1. The sample was given a test dose of 1.0 Gy prior to each TL measurement. In Protocol 1, TL A represents the TL measurements made before sample irradiation to 1000 Gy; TL B, the TL measurements made after the 1000 Gy irradiation and before the preheat to 700 °C and TL C, the TL measurements carried out after the preheat to 700 °C. In the modified Protocol 1, TL A represents the TL measurements made before 1000 Gy irradiation; TL B, the TL glow curves measured after 1000 Gy irradiation followed by a preheat to 700 °C and TL C, the TL measurements done after the second preheat to 700 °C.

the main peak is affected. The analysis was done using Chen's peak shape [9] and computer glow curve deconvolution (CGCD) methods. In the CGCD method, the TL glow curves were fitted by an equation of general-order TL [9].

The following are the results obtained by the CGCD method for three randomly chosen glow curves, one from each stage: for **TL A**, activation energy, E = 1.71 ± 0.01 eV, kinetic order, b = 1.87 ± 0.01; for **TL B**, E = 1.23 ± 0.01 eV, b = 1.33 ± 0.01 and for **TL C**, E = 1.71 ± 0.01 eV, b = 1.86 ± 0.01. We note that the values of the activation energy of the main peak (1.71 eV) and its order of kinetics (1.87) for **TL A** and **TL C** are equal and higher in value than those obtained in **TL B** i.e. 1.23 eV and 1.33, respectively. This result implies that both the degree of charge retrapping during stimulation and the energy depth of the main trap are essentially reduced due to radiation-induced defects.

Table 1 summarises the results obtained by the Chen's peak shape method [9]. It is notable that parameters of the TL main peak in **TL A** and **TL C** are identical. This indicates that thermal destruction of radiation-induced defects restores the original state of the sample. The value of the geometrical factor, μ, suggests that in the presence of radiation-induced defects, the TL main peak follows general order kinetics (μ = 0.44 ± 0.02) characterized by less retrapping whereas in the absence of these induced defects, the peak follows general-order kinetics (μ = 0.500 ± 02) characterized by heavy retrapping. In addition, the activation energy obtained in **TL A** and **TL C** for the main peak is significantly higher than that obtained in **TL B**. It is important to note that results obtained by these two methods of kinetic analysis are consistent with within experimental errors.

The results of the kinetic analysis suggest that one needs to exercise caution when analysing the main peak for kinetic parameters in α-Al_2O_3:C since its radiation history might affect the results. It is advisable that samples be heated to a temperature above 700C before use for reliable results.

3.4. Influence of the heavy irradiation dose on the post-heavy-irradiation OSL

We present the influence of heavy irradiation on the OSL measured after exposing a sample to a high beta-dose. Protocol 2 was followed in this investigation. As already indicated in Protocol 2,

Table 1
Activation energy of the main peak evaluated using Chen's peak shape method [9]. TL glow curves were measured to 500 °C following a 1.0 Gy test dose. **TL A** represents the TL measurements made before sample irradiation to 1000 Gy; **TL B**, the TL measurements made after the 1000 Gy irradiation and before the preheat to 700 °C and **TL C**, the TL measurements carried out after the preheat to 700 °C as outlined in Protocol 1.

	μ	Eτ (eV)	Eσ (eV)	Eω (eV)
TL A	0.50 ± 0.02	1.7 ± 0.1	1.7 ± 0.2	1.7 ± 0.1
TL B	0.44 ± 0.02	1.1 ± 0.1	1.1 ± 0.2	1.1 ± 0.1
TL C	0.50 ± 0.02	1.7 ± 0.1	1.7 ± 0.2	1.7 ± 0.1

OSL A represents the 10 OSL measurements made before sample irradiation to 1000 Gy; **OSL B** are the 10 OSL measurements recorded after the 1000 Gy irradiation and before the preheat to 700 °C and **OSL C** are the 10 OSL measurements carried out after the preheat to 700 °C.

Fig. 6(a) shows the shape of the OSL signal obtained in **OSL A**, **OSL B** and **OSL C**. It can be seen from Fig. 6(a) that the measured OSL signals are all peak-shaped. According to Chen and McKeever [11], peak-shaped CW-OSL is typical of transfer effects. Secondly, the OSL signals in **OSL A** and **OSL C** coincide. In addition, the signal in **OSL A** and **OSL C** seems to decay much faster than the one in **OSL B**. Furthermore, the initial intensities for the signal in **OSL B** are significantly higher than those in **OSL A** and **OSL C**.

Fig. 6(b) shows a plot of the peak position of the OSL signal with respect to the number of OSL runs. It can be seen from Fig. 6(b) that the peak position for the OSL signal in **OSL B** shifts towards earlier times. This shift to earlier times when OSL is measured in the presence of the radiation-induced defects suggests that direct recombination quickly dominates over retrapping of charge carriers during optical stimulation. This result is in good agreement with our earlier findings that in the presence of these radiation-induced defects, the sample follows general-order kinetics characterized by less retrapping i.e. b decreases from 1.87 to 1.33.

Fig. 6(c) shows a plot of the integrated OSL intensity with respect to the number of OSL runs. According to Fig. 6(c) the integrated OSL intensities in **OSL A** and **OSL C** are equivalent. In addition, the intensities are higher for OSL measured in **OSL B** compared to those measured in **OSL A** and **OSL C**. This result shows that the radiation-induced defects significantly change the OSL sensitivity of the sample. Further to that, the result confirms the role of heating to 700 °C in restoring the sample's initial sensitivity.

3.5. Effect of the heavy irradiation dose on the residual phototransferred thermoluminescence

The main peak observed in the TL glow-curve recorded after OSL measurement as indicated in Protocol 2, is due to residual charge carriers in the main trap and the phototransferred charge carriers from deep traps into main trap, hence the designation residual phototransferred thermoluminescence (RPTTL). In this investigation, which is based on Protocol 2, we focused on the effect of the heavy irradiation on the main RPTTL peak. Recall that **RPTTL A** represents the 10 RPTTL measurements made before sample irradiation to 1000 Gy; **RPTTL B** are the 10 RPTTL measurements recorded after the 1000 Gy irradiation and before the preheat to 700 °C and **RPTTL C** are the 10 RPTTL measurements carried out after the preheat to 700 °C.

Fig. 7(a) shows the TL glow curves measured in **RPTTL A**, **RPTTL B** and **RPPTL C**. The TL glow-curves of **RPTTL A** and **RPTTL C** coincide and show a relatively intense main peak centred at 177 °C and a high temperature secondary peak whereas that of **RPTTL B** shows an intense main peak centred at 190 °C alongside low temperature and high temperature secondary peaks. This dominant peak at 177 °C or 190 °C will be referred to as the main RPTTL peak.

Fig. 7(b) shows a plot of the position of the main RPTTL peak with respect to number of OSL runs for TL measurements in **RPTTL A**, **RPTTL B** and **RPTTL C**. The positions of the main peak lie in the range of 173–181 °C for TL glow curves in **RPTTL A**; 187–195 °C for those in **RPTTL B** and 172–180 °C for those in **RPTTL C**. This indicates that the position of the main RPTTL peak shifts towards higher temperatures when RPTTL is measured in the presence of radiation-induced defects. Note that the average temperatures of the position for the main RPTTL peak i.e. 177 °C for **RPTTL A** and

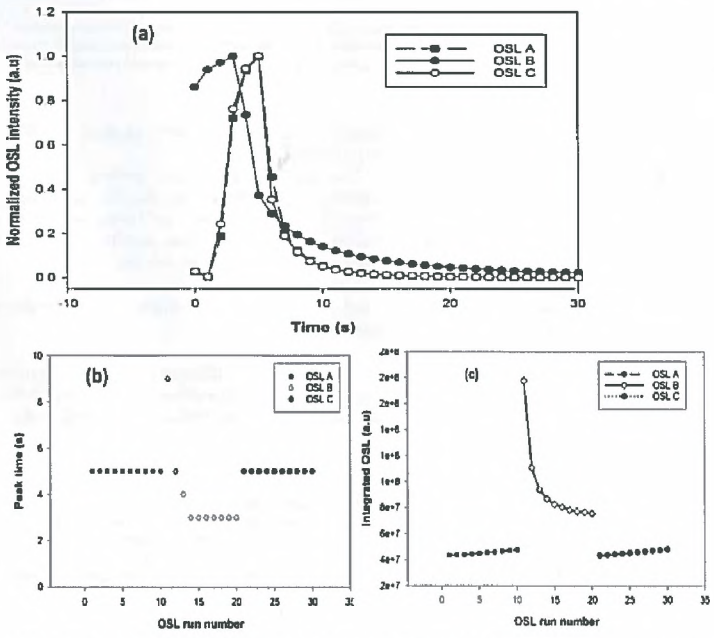

Fig. 6. OSL signals measured using Protocol 2 (a); behaviour of the peak position (b) and the integrated OSL intensities (c). The samples were stimulated by 470-nm blue LEDs for 200 s following irradiation to 1.0 Gy. **OSL A** represents the OSL measurements made before sample irradiation to 1000 Gy; **OSL B**, the OSL measurements made after the 1000 Gy irradiation and before the preheat to 700 °C and **OSL C**, the OSL measurements carried out after the preheat to 700 °C. Note that only the first 30 s have been shown in (a) for visual clarity.

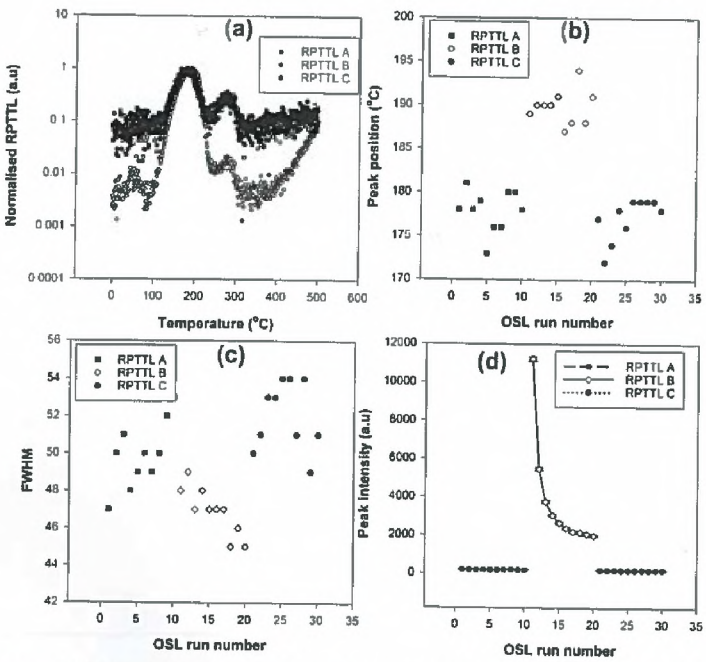

Fig. 7. The RPTTL glow curves measured at 1 °C/s to 500 °C following 470-nm blue LEDs stimulation for 200 s of a sample that was irradiated to 1.0 Gy (a). The behaviour of the position (b), the FWHM (c) and the maximum intensity (d) of the main RPTTL peak. **RPTTL A** represents the RPTTL measurements made before sample irradiation to 1000 Gy; **RPTTL B**, the RPTTL measurements made after the 1000 Gy irradiation and before the preheat to 700 °C and **RPTTL C**, the RPTTL measurements carried out after the preheat to 700 °C.

RPTTL C and 190 °C for **RPTTL B** are in general higher than those obtained for conventional TL i.e. 172 °C for **TL A** and **TL C** and 182 °C for **TL B** as shown in Fig. 3. This shift in position of the main peak in conventional TL towards higher temperatures in photo-transferred TL has already been reported [10].

Fig. 7(c) shows a plot of the FWHM of the main RPTTL peak with respect to number of OSL runs for TL measurements in **RPTTL A**, **RPTTL B** and **RPPTL C**. In general the FWHM of the main RPTTL peak is reduced when the RPTTL is measured in the presence of radiation-induced defects. This is in sharp contrast to the behaviour of the FWHM for conventional TL in which the FWHM increases for TL measured when the radiation-induced defects are present. It is also important to note that the average FWHM of the main RPTTL peak i.e. 51 °C for **RPTTL A** and **RPTTL C** and 47 °C for **RPTTL B** are in general higher than those obtained for conventional TL i.e. 33 °C for **TL A** and **TL C** and 38.5 °C for **TL B** as shown in Fig. 4.

Fig. 7(d) is a plot of the maximum intensity of the main RPTTL peak with respect to number of OSL runs. The maximum intensities in **RPTTL A** and **RPTTL C** are equivalent and considerably lower than those obtained in **RPTTL C**. Note that this plot is a complete replica of Fig. 7(b) in which the total OSL yield is plotted against OSL run number. This indicates a strong dependence of the intensities of the main RPTTL peak on the preceding OSL measurement.

4. Conclusion

We have shown that the salient features of TL and OSL obtained following a high irradiation beta-dose of α-Al_2O_3:C are significantly altered. For example, the main peak shifts towards higher temperatures; its FWHM increases; the activation energy decreases and its order of kinetics also decreases. These changes have been attributed to the defects induced by the heavy dose. These radiation-induced defects produce peaks in the range 480–650 °C. It has been observed that heating a sample to 700 °C after exposure to a high dose successfully removes the radiation-induced defects. Furthermore, these radiation-induced defects are more stable under sunlight conditions than the main trap.

References

[1] V. Kortov, I. Milman, Some new data on thermoluminescence properties of dosimetric α-Al2O3: C crystals, Radiat. Prot. Dos. 65 (1996) 179–184.
[2] A.I. Surdo, V.S. Kortov, I.I. Milman, Creation of aggregate f-centres in corundum irradiated with fast electrons, Technol. Phys. Lett. 11 (1985) 943–947.
[3] M. Izerrouken, T. Banyahioa, Adsorption and photoluminescence study of Al_2O_3 single crystal irradiated with fast neutrons, Nucl. Instrum. Methods Phys. Res. B 268 (2010) 2087–2090.
[4] V.S. Kortov, V.A. Pustovarov, S.V. Zvonarev, T.V. Shtang, Luminescence and radiation-induced color centres in anion-defective alumina crystals after high-dose irradiation, Radiat. Meas. (2016) 1–4.
[5] E.A. Kotomin, A.I. Popov, Radiation-induced point defects in simple oxides, Nucl. Instrum. Methods Phys. Res. B 141 (1998) 1–15.
[6] A.N. Nyirenda, M.L. Chithambo, Kinetic analysis of the main glow peak of α-Al2O3: C exposed to high irradiation dose, J. Nucl. Sci. 2 (2015) 23–30.
[7] M.L. Chithambo, Concerning secondary peaks in α-Al_2O_3:C, South African J. Sci. 100 (2004) 524–527.
[8] V.V. Haratyunyan, Radiation-induced effects in corundum single crystals, Armenian J. Phys. 8 (2015) 129–139.
[9] V. Pagonis, G. Kitis, C. Furreta, Numerical and Practical Exercises in Thermoluminescence, Springer, 2006.
[10] A.N. Nyirenda, M.L. Chithambo, G.S. Polymeris, On luminescence stimulated from deep traps using thermally-assisted time-resolved optical stimulation in α-Al_2O_3:C, Radiat. Meas. (2016) 1–4.
[11] R. Chen, S.W.S. McKeever, Theory of Thermoluminescence and Related Phenomena, World Scientific, Singapore, 1997.